

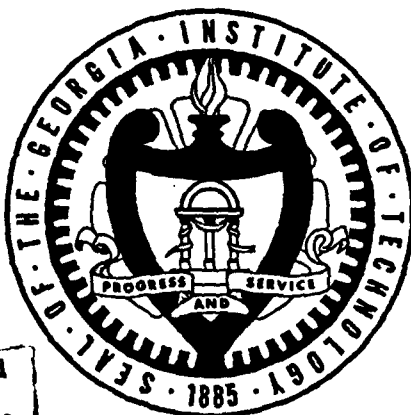
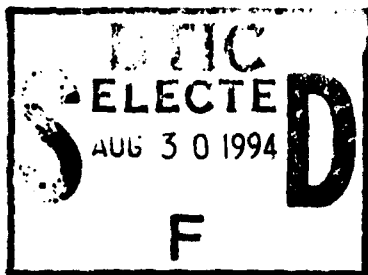
AD-A283 940



1

Georgia Institute of Technology  
and  
Office of Naval Research

# WORKSHOP ON CONDITION BASED MAINTENANCE



This document has been approved  
for public release and sale; its  
distribution is unlimited.

Sheraton-Atlantic Beach  
Atlantic Beach, North Carolina

November 15-17, 1993

DTIC QUALITY ASSURED 1

94-27792



94 8 29 055

**Best  
Available  
Copy**

Georgia Institute of Technology  
and  
Office of Naval Research

# WORKSHOP ON CONDITION BASED MAINTENANCE

Sheraton-Atlantic Beach  
Atlantic Beach, North Carolina

November 15-17, 1993

Accession For	
NTIS CRA&I	<input checked="" type="checkbox"/>
DTIC TAB	<input type="checkbox"/>
Unannounced	<input type="checkbox"/>
Justification	
By	
Distribution /	
Availability Codes	
Dist	Avail and/or Special
A-1	

This document, beginning with an Executive Summary and ending with an Attendance List, contains copies of presentation materials and discussion group reports given at the WORKSHOP ON CONDITION BASED MAINTENANCE. The Agenda serves as a Table of Contents.

## EXECUTIVE SUMMARY

Georgia Institute of Technology  
and  
Office of Naval Research

### WORKSHOP ON CONDITION BASED MAINTENANCE

Sheraton-Atlantic Beach  
Atlantic Beach, N.C.

November 15-17, 1993

The Georgia Institute of Technology conducted a two and one-half day *Workshop on Condition Based Maintenance* at the Sheraton-Atlantic Beach Hotel in Atlantic Beach, N.C. on November 15-17, 1993. The workshop, sponsored by the Office of Naval Research, was held in conjunction with the Materials Engineering Division, Naval Aviation Depot of Cherry Point, N.C., and the Office of Naval Research. Representatives from academia, industry, national laboratories, and military services participated. Ward Winer of the George W. Woodruff School of Mechanical Engineering, Georgia Institute of Technology, and Peter Schmidt of the Chemistry and Materials Division of the Office of Naval Research served as co-chairs of the meeting. The purpose of the workshop was to promote the interchange of ideas and experimental techniques in support of the monitoring of military aircraft, ship, and land-vehicle components.

After a brief introduction and welcome, the first day of the workshop began with keynote addresses outlining the maintenance needs at Cherry Point, and sensor-monitoring requirements associated with component life and performance. This was followed by a tour of the Cherry Point Depot maintenance facilities. Upon return from the afternoon bus trip, breakout groups formed, chartered to discuss research and engineering needs for the implementation of specific monitoring procedures and component life improvements. Four subgroups were created by self-selection in the areas of Maintenance & Engineering, Chemistry & Physics, Sensors, and Signal Analysis.

The second day of the workshop focused attention on specific techniques for the in-situ monitoring of component life and performance, with brief presentations offered by numerous experts. The breakout groups refined the deliberations, and presented summaries to the plenary meeting for further discussion. As a result, four new subgroups formed to address issues related to Critical Equipment Failure and Maintenance, Failure Models, Sensors, and Signal Analysis.

The workshop ended with a morning plenary session. Group reports were presented and discussed. A summary of NADep drive issues concluded the meeting.

This document contains summaries from the breakout group deliberations and presentation materials used by the speakers, whose efforts were truly appreciated. A special thanks goes to ONR's Peter Schmidt and Georgia Tech's Steven Danyluk, Scott Bair, and Richard Cowan, for their "behind the scenes" efforts in making this a successful event.



Ward O. Winer  
Regents' Professor and Director  
Georgia Institute of Technology



**GEORGIA INSTITUTE OF TECHNOLOGY  
AND  
OFFICE OF NAVAL RESEARCH**

**WORKSHOP  
ON  
CONDITIONED BASED MAINTENANCE**

**Sheraton-Atlantic Beach  
Atlantic Beach, NC  
November 15-17, 1993**

**Co-Chair: Ward O. Winer  
Woodruff School of Mechanical Engineering  
Georgia Institute of Technology  
Atlanta, GA 30332-0405  
404/894-3200**

**Peter Schmidt  
Chemistry & Materials Division  
Office of Naval Research  
Arlington, VA 22217-566  
703/696-4362**

**AGENDA**

**Monday, November 15th**

- |                   |   |
|-------------------|---|
| <b>8:30 a.m.</b>  | <b>Ward O. Winer, Chair<br/>Welcome</b>   |
| <b>8:35 a.m.</b>  | <b>Peter Schmidt, ONR<br/>"INTRODUCTION AND OBJECTIVES OF THE WORKSHOP"</b>   |
| <b>8:45 a.m.</b>  | <b>John Cammett, Cherry Point-Navy<br/>"MAINTENANCE NEEDS"</b>  |
| <b>9:15 a.m.</b>  | <b>Don Kover, NSWC - Carderock, Annapolis, MD<br/>"TECHNOLOGY DEVELOPMENT PLAN FOR INTEGRATED MECHANICAL<br/>DIAGNOSTICS"</b> |
| <b>9:45 a.m.</b>  | <b>Paul Howard, Consultant<br/>"AN OVERVIEW OF CONDITIONED BASED MAINTENANCE"</b>   |
| <b>10:15 a.m.</b> | <b>15 Minute Break</b>  |

10:30 a.m. Frederick F. Ling, University of Texas-Austin  
**"COMPREHENSIVE AND CRITICAL LITERATURE REVIEW OF  
IN-SITU MICRO-SENSORS FOR APPLICATION IN MACHINERY  
DIAGNOSTIC"**

11:00 a.m.. Ronald Kadysewski, Vickers-Technology and  
John Reintjes, NRL  
**"OPTICAL DETECTION OF WEAR DEBRIS"**

11:30 a.m. Lunch

12:00 p.m. Bus Leaves For Tour to Cherry Point Maintenance Facilities  
John Cammett, host

5:30 p.m. Return to Hotel

8:00 p.m. Breakout Session Discussion, "What are the Issues?"

Self select in four groups in areas of:

- Maintenance & Engineering  
Chuck Stancil discussion leader
- Chemistry & Physics  
Irwin Singer discussion leader
- Sensors  
Steve Shaffer discussion leader
- Signal Analysis  
Tom McKenna discussion leader

(select a spokesperson to summarize issues and give brief notes on  
issues to Peter Schmidt or Ward Winer by 10:00 p.m.)

**Tuesday - November 16th**

8:30 a.m. Jan Achenbach, Northwestern University  
**"QUANTITATIVE NON-DESTRUCTIVE EVALUATION FOR CONDITIONED  
BASED MAINTENANCE"**

9:00 a.m. S. Ramalingam, University of Minnesota  
**"PEIZO-ELECTRIC SENSORS FOR REAL-TIME CONDITION MONITORING"**

9:30 a.m. Steven Danyluk, Georgia Tech  
**"WEAR AND LUBRICANT DEGRADATION MONITORED BY WORK  
FUNCTION MEASUREMENTS"**

9:50 a.m. Scott Bair, Georgia Tech  
**"SHEAR BANDS IN LUBRICANT FILMS-AN OPTICAL STRESS SENSOR"**

10:05 a.m. Rick Sewersky - Sikorsky Aircraft  
**"SIKORSKY HUM REQUIREMENT"**

10:15 a.m. Break

10:30 a.m. Dor Ben-Amotz, Purdue University  
**"RAMAN SPECTROSCOPY OF MOLECULAR MARKERS"**

10:40 a.m. Roger Barron and Gene Parker, Barron Associates  
**"SIGNAL PROCESSING"**  
 (On-Line Diagnostics and Prognostics for Early Malfunction Alerting and Conditioned Based Maintenance)

10:50 a.m. William Ruff and K.G. Krieder, NIST  
**"THIN-FILM FRICTION AND WEAR SENSORS FOR CONTINUOUS BEARING MONITORING"**

11:10 a.m. Irwin Singer, NRL  
**"SURFACE SCIENCE IN TRIBOLOGY"**

11:20 a.m. Francis Kennedy and Ursula Gibson, Dartmouth College  
**"SURFACE TEMPERATURE MEASUREMENT IN-SITU"**

11:30 a.m. Steve Hsu, NIST  
**"A MECHANO-CHEMICAL MODEL: REACTION TEMPERATURES IN A CONCENTRATED CONTACT"**

11:40 a.m. Bill Nickerson, Penn State University  
**"INITIATIVES IN CONDITIONED BASED MAINTENANCE"**

11:50 a.m. David Board, drme Corporation  
**"STRESS WAVE ANALYSIS"**

Ted Frison, Randle, Inc.  
**"SIGNAL ANALYSIS/SIGNAL PROCESSING"**  
 (Given on tour at Cherry Point Facility)

12:00 p.m. Lunch

1:30 p.m. Presentations from Breakout Session groups of 15 November.

3:30 p.m. Breakout session discussion.  
 Self select in four groups.

5:30 p.m. Dinner

8:00 p.m. Groups meet and prepare preliminary drafts of group reports for 17 November presentation.

**Wednesday - November 17th**

8:30 a.m.      Plenary Session  
Group Reports and Discussion

1. Critical equipment failure/maintenances issues: John Bowen
2. Failure Models: Tribology, LD Wedeven; Structural: Wm. Glaeser
3. Sensors: Steve Shaffer
4. Signal Analysis: Tom McKenna

10:00 a.m.      Billy Morgan, NADep  
**"NADep-DRIVE ISSUES SUMMARY"**

12:00 p.m.      Meeting Adjourned.

Workshop on Conditioned Based Maintenance  
**INTRODUCTION AND OBJECTIVES**

*The Georgia Institute of Technology, the Materials Engineering Division, Naval Aviation Depot, Cherry Point, NC, and The Office of Naval Research held a two and one-half day Workshop on Condition Based Maintenance in November, 1993 at the Sheraton Atlantic Beach Resort at Atlantic Beach, NC.*

*This workshop was supported by ONR.*

**The Issue**

America's military machines--ships, aircraft and land vehicles--are growing old. Many of the aircraft and ships we now rely on, for example, were designed and built twenty and thirty years ago. Unhappily, we can no longer plan to replace these old vehicles with next generation equipment; we must expect our older vehicles to remain in service well into the next century. But older vehicles can present problems of poor performance, inadequate safety, and increasingly expensive maintenance. It is our task to develop a maintenance system that can address these problem areas in older vehicles.

If we want our older equipment to operate safely and efficiently, we need to locate and address problems before they progress to the point of mechanical failure. But incipient failures are hard to locate, and current maintenance systems have only limited capabilities to do so. Current systems rely mainly on *time based inspection*, which requires that parts be inspected at specified intervals, and that they be replaced when deemed unfit for service. The problem with time based inspection is that it often fails to catch incipient failures, with disastrous consequences. An alternative to time based inspection is continuous monitoring of critical components; however, while this approach may be effective, it is also expensive.

These two approaches share one important flaw; they are based on inspection, and maintenance approaches based on inspection simply cannot provide *real time* information about the condition of a mechanical system. If we can collect such information, we can develop a *condition based maintenance* system which will be efficient, practical and safe. This report outlines our thinking about approaches to condition based maintenance, it suggests some avenues of study that researchers could fruitfully pursue, and it outlines some approaches that we could reasonably incorporate into our maintenance programs today.

**Current work**

The Navy has begun to address the need for real time information through an extensive program in mechanical fault diagnosis. The Navy's diagnostic method uses mechanical vibration sensors, which are attached to critical components and whose output is assessed through automated pattern recognition. A model system for helicopter transmissions will soon be tested in actual settings.

The Navy's work with mechanical vibration methods depends, of course, on vibration sensors.

But these sensors have limitations, and vibration may not always be the best indicator of pending mechanical failure. The job of this workshop is to explore other approaches to sensing, and to outline other parameters that may be critical in signalling mechanical failure. To this end, it is important to consider failures initiated by corrosion, to develop means of assessing lubricant degradation and contamination, and to detect surface fatigue and numerous modes of wear.

### **Areas of Study**

In order to make real progress addressing the issue of conditioned based maintenance, we need to address a number of questions:

- \* Do we know the physics and chemistry of the moving interface for metals and of materials subjected to high loads, high temperatures and corrosive environments?
- \* Which state variables--temperature, pressure, composition, electrical and magnetic variables, force--play a role in signalling the onset of a given problem?
- \* How will vibration sensing evolve?
- \* How can sensors be effectively placed on moving components in an oily environment?
- \* How will signal transduction from sensor to operator evolve?
- \* Can neural network analysis become a useful tool in development of our maintenance program?
- \* What other parameters merit consideration?

### **Practical Considerations**

Any study associated with maintenance should first identify critical elements which are bound to fail; these elements should have priority in our studies as they have priority in maintenance. For each critical element, we must consider the mechanism of failure and, if possible, develop a general failure model; this model should guide us in selection of the best mechanical, physical or chemical sensors to detect faults and pending failures. Then we must develop a means to analyze and correlate sensor output in order to provide an operator with reliable information about the state of the system.

Our summary of areas of study may seem to suggest a specific research program, but this sequence need not be followed in lockstep. Nor is it necessary to address all of the above questions before we introduce refinements into existing maintenance programs. We should consider, rather, that work in each of these areas will contribute to our knowledge of the state of the mechanical system in general, and the tribological interface in particular, and that we will all benefit from new understanding of friction, wear and mechanical failure.

P.P. Schmidt, Ph.D.  
Scientific Officer, ONR

## MAINTENANCE NEEDS

- Increased maintenance efforts with limited resources are anticipated at Cherry Point, given the closing of three of six inspection depots. Cherry Point(NC), Jacksonville(FL), and San Diego(CA) survived cuts.
- Cherry Point depot performs inspection and maintenance routines on an assortment of assemblies including jet engines, carrier components, C130 aircraft, and H46 helicopters.
- Standard maintenance and inspection routines at Cherry Point use such non-destructive aids as magnetic particles, ultrasonics, fluorescence, eddy current, and x-rays. The cracks, delamination and/or wear identified are generally attributed to fatigue and corrosion.
- Given the likelihood of failure with aged equipment and the effect of such an occurrence (e.g., loss of life, loss of platform), improved maintenance plans and inspection methods are a necessity. Field sensors are particularly desired.
- To provide the means for understanding what the Cherry Point maintenance facility does and needs, a tour of the depot will be conducted as part of the Workshop on Condition Based Maintenance, the afternoon of 15 November.

# **██████████ Integrated Mechanical Diagnostics**

**Presentation to  
the ONR Workshop on  
Condition Based Maintenance**

**15 - 17 November 1993**

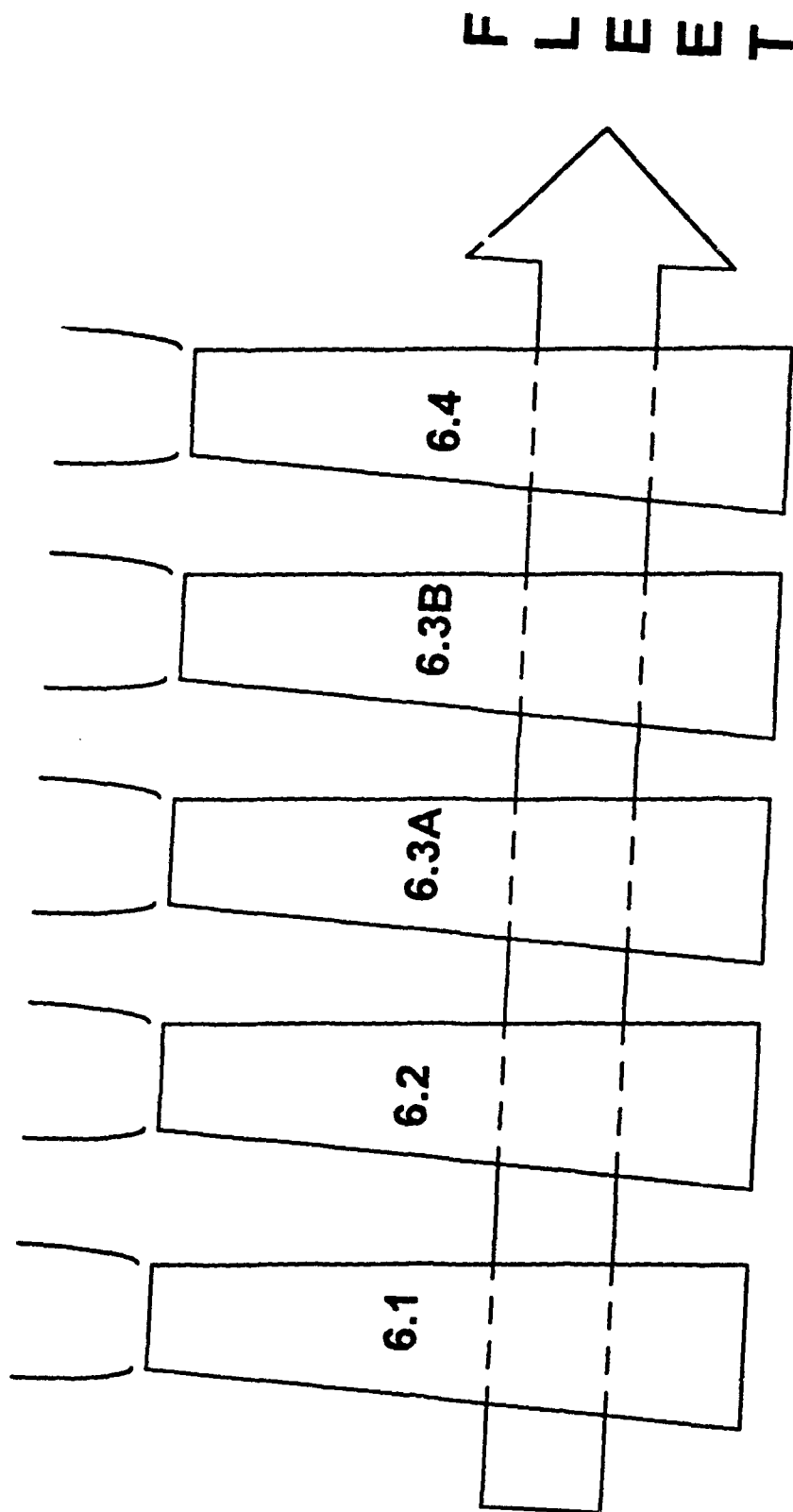
**by**

**Mr. Donald Kover  
CDNSWC Code 825**





# **Connectivity**



# ***The Problem***

- O&S budgets continue to shrink
- Fewer personnel for Maintenance & Repair
- Fleet size will markedly decrease and age
- Current diagnostic tools are inadequate,
- Current maintenance philosophy/infrastructure:  
slow and expensive
- Prognostics are lacking for mechanical systems



# **██████████** *Mechanical Systems Status*

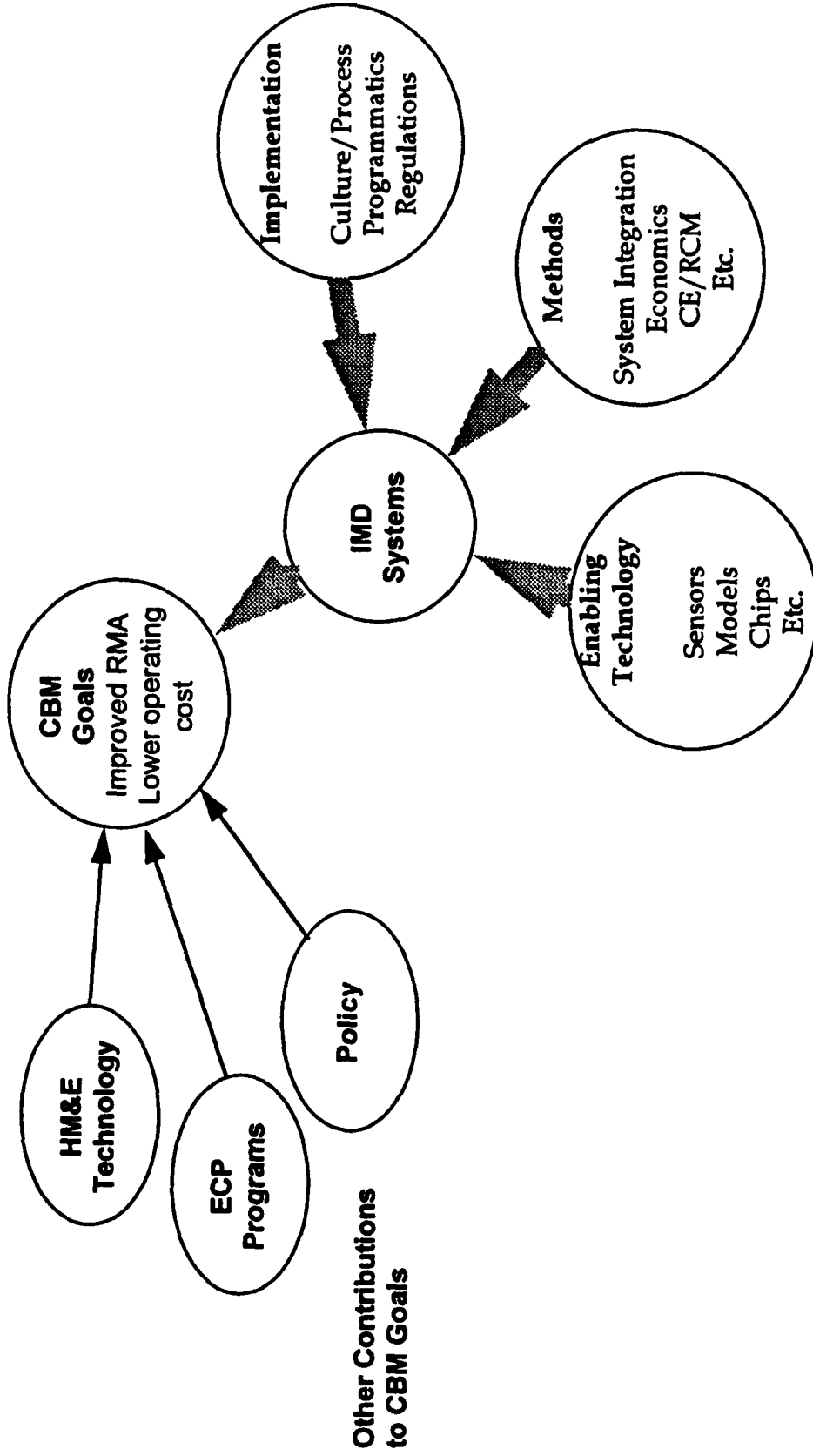
Achieved	Need
<ul style="list-style-type: none"><li>• RCM initiated*</li><li>• CBM initiated*</li><li>• Suboptimal MTBFs</li><li>• Unacceptable MTTRs</li><li>• Some Life warrantees</li><li>• Complexity in M&amp;R</li></ul>	<ul style="list-style-type: none"><li>• Realize RCM via IMD**</li><li>• Make CBM a way of life</li><li>• Merge training and O&amp;S</li><li>• Integrate RCM and CBM</li><li>• Concurrent Engineering</li><li>• Prognostics for IMD</li><li>• Reengineered methods</li><li>• A user friendly system</li></ul>

\* Initiated as policy, without supporting technology

\*\* Integrated Mechanical Diagnostics



# What is CBM and IMD?



# *Key IMD Technologies?*

- Oil Debris Monitoring
- Oil Condition Analysis
- Advanced Vibration Analysis
- Integrated, Multi-Function Sensors
- Advanced Signature Analysis
- Structural Life Usage Monitoring
- Integrated and Integral Sensors



## **What enables IMD?**

- Software development, tools and systems
- Information systems and methodologies
- Economic measures and models
- System integration
- Concurrent Engineering
- Failure & fault modeling
- Diagnostic modeling
- Interactive M&R documentation and training
- Advanced sensors and signal processing



# **████████** *CBM Implementation*

- **IMD technology**
- **Reengineering of Navy Maintenance & Repair infrastructure and processes**
- **A solid and realistic investment strategy**
- **Management and organization**
  - Leadership
  - Responsibility
  - Structure
  - Knowledge
- **A vision of IMD in the Navy**
  - “on-line, on-the-fly diagnostics at the O-level”





# *Advanced Diagnostic Techniques*

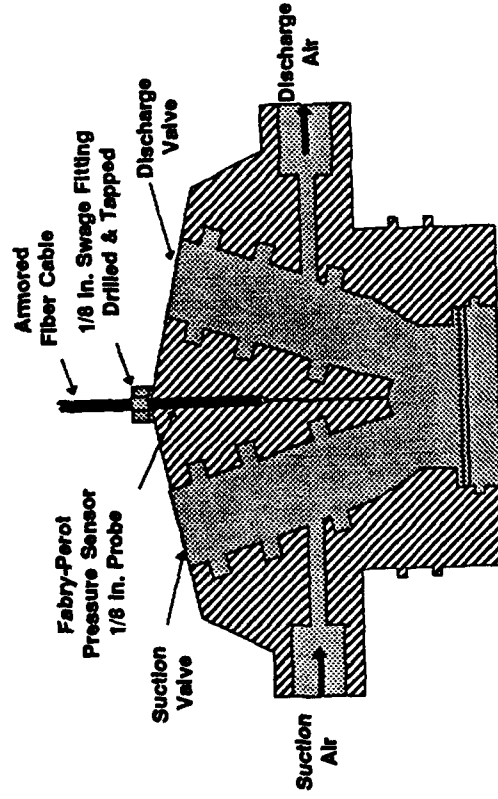
- Sensors for Advanced Mechanical Diagnostics
- Engine Diagnostics Using Exhaust Pattern Recognition
- Analytical Modeling for Mechanical Diagnostics
- Air Vehicle Gearbox Diagnostics
- Rotor System Load Monitoring and Fault Detection
- Optical Oil Debris Sensor



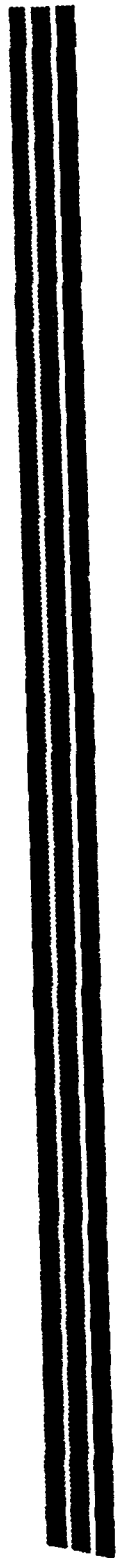
# **Sensors for Advanced Mechanical Diagnostics**

As the number of sensors has increased with advancing control and monitoring systems, the need for advanced sensors has become apparent

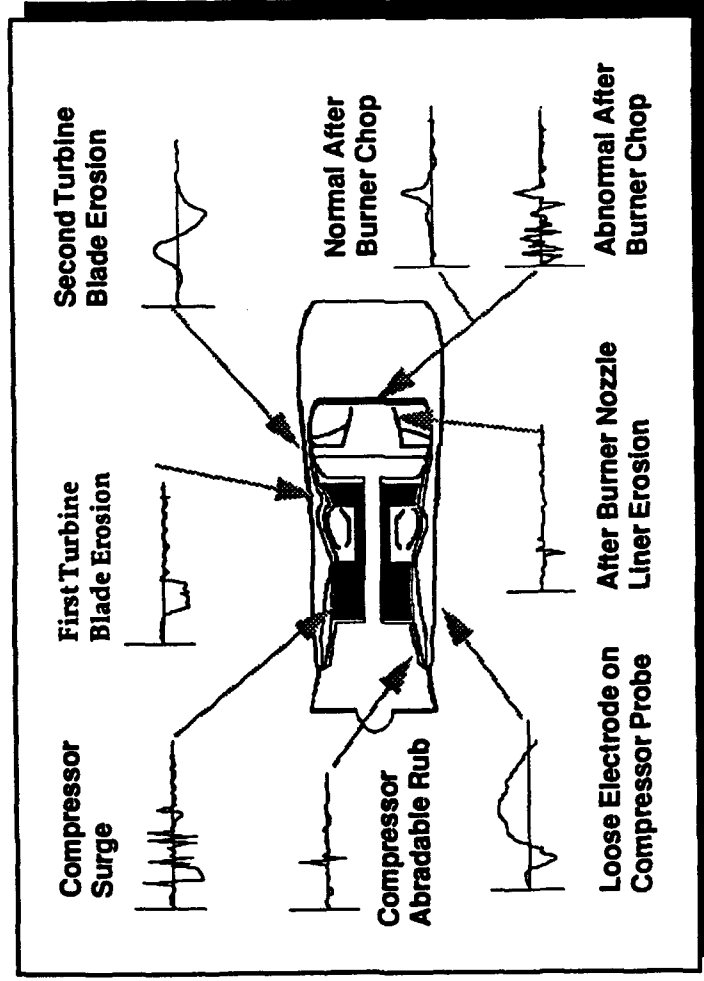
Develop fiber optic sensor technology and embedding techniques.



Cross Section of Third Stage Cylinder Head



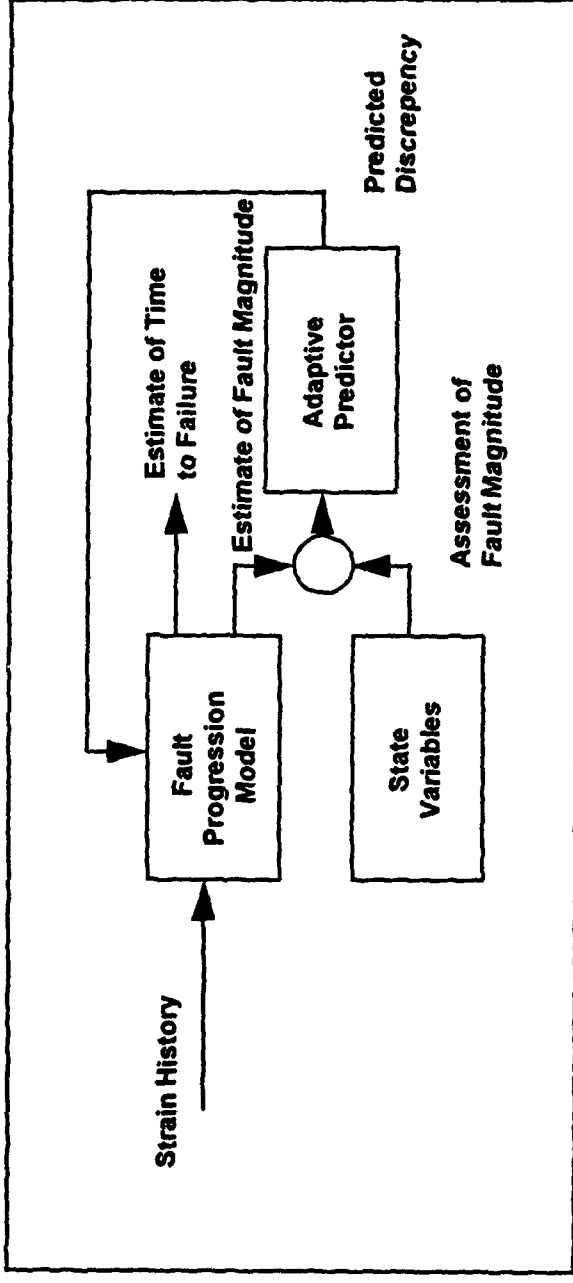
# Engine Diagnostics Using Exhaust Pattern Recognition



Evaluate the capability to  
diagnose engine problems  
from exhaust ion patterns.



# *Analytical Modeling for Mechanical Diagnostics*



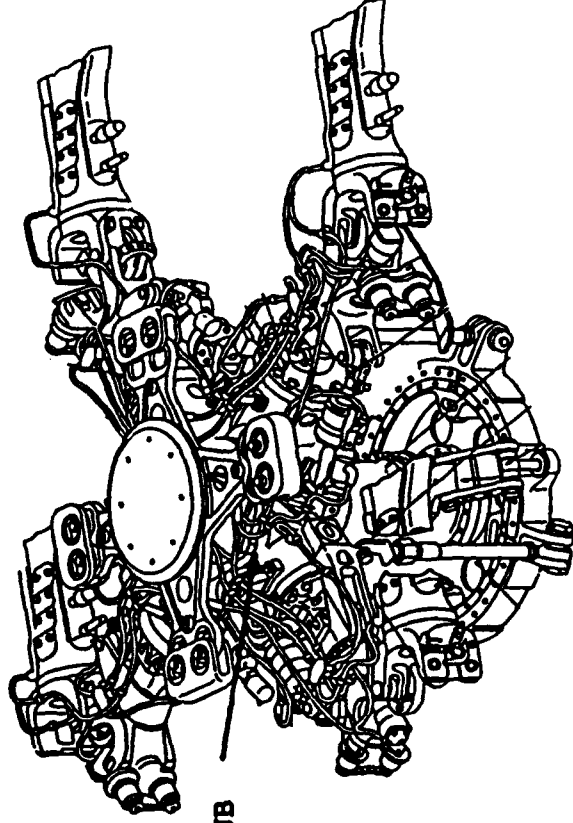
**Identify a multi-dimensional state space where the magnitude of deviation from normal relates to fault severity and the direction of deviation relates to the type of fault.**

# *Air Vehicle Gearbox Diagnostics*

**Demonstrate that advanced time/frequency transforms and neural network classifiers can resolve complex interactions of mechanical components to detect and classify faults near real-time.**



# **██████████** Rotor System Load Monitoring and Fault Detection



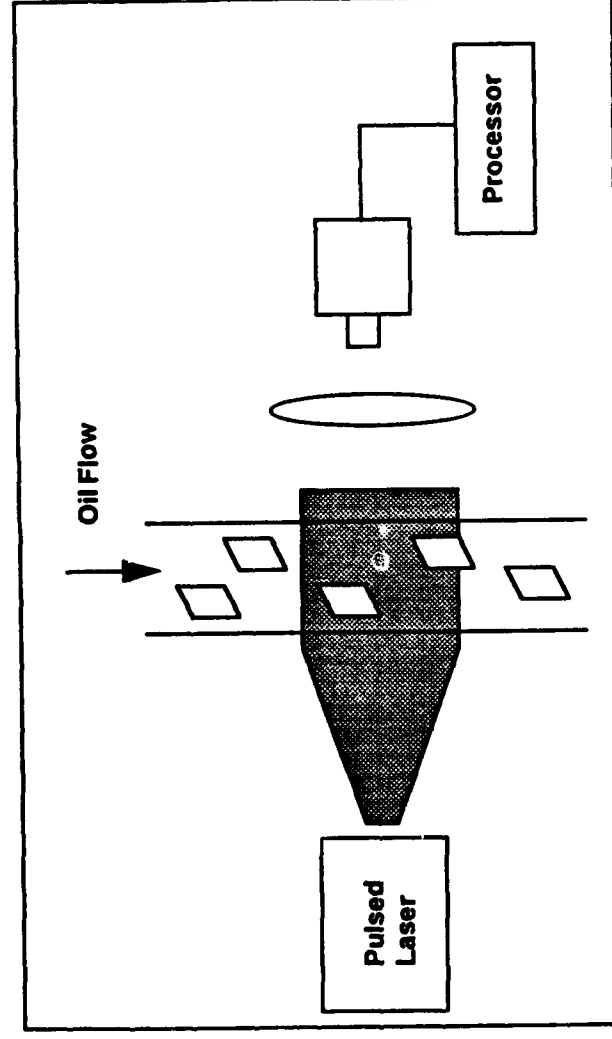
ROTOR HUB

Two approaches are being developed to continuously monitor rotor system health:

- (1) neural net to predict & monitor dynamic loads;
- (2) analytical model to predict structural faults.



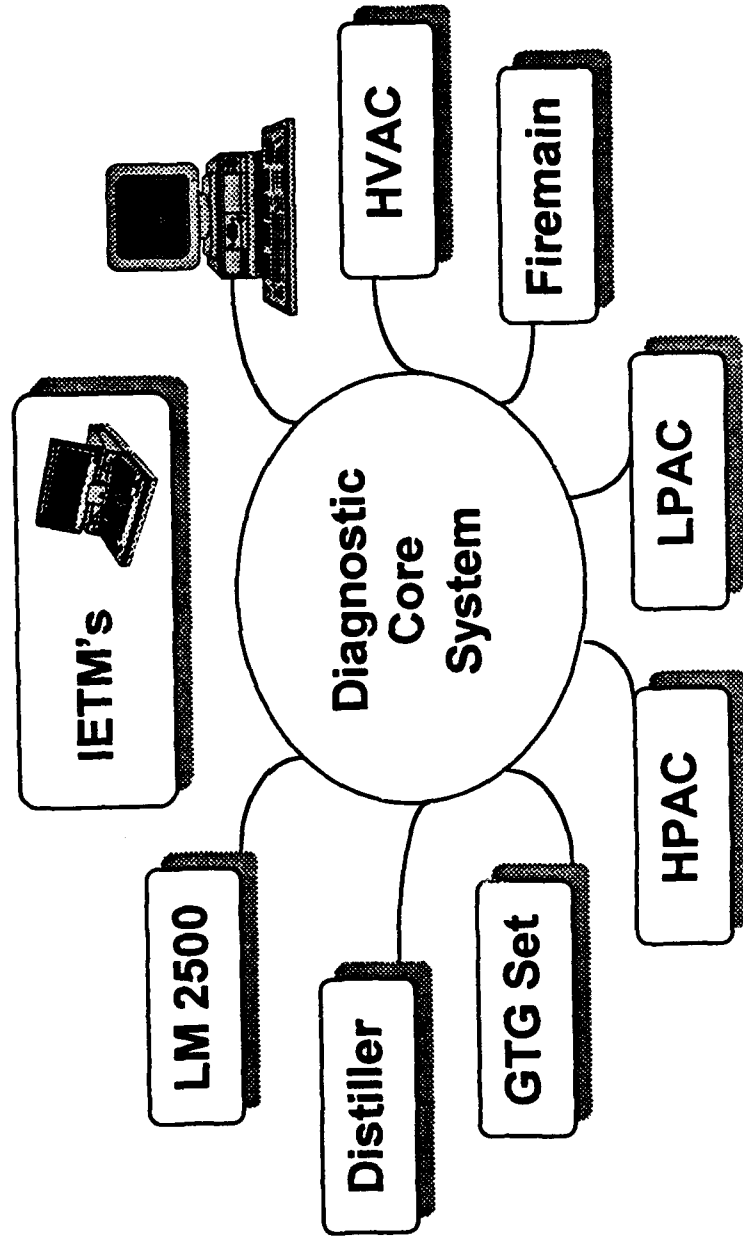
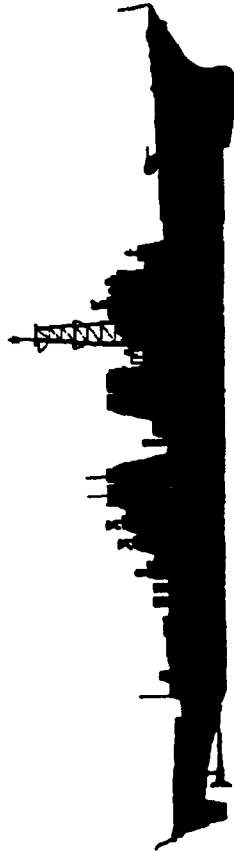
# **Optical Oil Debris Monitoring**



Develop the capability to optically detect and identify metallic and non-metallic wear/failure debris particles in lube oil systems in real-time.

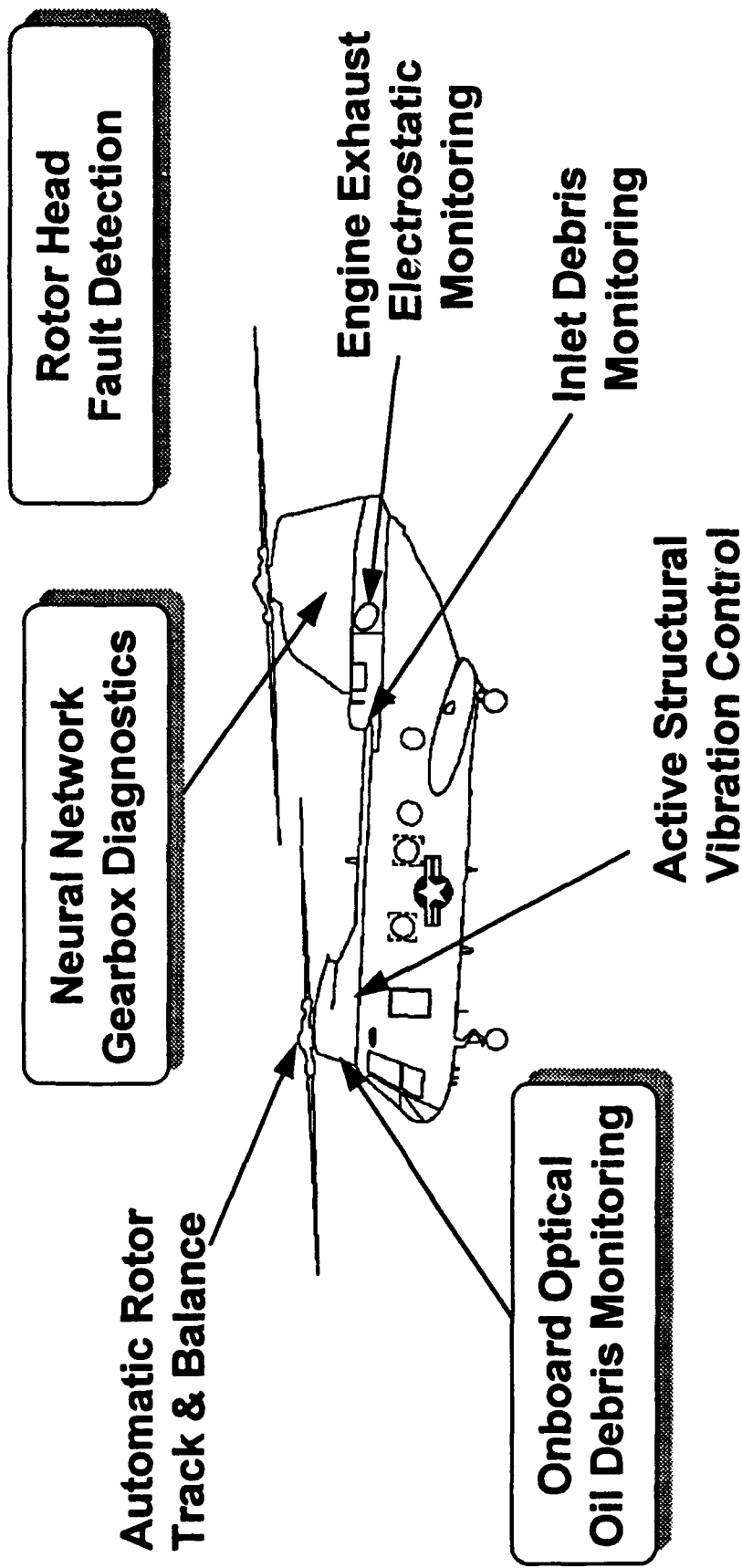


# **Integrated Mechanical Diagnostic Demonstration**





# ***Air Vehicle Diagnostic System***



# *Summary*

- **Current Efforts**
  - Introduce Draft TDP
  - 6.2 Logistics Technology Program
- **Invite Private Industry Participation**
- **Recommend Approach**



# *Approach*

- Machine Testability
- Research for Technology Development
- Interface and Technology Integration Requirements



PAUL L. HOWARD

*Consultant*

*to*

*Government and Industry*

Telephone  
215-692-0152

1212 CLEARBROOK ROAD  
WEST CHESTER, PA 19380

FAX  
215-692-5084

# DIAGNOSTIC TECHNOLOGY TRENDS AND EMERGING TECHNOLOGY

## Briefing

TECHNOLOGY APPLICATION

•

BUSINESS DEVELOPMENT

•

STRATEGIC PLANNING

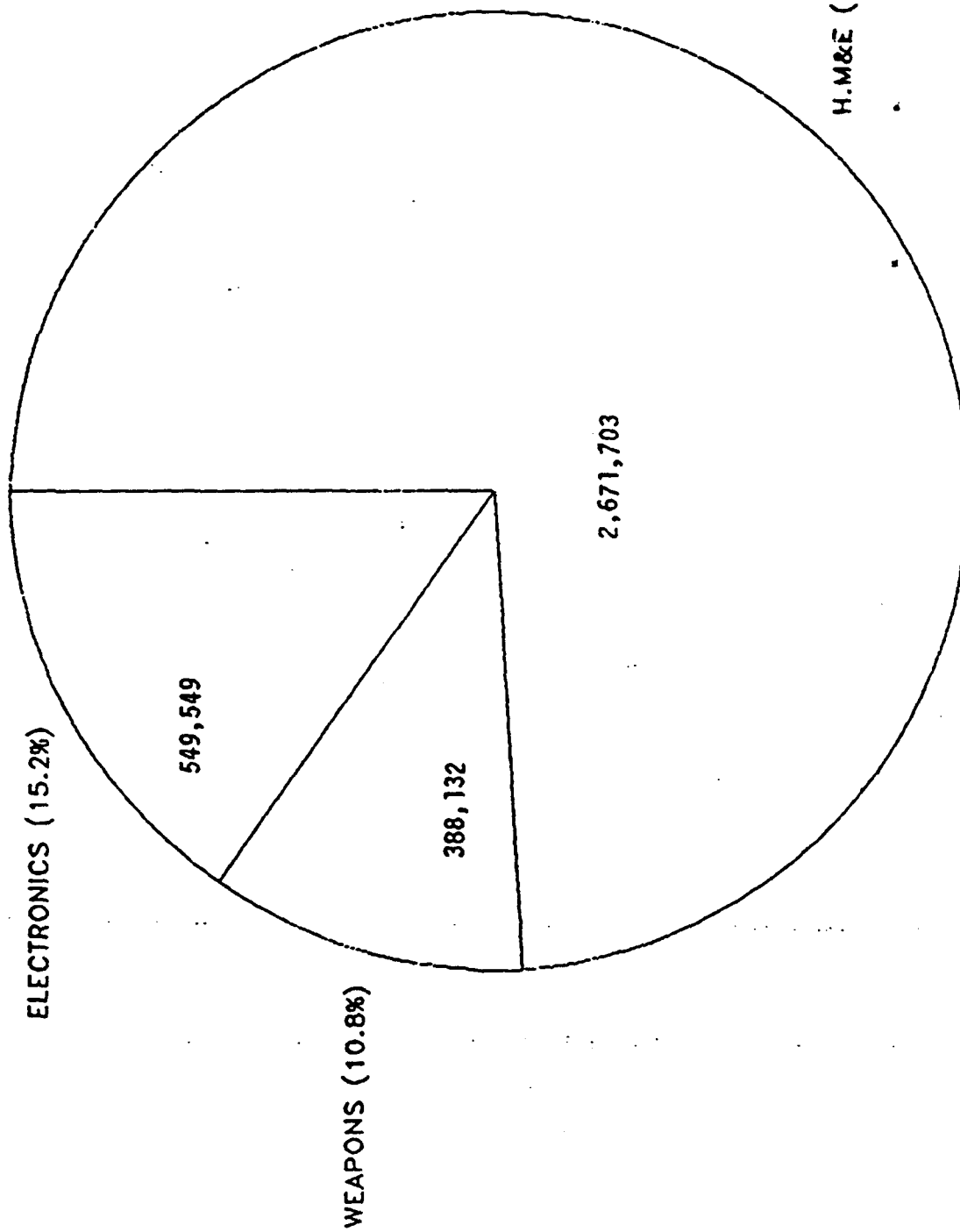
\*\*\*\*\* Paul Howard, "An Overview of Conditioned Based Maintenance" \*\*\*\*\*

SOME KEY ASPECTS  
OF THE  
CURRENT WEAPON SYSTEM  
SUPPORT ENVIRONMENT

- AGING FLEET --- ESPECIALLY HELO
  - INCREASED MAINTENANCE BURDEN
  - ATTRITION -- WEAROUT.
  - NO ASSET REPLACEMENT LINE ITEM
  - FEWER NEW WEAPON SYSTEM STARTS
- SUPPORT ASSETS REDUCED
  - PERSONNEL ROTATION, RIF, SHORTAGES
  - FEWER STAFF, SAME MISSION IN OPERATIONS.
  - HIGHER SPARES COSTS/PRESSURE TO REDUCE USAGE.
- NAVY STRATEGY DIRECTIONS ( HOW TO COPE)
  - EXTEND LIFE OF ASSETS --- SLEP
  - CONSERVE ASSETS --- LOWER MAINT. BURDEN BY  
BETTER DIAGNOSTICS
  - REDUCE SPARES USAGE --- REDUCE FALSE REMOVALS.
  - IMPLEMENT A BALANCED RISK REDUCED TECHNOLOGY  
PROGRAM TO ACHIEVE TBO TO CBM TRANSITION
    - ON-BOARD DIAGNOSTICS
    - MAINTAINERS ASSOCIATES
    - EMBEDDED TRAINING
  - FUNDED FROM CURRENT R&D LINES+CIP
  - RISK ABATEMENT
    - PROVEN TECHNOLOGY
    - TECHNOLOGY DEMONSTRATIONS-- ATD ROUTE
    - TECHNOLOGY DEVELOPMENT -- 6.2, 6.3, IR&D

DD-963 CLASS

MAINTENANCE MANHOURS (1/1/87 - 6/30/89)



## WHAT MUST IT DO?

### MACHINERY MONITORING REQUIREMENTS

- 0 DETECT FAILURE ONSET, DETERMINE SEVERITY AND TRACK PROGRESSION
- 0 MONITOR PERFORMANCE, DETECT DEGRADATION AND TREND
- 0 MEASURE LIFE USAGE OF LIFE-LIMITED PARTS AND TREND
- 0 PROGNOSE FUTURE CONDITION
- 0 AUTOMATED -- REDUCED LABOR INTENSITY
- 0 OPERATE ON-BOARD AUTONOMOUSLY -- ELIMINATE DIAGNOSTIC EXPERT DEPENDENCE.

# VIBRATION TECHNOLOGY



# VIBRATION TECHNOLOGY FRAMEWORK

---

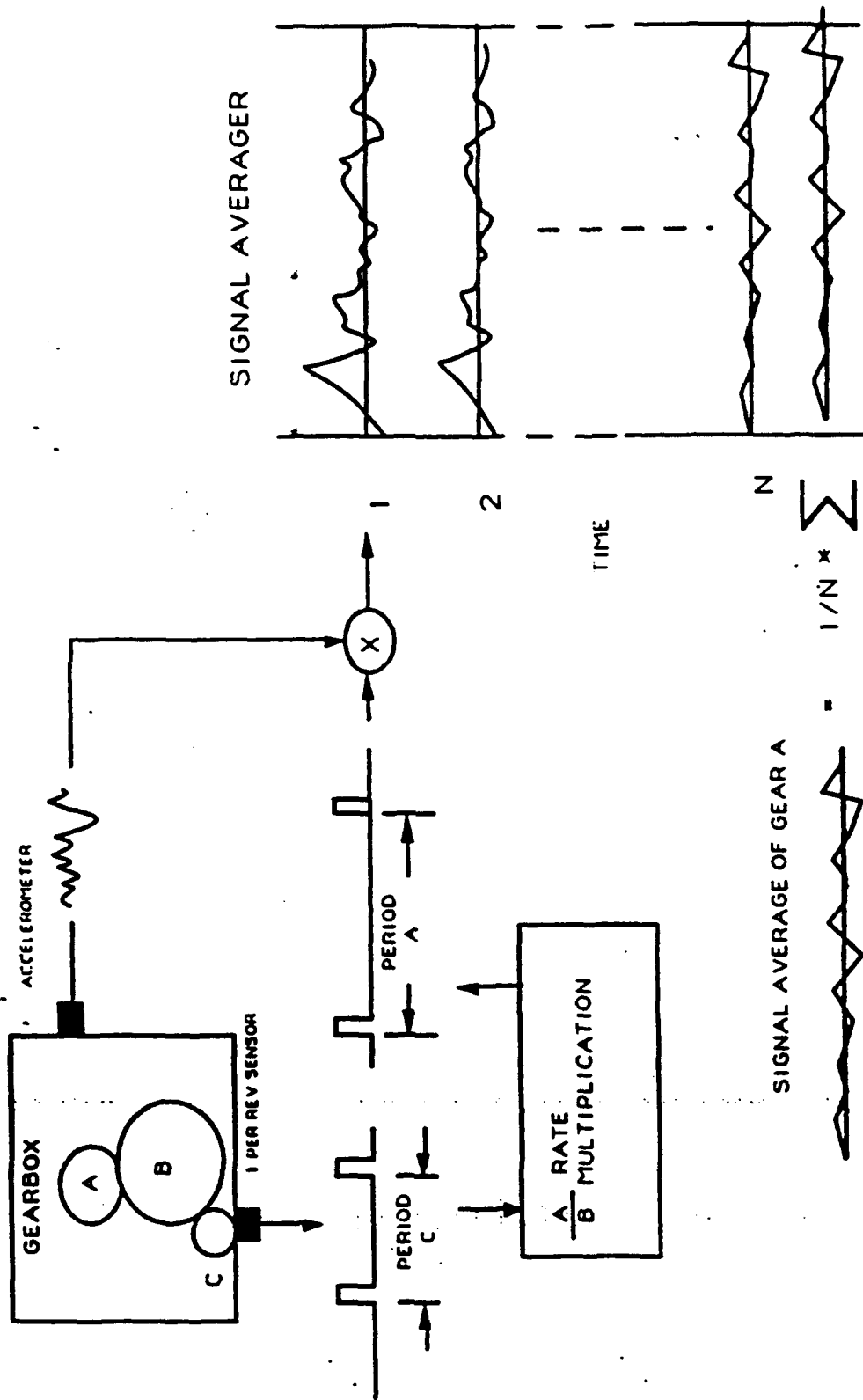
- DIAGNOSTIC FREQUENCY RANGE
  - LOW (<10KHZ)
  - HIGH (10KHZ--50KHZ)
  - ULTRA HIGH (50KHZ--500KHZ)
- ANALYSIS DOMAIN
  - FREQUENCY DOMAIN
  - ORDER DOMAIN
  - TIME DOMAIN
- DIAGNOSTIC TOOL CLASS
  - PATTERNS
  - FEATURES
  - ENERGY/RMS--BROAD/NARROW BAND
- FAULT DIAGNOSTIC BASIS
  - HEURISTIC
  - MODEL BASED
- ANALYSIS MODE
  - MANUAL--OPERATOR INTERPRETATION OF DATA
  - SEMI AUTOMATIC-- OPERATOR INTERPRETATION OF INFORMATION
  - AUTOMATIC
- OPERATIONAL MODE (MEASUREMENT/ANALYSIS)
  - OFF--LINE
  - ON--LINE/OFF--LINE
  - ON--LINE

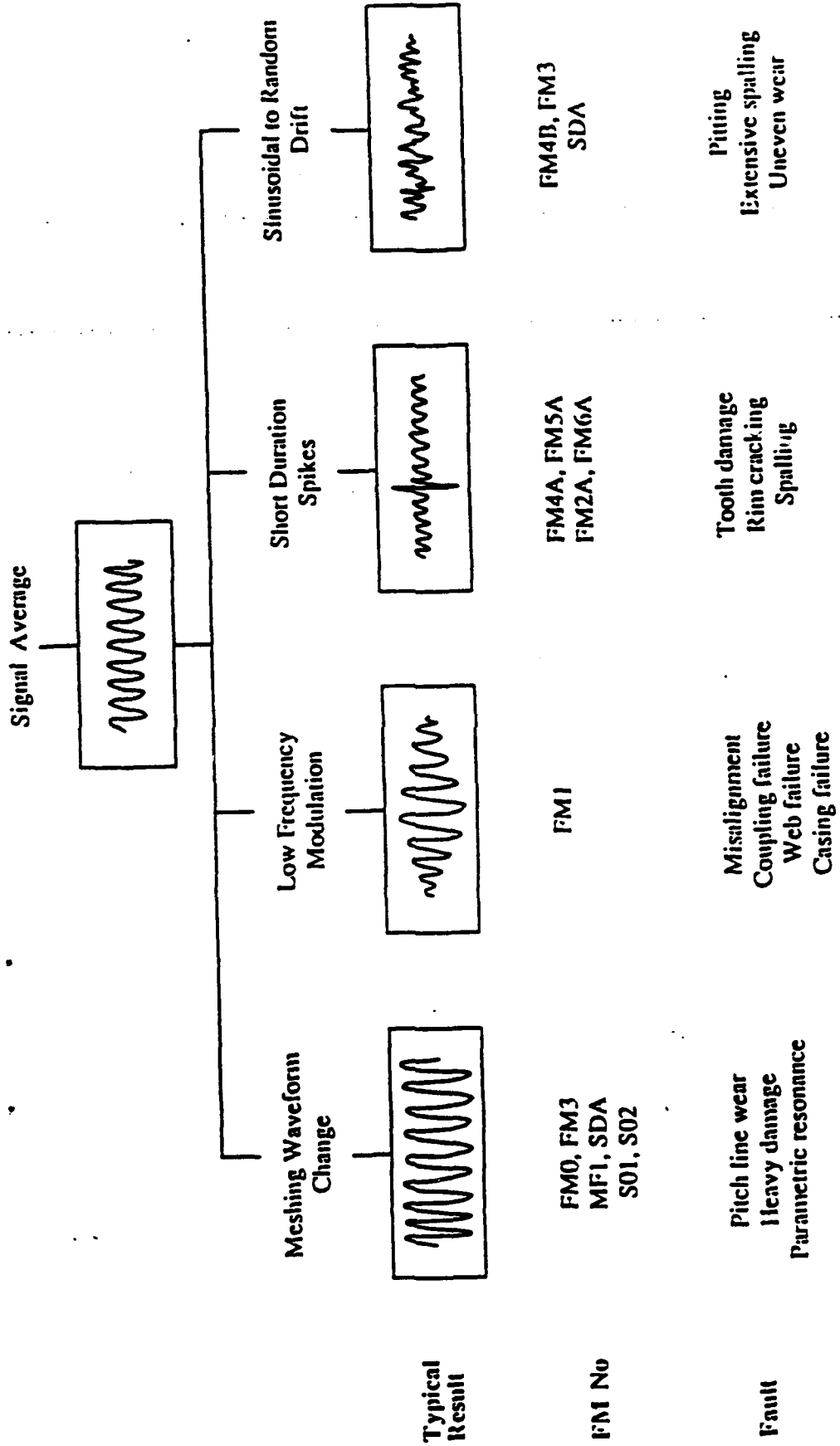
# VIBRATION TECHNOLOGY DIAGNOSTIC REQUIREMENTS

---

- RELIABILITY – SENSORS AND COMPUTATION
- DIAGNOSTIC CLARITY – UNAMBIGUOUS FD/FI
- FALSE ALARM RATE/CONDITIONS
- HIT RATIO
- DIAGNOSTIC SENSITIVITY – MINIMUM DEFECT  
DETECTABLE IN OPERATING ENVIRONMENT
- DETECTION DYNAMIC RANGE – RATIO OF MINIMUM  
DEFECT TO FAILURE DETECTION LEVELS
- SIGNAL/NOISE CAPABILITY
- DIAGNOSTIC LINEARITY – TRENDING AND PROGNOSTICS
- MATURITY
- APPLICATION SENSITIVITY – WIDE/NARROW APPLICATION
- BIT/SELF CALIBRATION

# GEAR BOX SIGNAL AVERAGING DIAGRAM





**OIL AND OIL DEBRIS  
MONITORING TECHNOLOGY**

## LUBRICANT CONDITION MONITORING

- LUBRICANT FAILURE LEADS TO MECHANICAL FAILURE
- PERFORMANCE FACTORS
  - FILM STABILITY – LOAD CAPABILITY
  - CHARACTERISTICS – VISCOSITY, THERMAL
- MONITORING PARAMETERS
  - ADDITIVE PACKAGE DEPLETION
  - TAN – WATER INGESTION
- TECHNOLOGY
  - COBRA – COMPLETE OIL BREAKDOWN RATE ANALYZER
  - RULLER – REMAINING USEFUL LUBRICANT LIFE EVALUATION RIG

## OFF-LINE SAMPLING TECHNIQUES

---

- SOAP (SPECTROGRAPHIC OIL ANALYSIS PROGRAM):

ELEMENTAL ANALYSIS OF A SMALL OIL  
SAMPLE BY ATOMIC EMISSION or ABSORPTION  
TECHNIQUES IN LAB AND PLANESIDE

- FERROGRAPHY:

FERROUS DEBRIS SIZE vs. AMOUNT

- X-RAY BACKSCATTER:

ELEMENTAL ANALYSIS OF OIL SAMPLE or  
DEBRIS DEPOSITS ON FILTER PATCH or  
SEGMENT

- DEBRIS TESTER UNIT:

ANALOG INDUCTIVE MEASUREMENT OF  
FERROUS DEBRIS ACCUMULATION (REMOVED  
FROM IN-LINE MAGNETIC PLUGS)

## REAL-TIME ON-LINE DEBRIS MONITORING TECHNIQUES

---

- DEBRIS MONITORING APPROACHES:
  - DEBRIS CAPTURE TECHNIQUES
    - ADVANTAGES
      - EVIDENCE OF FAILURE RETAINED FOR ANALYSIS
      - DEBRIS REMOVED FROM SYSTEM
    - DISADVANTAGES:
      - PRESSURE DROP vs. CAPTURE EFFICIENCY
      - WEIGHT vs. CAPTURE EFFICIENCY
  - FLOW-THROUGH SENSING:
    - ADVANTAGES
      - LOWER PRESSURE DROP
      - LESS APPLICATION RESTRICTIVE
    - DISADVANTAGES:
      - FLOW DIAMETER TO MINIMUM PARTICLE SIZE RELATION
      - COMPLEXITY vs. SENSITIVITY TO BUBBLES



---

---

# INTEGRATING DIAGNOSTIC TECHNOLOGIES

---

---

# INTEGRATING DIAGNOSTIC TECHNOLOGIES

[VIBRATION – VIBRATION – OIL DEBRIS – STATE VARIABLES]

## GOALS

- IMPROVED FAULT COVERAGE (FD/%)
- REDUCE FAR/IMPROVE HIT
- EXPAND DETECTION DYNAMIC RANGE  
& LINEARITY
- IMPROVED RELIABILITY (BACKUP  
DETECTION MODES)

# Functions

- Forewarn Crew of Catastrophic Failures
- “Watchdog” for Unanticipated Failures in Modified or Aging Aircraft
- Gather Engineering Data for Smart ECP's

## ISSUES

---

- MATURING DIAGNOSTIC TECHNOLOGIES
  - PROGRAMS
  - METRICS
  - FACILITIES
  - RETENTION OF DATA
  - METHODOLOGY
- "CURE IS WORSE THAN THE DISEASE"  
SYNDROME – COMPLEXITY
- BASIC FAILURE MECHANISMS R&D
- TESTABILITY IMPROVEMENT – FIELD  
SYSTEMS
- STRATEGY – DIAGNOSTICS FOR FD/FI  
(FD/FI + GEARBOX ECP)

# POTENTIAL IMPLEMENTATION ROADBLOCKS

- HEURISTIC TECHNIQUE "LEARNING"

DATA BASE SIZE

METRIC VALUE (M.V.)

GEARBOX  
OPERATING  
HOURS

NUMBER OF  
GEARBOXES  
TESTED

BUILD VARIATION

GOOD

GOAL: M.V. FAULT >5X M.V GOOD  
(MINIMUM)

AGING

- SENSOR DYNAMIC RANGE:

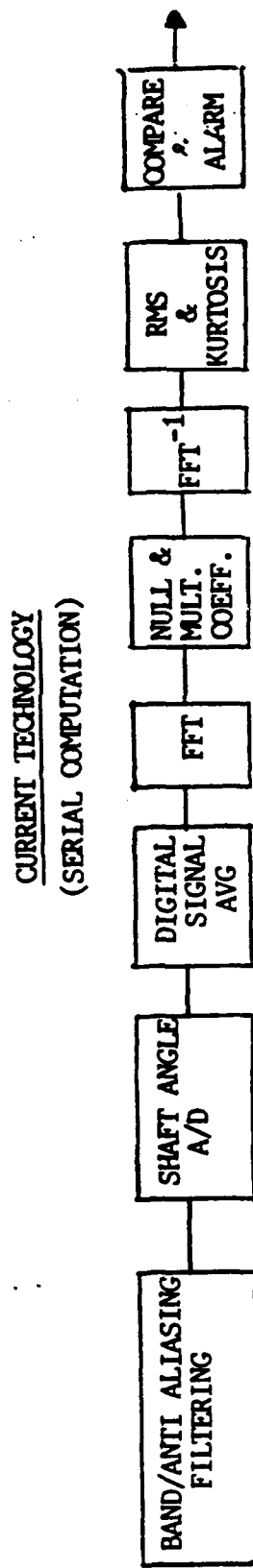
FAULT SIGNAL/TOTAL SIGNAL RATIO

- TECHNIQUE COMPUTATIONAL INTENSITY:

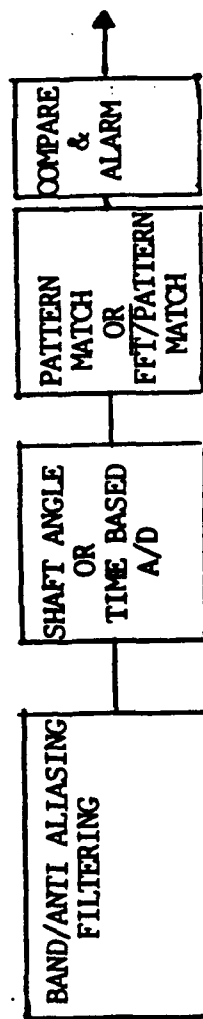
MIPS/FAULT TYPE DETECTION

- DIAGNOSTIC COMPUTER FAILURE RATE  
IS TEN TIMES GEAR FAILURE RATE

FLOW CHART OF  
GEAR FAULT DIAGNOSTICS BY VIBRATION ANALYSIS



"NEXT PLATEAU" TECHNOLOGY  
(PARALLEL COMPUTATION)



IDEAL  
CHARACTERISTICS  
OF THE  
DIAGNOSTIC CHIP

- o INTERNAL / EXTERNAL POWERED
- o INTEGRAL SENSORS --- ACCELERATION, STRAIN, TEMPERATURE, CHEMICAL (POSSIBLE)
- o SIGNAL CONDITIONING FOR EXTERNAL SENSOR INPUTS --- ABOVE PLUS STATE VARIABLES.  
( ANALOG )
- o DATA I/O --- BUSS PLUS TRANSMITTER(FM/FM FORMAT)
- o STACKING ABILITY --- TRANSPUTER EQUIVALENT AS A MINIMUM.
- o REDUNDANT / PARALLEL , HIGH RELIABILITY , HIGH TEMPERATURE ( $> 150^{\circ} \text{C}$  ),  
CHEMICAL RESISTANT

DIAGNOSTIC CHIP  
FUNCTIONS

- o NEURAL NET PATTERN MATCH --- 64 X 64 MINIMUM , 150 PATTERN REPERTIORE.
- o SIGNAL CONDITIONING --- VOLTAGE / CURRENT SOURCES , HIGH INPUT IMPED. ,  
SELECTABLE LO/HI PASS FILTERING, ETC.
- o A / D , D / A EXTERNALLY / INTERNALLY CLOCKED.
- o USE REGIME COMPUTATION AND PROGRAMMABLE LOOK UP TABLES --- LIFE USEAGE.
- o DSP FUNCTIONS --- FFT , PSD ,  $FFT^{-1}$  , KURTOSIS --- SELECTABLE SEQUENCE.
- o LIMIT EXCEEDENCE --- ALARM --- TREND CALCULATION CIRCUITS
- o SERIAL / PARALLEL I/O INCLUDING DSP FUNCTIONS FOR STACKING.
- o INTERNAL POWER GENERATION --- TEMP. OR VIBRATION INDUCED.
- o FM/FM TELEMETRY TRANSMIT MODE.
- o EXTERNAL POWER INPUT / CONDITIONING CAPABILITY.



SOME TYPICAL USES  
OF THE  
DIAGNOSTIC CHIP

- o GEAR BOX FAULT DIAGNOSTICS --- SELF CONTAINED
- o ROTOR HEAD STRUCTURAL FATIGUE DETECTOR --- SELF CONTAINED , SELF POWERED ,  
TRANSMITTING DATA TO AIRFRAME.
- o ELECTRIC MOTOR CURRENT ANALYSER --- FAULT DETECTOR.
- o EMBEDDED / INTEGRAL STRUCTURAL FATIGUE MONITOR --- REGIME RECOGNITION.
- o ENGINE GAS PATH DEBRIS / OIL DEBRIS ANALYSER.

AN INTERIM REPORT

of

OFFICE OF NAVAL RESEARCH PROJECT

under

Contract No. N00014-93-1-0674

COMPREHENSIVE AND CRITICAL LITERATURE REVIEW  
ON IN-SITU MICRO-SENSORS FOR APPLICATION  
IN MACHINERY DIAGNOSTICS

by

Frederick F. Ling

Earnest F. Gloyna Regents Chair in Engineering  
The University of Texas at Austin

THE UNIVERSITY OF TEXAS AT AUSTIN

✓ INTRODUCTION

SELECTED RECORDS FOR INTERIM REPORT

A. GENERAL

SELECTED RECORDS FOR INTERIM REPORT

B. PERTAINING TO MACHINERY CONDITION

TEN EXAMPLES FOR DETAIL DISCUSSION

SOME CONCLUDING REMARKS

# INTRODUCTION

## FILTERS ADOPTED IN THE SEARCH OF LITERATURE

- ONLY THOSE WHICH MIGHT HAVE RELEVANCE, DIRECT OR POTENTIAL, TO MACHINERY CONDITION SENSING ARE INCLUDED.
- ONLY THOSE WHICH MIGHT LEND THEMSELVES TO, PRESENTLY OR POTENTIALLY, FIBER-OPTICAL MODE OF INFORMATION TRANSMISSION ARE INCLUDED.
- DEFERRED IS THE IMPORTANT AND COMPLEMENTARY INFORMATION PROCESSING AND SOFTWARE ENGINEERING LITERATURE.

# **INTRODUCTION - continued**

## **BASES OF LITERATURE**

- **THE UNIVERSITY OF TEXAS AT AUSTIN'S U-SEARCH**
- **THE ENGINEERING INDEX**
- **LIMITED USE OF COMMERCIAL DATA BASES**

## **PERIOD COVERED FOR THE INTERIM REPORT**

- **SYSTEMATIC SEARCH : 1986 - 1993**
- **SELECTED AREAS FOR EARLIER YEARS**

## INTRODUCTION - continued

### CHARACTERISTICS OF THIS INTERIM REPORT

- 23,000 RECORDS HAVE BEEN REVIEWED
- 190 RECORDS HAVE BEEN SELECTED; THESE ARE SHOWN LATER IN THIS REPORT
- THE SELECTED RECORDS ARE SHOWN IN 13 CATEGORIES, MOST OF WHICH ARE FUNCTION-ORIENTED; THERE ARE FEW EXCEPTIONS, e.g., FIBER OPTICS.

## INTRODUCTION

### ✓ SELECTED RECORDS FOR INTERIM REPORT

#### A. GENERAL

### SELECTED RECORDS FOR INTERIM REPORT

#### B. PERTAINING TO MACHINERY CONDITION

### TEN EXAMPLES FOR DETAIL DISCUSSION

### SOME CONCLUDING REMARKS

## SELECTED RECORDS - A. GENERAL

### ACCELEROMETER

- 1993 mechanical resonator monolithically integrated with  
laser diodes on gallium arsenide - *Ukita et al*
- 1992 smart accelerometer with on-chip electronics fabricated by a  
commercial CMOS process - *Riethmuller et al*
- 1992 analysis of twin-mass structure for a piezoresistive accelerometer  
- *Shen et al*
- 1992 piezoresistive acceleration sensor for automotive application -  
*Tsugai et al*
- 1991 fabrication and characterization of silicon micromachined  
threshold accelerometers - *Lobe et al*
- 1991 surface micromachined accelerometer - *Payne*
- 1990 piezoelectric quartz vibrating beam in a digital accelerometer -  
*Meldrum*
- 1987 fiber optics acceleration sensor - *Daneshvar et al*



## ACOUSTIC EMISSION

- 1992 intrinsic optical fibre sensor for detecting acoustic emission -  
*Zheng et al*
- 1991 ultrasonic transducers with piezoelectric polymer foil - *Harnisch et al*
- 1991 general problem of acoustic emission sensors - *Higo and Inaba*
- 1991 piezoceramics and sensor applications - *Petrucci*
- 1990 gear box failure - *Aatola and Leskinen*
- 1990 on-line ultrasonic for bearing wear - *Chann*
- 1990 detecting hydrogen assisted cracking of low alloy steel - *Hayashi*
- 1989 testing of F-111 - *Carlyle*
- 1989 Surface Acoustic Wave (SAW) sensors - *D'Amico and Verona*
- 1989 rolling element bearings - *Hawman and Galinaitis*
- 1989 wear of high speed ceramic insert - *Young and Houghton*

ACOUSTIC EMISSION - continued

- 1988 grinding process - *Sarshevskii*  
1988 incipient bearing failure by noise cancellation - *Tau*  
1988 sensors manufacturing - *Tse and Dornfeld*  
1987 tool fracture by acoustic emission - *Diei and Dornfeld*  
1987 hot tearing in castings - *Ohtaki et al*  
1987 review of acoustic emission in pressure vessels - *Tonolini et al*  
1986 manufacturing process - *Dornfeld*  
1986 in-process detection of grinding cracks - *Eda*  
1986 acoustic emission in the plastic industry - *Fowler*  
1986 status and future of acoustic emission in nuclear reactor systems -  
*Houlton*  
1986 high fidelity transducers - *Proctor*  
1986 in-process tool wear - *Tse*

## ELECTRIC CONTACT RESISTANCE AND CAPACITANCE SENSING

- 1992 Proceedings of EUROSensors V - 69 papers including capacitance-based sensors and many other types - *D'Amico, ed.*
- 1992 controlled selectivity of polysiloxane coatings: their use in capacitance sensors - *Hang et al*
- 1992 micromachined sensor structures with linear capacitive response - *Rosengren et al*
- 1992 capacitive oil deterioration sensor - *Saloka and Meitzler*
- 1987 state of oil film - *Nakashima and Takafuji*
- 1986 gear tool noise - *Atherton*
- 1986 AC impedance measurements of the resistance and capacitance of lubricant film - *Wang et al*
- 1986 new instrument for measuring electric contact resistance - *Watanabe*

## FIBER OPTICS

- 1993 optical sensors, fiber optic sensors - *Goure*
- 1992 Large band-width reflection fiber-optic sensors for turbomachinery rotor blade diagnostics - *Andrenelli and Rossi*
- 1992 Naval fiberoptic system development program - *Blackwell*
- 1992 long-term performance of fiber optic cable plant in Navy ships - *Brown et al*
- 1992 fiber-optic Bragg-grating differential-temperature sensor - *Kersey and Berkoff*
- 1992 evaluation of commercial fiber optic sensors in a marine boiler room - *Musselman*
- 1991 planar fiber optic acoustic sensors - *Lagakes et al*
- 1989 implementation of fibre optics in U.S. Naval combatants - *Johnston and Stewart*
- 1989 fibres are ready made sensors - *Parry*
- 1989 temperature sensors - *Schaefer*
- 1989 using fiberoptics for practical sensing - *Wohstein*

## FIBER OPTICS - continued

- 1988 fiber optic and laser sensors IV - *DePaula, ed. and Udd, ed.*
- 1988 fiber optic displacement sensor for detecting roller bearing condition - *Philips*
- 1987 fiber optic sensors - *Arditty et al*
- 1987 fiber optic sensors, a review - *Jackson*
- 1987 industrial sensors using laser scanning - *Jones*
- 1987 implementation of fiber optic technology in naval combatants - *Morais*
- 1987 fiber optics in machine vision - *Vinarub and Flom*
- 1987 non-contact surface flow detection by fiber optic reflection sensors - *Waegli et al*

## FLUID FLOW AND HEAT TRANSFER

- 1992 optical fiber vortex sensor for flowrate measurements - *Herzog*
- 1992 liquid density sensing by using a photothermal vibration -  
*Inaba*
- 1992 a liquid shear stress sensor fabricated using wafer bonding  
technology for use in fluid environment - *Ng et al*
- 1992 monolithic flow sensor for measuring millilitre per minute  
liquid flow - *Yang and Soeberg*
- 1991 quartz crystal oscillator for under-liquid sensing - *Barnes*
- 1991 optical fiber flowmeter - *Herzog et al*
- 1991 prediction of contact parameters by ultrasonic methods -  
*Krolkowski and Szczepek*
- 1991 small single-sensor for temperature, flow and pressure  
measurement - *Sun and Kamal*
- 1990 microsensors using micromachining: pressure, humidity,  
microviscometers, thermistors, thermocouples and flowmeters -  
*Udell et al*

## PRESSURE SENSING

- 1992 design of monolithic, signal conditioned pressure sensor - *Baslett et al*
- 1992 silicon pressure sensor with integrated bias stabilization and temperature compensation - *Crazzolara et al*
- 1992 comparison between micromachined pressure sensors using quartz or silicon vibrating beams - *Dufour et al*
- 1992 silicon optical pressure sensor - *Dzinban et al*
- 1992 merging micromachining and microelectronics - *Frank*
- 1992 silicon-on-oxide pressure sensor for high temperature - *French et al*
- 1992 fabrication of microdiaphragm pressure sensor using micromachining - *Fujii et al*
- 1992 fiber optic pressure sensor - *Ingold et al*
- 1992 multiplexed piezoelectric polymer tactile sensor - *Kolesar et al*
- 1992 optically excited silicon sensor for downhole pressure monitoring - *Kristeroy et al*
- 1992 smart CMOS capacitive pressure transducers with on-chip calibration capability - *Schnatz et al*
- 1992 optical pressure sensors based on semiconductor quantum wells - *Trzeciakonoski et al*

## PRESSURE SENSING - continued

- 1992 dynamic properties of pressure sensors based on Al GaAs films  
- *Zilionis et al*
- 1991 epitaxial silicon on zirconia (502) pressure sensors - *Chen et al*
- 1991 CMOS circuit for piezoresistive pressure sensor - *Gokkestad et al*
- 1991 surface micro-machine transducers - *Guckert*
- 1991 piezoresistive pressure sensors polycrystalline silicon - *Mosser et al*
- 1991 fiber-optic diaphragm pressure sensor - *Yuan and Qiu*
- 1991 Al GaAs semiconductor pressure sensor - *Zilionis and Stanheric*
- 1990 silicon capacitive pressure transducer - *Artyomov et al*
- 1990 cold silicon piezoresistive strain gauge - *Boyd et al*
- 1990 absolute pressure silicon sensor by air-tight electrical feedthrough structure - *Esashi*
- 1990 piezoresistive low-pressure sensor - *Sandmaier and Kuehl*
- 1989 piezoelectric ceramics for contact pressure measurement - *Oda et al*
- 1983 Raman spectroscopy to measure pressure in elastohydrodynamic lubricating film - *Gardiner et al*



## VIBRATIONS AND WAVES

- 1992 elastic wave sensors-quartz technological channel and silicon technology - *Handen et al*
- 1992 pattern recognition based bicoherence analysis of vibration in bearings - *Li et al*
- 1992 characterization of a new device for pressure sensing - *Lorenzini et al*
- 1992 simple fibre optic sensor for measuring vibration frequency - *Philip et al*
- 1992 correlating vibration measurement and tool wear in turning - *Sokolowski et al*
- 1990 rolling element bearing failure detection by changes in vibration response - *Reif and Lai*
- 1988 bearing behavior by statistical analysis of vibrations - *Gudonavicius et al*
- 1988 bearing condition by vibration analysis - *Mathew and Sefredson*
- 1988 time domain analysis of vibration in bearing behavior - *Springer*
- 1987 defects of power bearing by frequency spectrum - *Ivanov*
- 1987 machinery damage - *Kuoppala and Kuusisto*
- 1987 inspection of gear box by laser vibration measurement - *Watts et al*
- 1986 non-contact surface vibration analysis using a monomode fibre interferometer incorporating an open air path - *Lewin et al*

INTRODUCTION

SELECTED RECORDS FOR INTERIM REPORT

A. GENERAL

✓ SELECTED RECORDS FOR INTERIM REPORT

B. PERTAINING TO MACHINERY CONDITION

TEN EXAMPLES FOR DETAIL DISCUSSION

SOME CONCLUDING REMARKS

## CHEMICAL SENSING

- 1993 fiber-optic photothermal interferometric sensor: a novel technique for chemical measurements - *Balconi et al*
- 1993 micromachined miniature capillary electrophoresis-based chemical analysis system on a chip - *Harrison*
- 1992 mechanical resonance gas sensors with piezoelectric excitation and detection using PVDF polymer foils - *Bloch et al*
- 1992 optical and piezoelectric analysis of polymer films for chemical sensor characterization - *Bowman et al*
- 1992 Proceedings of EUROSENSORS V - 56 articles on mostly chemical and biochemical sensors - *D'Amico, ed.*
- 1992 Proceedings of EUROSENSORS V - 89 papers on chemical and electrochemical sensors - *D'Amico ed.*
- 1992 optical chemical sensor based on surface plasma on interrogation - *De Maria and Martinelli*
- 1992 gas sensor system with dielectric and mass sensors - *Endres et al*

## CHEMICAL SENSING - continued

- 1992 selective detection of organic molecules with polymers and supramolecular compounds - *Schierbaum et al*
- 1992 application specific design of a piezoelectric chemosensor array - *Schmantz*
- 1992 silicon integrated miniature chemical analysis system - *Van der Schoot et al*
- 1991 diffusion of extreme pressure-antiwear additives in oil by holographic interferometry - *Dudler et al*
- 1991 calorimeter gas sensor - *Miuro et al*
- 1990 piezoelectric resonator for - *Maramatsu et al*
- 1987 oxidative stability of lubricants by chemical luminescence - *Benor and Murray*
- 1986 chemical analysis with fibre optics - *Krohn*
- 1986 sensing chemicals with optical fibres - *Narayan and Swamy*
- 1979 emission microspectrophotometer for surface analysis in lubrication - *Lauer and King*

## DISPLACEMENT, STRAIN AND FILM THICKNESS SENSING

- 1993 Bragg grating-timed fiber laser strain sensor system - *Melle et al*
- 1992 real-time holographic interferometry through fibre optics - *Dudderar and Gilbert*
- 1992 non-contact absolute position measurement using a compact disc player optical pick-up - *During et al*
- 1992 a high precision, six degree-of-freedom single-sided noncontact, optical sensor suitable for assembly automation - *Mancevski et al*
- 1992 fiber optic sensors focus on smart systems, e.g., all-fiber, intrinsic Fabry-Pecot strain sensors - *Measures and Liu*
- 1992 polycromatic birefringence sensing for optical fibre monitoring of surface strain - *Murphy and Jones*
- 1992 silicon subminiature microphone based on piezoresistive polysilicon strain gauges - *Schellin and Hess*

## DISPLACEMENT, STRAIN AND FILM THICKNESS SENSING

- continued

- 1991 oil film thickness between piston ring-cylinder by laser  
fluorescence - *Lux and Hoult*
- 1991 three-dimensional position determination - *Nashman and  
Karen*
- 1991 R-C oscillation technique for measuring oil film thickness in  
elastohydrodynamic lubrication - *Zhang et al*
- 1991 simple capacitive displacement sensor - *Zhu et al*
- 1990 angular displacement by intensity of reflected light  
measurement - *Partaatmadja et al*
- 1990 strain field in sliding contacts by laser speckle and  
metallographic techniques - *Seif et al*
- 1988 fiber optic lever displacement transducers - *Kissinger*
- 1982 laser interferometer for air bearing separation measurement -  
*Nigam*

## FORCE AND FORCE-RELATED SENSING

- 1992 Proceedings of EUROSENSORS V - 45 papers on various physical sensors including three for force measurements - *D'Amico, ed.*
- 1992 new tactile sensor like the human hand and its application - *Omata and Terunuma*
- 1992 tactile imaging; review of design problems and the state-of-art of tactile sensing - *Regtieu*
- 1992 non-contacting torque measurement by a modified moire-fringe method - *Spoencer et al*
- 1992 capacitive tactile sensor for shear and normal force measurements - *Zhu and Spronck*
- 1991 dynamometrical sensors - *Bethe*
- 1991 silon on sapphire strain gauge sensors - *Stuchebrukov*
- 1991 piezoelectrically driven silicon beam force sensor - *Van Mullen*
- 1989 fiber optic torquemeter design and development - *Rudd et al.*
- 1987 fiber optic sensor sensitive to normal pressure and shear stress - *Cuomo et al*

## LUBRICANT CONDITION CHARACTERIZATION

- 1992 measuring engine oil film, using fiber optics and laser induced fluorescence - *Richardson and Borman*
- 1992 fluorescent sensor as an engine oil quality indicator - *Vinas et al*
- 1991 in-lubro of elastohydrodynamic lubrication contracts by FTIR adsorption spectroscopy - *Caun and Spikes*
- 1991 in-situ electro-charging for friction reduction and wear resistant film formation - *Tung and Wang*
- 1990 analysis of lubricant oxidation products by digital imaging processing techniques - *Schilowitz et al*
- 1989 shear in elastohydrodynamic contacts - *Caun and Spikes*
- 1987 in-situ SEM study of boundary lubricated contacts - *Holzhauser and Ling*
- 1987 coolant contamination of lubricating oil using radioisotope
- 1985 advanced mass spectrometry - *Campana and Freas*



## SURFACE TEMPERATURE SENSING

- 1993 quartz crystal socillator used as temperature sensor - *Azcondo and Peire*
- 1992 wavelength-demultiplexed fiber-optic temperature measurement instrument - *Andrew et al*
- 1992 pure and calcium-modified lead titanate ceramics for pyroelectric sensors de Frutos and Jiminez
- 1992 high speed sensitive thermovoltaic IR detectors - *Marchetti and Simili*
- 1992 all-fibre optically addressed silicon microresonator sensor for pressure and temperature measurements - *Rao et al*
- 1992 thin film thermocouple for contact temperature measurement - *Tian et al*
- 1992 effect of process parameter variation on polysilicon temperature transducer characteristics - *Zucker et al*
- 1991 in-process workpiece temperature - *Cogdell*
- 1989 thin film thermopile detector - *Hamel*
- 1989 fibre-optic and quartz sensors - *Schaefer*
- 1988 infrared technique in EHD contacts - *Hou*
- 1988 bearing defects by pattern recognition analysis of vibrations - *Li*
- 1986 temperature measurement in subsurface layer - *Ko*

## WEAR AND BEARING DAMAGE SENSING

- 1992 ferrographic analysis of failure process in journal bearing -  
*Akagaki and Kato*
- 1992 dynamic wear tests in the SEM - *Calabrese et al*
- 1992 initial fault detection of a tapered roller bearing - *Su and Lin*
- 1991 adhesive and abrasive wear - *Boness and McBride*
- 1991 wear processes by acoustic emission - *Hanchi and Klawecki*
- 1991 automated image analysis for study of wear particles in oil-lubricated systems - *Uedelhoven and Guttenberger*
- 1990 in-situ friction and wear measurement in integrated polysilicon mechanisms - *Gabriel et al*
- 1990 high-speed ellipsometer for on-line wear of recording media - *Nunnelley et al*
- 1990 on-line tool wear sensing by pneumatic sensor - *Sanjanwala et al*

WEAR AND BEARING DAMAGE SENSING - continued

- 1988 antifriction bearing fault detection - *Burgess*
- 1988 complete oil breakdown rate analyzer (COBRA) and quantitative debris monitor (QDM) - *Centers and Price*
- 1988 Quantimet in thin-film lubrication wear and galling of aircraft fuel pump shafts and gears by surface activation techniques - *Gallmann et al*
- 1988 on-line severity assessment of bearing damage - *Li and Wu*
- 1988 in-situ friction/wear/electrical contact resistance in scanning Auger microprobe - *Pope and Peebles*
- 1987 machinery faults - *Lim*
- 1987 ferrography in conjunction with - *Roylance and Vaughan*
- 1986 process on the basis of wear particles - *Barwell*
- 1972 wear particles in lubricating oils - *Seifert and Westcott*

**INTRODUCTION**

**SELECTED RECORDS FOR INTERIM REPORT**

**A. GENERAL**

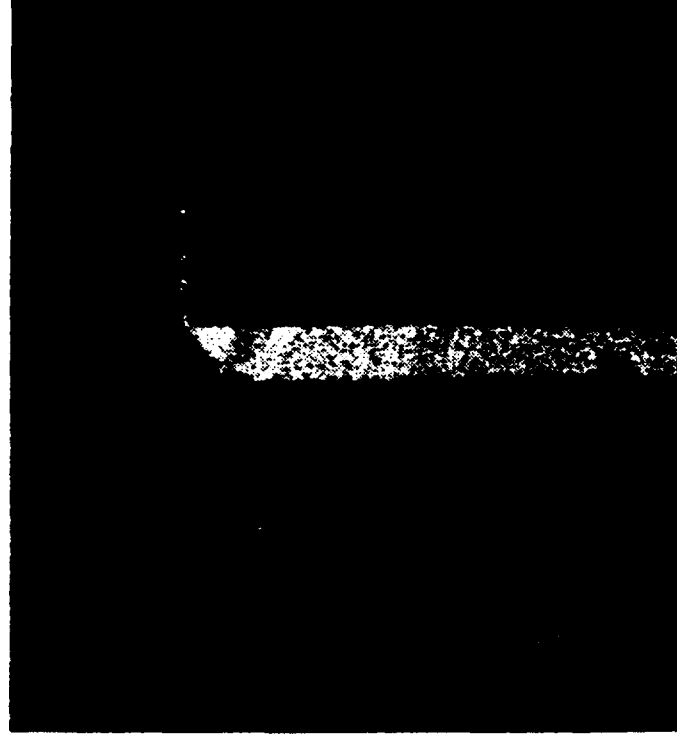
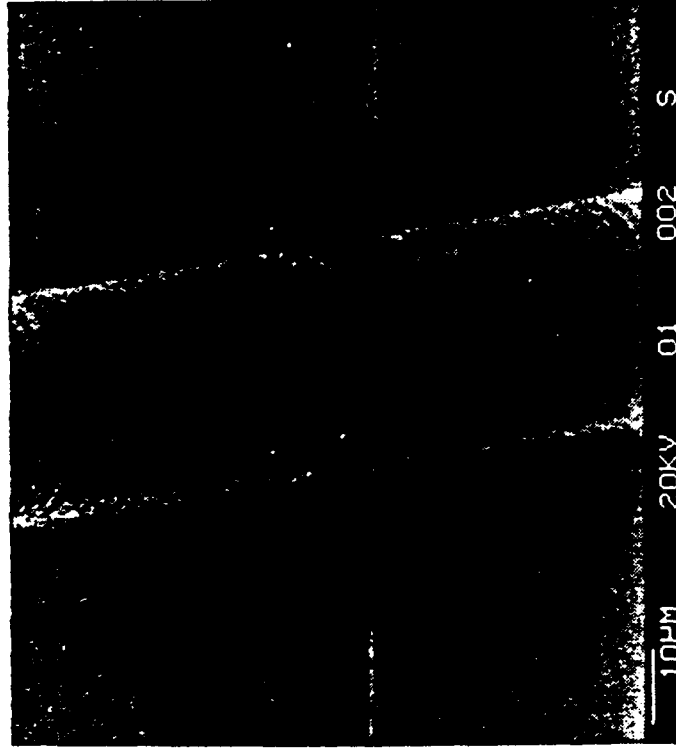
**SELECTED RECORDS FOR INTERIM REPORT**

**B. PERTAINING TO MACHINERY CONDITION**

✓ TEN EXAMPLES FOR DETAIL DISCUSSION

**SOME CONCLUDING REMARKS**

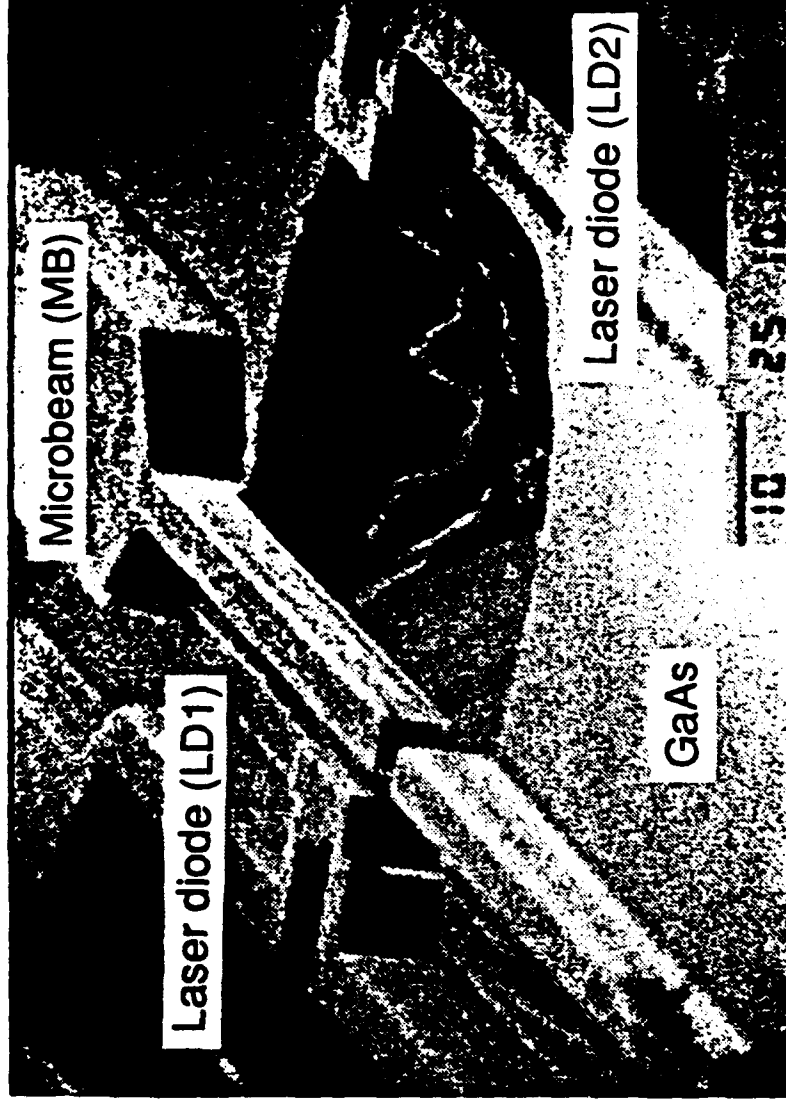
Harrison et al (1993): MICROMACHINING A MINIATURE ZED CAPILLARY  
ELECTROPHORESIS-BASED CHEMICAL ANALYSIS  
SYSTEM ON A CHIP



THE UNIVERSITY OF TEXAS AT AUSTIN

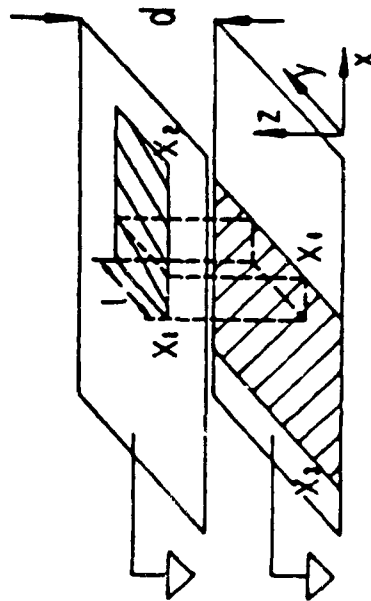
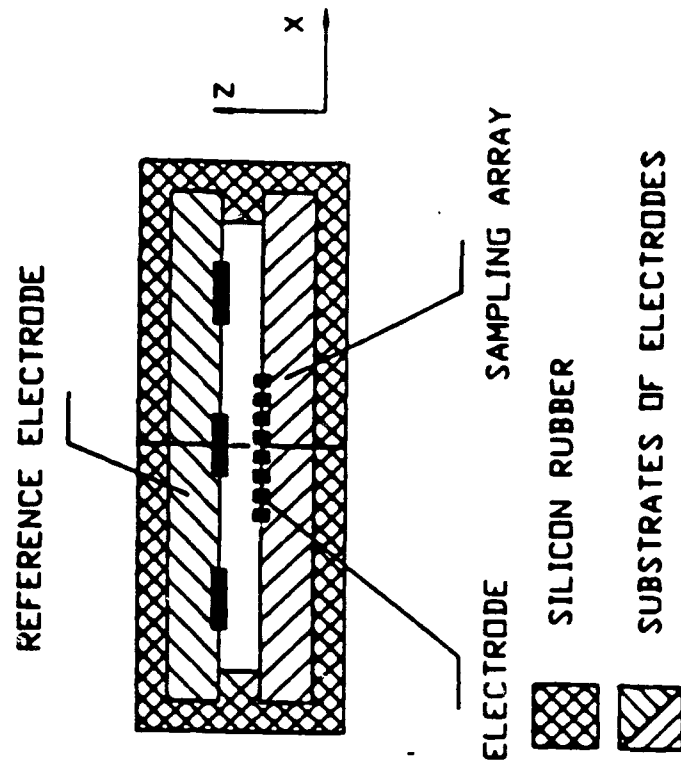
Ukita et al (1993):

MECHANICAL RESONATOR MONOLITHICALLY  
INTEGRATED WITH LASER DIODES ON GaAs



Zhu and Spronck (1992):

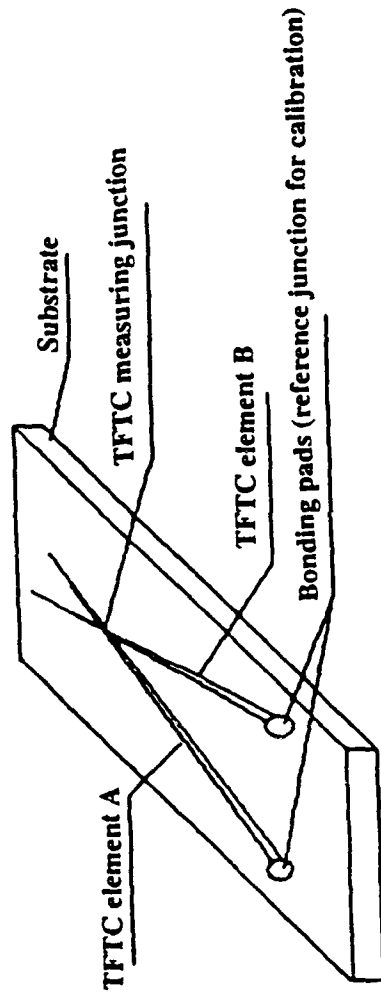
CAPACITIVE TACTILE SENSOR FOR SHFAR  
AND NORMAL FORCE MEASUREMENT



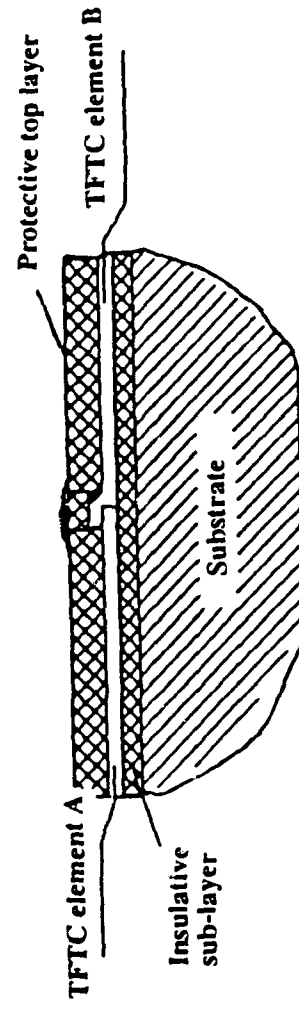
THE UNIVERSITY OF TEXAS AT AUSTIN

Tian et al (1993):

# THIN FILM THERMOCOUPLES FOR CONTACT TEMPERATURE MEASUREMENT



(a)—Schematic diagram of thin film thermocouple.



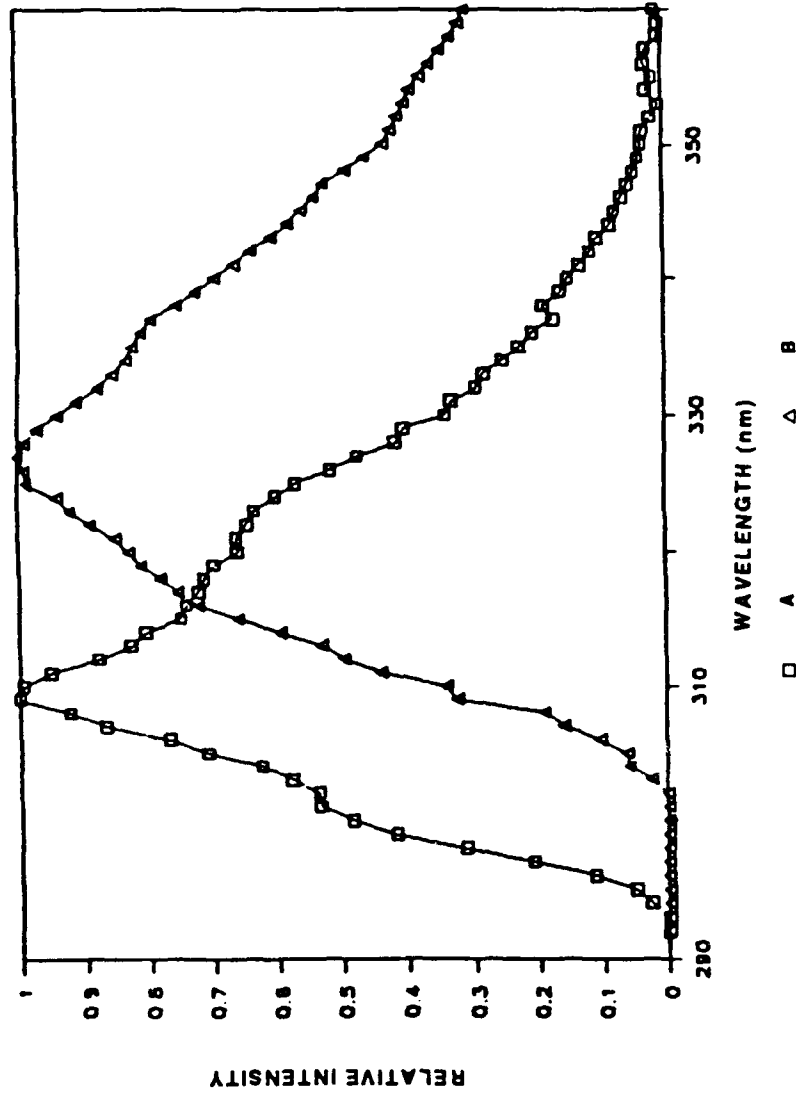
(b)—Schematic cross-section of thin film thermocouple.



Vinas et al (1992):

FLUORESCENT SENSOR AS AN ENGINE OIL  
QUALITY INDICATOR

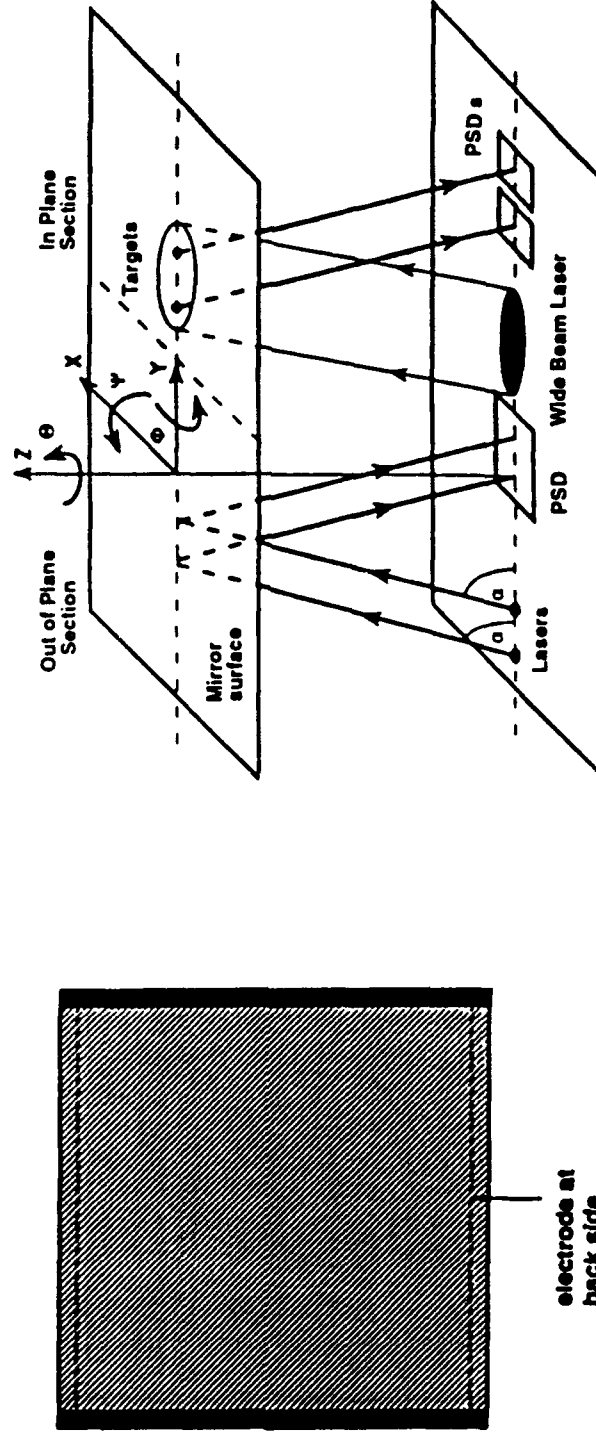
$$\Delta E = -\frac{2}{a^3} f(D, n) \bar{\mu}_i \bullet \bar{\mu}_i, -\frac{1}{a^3} g(n) \bar{\mu}_i \bullet \bar{\mu}_i, -\frac{4\pi\rho\alpha}{3a^3} \bar{\mu}_o \bullet \bar{\mu}_o + D$$



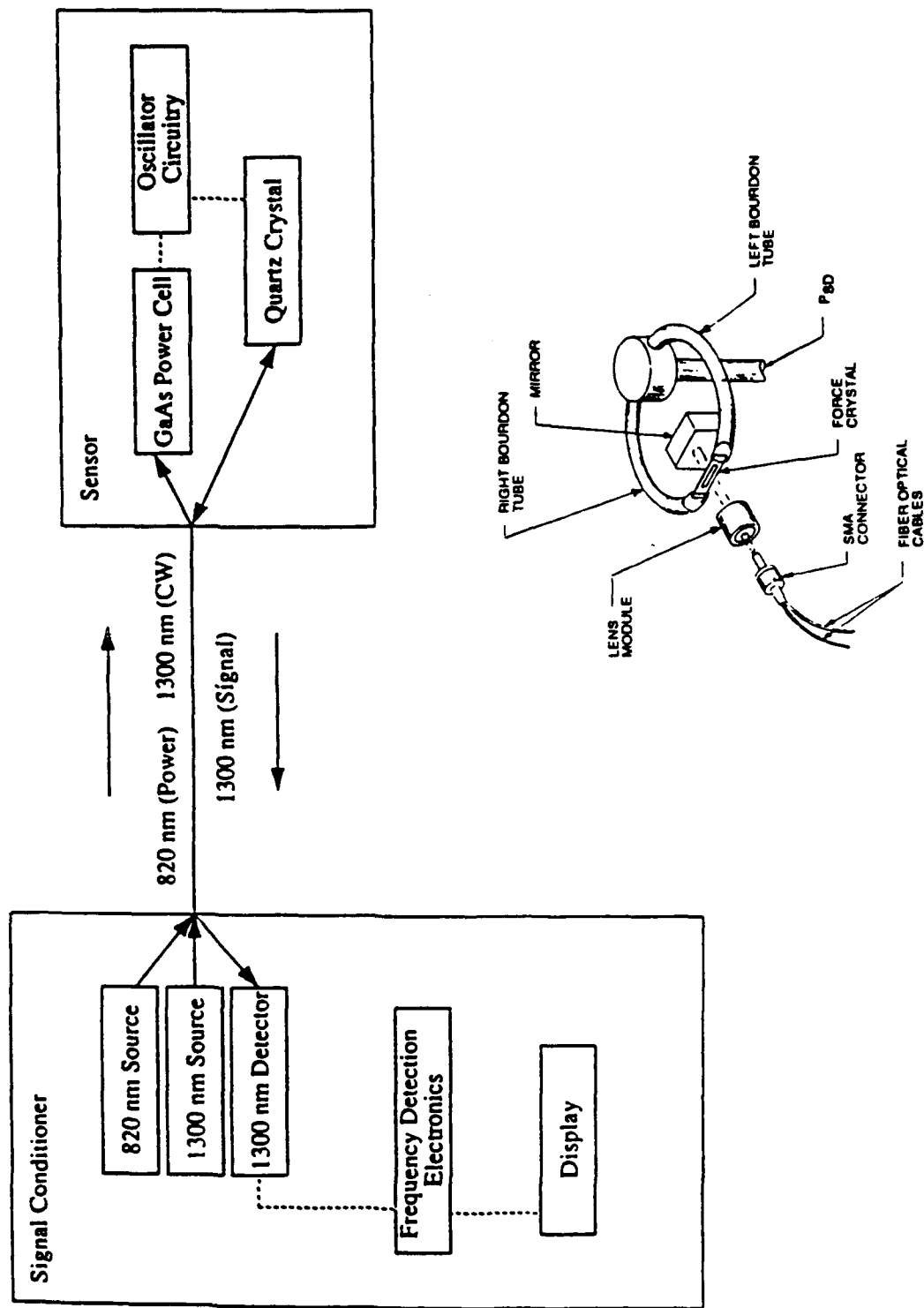
THE UNIVERSITY OF TEXAS AT AUSTIN

Mancevski et al (1993):

HIGH PRECISION, SIX DEGREE-OF-FREEDOM,  
NONCONTACT, OPTICAL SENSOR



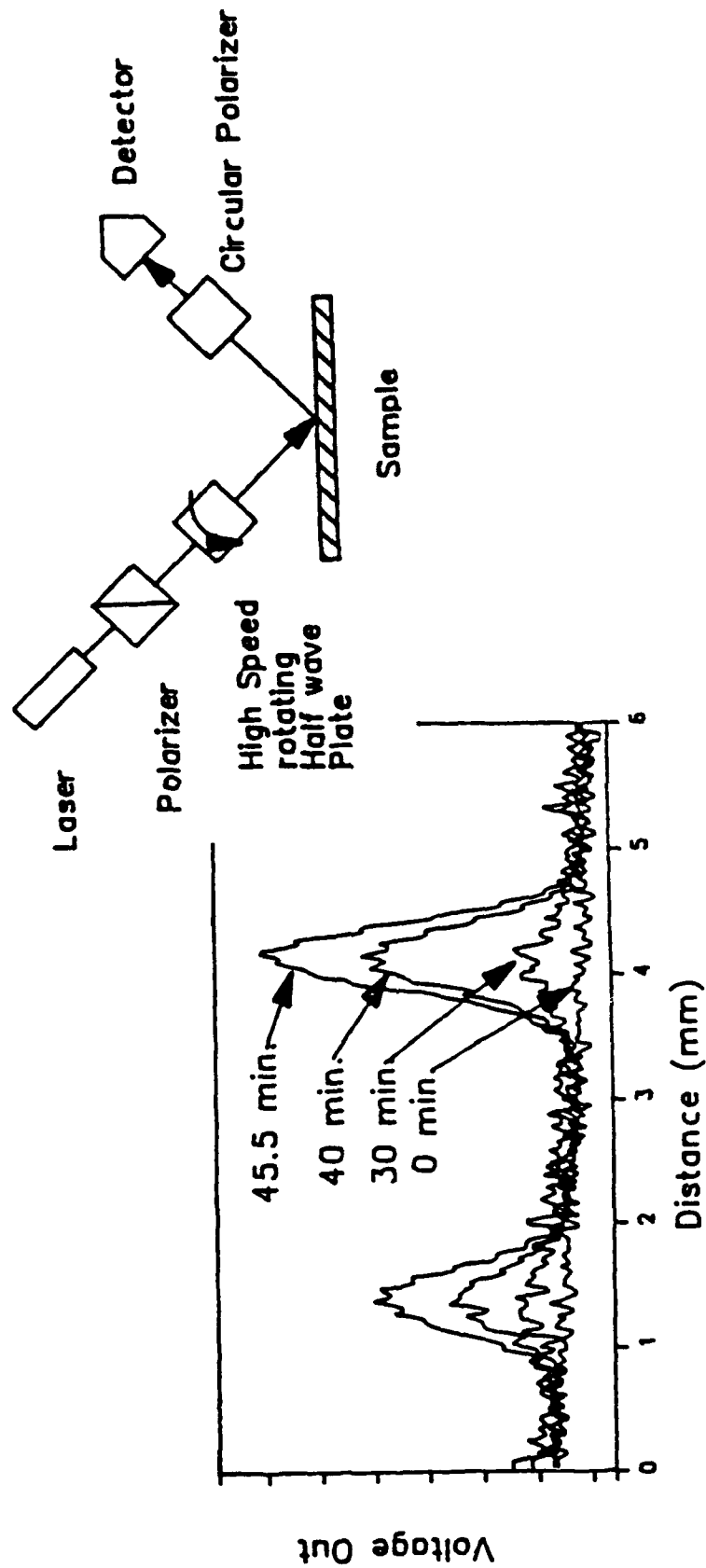
# Ingold et al (1991): FIBER OPTIC PRESSURE SENSOR



THE UNIVERSITY OF TEXAS AT AUSTIN

Nunnelley et al (1990):

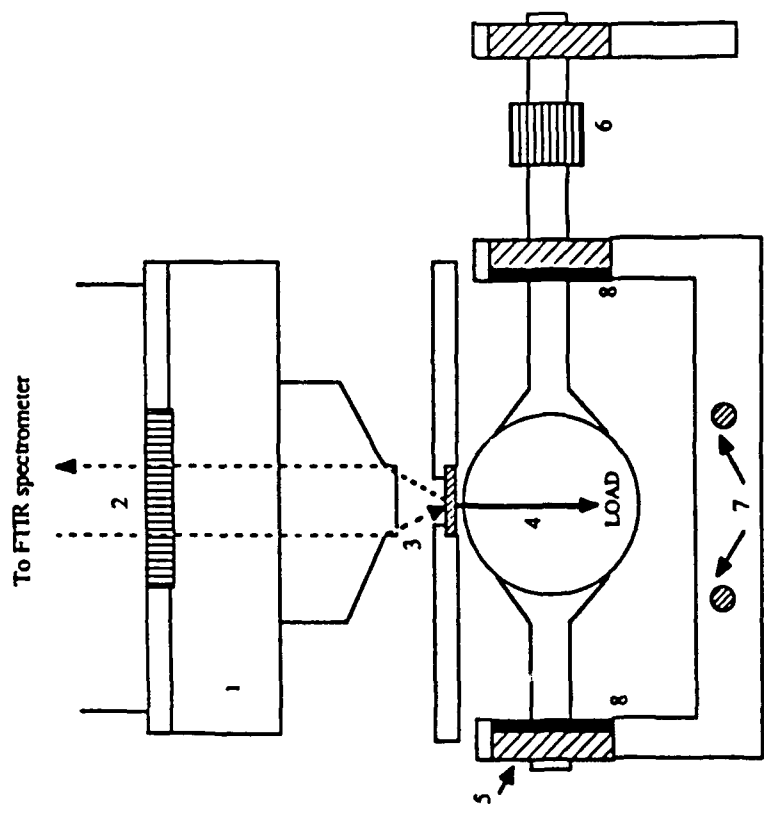
ON-LINE WEAR MEASUREMENTS OF  
RECORDING MEDIA



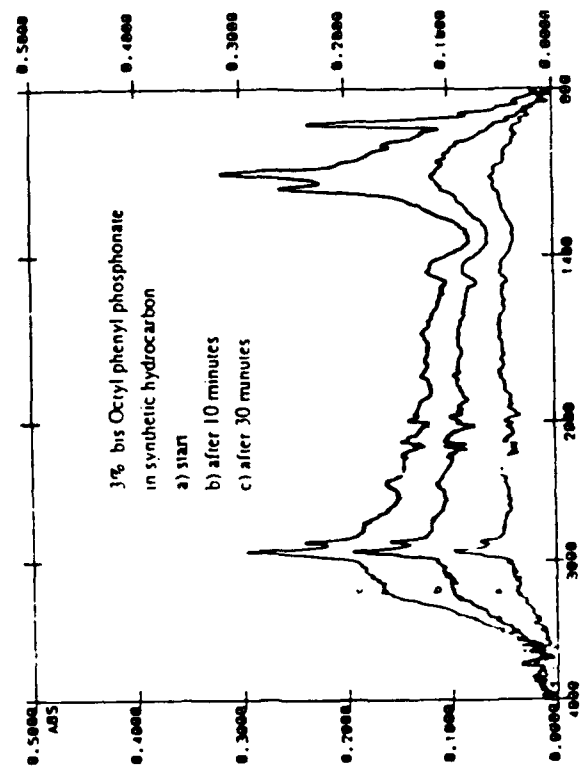
THE UNIVERSITY OF TEXAS AT AUSTIN

Cann and Spikes (1991):

STUDIES OF LUBRICANTS IN EHD CONTACTS  
USING FTIR ADSORPTION SPECTROSCOPY



- 1. IR microscope
- 2. Polariser position
- 3. Diamond window
- 4. Steel ball
- 5. Bearings
- 6. Belt and pulley drive
- 7. Heating rods
- 8. Oil seals



THE UNIVERSITY OF TEXAS AT AUSTIN

**INTRODUCTION**

**SELECTED RECORDS FOR INTERIM REPORT**

**A. GENERAL**

**SELECTED RECORDS FOR INTERIM REPORT**

**B. PERTAINING TO MACHINERY CONDITION**

**TEN EXAMPLES FOR DETAIL DISCUSSION**

✓ **SOME CONCLUDING REMARKS**

## SOME CONCLUDING REMARKS

- ONE ESTIMATE OF WORLD MARKET OF FIBER OPTIC SENSOR SYSTEMS  
\$4.88 billion by Year 2000, from \$268 Million in 1990\*
- WE HAVE GIVEN EMPHASIS TO NEW IDEAS WHICH, THROUGH ADDITIONAL RESEARCH, WOULD MOST LIKELY LEAD TO SENSOR TECHNOLOGIES PERTAINING TO MACHINERY CONDITION IN THE NEXT CENTURY
- ALTHOUGH WE HAVE DEFERRED REVIEWING THE COMPLEMENTARY WORKS ON INFORMATION PROCESSING AND SOFTWARE ENGINEERING, ADVANCES THEREIN HAVE BEEN TAKEN INTO CONSIDERATION IN THIS STUDY
- NEXT GENERATION OF POWERFUL SENSORS WILL BE BUILT ON THE TWO-PRONG FOUNDATION\*\* OF:

- (1) MATERIALS RE SURFACE AND MICRO-ANALYSIS METHODS
- (2) SOFTWARES RE KNOWLEDGE-BASED INFORMATION PROCESSING

\* Montgomery, J.D. and Glasco, J., "Fiber Optic Sensors Long-Range Market Forecast." Proceedings on Fiber Optic Sensors, Arditty, H.J. and Jeunhomme, L.B., eds., SPIE, 586, 2-13 (1985).

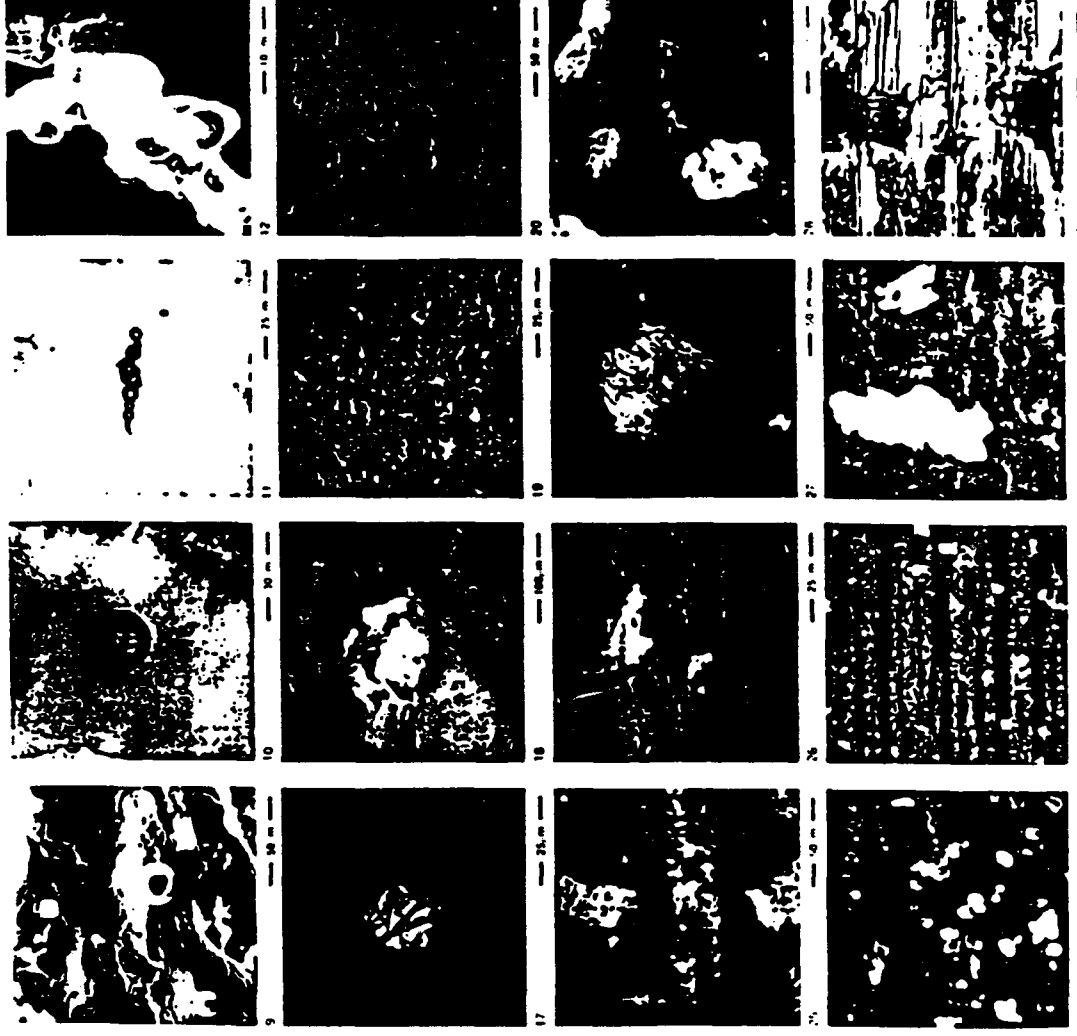
\*\* Keinschmidt, P. and Hanrieder, W., "The Future of Sensors, Materials Science or Software Engineering," Sensors and Actuators, A, 33, 5-17 (1992).

## PROMISING APPROACHES/IDEAS

Limiting this discussion to potential research arena, we see:

- Great opportunities to sense, or otherwise detect, symptoms of impending failure modes of machinery through chemical considerations in addition to physical ones which are most often used today.
- Indeed, these opportunities are projected in the in-situ and micro-miniature realm.
- Advanced modeling of processes leading up to failures will greatly enhance the capabilities of the aforementioned potential for sensing devices.





## CONDITION BASED MAINTENANCE

VICKERS-TEDECO  
GLENOLDEN, PA.

A

TRINOVA COMPANY  
MAUMEE, OHIO

## TECHNOLOGY NICHES

### NATURE OF PRODUCT

ELECTRONIC SYSTEMS AND COMPONENTS FOR REAL TIME, ON-LINE MONITORING  
OF LUBRICATION SYSTEMS FOR TURBINE ENGINES AND GEARBOXES.

### CUSTOM PRODUCTS

DEBRIS SENSORS AND DETECTORS, POWER MODULES, SIGNAL CONDITIONERS,  
DATA PROCESSORS, INTERFACE CIRCUITS, LEVEL SENSORS, SEPARATORS.

### FUNCTIONS PERFORMED

- FERROUS DEBRIS DETECTING/SENSING
- FLUID SYSTEMS LEVEL DETECTION AND MONITORING
- SIGNAL CONDITIONING
- DATA PROCESSING
- COMMUNICATION INTERFACES
- SENSOR CONTROL MODULES

## CONDITION BASED MAINTENANCE

### TECHNOLOGIES

- FLUID BASED SYSTEM SENSING, MONITORING, CONTROL AND DIAGNOSTICS
- FERROUS AND NON-FERROUS METALLIC DEBRIS DETECTION AND MONITORING
- DESICCANT MATERIAL PERFORMANCE AND CHARACTERISTICS
- FIBER-OPTIC SIGNAL/DATA LINK
- MAGNETIC SENSING
- ELECTRO-OPTIC SENSING
- INDUCTIVE SENSING
- CAPACITIVE SENSING
- SIGNAL CONDITIONING/PROCESSING ELECTRONICS
- DATA INTERFACE ELECTRONICS

## **CONDITION BASED MAINTENANCE**

### **ELECTRONICS**

#### **CHARACTERISTICS**

- FERROUS PARTICLE SENSING SENSITIVITY TO 0.04 MILLIGRAM
- FERROUS MASS SENSING SENSITIVITY TO 0.01 MILLIGRAM
- LOW LEVEL (MILLIVOLT) ANALOG SENSOR SIGNAL AMPLIFICATION
- LOW FREQUENCY SIGNAL FILTERING
- DIGITAL DATA PROCESSING
- ANALOG/DIGITAL COMMUNICATION INTERFACING
- HIGH CURRENT SENSOR CONTROL PULSES
- ELECTRO-OPTIC DETECTION

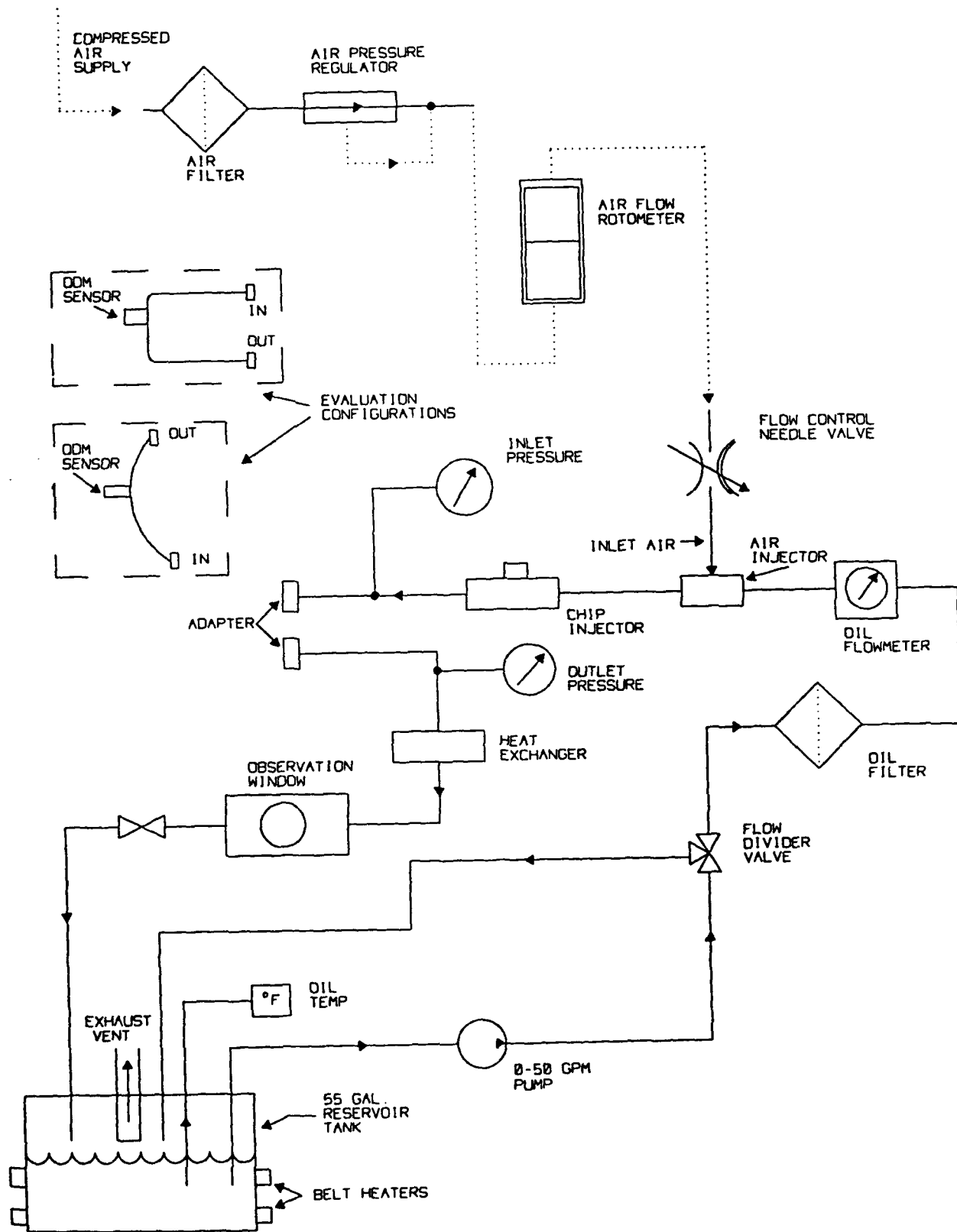
## CONDITION BASED MAINTENANCE

### PRODUCTS

- QDM® — SENSORS, SIGNAL CONDITIONING/PROCESSING ELECTRONICS
- FERROUS DEBRIS DETECTORS
- ELECTRIC CHIP DETECTOR, ZAPPER® SYSTEMS
- ELECTROMESH, METALLIC NON-FERROUS DEBRIS MONITORS
- LEVEL SENSORS — ELECTRO-OPTIC, FLOAT, FIBER-OPTIC
- LUBRICLONES® — AIR/OIL/DEBRIS SEPARATORS

# CONDITION BASED MAINTENANCE

## LUBRICATION SYSTEM TESTING



**OPTICAL OIL DEBRIS MONITOR**

**J. REINTJES  
NAVAL RESEARCH LABORATORY  
WASHINGTON, DC 20375**

**ONR WORKSHOP  
CONDITION BASED MAINTENANCE**

**ATLANTIC BEACH NC**

**11/15-17, 1993**



## OPTICAL OIL DEBRIS MONITOR

### NEEDS

- OIL DEBRIS MONITORING IS ONE OF TWO MAIN MECHANICAL  
DIAGNOSTIC SYSTEMS FOR ON LINE HEALTH MONITORING
- IMPROVED HEALTH MONITORING OF ENGINES ALLOWS CONDITION  
BASED MAINTENANCE
  - COST SAVINGS ON PARTS INVENTORY
  - SAVE LIVES
- OPTICAL OIL DEBRIS MONITOR WILL
  - PROVIDE ADDITIONAL CAPABILITY NOT CURRENTLY AVAILABLE
  - OPERATE WITH CERAMIC BEARINGS EXPECTED IN NEXT GENERATION OF  
ENGINES





## OPTICAL OIL DEBRIS MONITOR

STATE OF THE ART

### ● CURRENT CHIP DETECTORS

- MAGNETIC PLUGS (MP)
- ELECTRIC CHIP DETECTORS (ECP)
- ON LINE DEBRIS DETECTORS/COUNTERS (DD)

### ● MAIN SHORTCOMINGS

- OFF LINE ONLY (MP)
- DON'T DISTINGUISH SOURCE OF DEBRIS (ECP, DD)
- PARTICLE SIZE LIMITED (300-400  $\mu\text{m}$  MINIMUM)
- ELECTROMAGNETIC ENVIRONMENT SENSITIVE
- DETECT ONLY MAGNETIC/METALLIC PARTICLES
  - \* WON'T WORK ON ADVANCED BEARING MATERIALS (CERAMIC)
  - \* WON'T WARN OF INGESTED PARTICLES (SAND, ETC)



## OPTICAL OIL DEBRIS MONITOR

### TECHNICAL OBJECTIVE

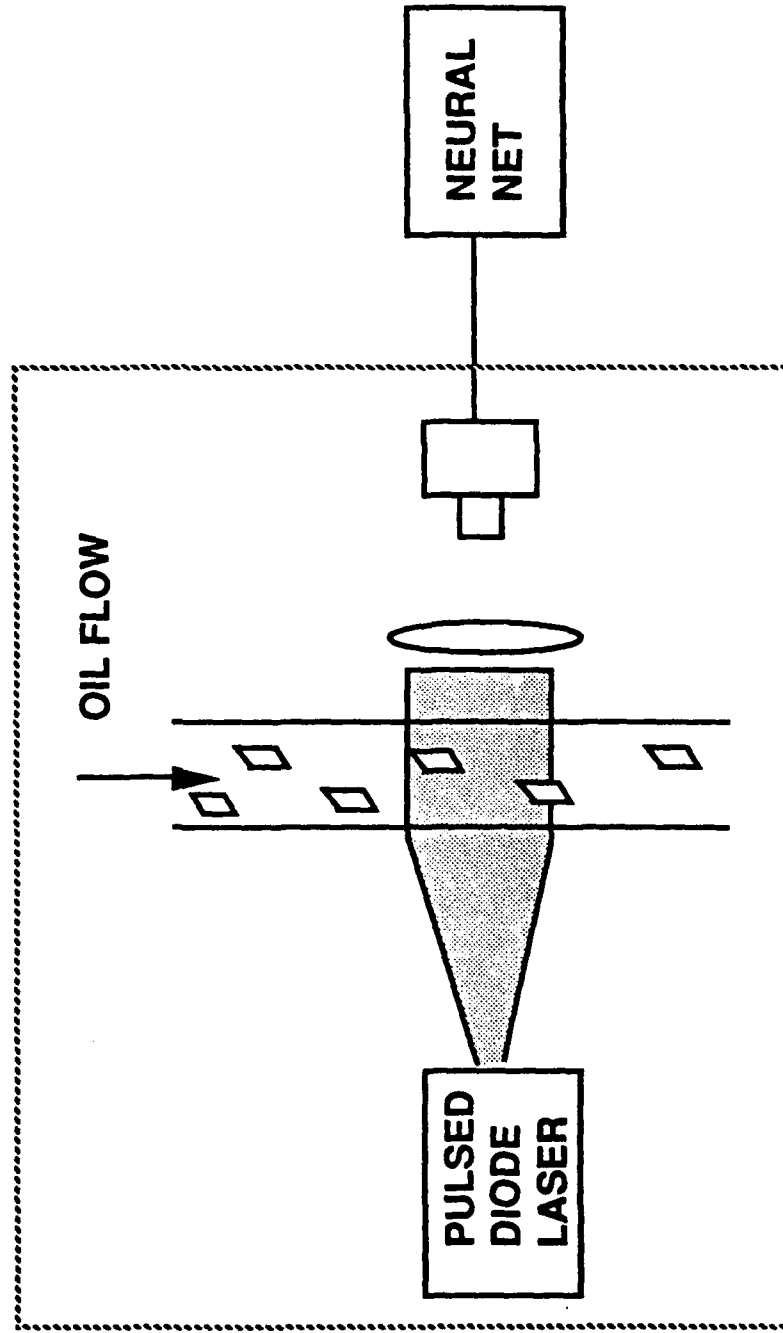
- **ON LINE OPTICAL OIL DEBRIS MONITOR**
  - REAL TIME IDENTIFICATION OF DEBRIS SHAPE/SIZE WITH OPTICAL IMAGING/NEURAL NET ANALYSIS
- **USE OF CHIP MORPHOLOGY/SIZE ALLOWS**
  - IDENTIFICATION OF SOURCE OF FAILURE
  - DISTINCTION OF CHIPS FROM AIR BUBBLES
  - DISTINCTION OF FAILURE RELATED DEBRIS FROM NON FAILURE DEBRIS (MACHINE CURLS, E. G. )
  - DETECTS ANY PARTICULATE MATERIALS - FERROUS, NON FERROUS, NON METALLIC (SAND, CERAMIC BEARINGS)
- **PROVIDES**
  - CUMULATIVE RECORD OF ENGINE HEALTH
  - CATASTROPHIC WARNING



## OPTICAL OIL DEBRIS MONITOR

### TECHNICAL APPROACH

- OPTICAL OIL DEBRIS MONITOR
  - IMAGES DEBRIS IN TRANSMISSION USING LASER ILLUMINATOR
  - ANALYZES DEBRIS SHAPE/SIZE WITH NEURAL NETWORK





# OPTICAL OIL DEBRIS MONITOR

## EXAMPLE SYSTEM PARAMETERS

COMPONENT	VALUE	DETERMINED BY
LASER WAVELENGTH	850 - 950 nm	OIL TRANSMISSION/ DETECTOR SENSITIVITY
PULSE DURATION	1 $\mu$ sec	RESOLUTION/ FLOW SPEED
REP RATE	1 kHz	AREA COVERAGE/ FLOW SPEED
DETECTOR ARRAY	1000 x 1000	AREA COVERAGE, RESOLUTION
OIL TRANSMISSION (2 cm)	0.1	790 HOUR GEAR BOX SAMPLE
LASER POWER	1 W PEAK    1 mW AVERAGE	OIL TRANSMISSION/ DETECTOR SENSITIVITY
SIGNAL	$4 \times 10^5$ PHOTONS/PIXEL	COMPATIBLE WITH CCD ARRAYS



## OPTICAL OIL DEBRIS MONITOR

### TECHNICAL ALTERNATIVES

● LASER SOURCES	DIODE ONLY PRACTICAL ONE
● LASER WAVELENGTH	CHOSEN FOR COMBINATION OF OIL TRANSMISSION,
● LASER POWER	DETECTOR SENSITIVITY AND SOURCE AVAILABILITY
● LASER TRANSVERSE MODE STRUCTURE	SINGLE MODE - BETTER RESOLUTION MULTI MODE - HIGHER POWER/CHEAPER
● IMAGING GEOMETRY	CHOSEN TO SATISFY REQUIREMENTS OF FIELD OF VIEW, RESOLUTION AND DEPTH OF FIELD SIMULTANEOUSLY
● ILLUMINATION GEOMETRY (MULTIPLE AXIS VIEWING)	DESIRABLE FOR OBSCURED CHIPS, IDENTIFYING FLAKES VS SPHEROIDS
● NEURAL NET	RETINAL NETS - OPTICAL TRANSISTORS CCD ARRAYS CCD DETECTOR/ELECTRONIC NET

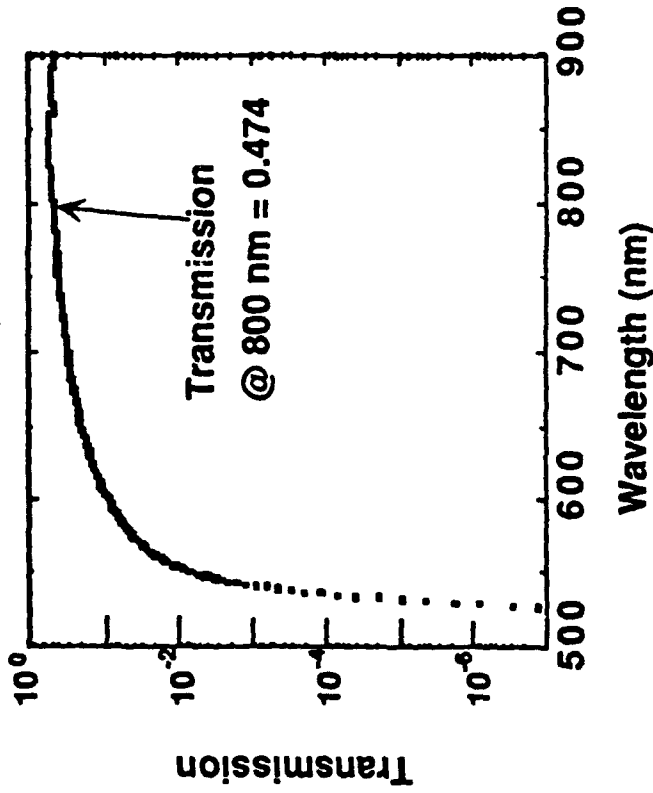


# OPTICAL OIL DEBRIS MONITOR

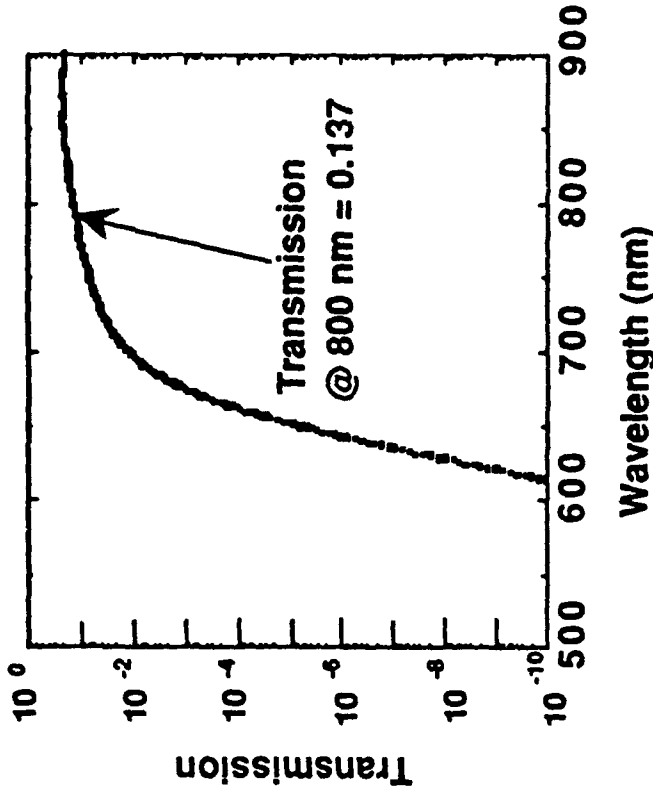
WORK PROGRESS FY92

## OPTICAL TRANSMISSION OF USED OIL

Used Engine Oil 790 Hours  
3/4" path



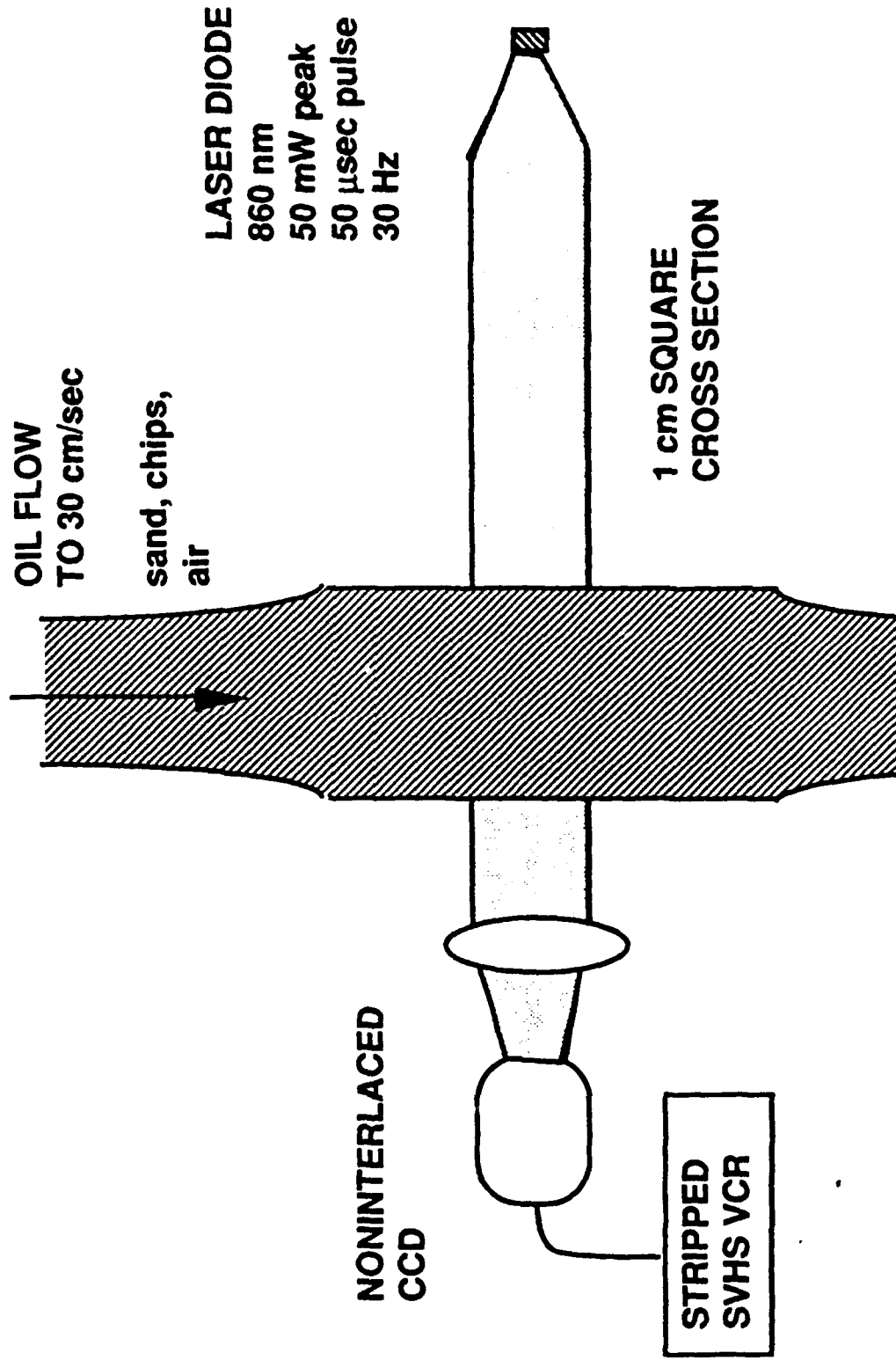
Used Gear Box Oil 790 Hours  
3/4" path





# OPTICAL OIL DEBRIS MONITOR

WORK PROGRESS - FY93/NRL TESTS





# OPTICAL OIL DEBRIS MONITOR

FY93 WORK PROGRESS - NRL LAB TESTS

## GOAL

- INCREASE RESOLUTION
- DEVELOP ILLUMINATION SYSTEM FOR FIELD TESTING
- MOVE TOWARD MORE REALISTIC CONDITIONS
- TEST ALTERNATIVE GEOMETRIES

	LAB	PROJECTED REAL SYSTEM
LASER	DIODE	DIODE
POWER	50 mW	1 W
PULSE DURATION	50 $\mu$ sec	1 $\mu$ sec
RESOLUTION	15-25 $\mu$ m	20 $\mu$ m
FRAME RATE	30 Hz (LIMITED BY VCR)	1 kHz
FLOW RATE	30 cm/sec (TO MATCH FRAME RATE)	10 m/sec



Chips and bubbles  
TM 42.46  
860 nm illumination

1 mm



Curls and small bubbles  
TM 9 07  
860 nm illumination

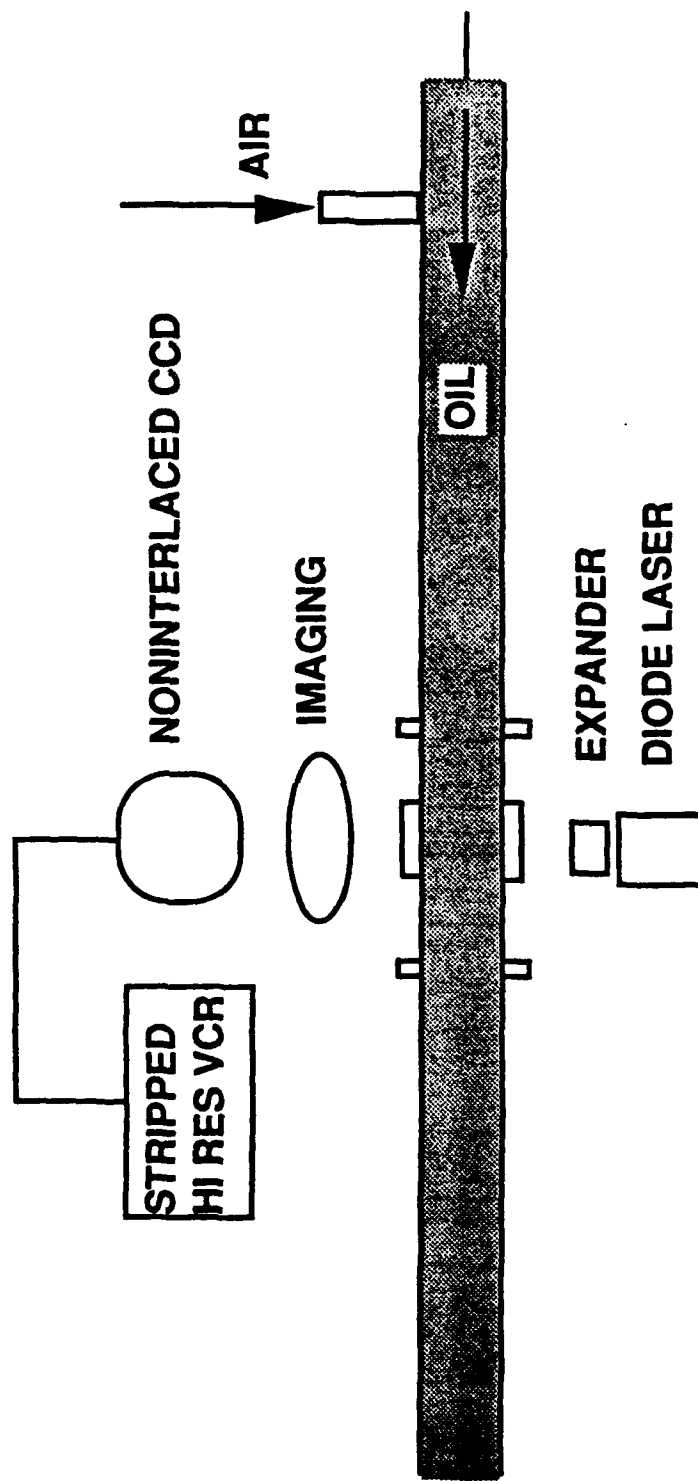
1 mm





# OPTICAL OIL DEBRIS MONITOR

WORK PROGRESS - FY93 FIELD TESTS





## OPTICAL OIL DEBRIS MONITOR

WORK PROGRESS - FY93 FIELD TESTS - TEDECO

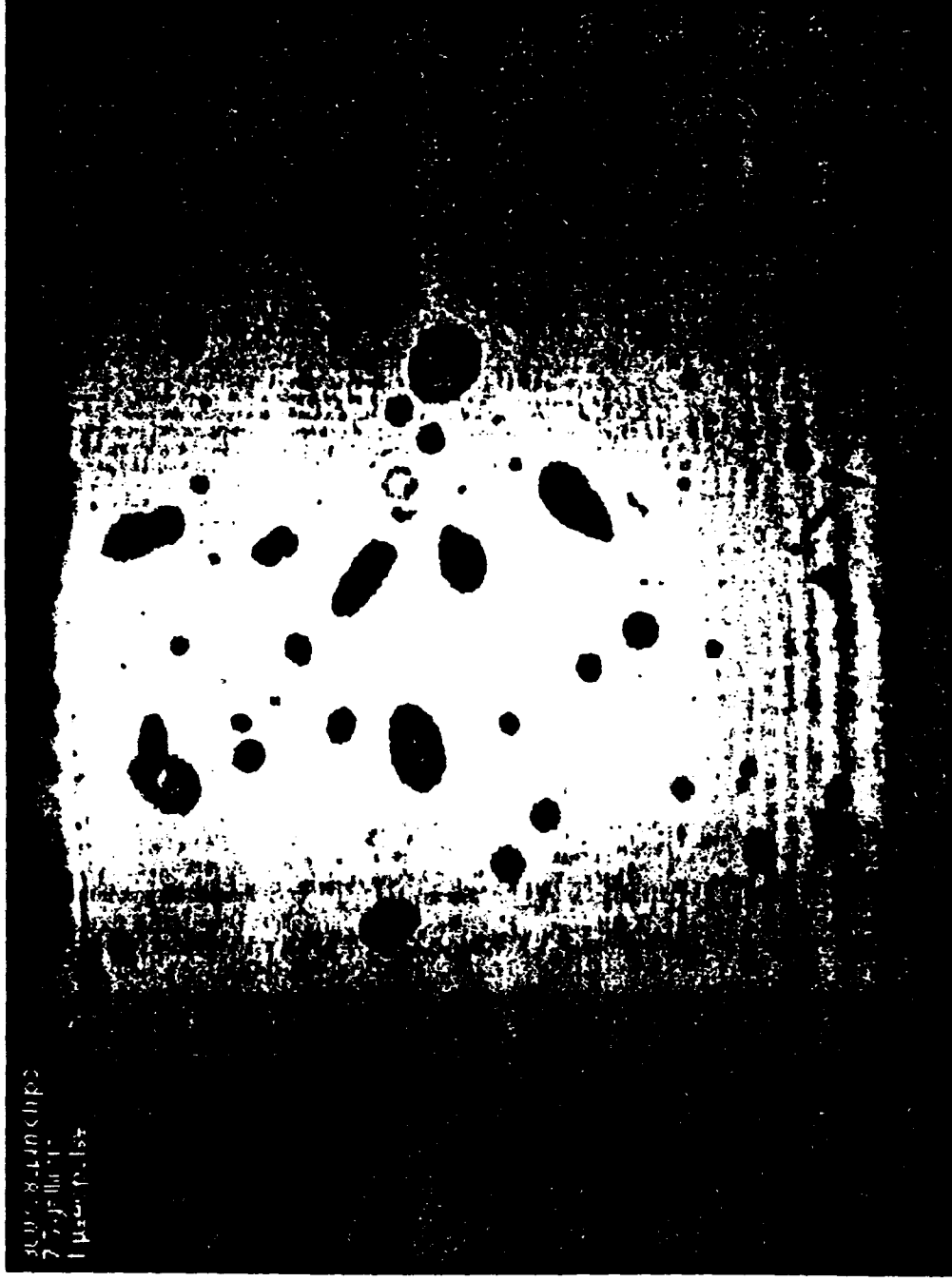
	FIELD TEST	ACTUAL
LASER	DIODE	DIODE
POWER	100 mW	1 W
PULSE DURATION	1-10 $\mu$ sec	1 $\mu$ sec
RESOLUTION	15-25 $\mu$ m	20 $\mu$ m
FRAME RATE	30 Hz	1 kHz
FLOW RATE	up to 7 m/sec	10 m/sec
OIL COLUMN	1 cm	2 cm
AIR CONTENT	VARIABLE	VARIABLE
CHIPS	SYNTHETIC/ REAL DEBRIS/ SAND	REAL DEBRIS
OIL TRANSMISSION	.01 (1 cm)	0.14 (2 cm)

# OPTICAL OIL DEBRIS MONITOR

## FIELD TESTS

FLOW RATE 5.2 m/sec

Synthetic chips 300x380  $\mu\text{m}$



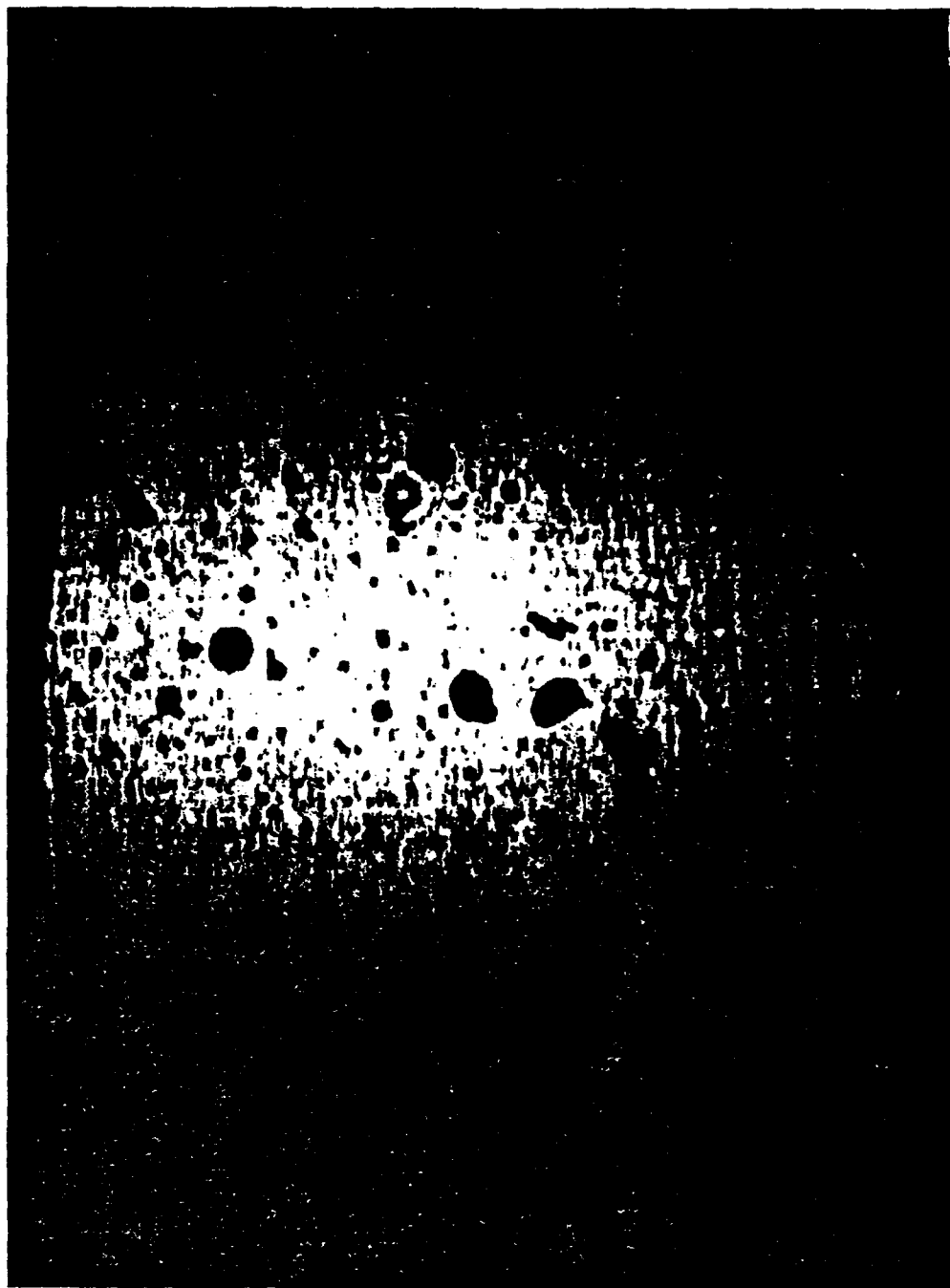
1 mm

# OPTICAL OIL DEBRIS MONITOR

## FIELD TESTS

FLOW RATE 0.6 m/sec

H-60 DEBRIS



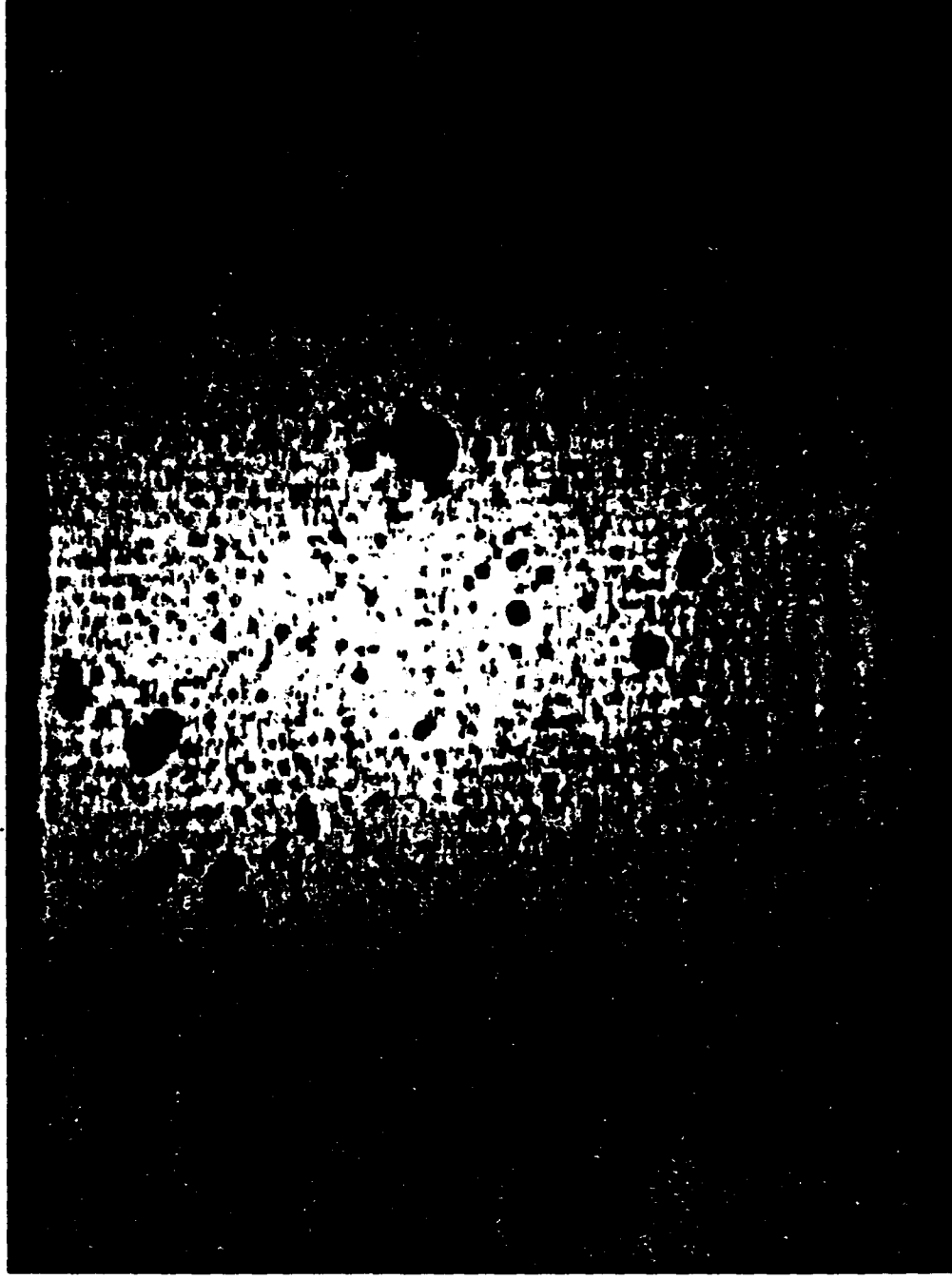
1 mm

# OPTICAL OIL DEBRIS MONITOR

## FIELD TESTS

FLOW RATE 5.2 m/sec

SAND



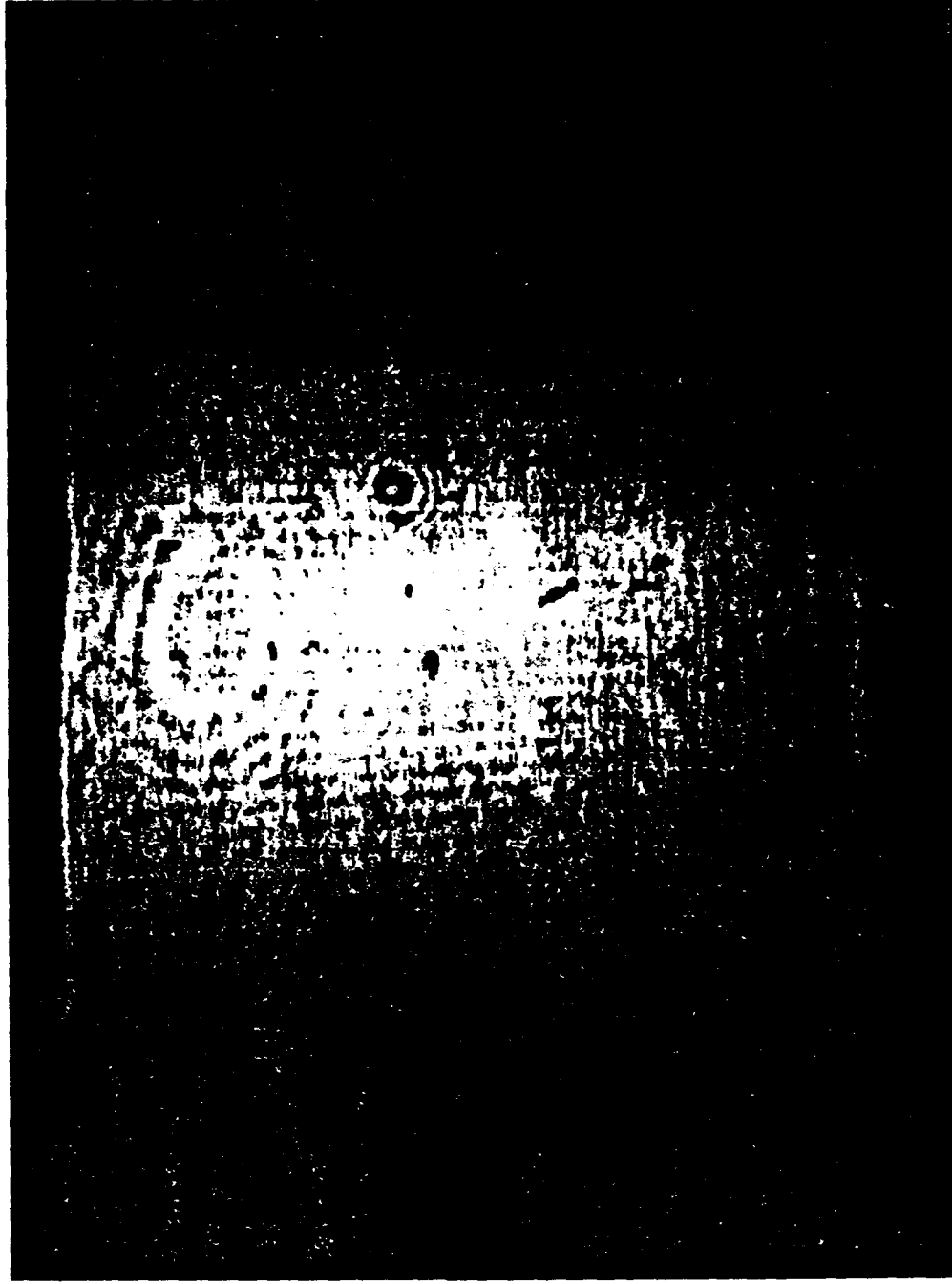
1 mm

# OPTICAL OIL DEBRIS MONITOR

## FIELD TESTS

FLOW RATE 0.6 m/sec

40  $\mu$ m IRON FILINGS



1 mm



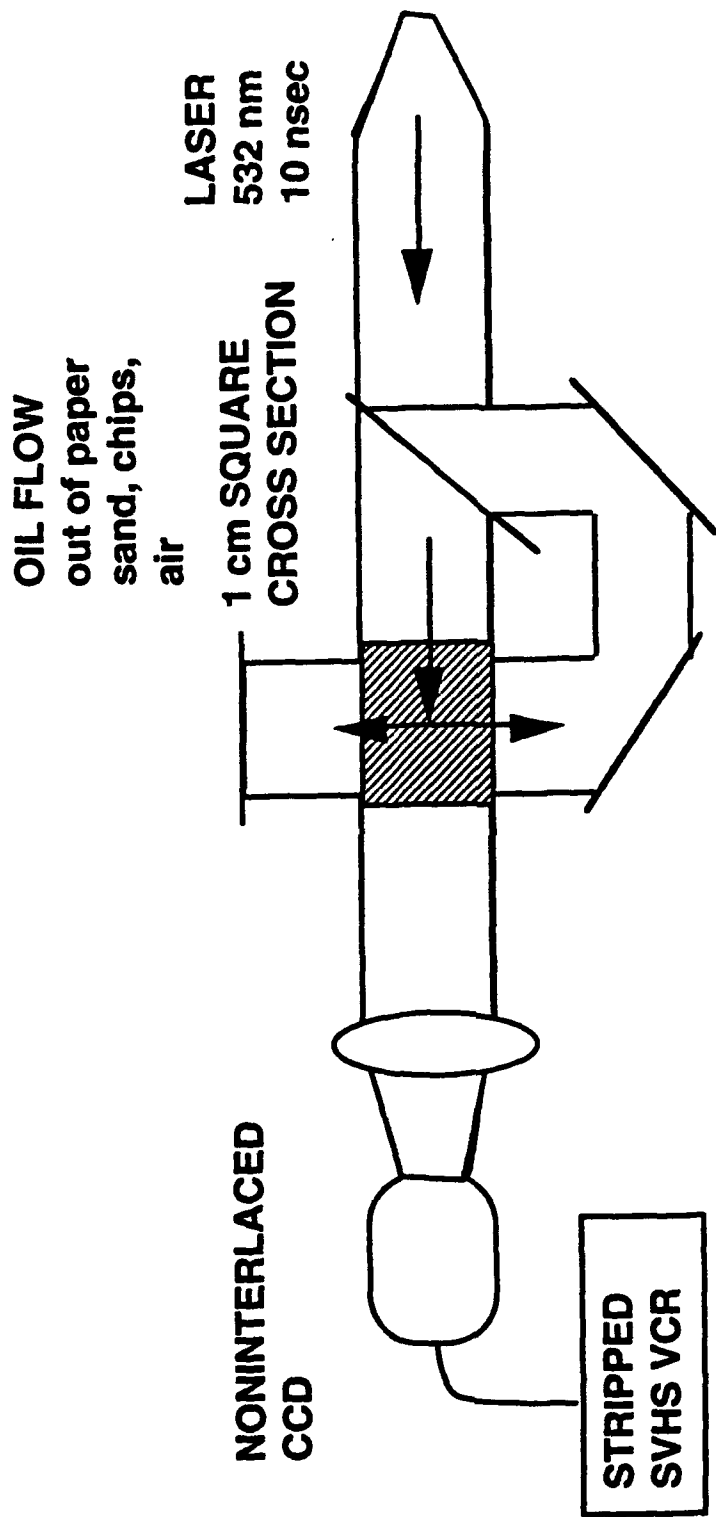
## **CURRENT STATUS/CONCLUSIONS**

- **OPTICAL IMAGING WELL IN HAND**
- **POWER REQUIREMENTS COMPATIBLE WITH LASER DIODES**
- **LIBRARY OF BEARING DEBRIS SHAPES BEING COMPILED**
- **ADDITIONAL STUDIES OF OPTICAL PROCESSING UNDERWAY**
- **MORE EXTENSIVE STUDIES UNDER VARIOUS FLOW CONDITIONS TO BE**

**DONE FY 94**

# OPTICAL OIL DEBRIS MONITORING

## CROSS ILLUMINATION



Chips and bubbles  
TM 14.56  
532 nm two-way  
illumination

1 mm



120 grit and bubbles  
TM27.51  
532nm two-way illumination

1 mm

## **CURRENT STATUS/CONCLUSIONS**

- **IMAGE PROCESSING BEING ASSESSED**
- **MAJOR ISSUE - CLUTTER IN IMAGE REQUIRES HIGH PROCESSING SPEED**
- **RETINAL SHIPS DESIRABLE FOR SPEED**
- **PROCESSING OF SHAPES SEEMS STRAIGHTFORWARD WITH NEURAL NETS OR PERHAPS OTHER PARALLEL APPROACHES**
- **FAST PREPROCESSING (OBJECT ISOLATION, EDGE DEFINITION) FOR BUBBLE REJECTION BEING INVESTIGATED**

## ISSUES TO BE ADDRESSED BY BREAKOUT GROUPS

1. **FAILURE MECHANISM MODELS**
2. **FOR WHICH FAILURE MODES/TYPES?**
3. **WHAT USEFUL MEASUREABLE INFORMATION COMES OUT OF COMPONENT?**
4. **HOW CAN IT BE MONITORED?**
  - Sensors
    - Oil Analysis Issues (e.g., debris, chemistry)
    - Physical State(s)
5. **DATA PROCESSING**
  - Real Time Analysis
  - Multichannels
6. **DECISION MAKING**
  - Probabilistic Aspects
  - Stochastic/Nonlinear Aspects
7. **DATABASE DEVELOPMENT**

Four groups were formed to discuss the issues of conditioned based maintenance relative to the disciplines of Chemistry & Physics, Maintenance & Engineering, Sensors, and Signal Analysis. Suggestions from the Chemistry & Physics subgroup follow. Results from the other subgroups are incorporated in the Plenary Session reports of 17 November, 1993.

CBM workshop, 15-17 Nov. Cherry Point. Sheraton Atlantic Beach. Atlantic Beach, NC.

Summary of the first night panel on physics and chemistry tasks in CBM.

We addressed the approaches that might be used to tackle the three problems below, listed in priority order:

1. detection of fatigue cracking in corrosive environments.
  - a. inspection methods to detect cracks 100  $\mu\text{m}$  in size.
  - b. microdetectors for corrosion products
  - c. thin film devices to monitor interface properties
    - i. surface chemistry e.g. corrosion products
    - ii. surface integrity e.g. crack sensitive films
2. detection of fine (20 - 70  $\mu\text{m}$ ) debris, both ferrous and non-ferrous, such as Al and bronzes.
  - a. centrifuge
  - b. filter trap sensors
  - c. mass detectors such as quartz crystal monitors
  - d. in-line chemistry detectors tuned to specific species e.g.  $\text{Fe}_2\text{O}_3$ :
    - i. Raman
    - ii. Fluorescence
      - (1) "dopant labeled" ceramics
  - e. thin film activation detectors
  - f. zeta potential
  - g. charged particle detectors
  - h. electrochemistry with micro-electrodes
  - i. coatings, with markers based on
    - i. ion implantation
    - ii. multilayer markers
3. monitor oil condition and additive-depletion of lubricants.
  - a. fluorescence of oxidized products
  - b. additive-depletion using chemical microsensors

Irwin Singer, Scribe.

QUANTITATIVE NON-DESTRUCTIVE EVALUATION

( QNDE )

FOR

CONDITION-BASED MAINTENANCE

J. D. ACHENBACH

CENTER FOR QUALITY ENGINEERING AND  
FAILURE PREVENTION

NORTHWESTERN UNIVERSITY

EVANSTON

IL 60208

\*\*\*\*\* Jan Achenbach, "Quantitative Non-Destructive Evaluation for Conditioned Based Maintenance" \*\*\*\*\*



## POINTS IN LIFE CYCLE WHEN QNDE IS NEEDED

1. DESIGN OF COMPONENT
2. CONTROL OF PROCESSING OF BASIC MATERIALS
3. CHECK THAT QUALITY OF INCOMING MATERIAL IS SATISFACTORY FOR ADDING MANUFACTURING VALUE
4. CHECK OF INTEGRITY OF MANUFACTURED COMPONENTS
5. DETERMINATION OF IN-SERVICE DEGRADATION

IN-SERVICE DAMAGE

FATIGUE DAMAGE : MATERIAL DETERIORATION  
CRACK ( NEAR STRESS RAISER )

WEAR

CORROSION

ADHESIVE FAILURE

IMPACT DAMAGE ( COMPOSITES )

MOISTURE INFILTRATION

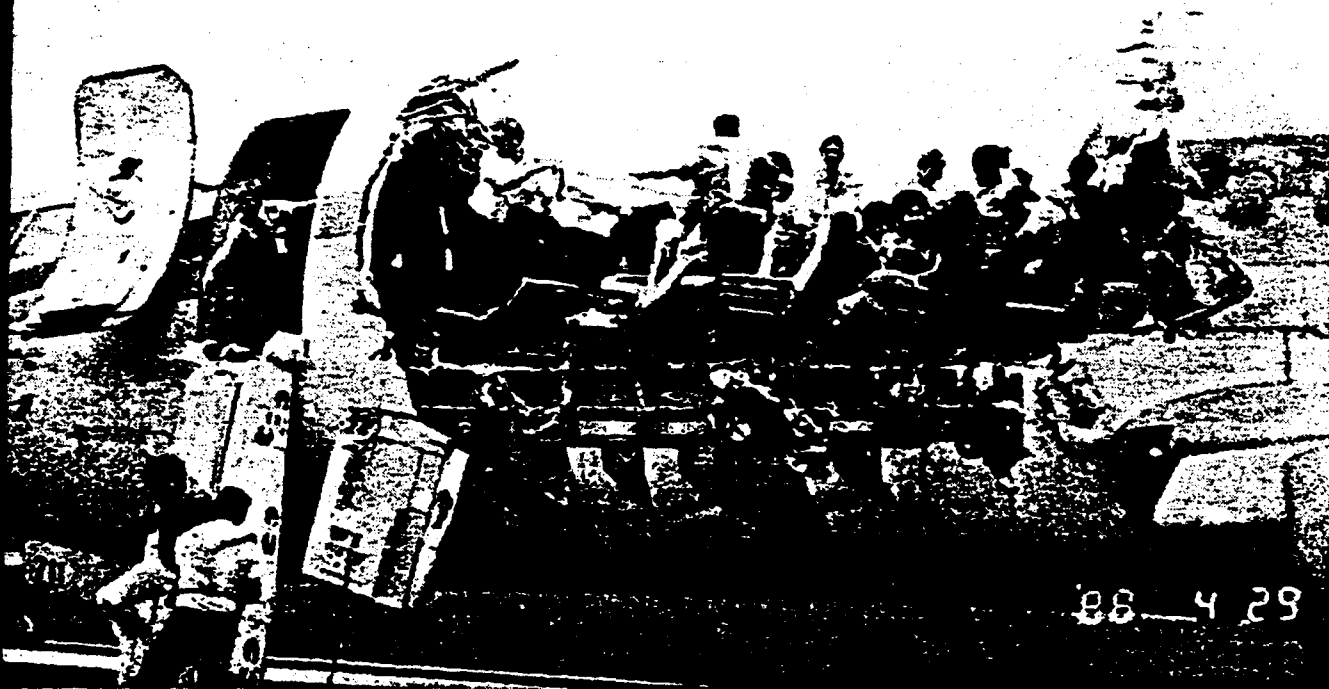
PROBABILITY OF DETECTION ( POD )

DAMAGE TOLERANT DESIGN PHILOSOPHY

RETIREMENT FOR CAUSE

REPAIR

Boeing's three varieties of 737, including | Technology also contributes to the trend.



©1988 Robert Nichols/Black Star

**Coming apart at the seams?** *A 19-year-old Boeing 737 split apart last April along a weak skin splice that had been the subject of concern since 1972.*

NEWS & COMMENT 595

-4-



Figure 5.7A

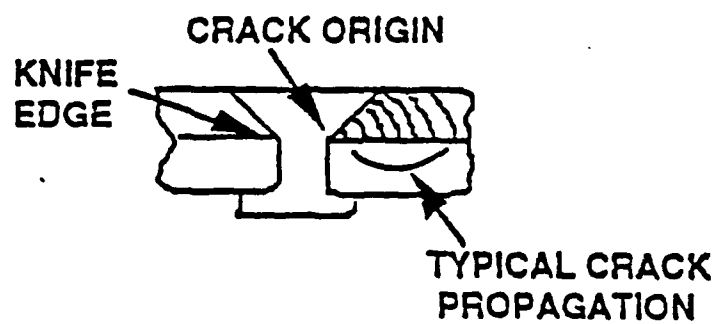
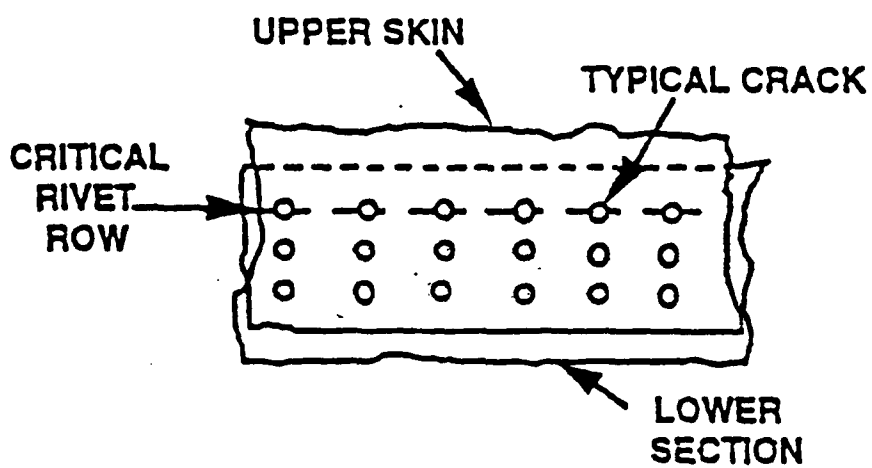
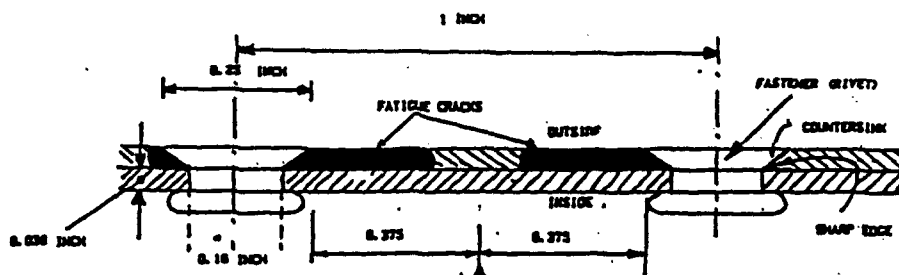


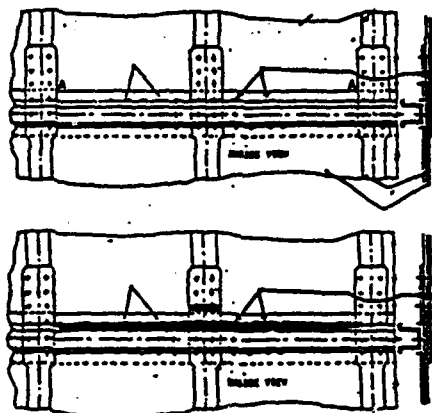
Figure 5.7B

Figure 5.7A and 5.7B Lap Joint And Crack Formation

a. MSD



b. Structure



c. Sequence of events

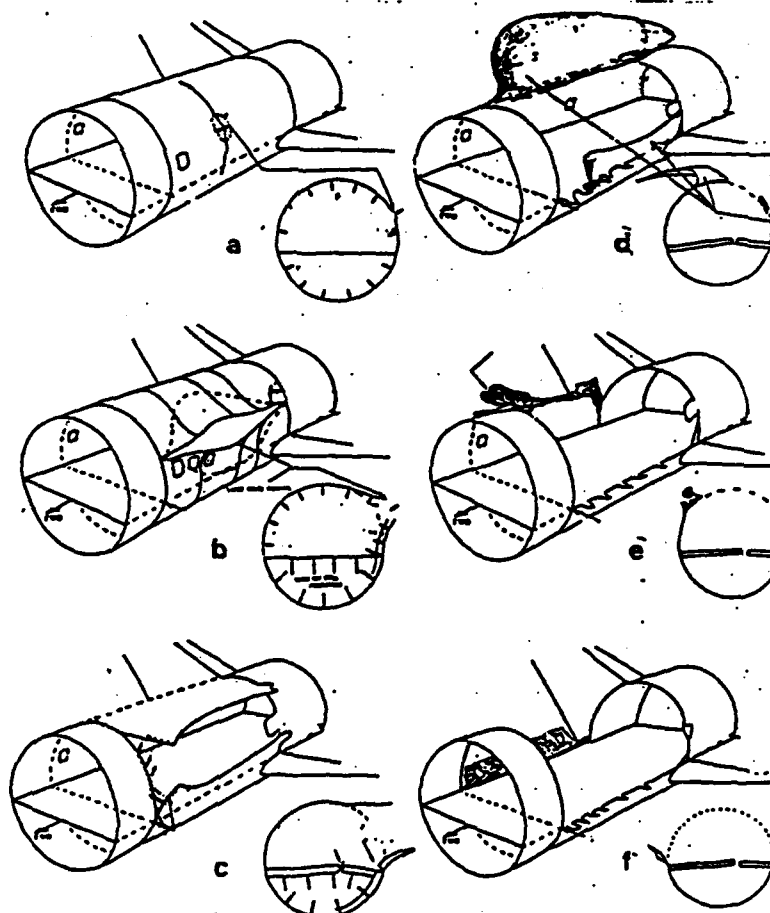


Figure 6. The Aloha case

1. DAMAGE GENERATION  
    SIGNAL : ACTIVE , PASSIVE  
    EXAMPLES :  
        PASSIVE : ACOUSTIC EMISSION  
                  THERMAL  
                  MAGNETIC  
        ACTIVE : ULTRASOUND  
                  EDDY CURRENTS  
                  X-RAY  
                  THERMAL WAVES  
                  OPTICAL INTERFEROMETRY  
                  E-M WAVES
2. SENSOR(S)
3. MEASUREMENT MODEL
4. DATA COLLECTION
5. DATA PROCESSING
6. INTERPRETATION  
    HUMAN  
    EXPERT SYSTEM  
    NEURAL NETWORK
7. CORRECTIVE ACTION

## MEASUREMENT MODELS FOR QUANTITATIVE ULTRASONICS

**PURPOSE:** TO PREDICT FROM FIRST PRINCIPLES THE MEASUREMENT  
SYSTEM'S RESPONSE TO SPECIFIED ANOMALIES IN A  
GIVEN MATERIAL OR STRUCTURE

(CRACKS, VOIDS, DISTRIBUTED DAMAGE, CORROSION, ETC.)

REQUIRES CALCULATION OF :    GENERATION  
   PROPAGATION  
   REFLECTION  
   TRANSMISSION  
   SCATTERING  
   RECEPTION  
  
   OF ULTRASOUND

### BENEFITS :

1. DESIGN AND OPTIMIZATION OF EFFICIENT TESTING  
CONFIGURATIONS
2. INTERPRETATION OF DATA
3. DETERMINE POD (PROBABILITY OF DETECTION)
4. IDENTIFY CHARACTERISTIC FEATURES, INVERSE PROBLEM
5. DEVELOP TRAINING SET FOR NEURAL NETWORK AND/OR  
KNOWLEDGE BASE FOR EXPERT SYSTEM

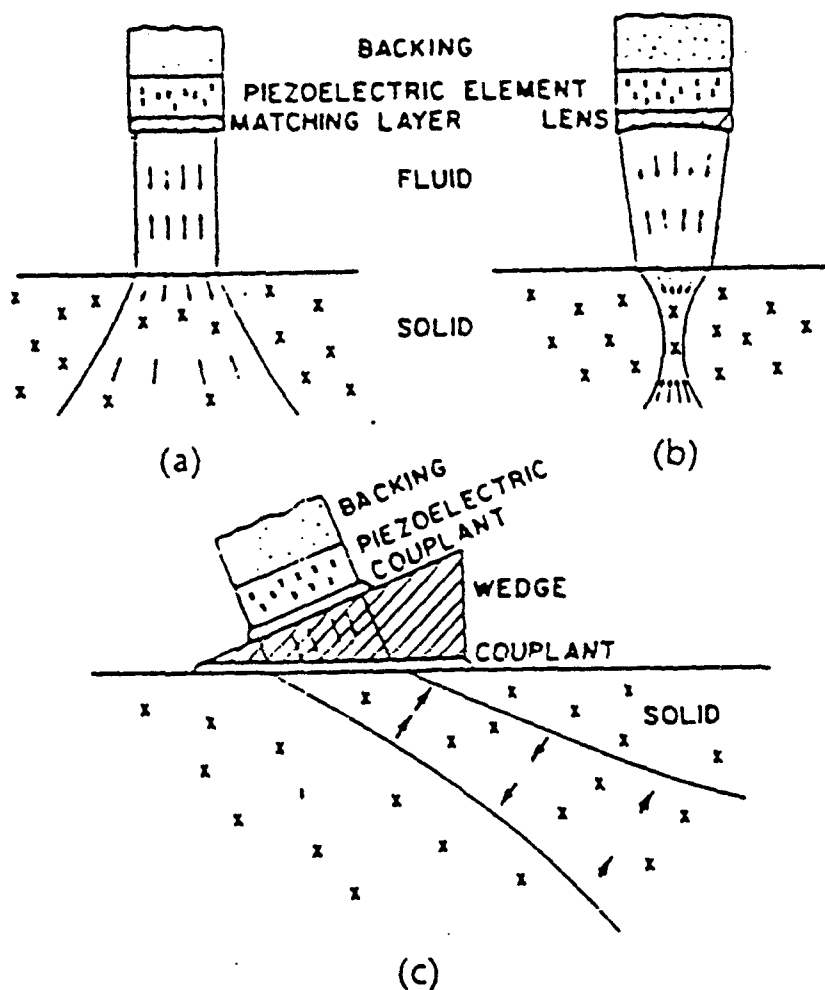


Fig. 12. Selected ultrasonic probe types (see Fig. 10 for contact probe). (a) Immersion. (b) Focussed immersion. (c) Contact angle shear.



# LASER-BASED ULTRASONICS

## OBJECTIVES

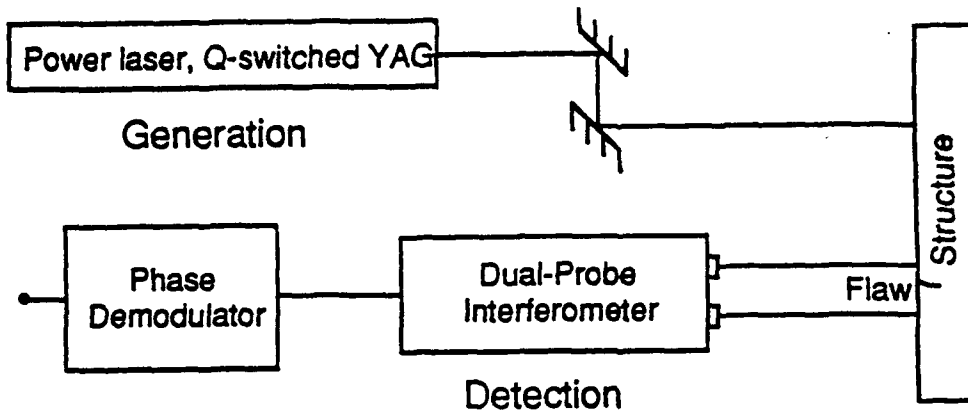
To exploit the advantages of laser-based ultrasonics for NDE of aircraft structures:

- . Non Contact
- . Point Generation and Detection
- . Wide Frequency-Band Measurements
- . Curved Surface Applicability
- . Absolute Displacement Calibration
- . Both Broad Band and Narrow Band Signal Generation
- . Easy Scanning
- . Remote Application by Use of Fiber Optics

The technique uses a laser or a transducer to excite ultrasound and a dual-probe laser interferometer for the measurement of ultrasonic signals.

# ***LASER-BASED ULTRASONICS FOR QNDE***

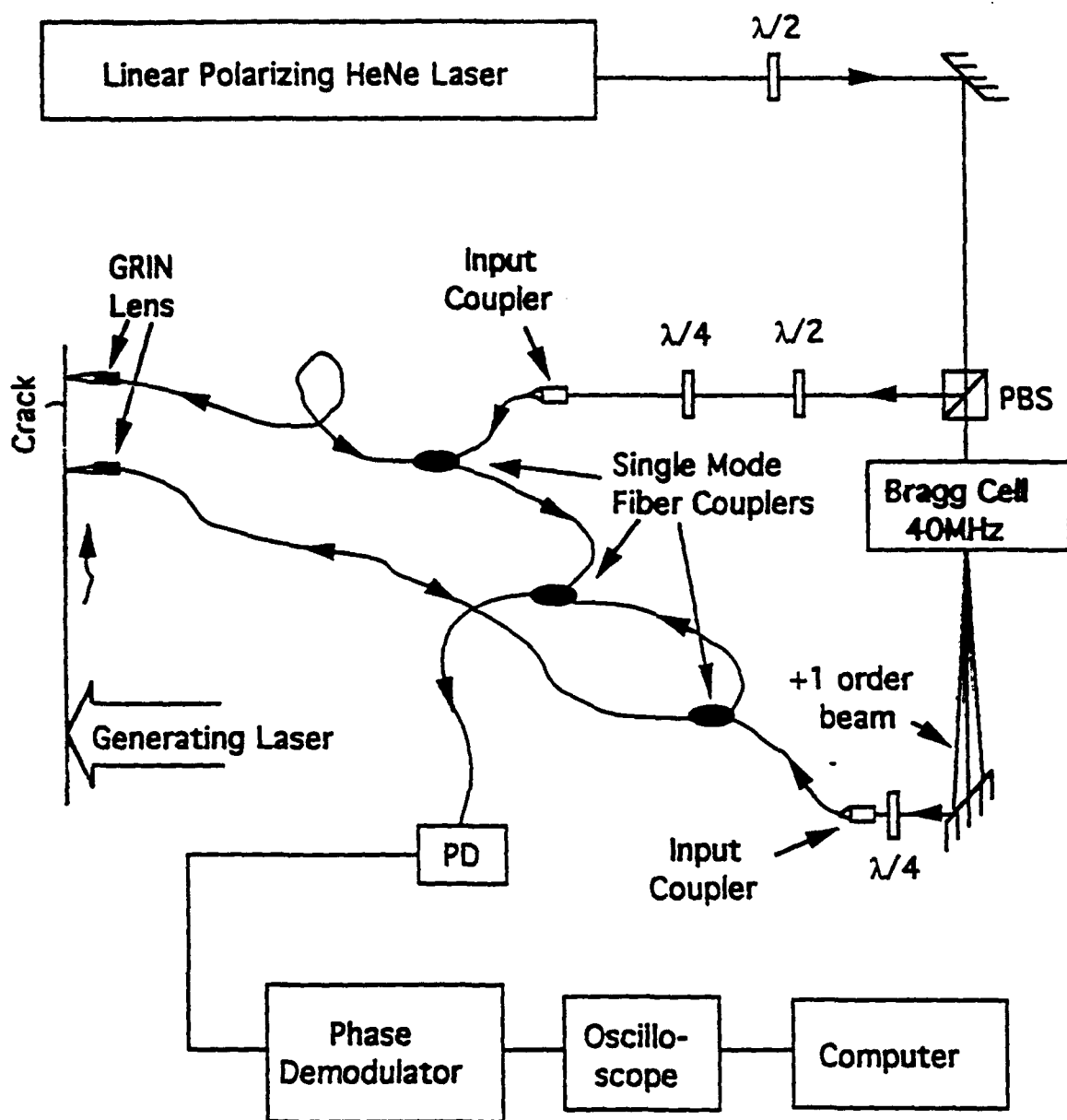
## **Schematic:**



## **Applications Implemented:**

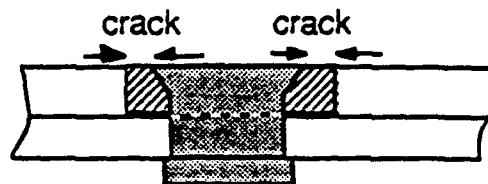
- Characterization of Surface Roughness
- Evaluate Fatigue Damage
- Determine Material Anisotropy
- Measure Thin Film Elastic Constants
- Detect Cracks in Fuselage Panel
- Fiber Guided Remote Crack Detection

# DIAGRAM OF THE DUAL-PROBE FIBER INTERFEROMETER

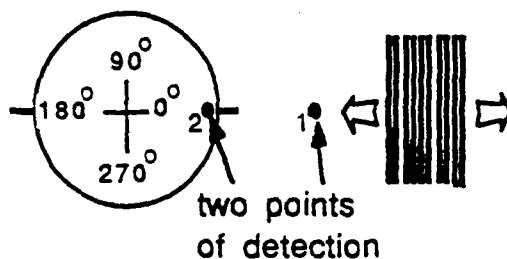


# APPLICATION OF NARROW BAND SIGNAL GENERATION AND DUAL-PROBE DETECTION TO RIVET CRACK INSPECTION

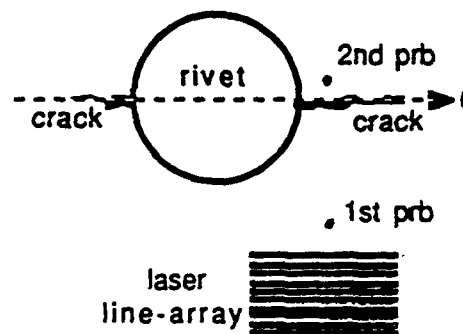
Specimen Schematics



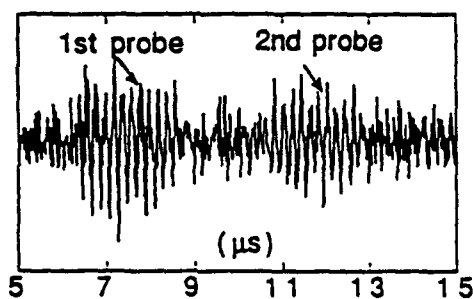
Circumferential Scan



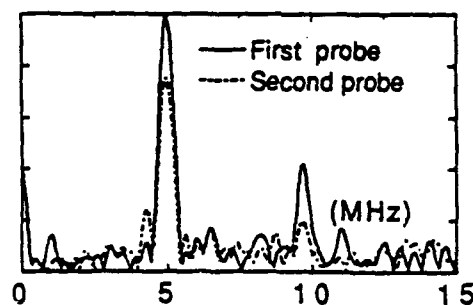
Radial Scan



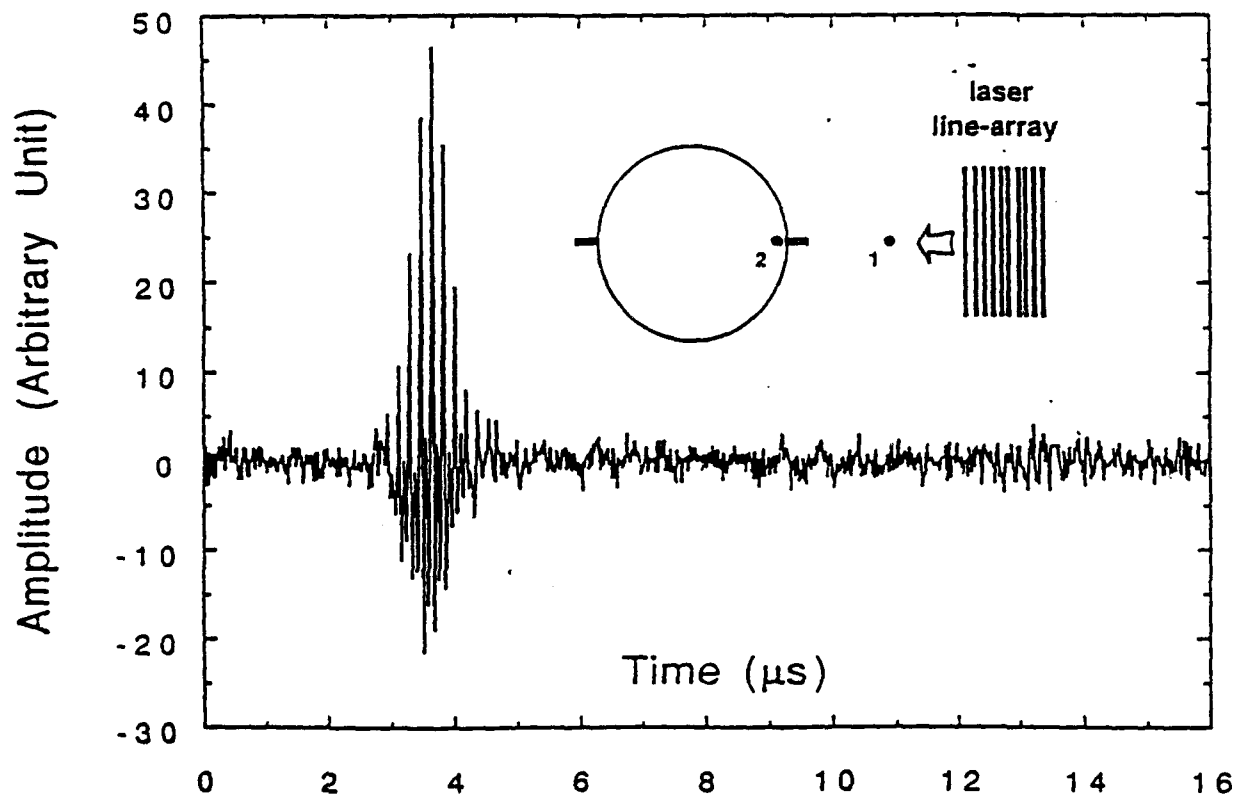
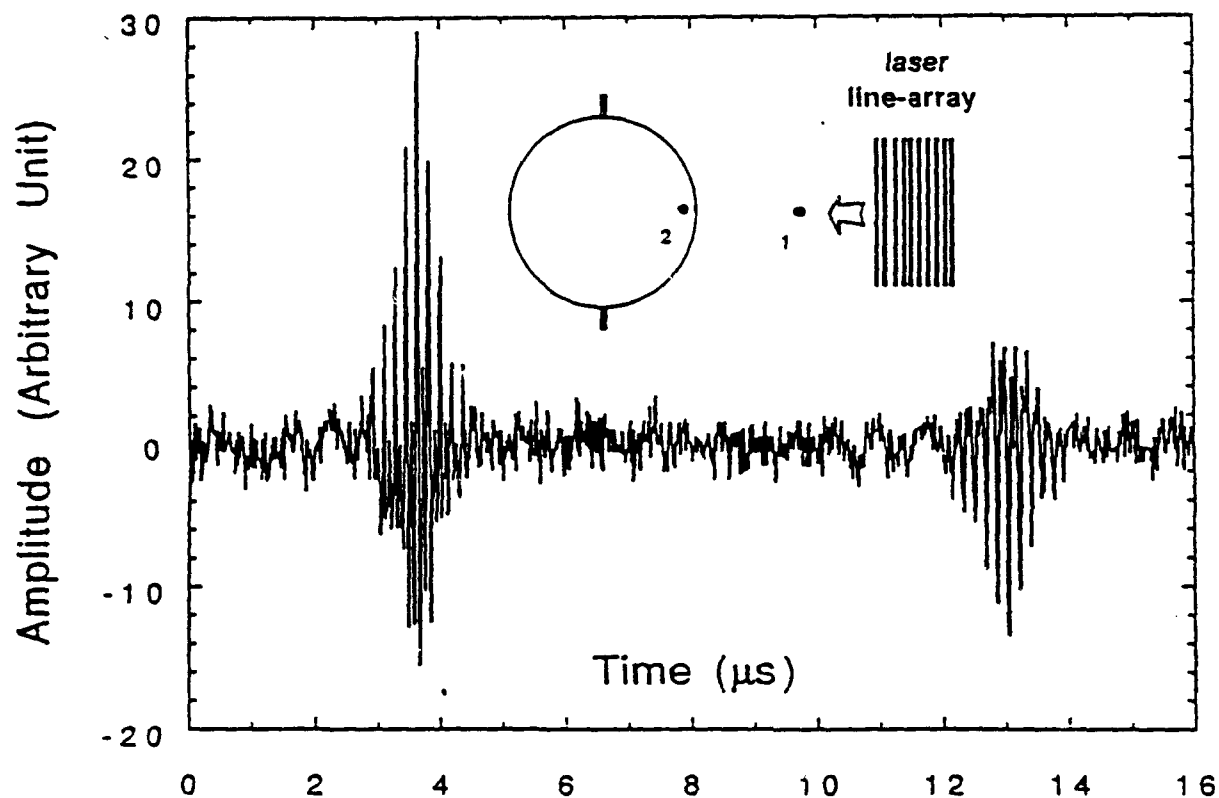
Signal in Time Domain



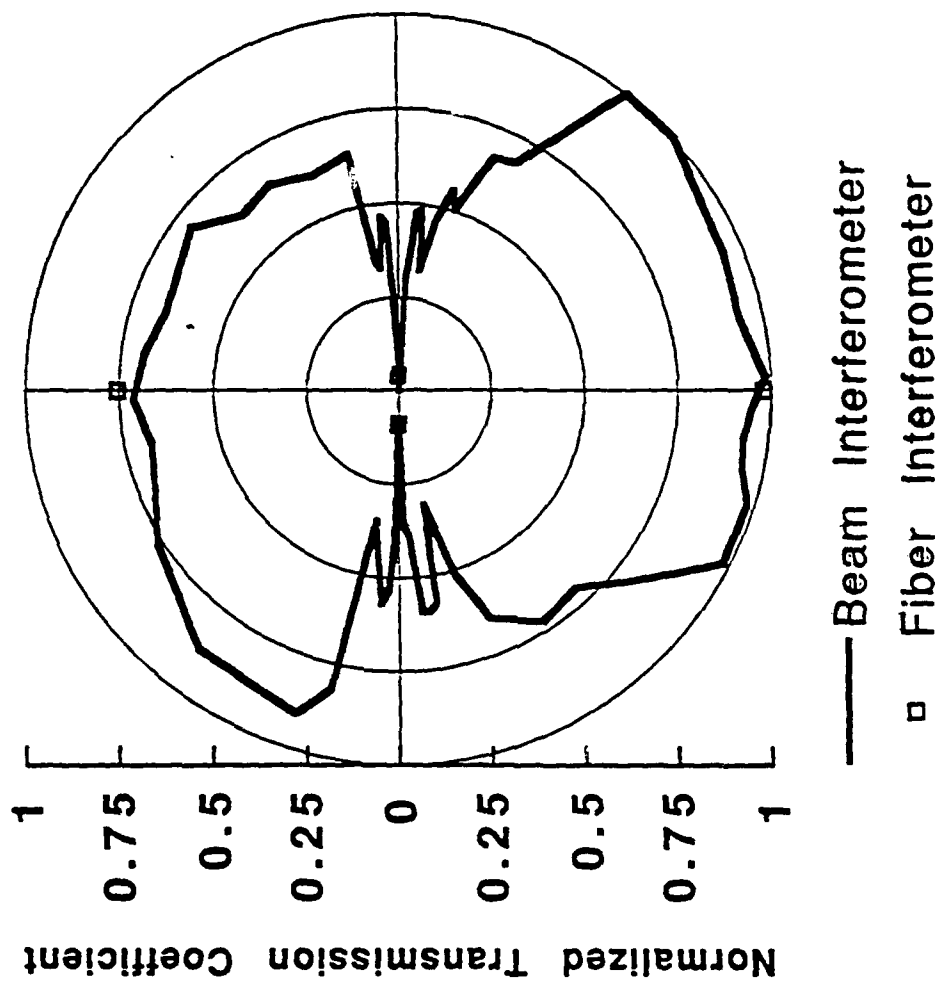
Signal in Frequency Domain



# Dual-Probe Fiber Interferometer Detection with Laser Generated Narrow-Band Signal

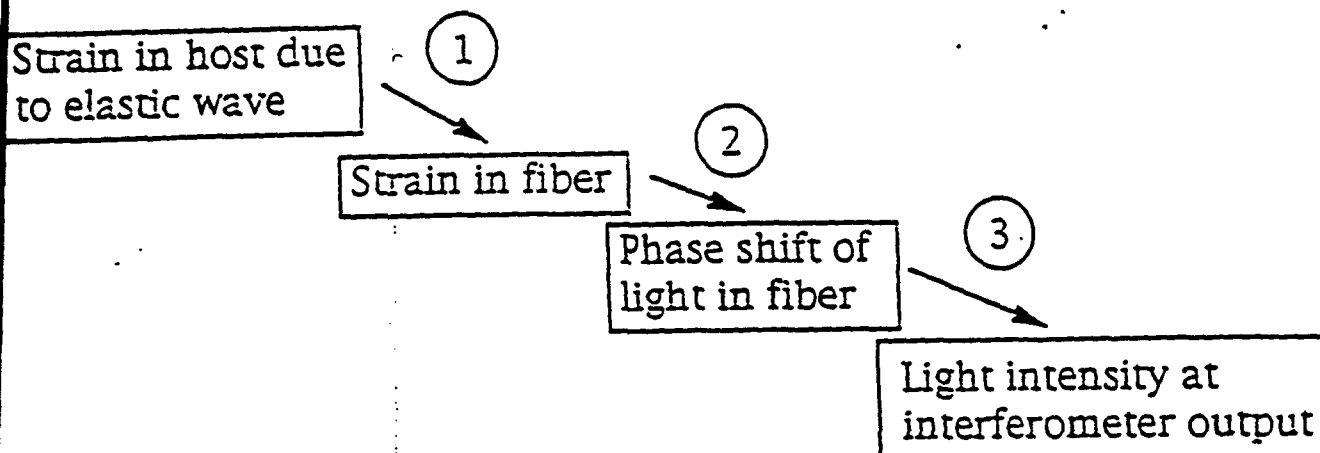


# Circumferential Scan of a Rivet Head

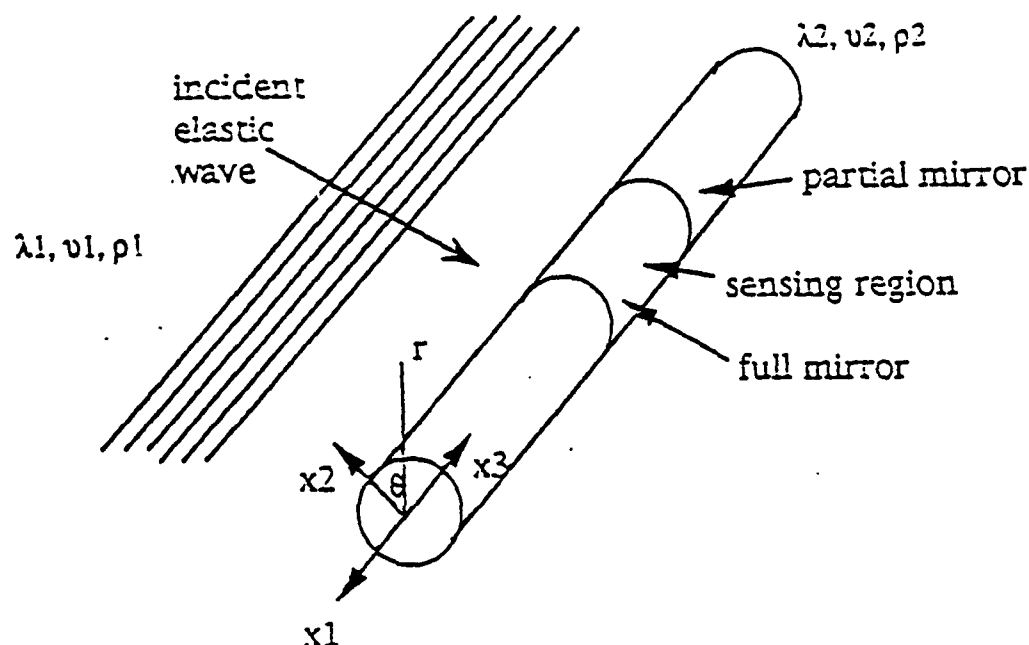


# Mechanical Interaction of Detector Components with Host

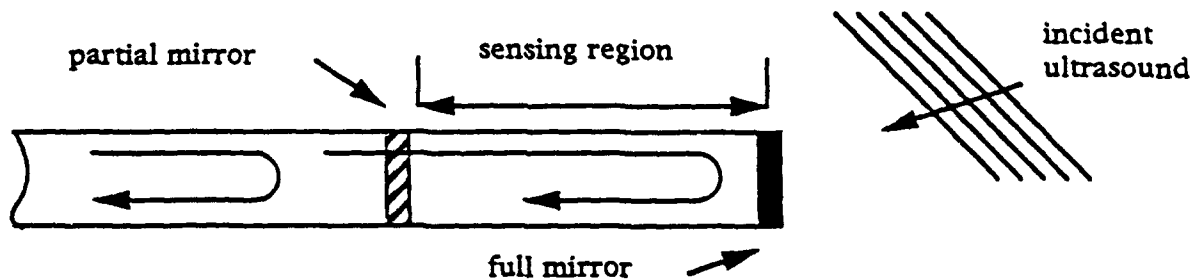
Steps in analysis:



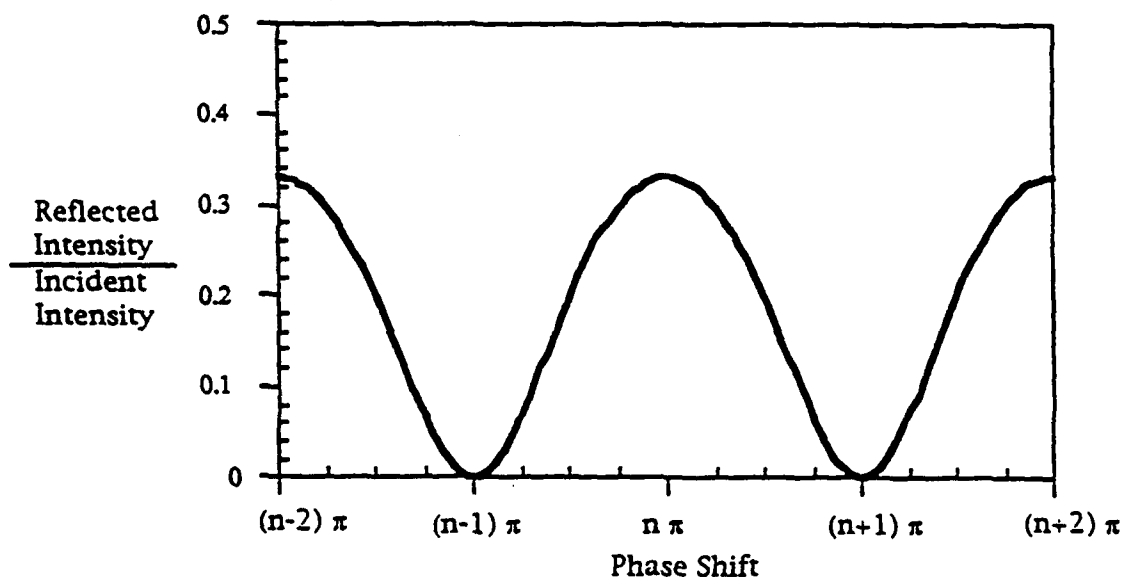
Geometry for analysis:



## Ultrasound Detection using Fiber Optic Fabry Perot Sensors



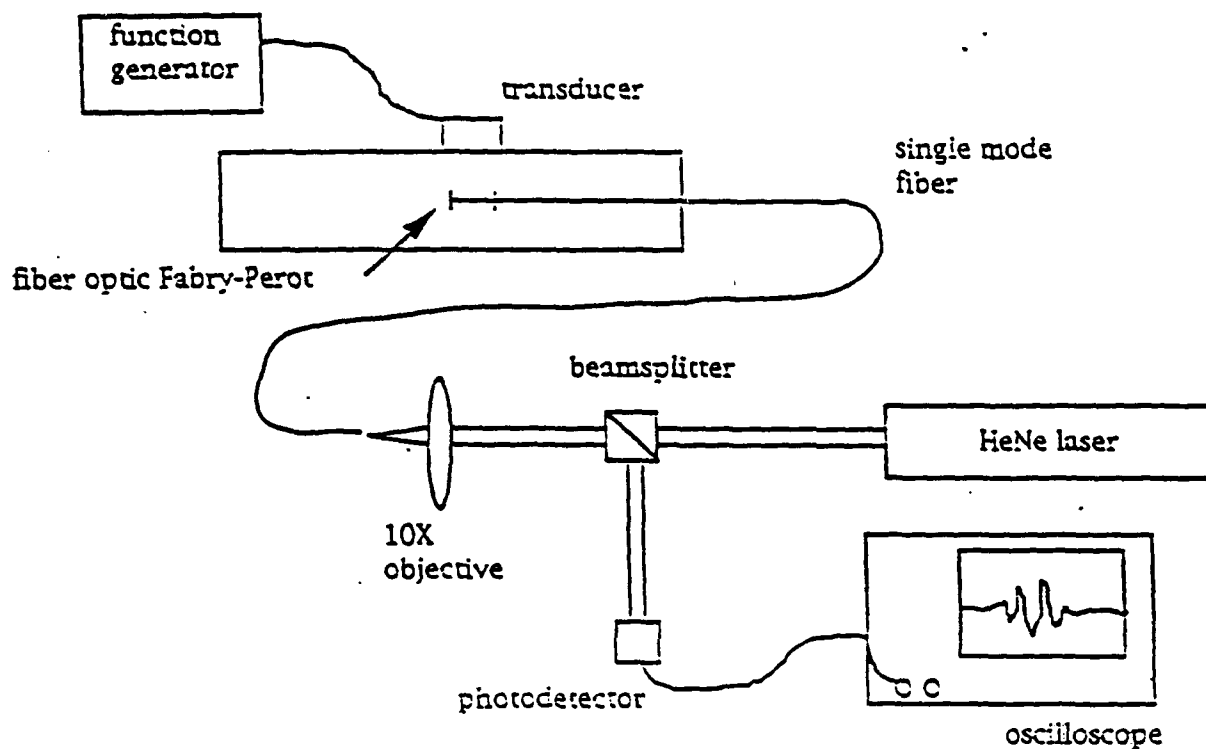
- Ultrasound induces length and refractive index changes in fiber producing phase shifts of light in fiber
- Phase differences between the light reflected from the full mirror and the partial mirror cause changes in the intensity of light reflected from the Fabry Perot cavity



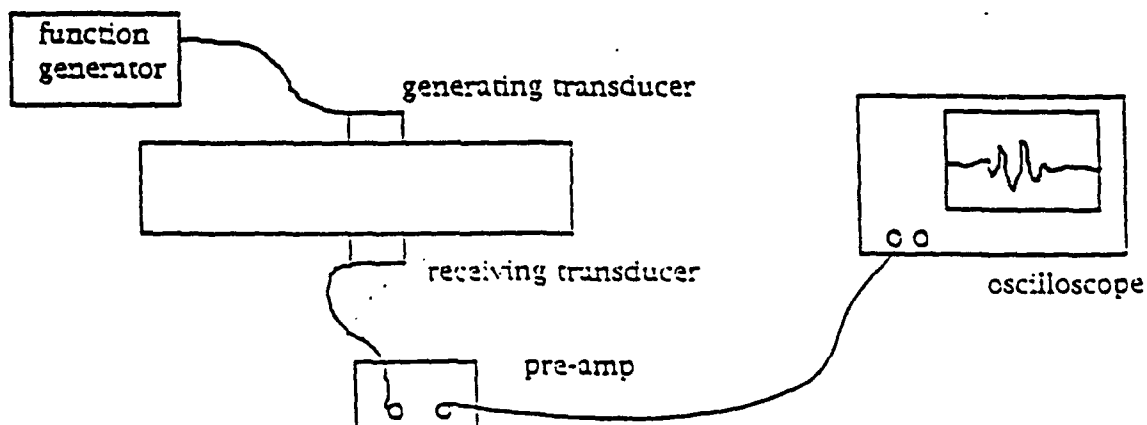
- Large amplitude signals produce large phase shifts and the reflected intensity sweeps through several maxima
- Ultrasound produces small phase shifts and the reflected intensity oscillates about a point
- From the measured light intensity output and knowledge of the Fabry-Perot sensor response, the ultrasonic signal can be obtained.



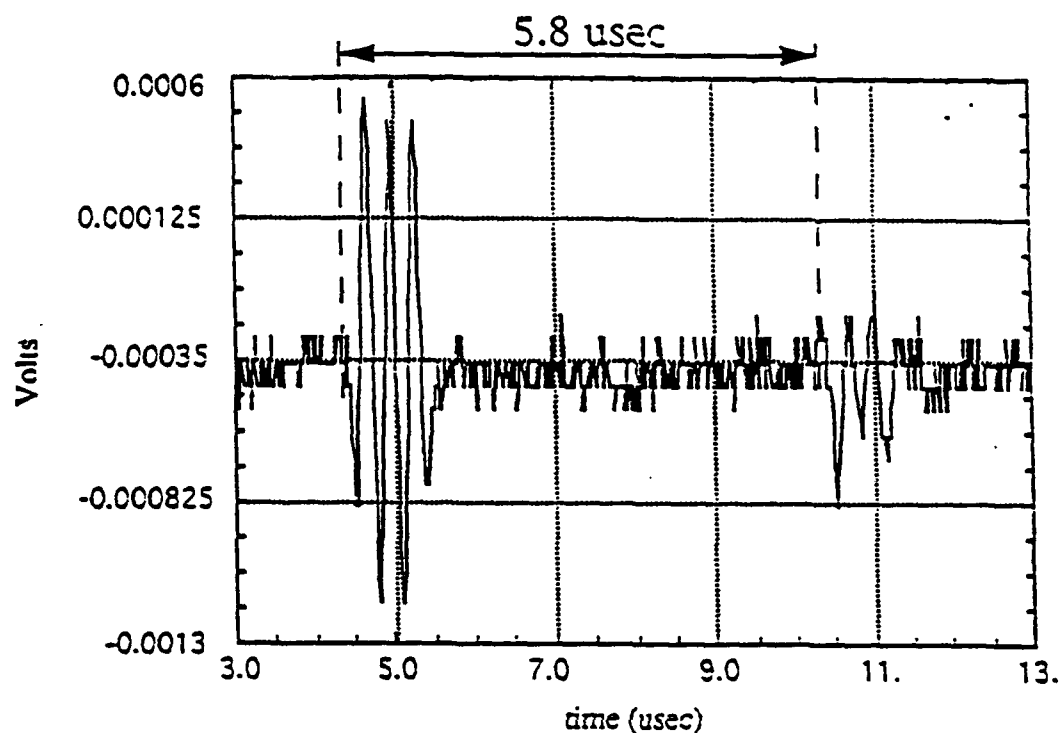
## Ultrasound Detection using Fiber Optic Fabry-Perot



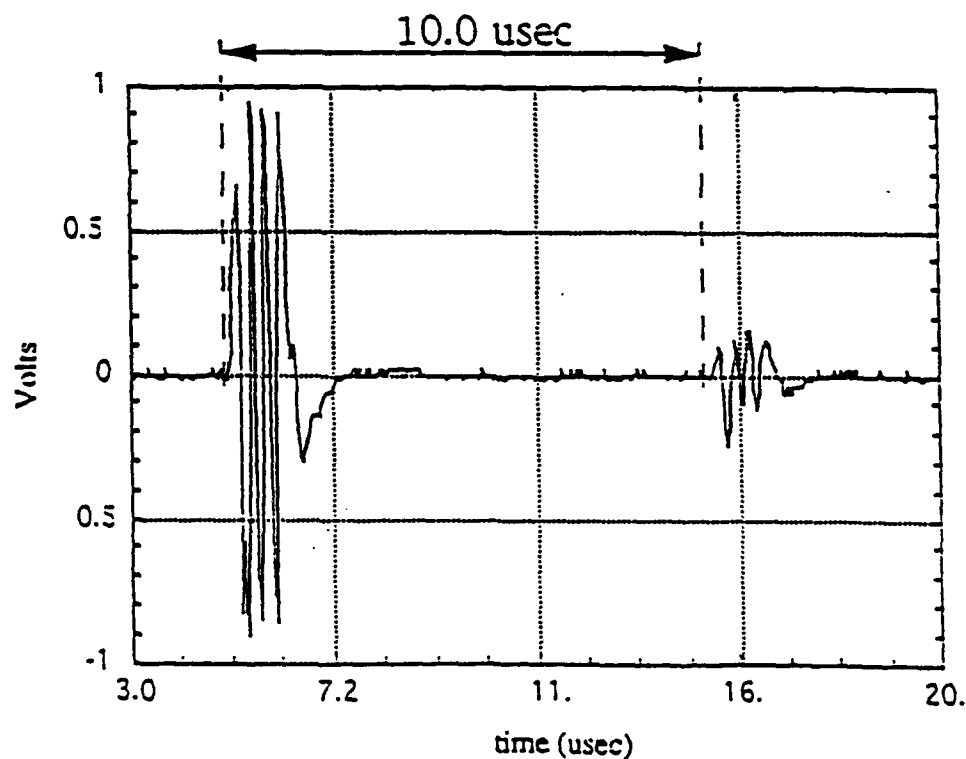
## Ultrasound Detection using Transducer



# 3.5 MHz three cycle tone burst detected with FOFP



## 3.5 MHz three cycle toneburst detected with transducer



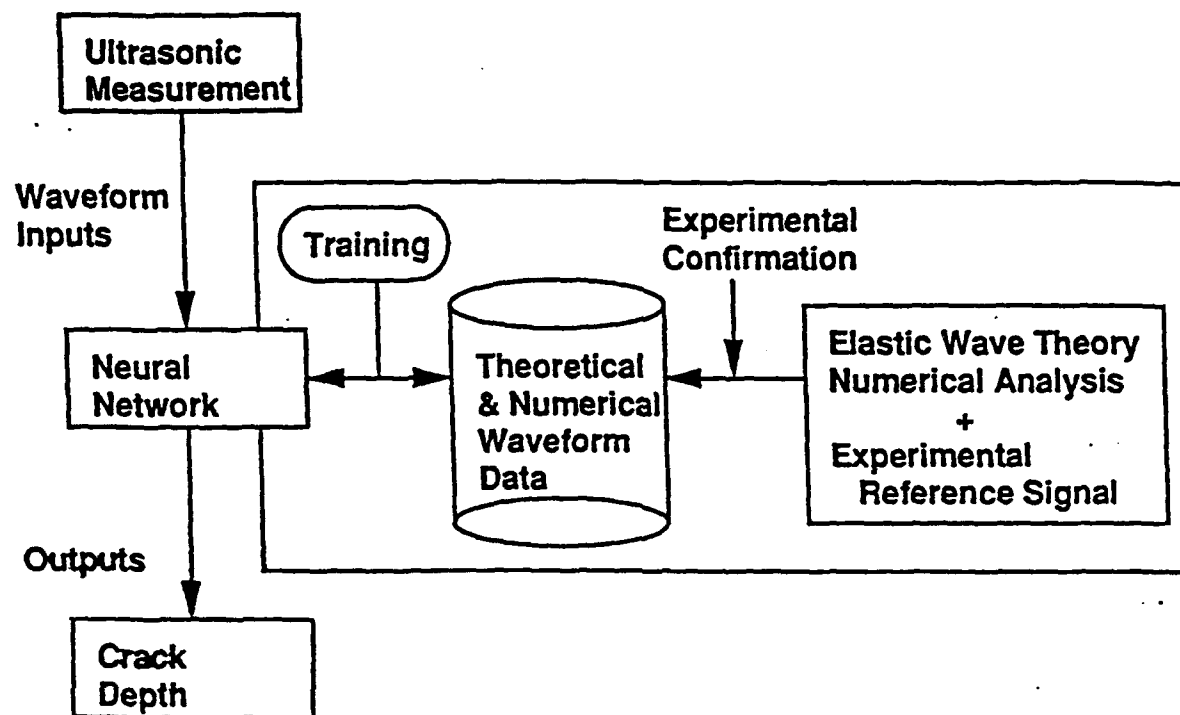
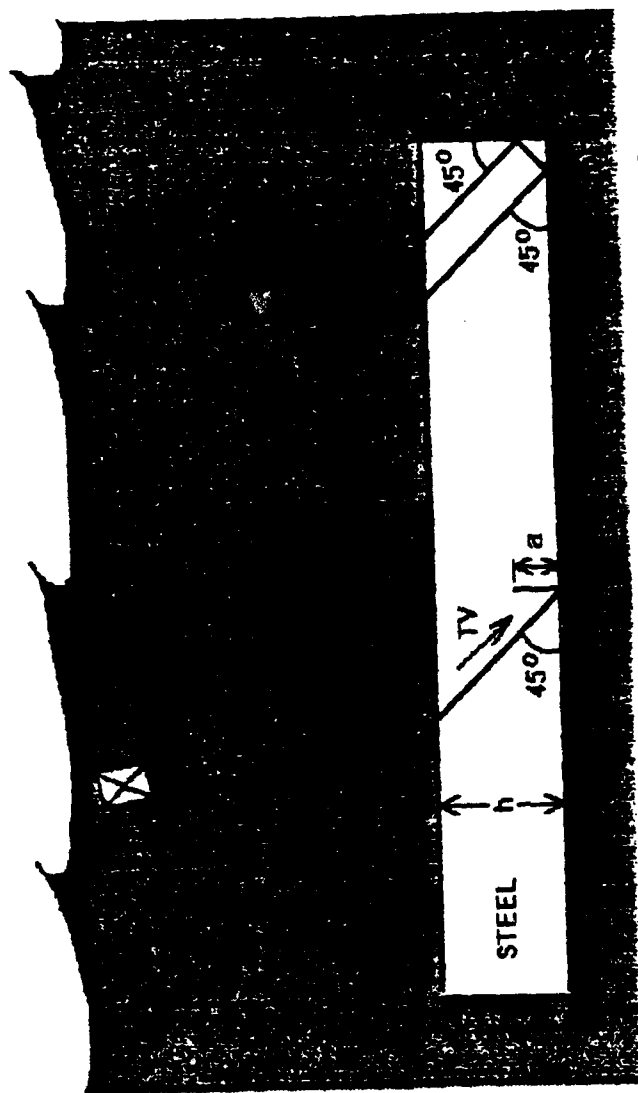
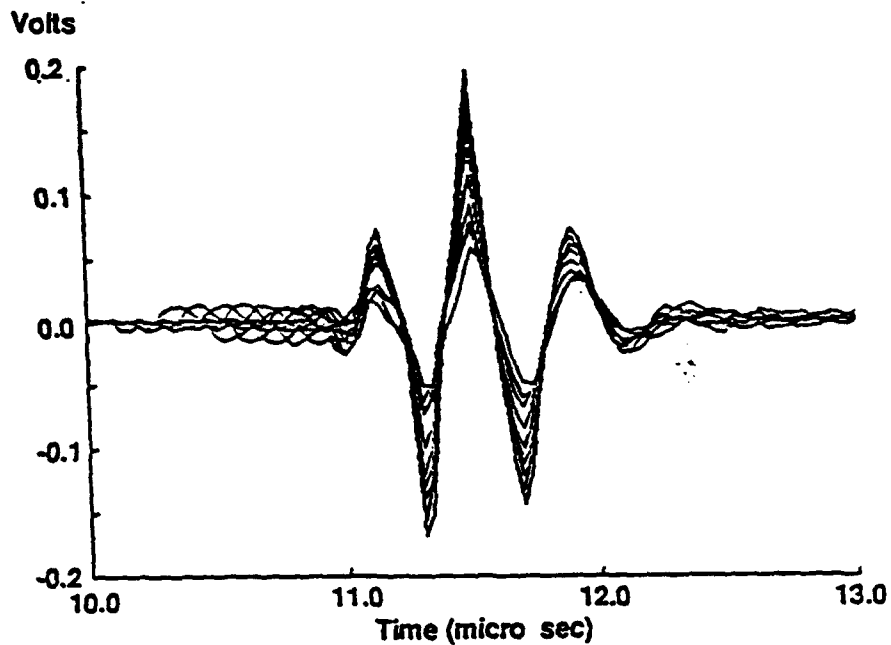


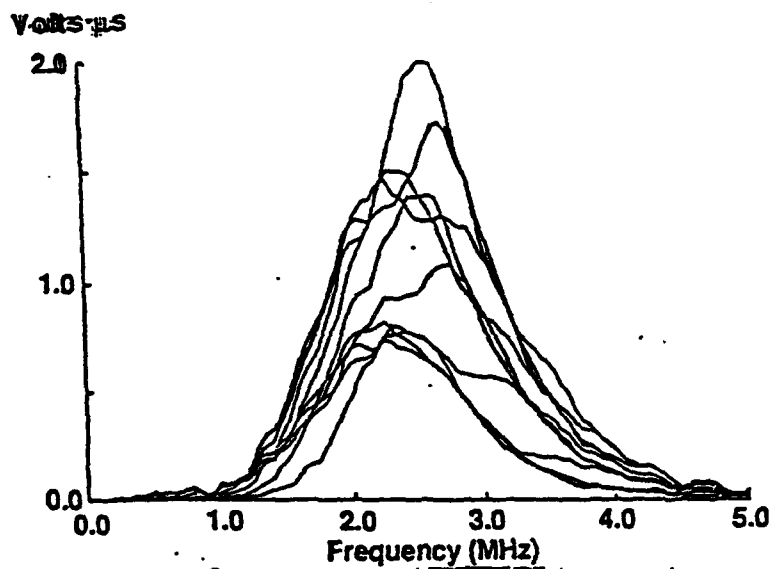
Fig. 3 Neural network system.



Surface breaking crack of depth 'a' in a steel plate (a).  
and corner reflection of the reference signal (b).



(a) Time domain training data



(b) Frequency domain training data

Fig. 4 Theoretical training signals for ten notch depths ranging from 0.6mm to 2.4mm with 0.2mm increments.

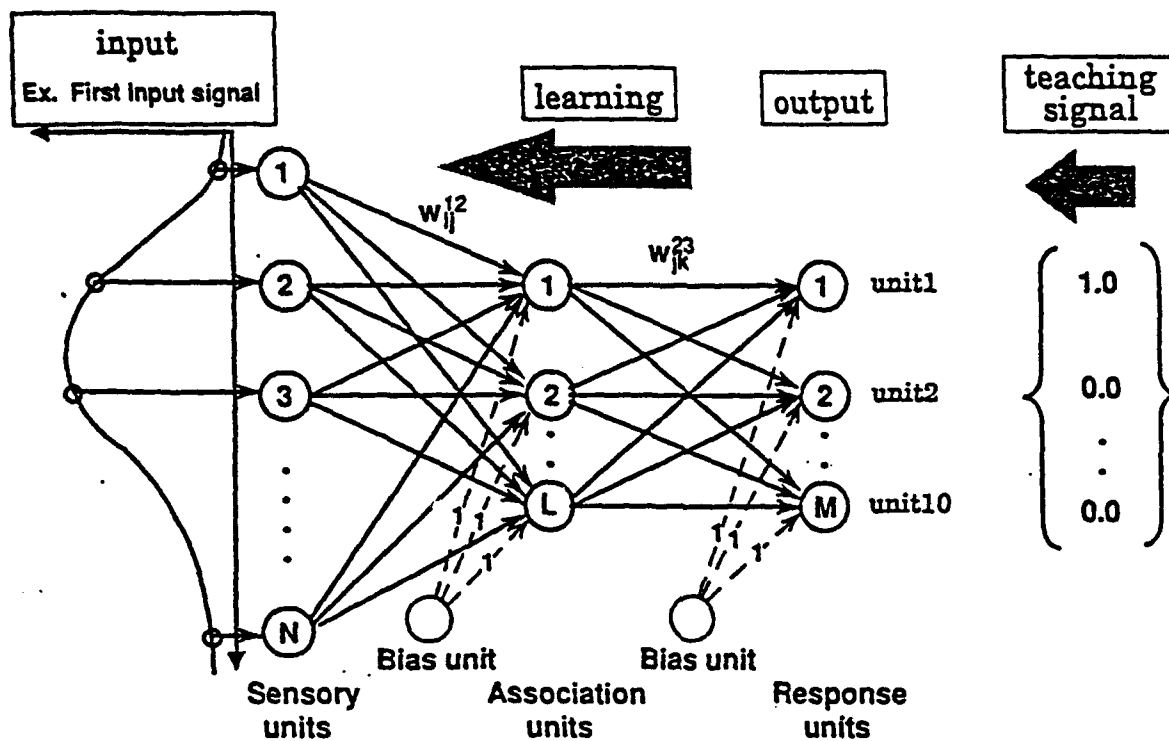


Fig.4 Three-layered feedforward network and an input signal, teaching signal and bias units.

	output unit	0.60	0.80	1.00	1.20	1.40	1.60	1.80	2.00	2.20	2.40
1.05mm	time	-	0.22	0.97	-	-	-	-	-	-	-
	freq.	-	-	-	0.99	-	-	-	-	-	-
1.49mm	time	-	-	-	-	0.52	0.45	-	-	-	-
	freq.	-	-	-	-	0.29	1.00	-	-	-	-
2.19mm	time	-	-	-	-	-	-	-	-	0.97	-
	freq.	-	-	-	-	-	-	-	-	0.98	-

## CONCLUSIONS

Quantitative Non-Destructive Evaluation is a systems approach which integrates the identification of appropriate state variables defining damage states and failure criteria with diagnostic techniques using suitable sensors, measurement models and data processing techniques to predict the reliability and safety of components.

Quantitative Non-Destructive Evaluation is the most important component of an interdisciplinary approach to Condition-Based Monitoring.

### SOME RELEVANT REFERENCES

(with D.O. Thompson), "Towards Quantitative Non-Destructive Evaluation of Aging Aircraft", in Structural Integrity of Aging Aircraft, Springer Series in Computational Mechanics, S.N. Atluri, S.G. Sampath and P. Tong (eds), 1990, pp. 1-13.

(with Jin Huang), "Dual-probe laser interferometer", J. Acoust. Soc. Am. 90, pp. 1269-1274, 1991.

(with Jin Huang and Sridhar Krishnaswamy), "Laser-generation of narrow-band surface waves", J. Acoustic Soc. Am. 92, pp. 2527-2531, 1992.

(with I.N. Komsky, Y.C. Lee and Y.C. Angel), "Self-Calibrating Ultrasonic Technique for Crack Depth Measurement", J. of Nondestr. Eval. 11, pp. 103-108, 1992.

"Measurement Models for Quantitative Ultrasonics", J. Sound and Vibration, 159, pp. 385-401, 1992.

(with M. Takadoya and M. Notake, M. Kitahara, Q.C. Guo and M.L. Peterson), "Crack-Depth Determination by a Neural Network with a Synthetic Training Data Set", Review of Progress in Quantitative Nondestructive Evaluation, Vol. 12, Eds. D.O. Thompson and D.E. Chimenti, pp. 803-810, 1993.

(with Yung-Chun Lee and Jin O. Kim), "V(z) curves of layered anisotropic materials for the line-focus acoustic microscope", J. Acoust. Soc. Am. 94, pp. 923-930, 1993.

(with S.M. McGuire, M.E. Fine, and O. Buck), "Nondestructive detection of fatigue cracks in PM 304 stainless steel by internal friction and elasticity", J. Mater. Res., 8, pp. 2216-2223, 1993.



# Aluminum nitride thin film sensor for force, acceleration, and acoustic emission sensing

L. Zheng, S. Ramalingam, T. Shi, and R. L. Peterson

*Productivity Center, Mechanical Engineering Department, University of Minnesota, Minneapolis, Minnesota 55455*

(Received 30 November 1992; accepted 27 March 1993)

To meet the real-time process monitoring and control needs in machining automation, aluminum nitride thin film sensors have been implemented on WC-Co cutting inserts by rf sputtering. These piezoelectric sensors detect force, acceleration, and acoustic emission signals. Method of constructing, characterizing and evaluating AlN piezoelectric sensors are presented here. It is shown that *c*-axis oriented AlN films can be deposited on WC-Co substrates to sense force, acceleration and acoustic emission signals. As the transducer characteristics vary with rf sputtering conditions, parametric studies have been carried out to determine "best processing" conditions to obtain the needed transducers sensitivities and process reproducibility. Results of these studies are also presented here. It is shown, in addition, that AlN films deposited WC-Co can provide useful signals even though the cutting tool substrate may experience temperature rise during use in metal machining.

## I. INTRODUCTION

Chemical vapor deposition (CVD) and physical vapor deposition (PVD) processes are now in wide use to improve the wear life of cutting tools. To secure best benefit from the single or multilayer hard compound films deposited with these processes, coated tools are used at higher metal removal rates so that the tool life obtained in cutting is between 20 and 60 min. The frequent tool replacement necessitated by this is a problem in automated machining since frequent operator attention is called for. If tool replacement by the operator is scheduled at fixed time intervals, some tools are replaced prematurely and some tools will continue in use beyond wear limit. This is due to distributed wear life common in coated and uncoated cutting tools. Weibull-distributed life, for example, is common in TiN-coated drills. Tool condition monitoring can be useful to overcome the distributed life problem in automated machining. By condition monitoring, the actual end point of tool life is detected so that every tool is used to the limit of its useful life.

Force, acceleration, and acoustic emission signal sensing are frequently used to determine the tool condition during machining. Strain gage and piezoelectric crystal dynamometers can be used to sense the change in the magnitude and direction of the cutting forces with tool wear<sup>1,2</sup> to determine the tool condition. Piezoelectric accelerometers may be used to sense changes in vibration modes to infer tool condition. Acoustic emission (AE) signals generated during machining and from tool fracture may also be used for tool condition monitoring.<sup>3,4</sup>

Thin film piezoelectric transducers exhibit natural frequencies in the MHz range. Sputter deposited, piezoelectric sensors, constructed directly on a nonworking surface of a cutting tool, offer a means of implementing acoustically bonded AE transducers in cutting tools. High transducer sensitivity is realized by positioning the transducer close to the signal source and the signal distortions avoided

by doing so can make less severe demands on signal conditioning circuitry. Robust and affordable tool condition monitoring systems then become accessible by integrating the transduction function of the thin film sensor with the cutting function of the carbide substrate.

When transducer sensitivity is high, by positioning the signal conditioning electronics close to the transducer, useful dc as well as ac signals can be secured. Hence, with thin film piezoelectric transducers force, acceleration, and acoustic emission signals can all be acquired with a single sensor to implement a robust, multiparameter tool condition sensing system.

We have constructed piezoelectric thin film transducers on WC-6% Co substrates. Proof-of-principle was demonstrated with ZnO sensors.<sup>5</sup> Sputtering and photolithographic processes were used for film deposition and sensor delineation respectively on commercially available WC-Co cutting inserts. Subsequently aluminum nitride transducers have been implemented. As AlN transducer sensitivity varies with film deposition conditions, studies have been carried out to identify the film deposition conditions which provide better transducer sensitivities and yields. Force, acceleration, and acoustic emission sensing characteristics of instrumented cutting inserts have been determined. Performance characteristics of the integrated sensor have also been evaluated in machining tests. Results obtained are presented and discussed in this article.

## II. EXPECTED TRANSDUCER CHARACTERISTICS

Cobalt-bonded tungsten carbide cutting inserts (square, triangular and other standard shapes) are in wide use for machining. Edge dimensions of the cutting inserts vary between 10 and 40 mm, and thicknesses range between 3 and 15 mm. To develop the notion of an *instrumented* insert with an integral thin film piezoelectric sensor and to estimate the anticipated sensor characteristics, we assume use of a 12 mm square cutting insert, 3-5 mm in thickness,

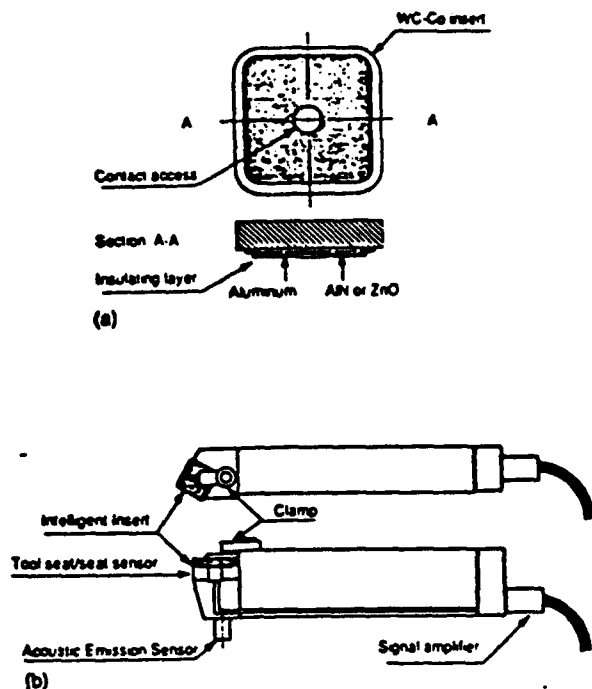


FIG. 1. (a) Schematic of a thin film sensor fabricated on a 12 mm square WC-6% Co insert. (b) Working configuration of the instrumented insert in the tool holder. An acoustic emission transducer is attached to the tool holder as shown to compare thin film sensor performance in the 100–500 kHz frequency band against that of a commercial AE sensor.

shown in Fig. 1(a). An insert of this type is held in a tool holder during use with finger clamps of the form shown in Fig. 1(b).

An instrumented cutting insert is realized by depositing a piezoelectric thin film sensor on the lower surface of the insert and overlaying it with a metal electrode. To prevent electrical shorting during use, the sensor is encapsulated with an insulating layer. A small opening is provided on the lower side of the insulating layer to make electrical contact with the piezotransducer. The substrate serves as the ground electrode of the piezosensor. One way of implementing an instrumented insert is shown schematically in Fig. 1(a).

A 10 mm square sensor can readily be implemented on a 12 mm square cutting insert. If the sensor implemented is 2  $\mu\text{m}$  thick, expected charge or voltage sensitivities of the transducer can be estimated from piezoelectric equations. Let  $E$ ,  $D$ ,  $T$ , and  $S$  represent the electric field, electric displacement, stress and strain respectively. Taking the electric field, strain, etc., to be in the same direction, and assuming a linear elastic material, the piezoelectric equations are:

$$D = dT + \epsilon^T E, \quad (1)$$

$$S = s^E T + d^E E, \quad (2)$$

where  $\epsilon^T$  is permittivity at constant stress and  $s^E$  is compliance at constant field. If the transducer surface area is

not changed by the stress applied, then  $d = d'$  is the piezoelectric charge constant in  $\text{C/N}$  units. Inverting Eq. (1) yields

$$E = gT + D(\epsilon^T)^{-1}. \quad (3)$$

Here  $g = d/\epsilon^T$  is the piezoelectric voltage constant.

Taking the sensor to be made of ZnO or AlN, and assuming that the thin film sensor is constructed such that the  $c$  axis of the film is normal to the substrate surface, the expected charge sensitivities for the piezotransducers are estimated from  $d_{31}$  values tabulated by Ikeda<sup>6</sup> as

$$\text{ZnO: } 12.4 \text{ pC/N}^{-1},$$

$$\text{AlN: } 5.0 \text{ pC/N}^{-1}.$$

Relative permittivities,  $\epsilon^T/\epsilon_0$ , of ZnO and AlN are 10.9 and 10.7 (data of Ikeda). For the assumed transducer dimensions, expected voltage sensitivities of ZnO and AlN sensors are therefore 2.57 and 1.06 mV/N, respectively.

Temporal response of a piezoelectric transducer, i.e., the charge decay time, is estimated from the dielectric relaxation time  $\tau_R$  given by

$$\tau_R = \rho \epsilon^T \epsilon_0, \quad (4)$$

where  $\rho$  is resistivity and  $(\epsilon^T \epsilon_0)$  is the dielectric permittivity. Thin film piezotransducers, however, exhibit much larger time constants than those predicted by the  $\rho \epsilon$  product. In thin film piezotransducer structures, film thickness  $t$  is much smaller than the Debye length  $L_D$ , and the large time constants observed have been attributed to the large  $L_D$ .<sup>7</sup>

The calculated charge and voltage sensitivities for the thin film ZnO and AlN transducers and the large dielectric relaxation times possible with thin film piezoelectric transducers suggests that dc cutting force measurements should be possible with the sensor dimensions envisaged (10 mm  $\times$  10 mm  $\times$  2  $\mu\text{m}$ ). As the principal cutting force under commercial cutting conditions can range from 100 N to a few kN, high gain (80–to 100 dB) signal amplifiers would not be necessary for tool condition monitoring with thin film piezotransducers.

Since induced accelerations from 10 to 100 g or more are probable when the cutting force on the tool holder is removed suddenly by cutting insert fracture, it should be possible to sense tool fracture in real-time by monitoring the ac component of the transducer signal in the 1–10 kHz frequency range (bandwidth of the dominant tool holder natural frequencies). The displacement amplitudes anticipated from acoustic emission signals are, however, very much smaller, and most probably in the nm range. Therefore, for the same transducer to function as a force, acceleration, and AE transducer, signal conditioning with a moderate amplifier gain (40–60 dB) would be necessary.

Calculated charge and voltage sensitivities suggest that both ZnO and AlN thin film sensors can fulfill the requirements for real-time tool condition monitoring. Transducer films deposited must have a preferred texture, i.e., the polycrystalline thin film transducers deposited must have  $c$ -axis oriented normal to substrate surface. Signal sensitivity will

vary with relative perfection obtained in film texture. Transducer dc performance will vary with film resistivity with high resistivity films preferred for best dc performance.

### III. PRIOR WORK ON PROOF-OF-PRINCIPLE

A number of materials are available to construct piezoelectric thin film transducers. They include relatively simple binary compounds (CdS, CdSe, ZnS, ZnTe, ZnO, AlN), and more complex ceramic materials (barium titanate, niobates, PZT). Some of these materials are well suited to implement piezoelectric sensors using PVD processes (PZT, ZnO, AlN). Two of these materials, ZnO and AlN, can be deposited on a range of substrate materials using inexpensive metallic targets.

To demonstrate proof-of-principle, ZnO films were rf sputter deposited on diamond-polished, cutting tool grade WC-6% Co substrates. The c-axis oriented, colorless, transparent piezofilms (1–1.5  $\mu\text{m}$  thick) deposited with an undoped zinc oxide target (200 mm diam) were covered with sputtered aluminum contact layers (0.5  $\mu\text{m}$ ). Photolithographic techniques were then used to delineate sensor geometry. Patterned transducers constructed were overlaid with glass films (0.5  $\mu\text{m}$ ; e-beam evaporation). An opening was then made in the glass layer (photolithography and etching) to acquire signals from the piezoelectric transducer.

Test stand measurements using an electromagnetic shaker and a calibrated force transducer showed that satisfactory ZnO-based piezosensors can be implemented on WC-Co substrates.<sup>8</sup> Machining tests with instrumented inserts demonstrated that real-time tool condition sensing and fracture detection are both possible with ZnO-based thin film sensors.<sup>9</sup> The transducers constructed exhibited substantial scatter in the measured piezoelectric voltage constant ( $g_{33}=0.022\text{--}0.072\text{ V m N}^{-1}$ ; 17.1%–56% of zinc oxide  $g_{33}$  values calculated with the data tabulated by Ikeda<sup>6</sup>) and a large decrease in  $g_{33}$  in the 25 to 110 °C temperature range (~75%–80%).

Bulk temperature rises of 200–300 °C or more are common in cutting inserts during commercial use in automated machining systems. Aluminum nitride, a covalent-bonded ceramic with a higher hardness ( $H_V\sim 12.60\text{ GN m}^{-2}$ ), a larger band gap (6 eV) and a much higher usable temperature range (1200 °C) is therefore a more appropriate transducer material. Aluminum nitride thin film piezoelectric sensors were hence implemented on carbide cutting inserts. Performance characteristics of the instrumented inserts vary as a function of AlN film deposition conditions. Work reported here is concerned primarily with this aspect of sensor fabrication and evaluation of performance characteristics.

### IV. ALUMINUM NITRIDE SENSOR CONSTRUCTION

Aluminum nitride films can be deposited by rf sputtering using an AlN target or by reactive sputtering in an Ar-N<sub>2</sub> ambient using an aluminum target. A 1.5 kW, 13.56 MHz rf power supply was used in this work for

reactive sputtering of AlN from a 200 mm diam, high purity aluminum target. A diffusion-pumped, 500 mm diam stainless steel vacuum chamber equipped with a throttling valve for pressure control was used. Following throttling, total chamber pressure and nitrogen partial pressure were controlled by varying argon and nitrogen gas flow rates. MKS Model 0258B flow meters and a capacitance gage (Baratron Model 370 HA) were used to monitor gas flow rates and chamber pressure. The chamber is equipped with a substrate carrier which could be heated or cooled as required. When needed, a Leybold Inficon Quadrex PPC 017-450-G1 quadrupole mass spectrometer was used to monitor chamber partial pressures.

Processing steps involved in substrate preparation before AlN film deposition are as follows: (a) lap commercial grade, WC-6% Co cutting tool insert substrates on cast iron laps using progressively smaller diamond grits till the substrate surface is "mirror finished" and free from scratches; (b) acetone clean in an ultrasonic bath for 5 min; (c) methanol clean in an ultrasonic bath for 5 min; (d) clean with fresh isopropyl alcohol in an ultrasonic bath for 5 min; (e) DI rinse, N<sub>2</sub> blow dry and load immediately into the vacuum chamber. Coating chamber was usually pumped over night (16–20 h) to obtain base pressure in the low  $10^{-7}$  Torr range. Before each coating run, substrates to be coated were preheated to 473 K for 1–2 h at base pressure.

The target was presputtered for 1 h with a shield in position. Presputtering and film deposition were carried out in an Ar-N<sub>2</sub> ambient. All sputtering operations were carried out at a chamber pressure in the mTorr range and cathode power in the 200–900 W range. The matching network used kept the reflected power below 10 W during all phases of film deposition. Measured film deposition rate under the sputtering conditions used was in the 0.2–0.5  $\mu\text{m h}^{-1}$  range. Typical coating runs lasted some 4–8 h to obtain 2  $\mu\text{m}$  thick transducer films. Due to electron and ion bombardment, substrate temperature tended to rise during film deposition. A substrate holder temperature control system was used to select and maintain the desired substrate temperature.

Without breaking vacuum, a 0.6  $\mu\text{m}$  thick aluminum contact layer was deposited on top of the AlN layer in a subsequent sputtering run after shutting off gas flows and reaching a base pressure of less than  $5\times 10^{-7}$  Torr. This usually required some 10–16 hour delay between AlN and Al deposition. Aluminum cathode was presputtered with a shield in position for 30 min to remove traces of nitrogen-poisoned layers from the cathode surface, and the metal film was then laid at a chamber pressure of 8 mTorr in a 100% Ar ambient. Film deposition was carried out at a cathode power of 400 W with substrates maintained at 373 K. Film deposition rate obtained was 1  $\mu\text{m/h}$ . Hence the electrode layer could be deposited in a 40 min coating run.

Transducer geometry was photo-lithographically delineated by spinning on Shipley S1400-27 photoresist at 3000 rpm for 25 s (1.5  $\mu\text{m}$  per spin cycle; 2 cycles for 2.0  $\mu\text{m}$  total resist thickness), soft baking the resist at 363 K for 30 min, exposing the resist with a photomask, and developing

the resist (5:1 developer-DI water solution) for 30 s. Following DI rinse and  $N_2$  blow drying, unwanted transducer/contact layer film around the periphery, defined by patterning, was etched off in a 1:1 DI:HCl solution (30 min etch). To encapsulate the transducer, a sol-gel film of Glassclad PS 233 was spun on at 700 rpm for 20 s ( $0.5 \mu\text{m}$  per spin cycle; 3 cycles for  $1.5 \mu\text{m}$  total thickness) and hard baked for 2 h at 573 K. Electrical access to the aluminum electrode layer was obtained by using a "stop-off" before spinning on the sol-gel layer and removing the stop-off with a solvent.

The completed transducer, thus, has a WC-Co substrate which serves as the ground electrode of the piezosensor and a sol-gel film encapsulation layer with a small opening in it for signal acquisition.

## V. SENSOR CHARACTERIZATION AND EVALUATION

### A. Sensor characterization with x-ray peak height measurements

Performance characteristics of fabricated sensors depend on the piezoelectric properties of the transducer film. For the transducer to be sensitive to the normal forces applied, the polycrystalline AlN films deposited must have c-axis oriented normal to the substrate surface. Piezoelectric voltage sensitivity of the sensor degrades rapidly with deviation from perfection in the preferred texture. X-ray diffractometry was used to assess this aspect of film quality with AlN x-ray peak height (0002 peak at  $2\theta = 36.04^\circ$ ) as a measure of texture perfection. An x-ray diffractometer with a copper target operating at a fixed acceleration voltage, beam current, detector voltage, and scanning speed was used. Peak heights (counts) were determined as a function of sputtering conditions to identify the "best process" for sensor film deposition.

### B. Sensor evaluation for quasi-static force sensing

When a quasistatic load is applied normal to the AlN sensor surface, force applied can be determined by measuring the charge output. dc sensitivity of AlN films deposited on WC-Co and silicon substrates were determined in an MTS load frame. A charge amplifier built for use with thin film transducers (Fastman, Inc., Bethlehem, PA) permitted the measurement of the charge signal generated in response to an applied load. Piezoelectric charge constant  $d_{33}$ , is determined directly under quasistatic loading conditions.

### C. Sensor evaluation for acceleration sensing

The sensitivity of the piezotransducer to low frequency dynamic signals was determined in a purpose-built test stand. A PZT disc, 50 mm in diameter (2 in. diam) and 3 mm in thickness ( $1/8$  in.), driven at 1 kHz was used to apply a time-dependent force to the instrumented insert held between the PZT driving crystal and a Kistler Model 912 H load cell. Drive signal obtained from a Krohn-Hite Model 5400 B function generator was used to drive a field

effect transistor (FET) power amplifier which in turn was used to excite the PZT driver. Calibrated load cell signal was amplified with a Kistler Model 5004 charge amplifier. Unamplified voltage signal from the instrumented insert and the load cell signal were simultaneously tracked and recorded in a digital oscilloscope.

This test provides voltage signal  $\Delta V$  generated by the application of a time-dependent  $\Delta F$  force, to derive a "generator coefficient"  $G$  (different from  $g_{33}$ ) defined as below. Let  $P$  be the polarization and  $s$  the strain in a piezoelectric material. For a piezoelectric functioning in the generator mode,  $G$  is defined as

$$G = \partial P / \partial s | \xi \text{ C m}^{-2}, \quad (5)$$

where  $\xi$  is the electric field. Since  $s = \sigma / E$ , where  $E$  is the elastic modulus,

$$G = E \partial P / \partial \sigma | \xi \text{ C m}^{-2}. \quad (6)$$

Application of an incremental force  $\Delta F$  to the piezofilm generates a change in polarization, i.e., an incremental charge  $\Delta Q$ . Capacitance  $C$  of the sensor comprised of the two electrodes with an intervening layer of a piezoelectric material with a dielectric constant  $\epsilon$ , responds to  $\Delta Q$  by exhibiting a change in voltage  $\Delta V$  corresponding to  $\Delta F$ . Measured voltage signal  $\Delta V$  and excitation  $\Delta F$  are related through the dimensions of the sensor (area  $A$  and thickness  $t$ ) and the properties of the sensor film ( $\epsilon$ , and  $E$ ).

$$G = (\epsilon \epsilon_0 A E / t) \Delta V / \Delta F \text{ C m}^{-2}. \quad (7)$$

$G$  value reported is a composite measure of film quality which includes variations in permittivity accompanying changes in film deposition conditions, and is based on measured  $\Delta V / \Delta F$ ,  $A$ , and  $t$ , and published<sup>6</sup> values for  $\epsilon$ , and  $E$ .

### D. Sensor evaluation for temperature sensitivity of the transducer

Temperature dependence of AlN sensors was determined by equipping the test stand with a small button heater (MINCO H7420115). The test assembly was heated and allowed to reach thermal equilibrium. Standard contact thermocouple temperature measurements were made to determine the instrumented insert/sensor temperature. Generator coefficient  $G$  of the transducer as a function of test temperature was then determined over the 298–473 K temperature range using the procedure described in the previous paragraph.

### E. Sensor evaluation: Bench tests for acoustic emission sensing

Acoustic emission characteristics in the 100–500 kHz frequency range were determined by using the Hsu lead-fracture test. A 0.5 mm diam (grade HB) mechanical pencil lead was fractured on the upper surface of the instrumented insert or seat sensor. Time-domain signal and frequency spectra from the AlN insert sensor and a commercial acoustic emission sensor were acquired to compare

the AE signal sensing characteristics of these two sensors. The commercial AE sensor was attached to the lower face of the tool holder, as shown in Fig. 1(b).

#### F. Sensor evaluation: Acoustic emission characteristics in cutting tests

To assess the AE sensing characteristics of the instrumented insert during metal machining turning tests were carried out in a numerically controlled lathe. Medium carbon steel work pieces were machined at a cutting speed of  $3.5 \text{ m s}^{-1}$ . Feed rates and depth of cut used were  $0.23 \text{ mm}$  per revolution and  $2 \text{ mm}$ , respectively. Signals from the thin film AlN sensor and a commercial AE sensor [attached to the tool holder as shown in Fig. 1(b)] were acquired. A 100–500 kHz band-pass filter was used.

### VI. RESULTS

#### A. Effect of process variables on film quality determined with x-ray peak height measurements

Variations in sputtering conditions, i.e., the coating pressure, coating ambient, cathode power and substrate temperature, affect film texture, i.e., sensor film quality. Peak height determined with x-ray diffraction analysis was used for process development. Figure 2(a) shows the (0002) peak from an AlN film deposited on silicon. Peak profiles obtained by x-ray diffraction scanning a WC-Co insert are shown in Fig. 2(b). A corresponding pattern from a WC-Co insert covered with rf sputtered aluminum nitride is shown in Fig. 2(c).

In films deposited with good *c*-axis orientation, (0002) planes lie parallel to the substrate surface. The dominant peaks observed at  $2\theta = 36.04^\circ$  in Figs. 2(a) and 2(c) indicate that the *c* axis of the polycrystalline AlN film is oriented normal to the surface of both the silicon wafer and WC-Co insert. X-ray diffraction trace of the WC-Co substrate, Fig. 2(b) shows a dominant peak at  $35.8^\circ$ , which makes it difficult to separate the AlN peak at  $36.04^\circ$  from the  $35.8^\circ$  peak in the WC-Co substrate. This difficulty was handled by comparing ratio of heights of the two dominant peaks observed and deriving the increment due to AlN in the largest peak.

Selected data, from a large number of process development runs, demonstrating the influence of sputtering process variables on AlN film texture on silicon, is presented in Table I. X-ray peak height in counts/second and the measured *G* coefficient are taken to be the primary indicators of transducer film quality.

Transducer elements deposited at 9 mTorr total pressure in a 50:50 argon-nitrogen ambient yielded transducers with the most sensitivity. Intensity of the (0002) peak observed indicates that these films have good *c*-axis orientation. Performance of sensor suffered as the  $\text{N}_2$  partial pressure is reduced, presumably due to loss of stoichiometry. It was noted that the resistivity of the film produced also decreased with a decrease in  $\text{N}_2$  partial pressure, implying deposition of a metal rich film. Depositions made at a lower total gas pressure exhibited reduced piezoelectric sensitivity. Possible reasons for this were not examined.

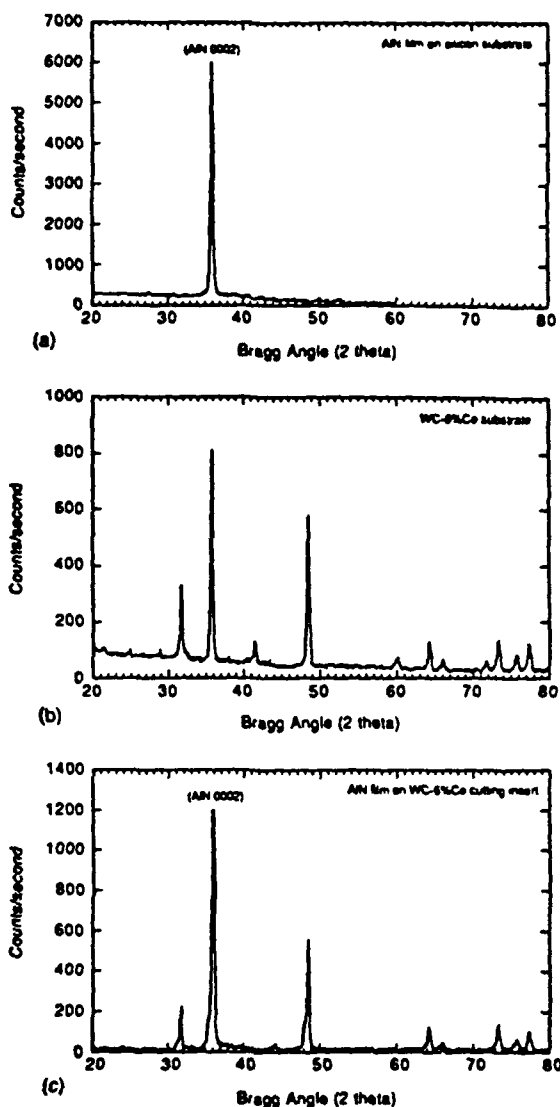


FIG. 2. (a) X-ray diffractometer trace from AlN on silicon showing the (0002) peak demonstrating *c*-axis orientation of the AlN film. Copper *K $\alpha$*  radiation with a wave length  $\lambda = 1.542 \text{ \AA}$ . (b) X-ray diffractometer trace from a WC-Co cutting insert. Dominant peak at  $2\theta = 35.8^\circ$  is close to AlN (0002) peak. Copper *K $\alpha$*  radiation. (c) X-ray diffractometer trace from AlN film on a WC-Co cutting insert. Substrate peak at  $2\theta = 35.8^\circ$  overlaps AlN (0002) peak at  $2\theta = 36.04^\circ$  copper *K $\alpha$*  radiation.

Increasing the total gas pressure tended to reduce film deposition rate, without improving film quality. Based on the results from parametric studies, all subsequent film depositions were made at a total system pressure of 9 mTorr in a 50:50 argon-nitrogen chamber ambient. Transducers fabricated exhibited sensor resistance in the high megaohm range implying minimum film resistivity in the  $10^9 \Omega \text{ m}^{-1}$  range.

Substrate preheating is required to obtain well-oriented polycrystalline films. Maintaining a stable temperature during film deposition tended to yield higher quality sensors. Substrate temperature control during sputtering required substrate holder cooling to maintain a constant tem-

TABLE I. Measured aluminum nitride film characteristics as a function of sputtering conditions.

Run No.	Temperature (K)	Power (W)	Pressure (mTorr)	0002 peak (x ray) (cps. AlN on silicon)	G coefficient ( $C m^{-2}$ on silicon)
901021	573	900	10; (40%Ar/60%N <sub>2</sub> )	< 100	< 0.08
901102	563	900	10; (60%Ar/40%N <sub>2</sub> )	1700	0.33
901025	548	900	10; (50%Ar/50%N <sub>2</sub> )	1020	0.31
901023	503	900	10; (50%Ar/50%N <sub>2</sub> )	< 100	< 0.10
901105	563	700	10; (50%Ar/50%N <sub>2</sub> )	2250	0.39
901101	563	650	8; (50%Ar/50%N <sub>2</sub> )	650	0.24
910713	548	650	9; (50%Ar/50%N <sub>2</sub> )	3500	0.40
920211	553	650	9; (50%Ar/50%N <sub>2</sub> )	6000	0.43

perature. Effect of substrate temperature was explored by film deposition at 498, 523, 548, 573, and 598 K. Films sputtered at lower temperatures ( $T < 523$  K) showed poorer (0002) orientation. Higher substrate temperature ( $T > 573$  K) during film deposition did not yield any improvement in film orientation. All subsequent film deposition runs were made at 553 K with a cathode power of 650 W.

Oxygen level in the vacuum background was found to have a significant effect on film orientation (oxygen background at base pressure was monitored with the mass analyzer). Residual oxygen tends to form  $Al_2O_3$  in the early stages of film growth and apparently prevents the AlN crystallites from growing with the desired, oriented microstructure. In several sputtering runs, even under the optimum sputtering conditions, good quality films could not be made because of leak or poor vacuum background. Particular care was exercised to assure low oxygen background before AlN film deposition.

Sputtering conditions identified in this section were determined from a large number film deposition runs carried out to identify the best processing conditions to obtain 'good' transducer characteristics on silicon. The same film deposition conditions yielded good quality transducers on WC-Co substrates as well.

#### B. AlN piezoelectric film response in quasistatic loading tests

Measured transducer sensitivity under quasistatic loading conditions in the MTS load frame in one of the transducers constructed is  $d_{33} = 3.16$  pC N<sup>-1</sup> for 2  $\mu$ m thick AlN film deposited on silicon. A transducer constructed on a WC-Co substrate under identical film deposition conditions exhibited a sensitivity of  $d_{33} = 1.67$  pC N<sup>-1</sup>. In both cases the transducers exhibit excellent linearity, as may be seen from Figs. 3(a) and 3(b). Measured piezoelectric charge coefficients  $d_{33}$  are smaller than those expected from bulk values for AlN ( $d_{33} = 5.00$  pC N<sup>-1</sup>) reported by Ikeda.<sup>6</sup>

#### C. AlN thin film sensor response in low frequency excitation tests and process reproducibility

Process reproducibility, i.e., process yield, is fairly high. This is shown by the transducer response in the more easily carried out ac excitation tests at 1 kHz. Measured genera-

tor coefficients  $G$  from six representative test samples constructed on silicon and on WC-Co substrates are presented in Table II. As observed in quasistatic loading tests, transducers constructed on WC-Co are less sensitive than those constructed on silicon substrates. Excitation signal used and the transducer response observed in the time domain are shown in Fig. 4(b). Good linearity was observed in all samples evaluated.

#### D. AlN thin film sensor response to substrate temperature rise

Since cutting inserts are subjected to temperature rise of 200 °C or more during machining, loss of transducer sensitivity with increase in substrate temperature can limit the

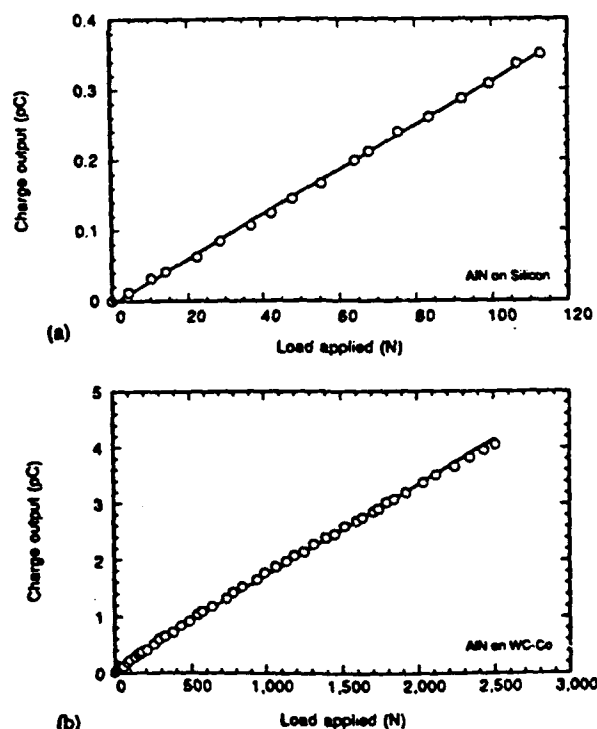


FIG. 3. Test results for quasistatic force calibration of aluminum nitride thin film sensors in an MTS load frame. Data from AlN on silicon and AlN on WC-Co substrates are shown.

TABLE II. Measured characteristics of AlN thin film sensors on Si and WC-Co (1 kHz).

AlN on silicon	$S_1$	$S_2$	$S_3$	$S_4$	$S_5$	$S_6$
$G$ ( $C m^{-2}$ )	0.40	0.43	0.37	0.40	0.42	0.33
$C$ (nF)	2.93	2.37	2.13	2.03	2.16	1.84
$d_{33}$ (pC/N)	4.72	3.65	3.13	3.39	3.56	2.80
$S_{33}$ (mV m N $^{-1}$ )	49	39	32	35	38	31
AlN on WC-Co	$W_1$	$W_2$	$W_3$	$W_4$	$W_5$	$W_6$
$G$ ( $C m^{-2}$ )	0.20	0.26	0.20	0.24	0.18	0.18
$C$ (nF)	5.02	4.96	4.98	5.16	5.01	4.98
$d_{33}$ (pC N $^{-1}$ )	1.79	2.18	1.71	2.03	1.52	1.56
$S_{33}$ (mV m N $^{-1}$ )	19	24	18	21	16	17

usefulness of the instrumented insert. To determine transducer temperature sensitivity,  $G$  coefficient was measured at 1 kHz, in the purpose-built test stand with the heater power turned on. Results obtained are shown in Fig. 5. Over 40% decrease in  $G$  coefficient is observed in AlN sensors constructed on silicon wafers in the 300–475 K temperature range. Over the same temperature range, the transducers constructed on WC-Co substrates exhibit a

loss of sensitivity of about 25%. Measured piezo characteristics suggest that aluminum nitride sensors possess useful sensitivity at temperatures likely under commercial machining conditions.

#### E. Sensor response for acoustic emission sensing: Bench top tests

Time domain signals obtained from the Hsu-Breckenberry test<sup>10</sup> are shown in Fig. 6. Signals from the thin film AlN sensor [Fig. 6(a)] compare favorably with those obtained simultaneously with PAC Model Nano 30 AE transducer [Fig. 6(b)]. Both signals were band pass filtered (100–500 kHz band). The same signals are shown in the frequency domain in Fig. 7. All the principal frequencies detected by the commercial AE transducer are

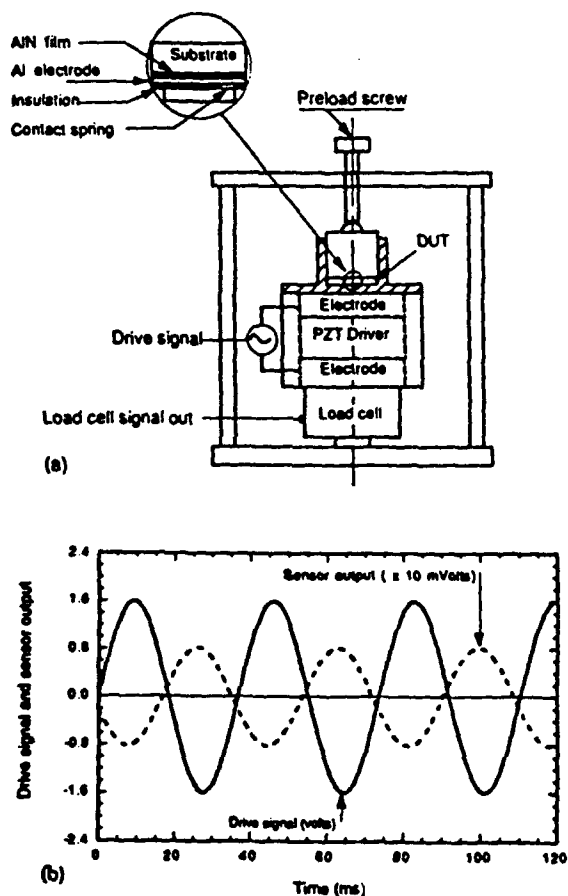


FIG. 4. (a) Schematic of the test stand used for ac calibration of thin film sensors at 1 kHz excitation test frequency. To measure the generator coefficient as a function of transducer temperature, a button heater is clamped between the test element and the preload assembly. (b) Drive signal used for excitation and the sensor response from a typical test run.

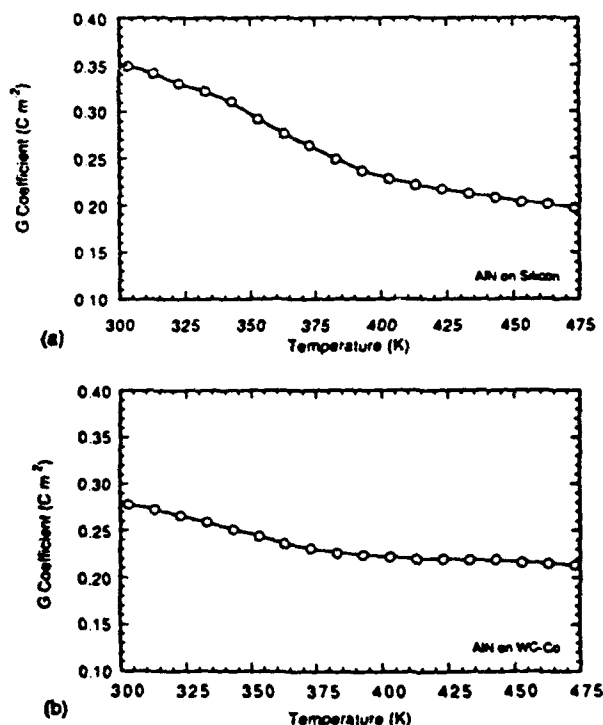


FIG. 5. Measured temperature dependence of the generator coefficient. (a) Aluminum nitride on silicon substrate. (b) Aluminum nitride on WC-Co substrate.

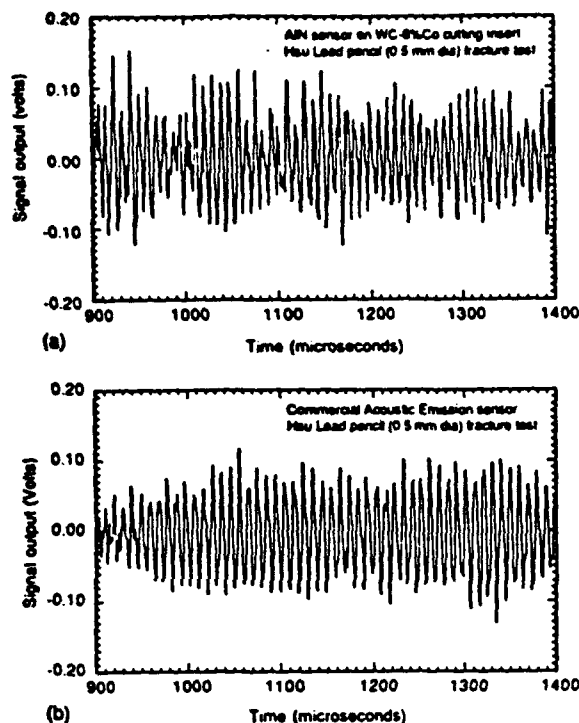


FIG. 6. Time domain signals detected by (a) the AlN thin film sensor on WC-Co cutting insert and (b) a commercial AE sensor attached to the tool holder as shown in Fig. 1. Mechanical pencil lead fracture test of Hsu (see the text for details). Signal from the AE transducer lags by a time corresponding to the distance between the thin film sensor and the AE transducer. Frequency content appears comparable.

detected by the thin film sensor. An additional peak close to the dominant peak at 100 kHz is also detected by the AlN sensor. It should be noted that while the commercial AE sensor contains a piezoelectric crystal and a backing plate, the AlN sensor is in a clamped condition with the insert holding finger exerting a compressive preload. Despite this, AlN sensors faithfully detect the AE signals originating from graphite rod fracture (0.5 mm diam; HB grade).

#### F. Sensor response for acoustic emission sensing: Machining tests

Band pass filtered (70–300 kHz) time domain signals obtained during machining are presented as frequency domain signals in Fig. 8. Every peak sensed by the commercial AE sensor is also sensed by the thin AlN film sensor. The richer frequency content of the thin film sensor suggests that the sensors constructed on the cutting insert may have a lower damping. Despite the difference in transducer boundary conditions, the thin film AlN sensors perform as well as commercial AE sensors during machining.

### VII. DISCUSSION

Film deposition conditions appropriate to deposit piezoelectrically active AlN sensors have been identified in this

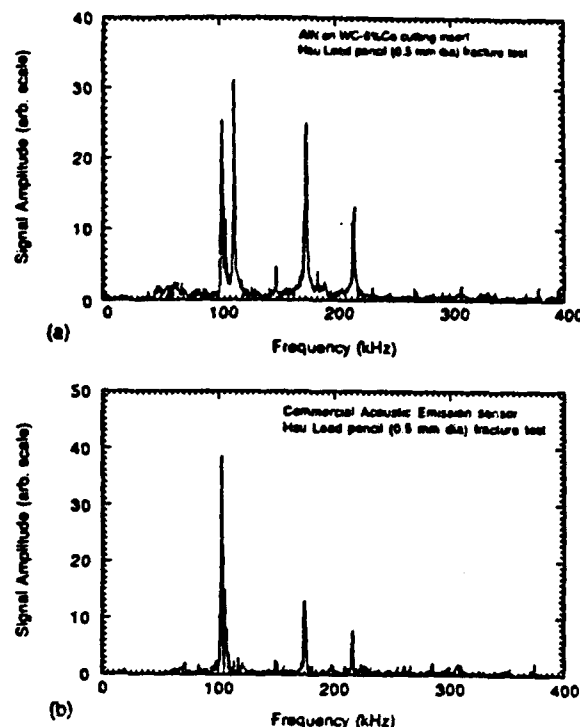


FIG. 7. Frequency domain signals detected by (a) the AlN thin film sensor on WC-Co cutting insert (b) a commercial AE sensor attached to the tool holder as shown in Fig. 1. Signals were band pass filtered (100–500 kHz). Mechanical pencil lead fracture test of Hsu (see the text for details). Frequency content is virtually identical. Source of the dominant peak just above 100 kHz observed in the signal from AlN on WC-Co insert has not been identified.

work with a group of parametric studies. It is shown that high resistivity films can be reproducibly deposited on silicon wafers as well as WC-Co substrates by rf sputtering in a reactive ambient containing 50% argon and 50% nitrogen. Substrate heating is necessary to make transducer elements with good sensitivity. Presence of oxygen in the coating ambient is detrimental.

Piezoelectric charge coefficients ( $d_{33}$ ) obtained in the transducers deposited on Si and WC-Co substrates are approximately 60% and 35% of the nominal value calculated from published data for AlN. Values reported are based on calculation of charge coefficients using a simple uniaxial loading model which ignores the strains induced in the film by substrate deformation in transverse directions. An expression can be written to calculate charge sensitivity which takes the Poisson expansion into account. Lower charge generation would be predicted as Poisson strains would tend to partially cancel the charge generated on the transducer surface by the compressive force.

Poisson expansion in lateral dimensions, proportional to the stress applied and  $\nu_{\text{substrate}}$ , will require continuity of displacements at the film-substrate interface in transducer films well bonded to the substrates. An unknown, nonuniform, biaxial tensile stress distribution will be generated in the transducer film when the substrate expands laterally in



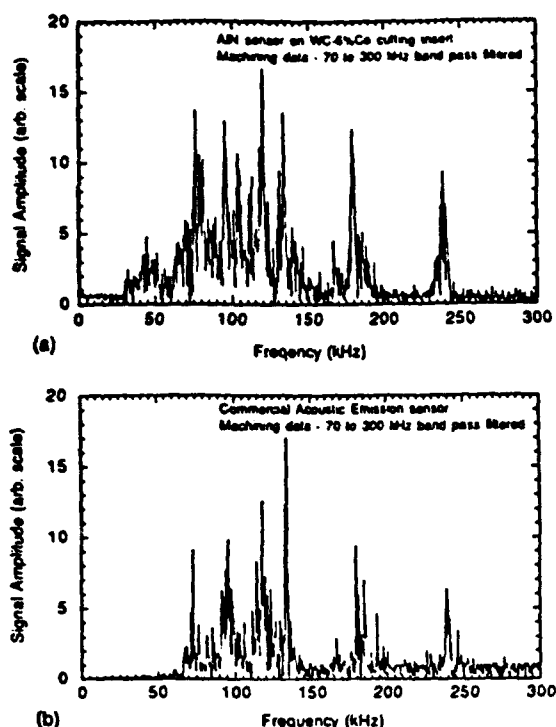


FIG. 8. (a) AE frequency spectra obtained from a machining test using a cutting insert equipped with the AlN thin film sensor. (b) AE frequency spectra obtained from the same machining test using a commercial AE transducer attached to the tool holder as shown in Fig. 1. Band pass filtered signals (70–300 kHz). Every peak detected by the commercial AE sensor is also detected by the AlN thin film sensor. See the text for details of cutting conditions.

response to compressive loading in the thickness direction.

The transducer-substrate assembly is clamped in position in the tool holder during use or placed on a metal platen during calibration measurements under compressive loading. In both cases unknown restraints to changes in lateral dimensions are introduced by friction. To avoid the uncertainties involved in estimating the actual lateral restraints a simpler model, used originally by White,<sup>11</sup> is employed here. A part of the discrepancy in calculated charge coefficients may be due to transverse strains not taken into account here.

Sputtered films are generally stressed and the film stresses vary with deposition conditions. Moreover, when film deposition is carried out on heated substrate holders, finite cooling stresses occur in the transducers deposited. Expected thermal stress  $\sigma_T$  is

$$\sigma_T = E_f(\alpha_f - \alpha_s)\Delta T / (1 - \nu_s), \quad (8)$$

where  $E_f$  is the Young's modulus of the film,  $\alpha_f$  and  $\alpha_s$  are the CTEs of the film and substrate,  $\Delta T$  is the deposition temperature minus room temperature, and  $\nu_s$  is the Poisson's ratio of the substrate. As the transducer and the substrate are both hard compounds ( $H_p = 12.30$  and  $23.50$  GN m<sup>-2</sup>, respectively, for AlN and WC-Co<sup>12</sup>) and high modulus materials (330 and 720 GPa<sup>12</sup>), the "as sputtered" films are expected to be stressed. Since the melting

temperatures of the transducer and substrate materials are both high (2250 and 2776 °C<sup>12</sup>), very little change in film stress would be expected from "aging". These unknown film stresses further justify the one dimensional model used to calculate  $d_{33}$ .

Aluminum nitride has been deposited here at low temperatures, i.e.,  $T/T_{MP}$  of the order of 0.20, where columnar crystallite growth is normal in sputtered films. Films laid at low temperatures are known to be prone to self-shadowing<sup>13</sup> with porosity along the columnar crystallite boundaries.<sup>14,15</sup> Films produced under these conditions are likely to have a distribution in crystallite orientations around a mean and are unlikely to be fully dense. These phenomena also tend to lower the charge coefficient.<sup>16</sup>

The discrepancy in calculated charge coefficients has a number of contributing factors which include unknown applied and intrinsic in-plane strains (stresses), deviation from perfection in texture generated, columnar structure and a level of porosity accepted to construct thin film transducers at low temperatures.

The generator coefficient  $G$  is found to decrease as a function of transducer temperature, as shown in Fig. 5. Decrease in  $G$  is larger for AlN on Si than for AlN on WC-Co. As the Si-AlN composite changes dimensions more rapidly with temperature (larger difference in coefficient of thermal expansion) than for AlN-WC-Co composite ( $\alpha_f$  is  $4.5 \mu\text{m m}^{-1} \text{K}^{-1}$ <sup>17</sup> for AlN,  $\alpha_s$  is  $2.8 \mu\text{m m}^{-1} \text{K}^{-1}$ <sup>18</sup> for Si and  $\alpha_s$  for WC-6% Co is  $5.0 \mu\text{m m}^{-1} \text{K}^{-1}$ <sup>19</sup>), a larger loss in charge sensitivity would be expected for the same temperature rise  $\Delta T$ , if larger in-plane stresses (and therefore strains) lead to larger charge displacements in AlN films. This is, in fact, observed. It is therefore reasonable to suggest that the larger reduction in charge sensitivity for AlN on Si is due to larger transverse stresses [stresses can be calculated with Eq. (8)] imposed by silicon on AlN films. Tungsten carbide and aluminum nitride have a better match in CTE. A smaller reduction in generator coefficient follows for AlN on WC-Co with increase in temperature.

Transducers constructed provide dc signals in quasi-static loading. Sensor response to low and high frequency excitations demonstrate that useful instrumented inserts with piezotransducers can be constructed. This is confirmed by bench top tests as well as machining tests in which the transducer-substrate assembly is subjected to temperature rise by the power dissipated during metal machining.

Both ZnO and AlN perform satisfactorily in machining. However, the higher hardness of AlN ( $H_p$  of ZnO<sup>20</sup> is  $4.0$  GN m<sup>-2</sup>), its modest decrease in charge coefficient with increase in temperature due to a better match in CTE and the much higher useful temperature limit,  $1200^\circ\text{C}$ ,<sup>21</sup> suggest that AlN is a better transducer material than ZnO.

## VIII. SUMMARY AND CONCLUSIONS

Piezoelectric thin film sensors for force, acceleration, and acoustic emission sensing based on sputtered AlN films have been developed. AlN thin film sensors are fabricated directly on WC-Co substrates in a reactive ambi-

ent. Film deposition conditions to reproducibly construct this class of sensors have been determined through parametric studies. Good c-axis orientation is readily obtained to construct AlN thin film sensors sensitive to normal forces on both silicon and WC-Co substrates by rf sputtering.

Sensors constructed exhibit good sensitivity, linear signal response and a large bandwidth. AlN films deposited also have sufficiently high resistivity to allow force sensing under quasistatic loading conditions. Satisfactory acceleration and AE sensing characteristics are obtained with rf sputtered AlN films laid on WC-Co substrates.

Unlike ZnO sensors, AlN sensors deposited on WC-Co substrates do not exhibit large losses in signal sensitivity with increase in tool temperature. This is due to a much better match in CTE for AlN films on WC-Co cutting inserts. Force, acceleration as well as acoustic emission signals can be tracked in real time to implement single parameter or more robust multiparameter tool condition monitoring systems to automate machining.

Cutting inserts with integral sensors have been evaluated in cutting tests in a computerized lathe. Machining conditions used were comparable to those employed in commercial cutting practice. Instrumented inserts perform satisfactorily in laboratory tests. Field trials carried out indicate that the sensor-equipped inserts are suitable for real-time tool condition sensing under commercial machining conditions.

Trials have also been carried out in which the sensor was constructed on WC-Co tool seats (see Fig. 1) as opposed to cutting inserts. Although the thin film sensor is now some 3–5 mm farther away from the cutting edge, seat sensors do not exhibit significant signal losses and have been found to be satisfactory for real-time tool condition sensing. Usable life of up to two days (six 8-h shifts) has been obtained with seat sensors. Seat sensors with life up to two weeks (30 shifts) are, however, preferred for industrial use. Future work on improving transducer durability may be necessary, when sensors are implemented in tool seats.

When sensors are implemented in cutting inserts, there could be a need for an in-tool temperature sensor to compensate for the changes in AlN transducer sensitivity with changes in cutting insert temperature. This assumes a tool condition monitoring system based on absolute signal values rather than relative changes. However, when the sensor

is implemented in tool seats, the transducer is farther away from the cutting edge. Thermal effects are then less significant. A temperature sensor is therefore unnecessary when the thin film transducer is implemented in seat sensors.

## ACKNOWLEDGMENTS

The authors acknowledge the support received from the GM Tech Center, Warren, MI, which made most of the work reported possible. We thank Martin Suchosky, GM Tech Center for his continued interest and encouragement. A part of the work reported here has received support from Wright Laboratory, USAF, WPAFB, Ohio through a sub-contract with Fastman, Inc., Bethlehem, PA (now at Austin, TX) and from the National Science Foundation, Grant No. DDM 9022550.

<sup>1</sup>S. Birla, GM Tech Center Report No. GMMD-80-026, General Motors Technical Center, Warren, MI, 1980.

<sup>2</sup>J. Tlustý and G. C. Andrews, *Ann. CIRP* 34, 87 (1985).

<sup>3</sup>T. Moriwaki and K. Iwata, *Ann. CIRP* 25, 21 (1977).

<sup>4</sup>Y. Kakino, *J. Acou. Emis.* 5, 108 (1984).

<sup>5</sup>W. P. Robbins, B. Bischoff, and S. Ramalingam, *Thin Solid Films* 166, 387 (1988).

<sup>6</sup>T. Ikeda, *Fundamentals of Piezoelectricity* (Oxford University Press, Oxford, England, 1990), p. 222.

<sup>7</sup>D. L. Polla, Ph.D. dissertation, University of California, Berkeley, CA, 1985.

<sup>8</sup>B. Bischoff, M.S. thesis, University of Minnesota, Minneapolis, MN, 1985.

<sup>9</sup>B. Bischoff et al., in *Sensors for Manufacturing*, ASME Special Publication PED-26 (ASME, New York, 1987), p. 69.

<sup>10</sup>N. N. Hsu, U.S. Patent No. 4 018 084, 1976.

<sup>11</sup>R. M. White, *IEEE Trans. Son. Ultrason.* SU-28, 8 (1981).

<sup>12</sup>H. Holleck, in *Harstoffschichten zur Verschleissminderung*, edited by H. Fleischmeister and H. Jehn (Informations Gesellschaft Verlag, city, 1986), p. 25.

<sup>13</sup>K. H. Müller, *J. Appl. Phys.* 58, 2573 (1985).

<sup>14</sup>J. A. Thornton, *Annu. Rev. Mater. Sci.* 7, 239 (1977).

<sup>15</sup>H. Pulker, *Coatings on Glass* (Elsevier, Amsterdam, 1984).

<sup>16</sup>Q. Zhenxing, Z. Xiaozhong, Z. Mingzhou, W. Xizhang, and L. Yujin, *IEEE Trans. Son. Ultrason.* SU-32, 630 (1985).

<sup>17</sup>W. B. Carter and M. V. Papageorge, *J. Vac. Sci. Technol. A* 10, 3460 (1992).

<sup>18</sup>*Electronic Materials Handbook* (American Society for Metals, Metals Park, OH, 1989), Vol. 1, p. 1120.

<sup>19</sup>*Metals Handbook*, 7th ed. (American Society for Metals, Metals Park, OH, 1967), Vol. 1, p. 664.

<sup>20</sup>*Wear Control Handbook*, edited by M. B. Peterson and W. O. Winer (ASME, New York, 1980), p. 1317.

<sup>21</sup>*Ultrasonic Testing*, edited by P. McIntire (American Society for Non-destructive Testing, Columbus, OH, 1991), p. 849.

# WEAR AND LUBRICANT DEGRADATION MONITORED BY WORK FUNCTION MEASUREMENTS

Steven Danyluk

Elmer Zanoria

Ligang Xu

Georgia Institute of Technology

- Describe vibrating probe (Kelvin) technique to measure contact potential difference (CPD)
- Applications to Tribology
- Data of sensitivity and spatial resolution for CPD
- Suggestions on applications

Lord Kelvin - ~1870  
Zisman - ~1935-1940  
- 1940's surface science

- Describe vibrating probe (Kelvin) technique to measure contact potential difference (CPD)

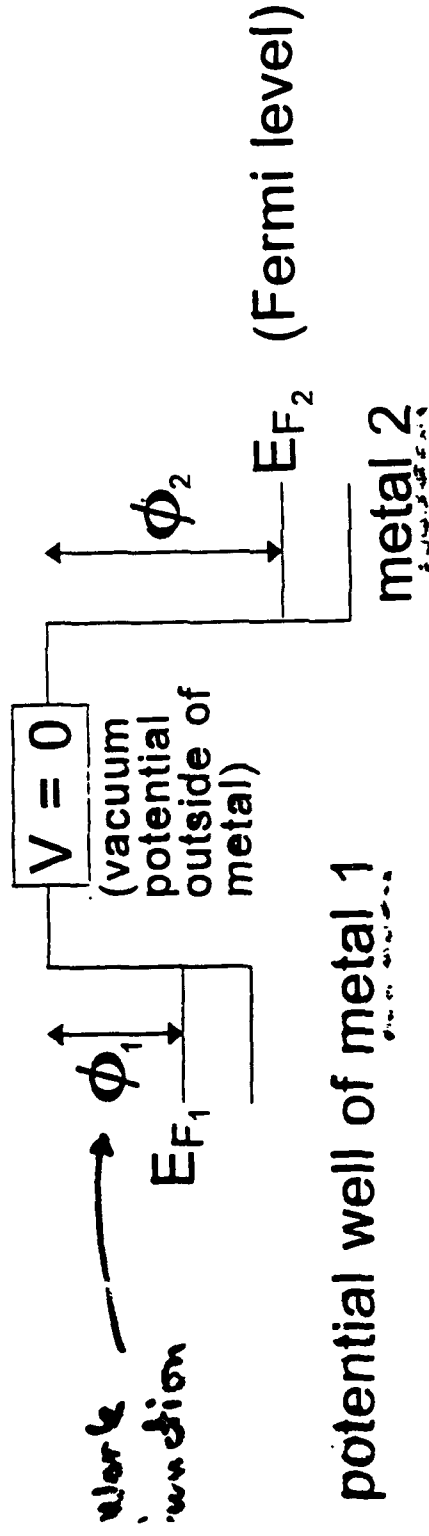
- refers to differences in work function  
surface condition

- Applications to Tribology
- Data of sensitivity and spatial resolution for CPD
- Suggestions on applications - to condition base monitoring

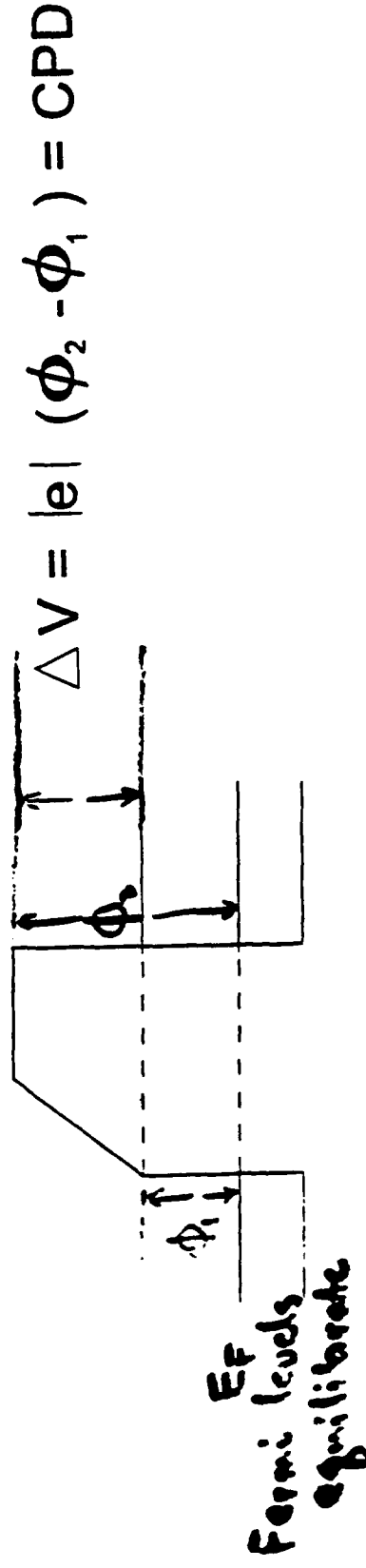
# Physics of Surface Potential (Work Function) Measurements

Applied to Metals:

(a) prior to contact: vacuum potential = 0



(b) after contact:  $E_{F_1} = E_{F_2} = E_F$

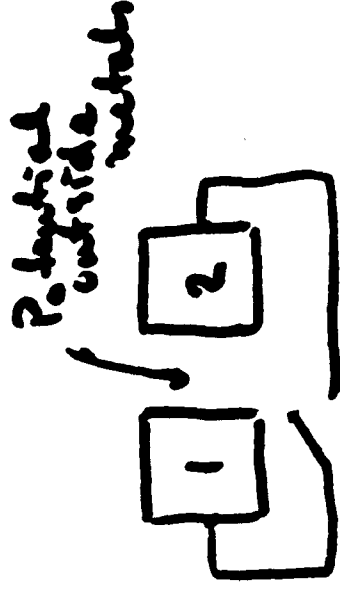
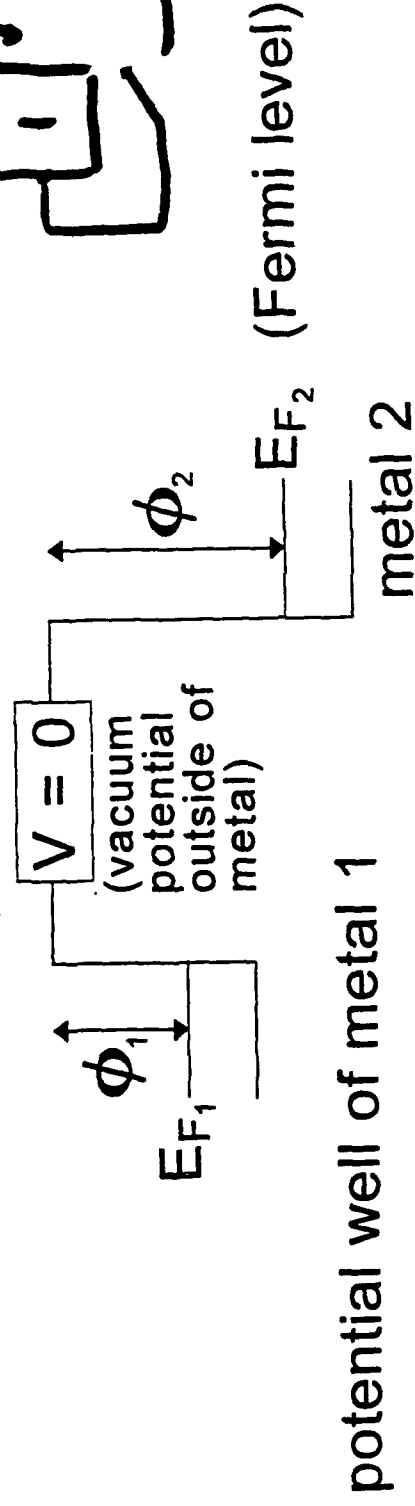


# Physics of Surface Potential (Work

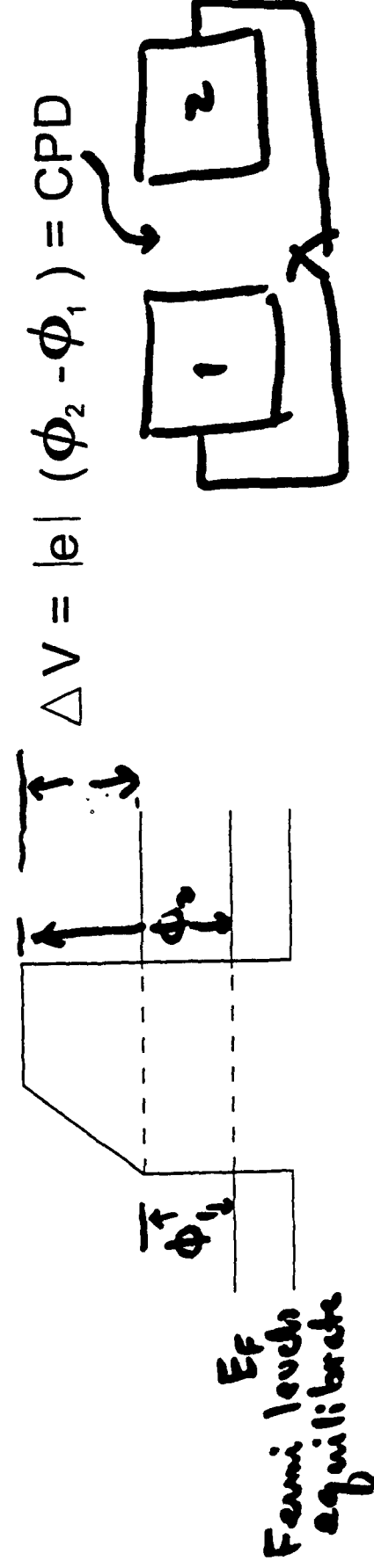
## Function) Measurements

Applied to Metals:

(a) prior to contact: vacuum potential = 0

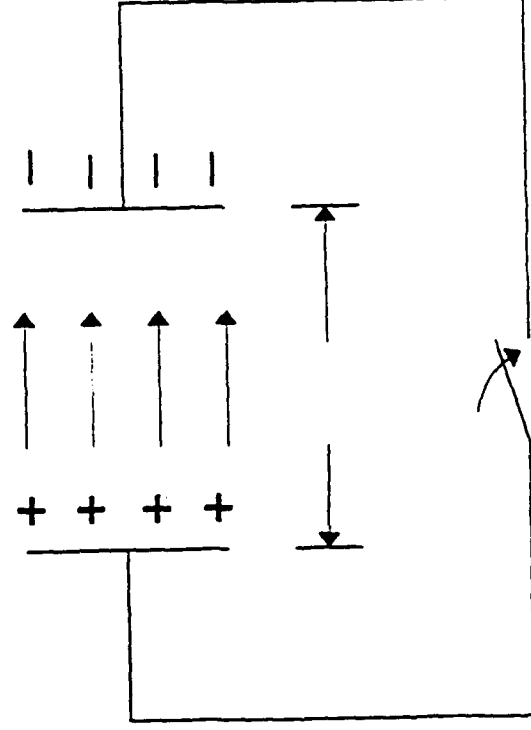
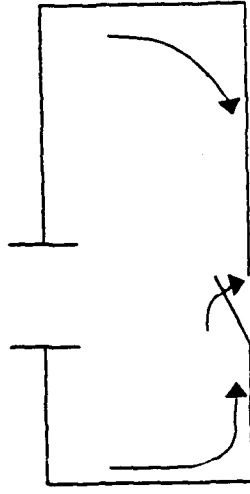


(b) after contact:  $E_{F1} = E_{F2} = E_F$



# Measurement of Current Flow

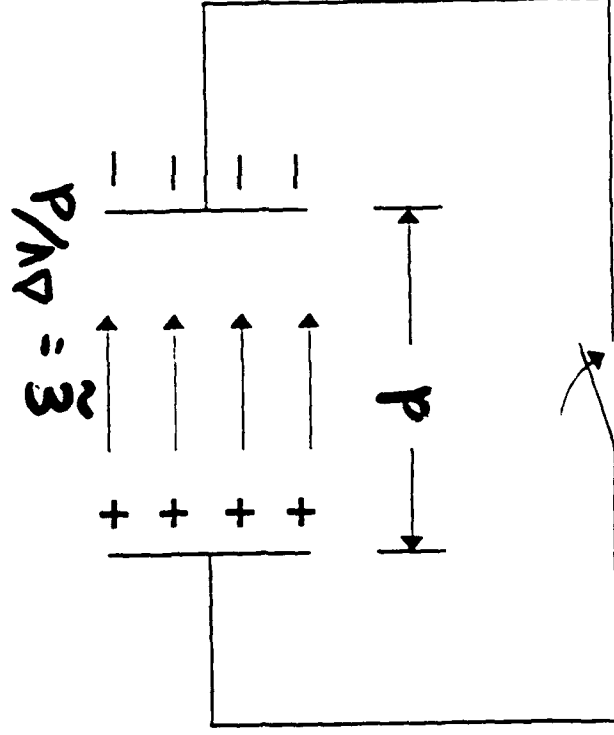
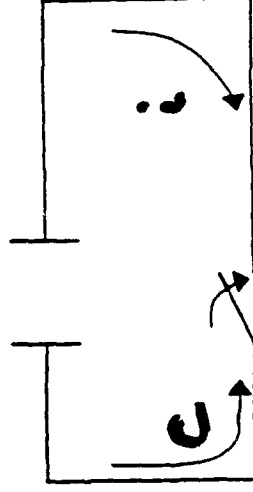
metal 1   metal 2





# Measurement of Current Flow

metal 1 metal 2



$$Q = C \Delta V$$

$$\frac{dQ}{dt} = \frac{d}{dt} (C \Delta V)$$

when  
switch  
is closed

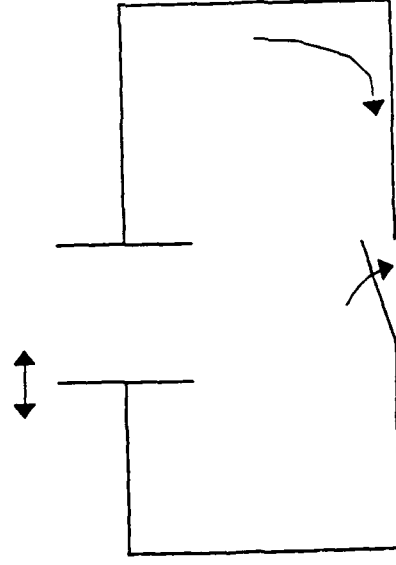
$$\frac{dQ}{dt} = \Delta V \frac{dC}{dt} + C \frac{d(\Delta V)}{dt}$$

$$\frac{dQ}{dt} = i = (\Delta V) \frac{dC}{dt}$$

← capacitance

For a parallel plate capacitor

Vibrating one plate (reference electrode)



For a parallel plate capacitor

$$C = \frac{\epsilon_0 A}{d}$$

Vibrating one plate (reference electrode)

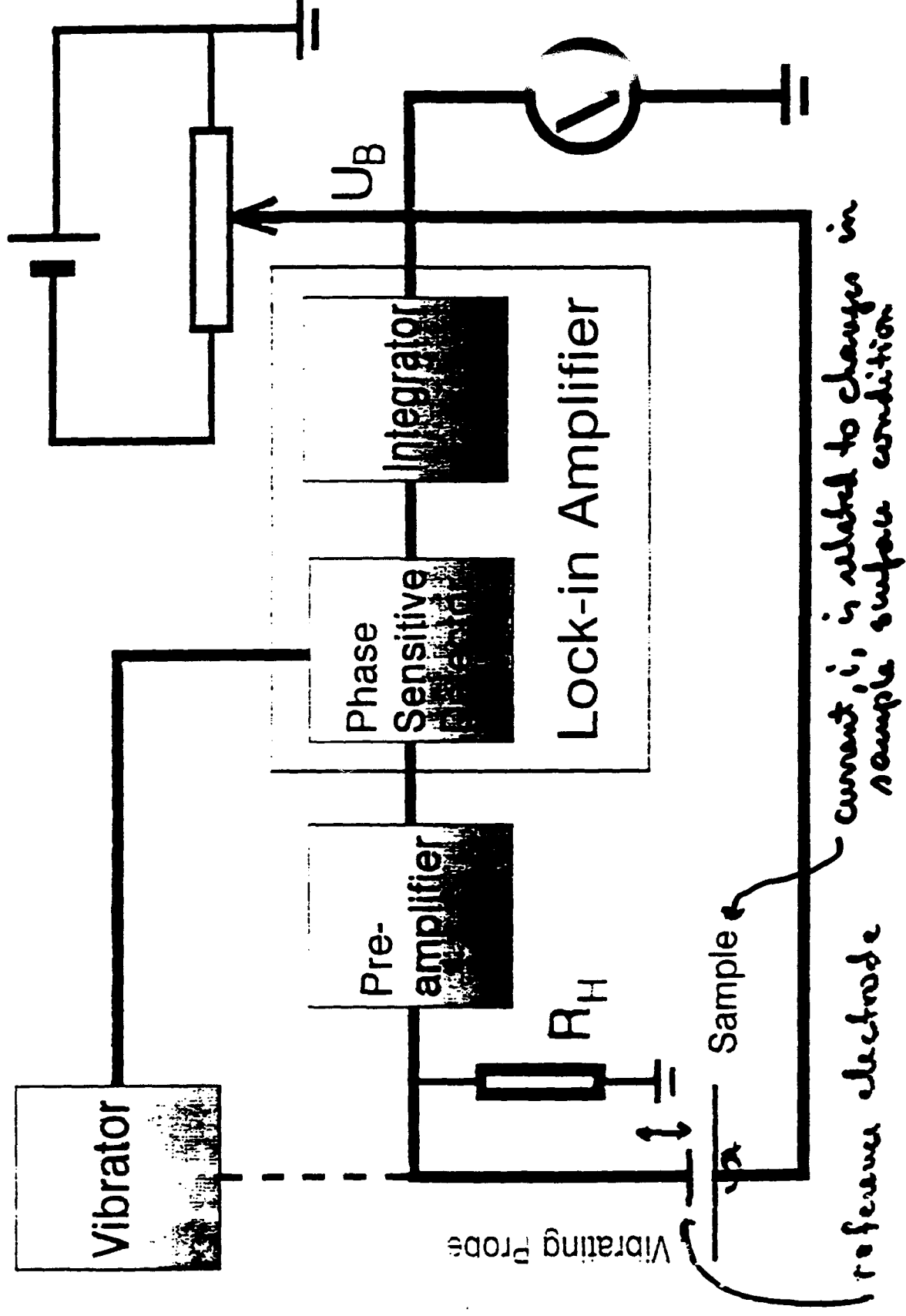
$$d = d_0 \sin \omega t$$

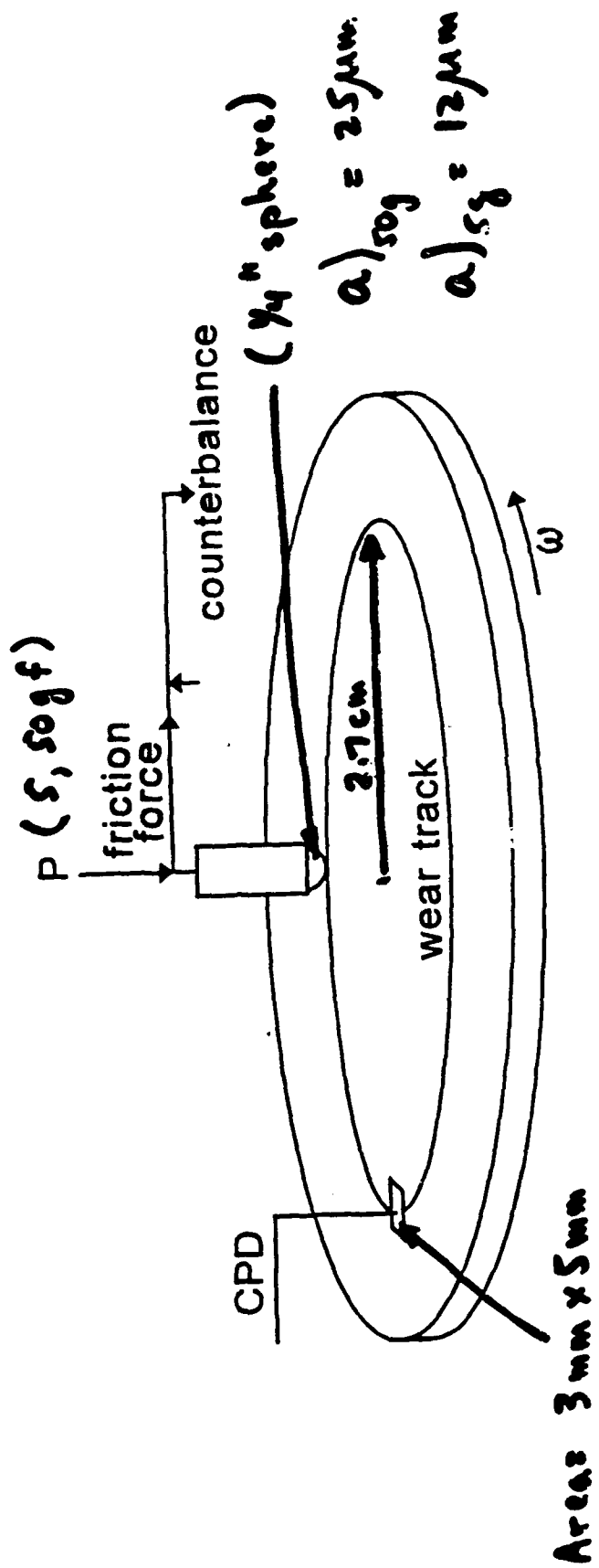


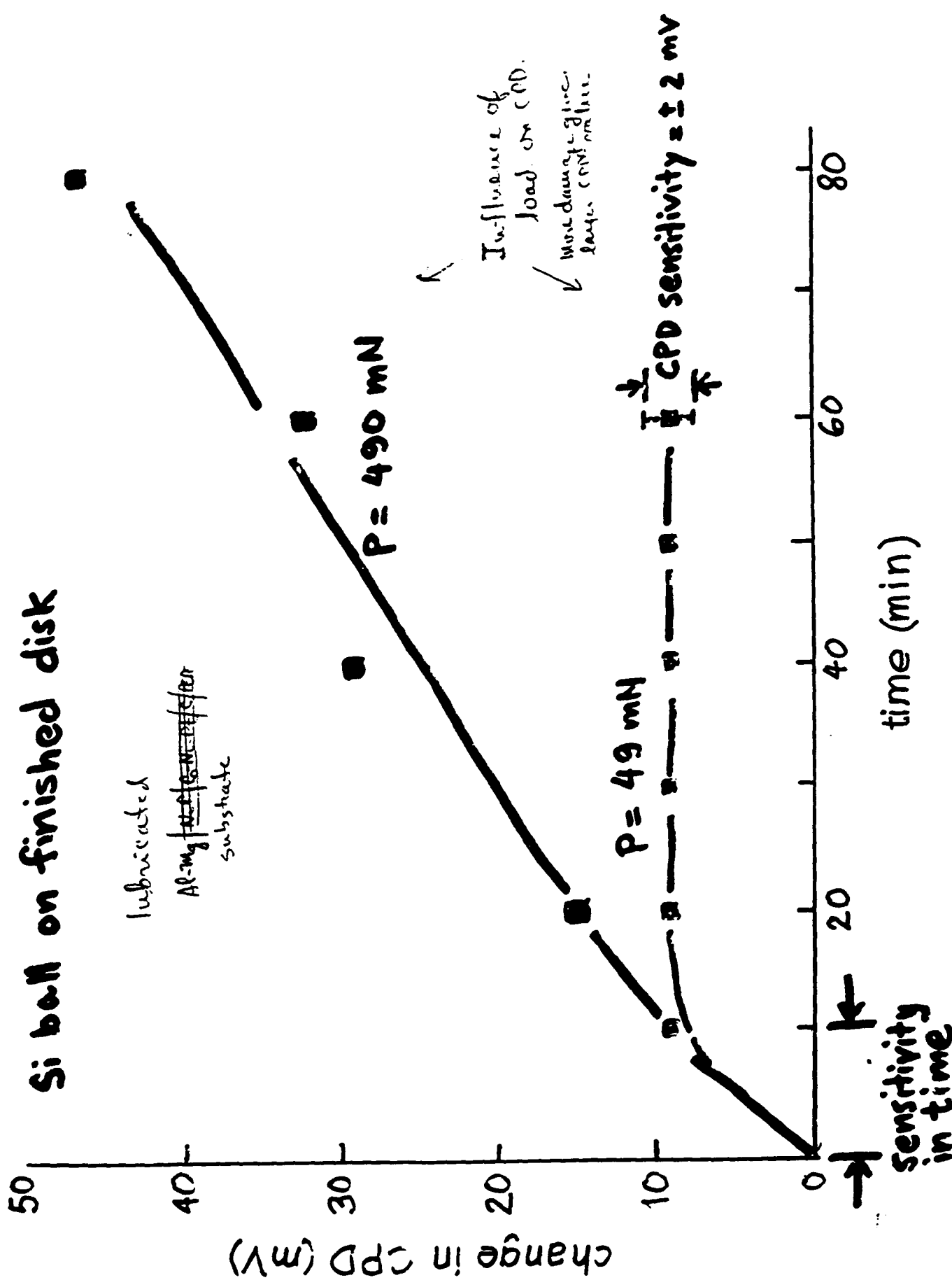
$$C = \frac{\epsilon_0 A}{d_0 \sin \omega t}$$

$$i = \Delta V \left( \frac{\epsilon_0 A}{d_0} \right) \frac{d}{dt} \left( \frac{1}{\sin \omega t} \right)$$

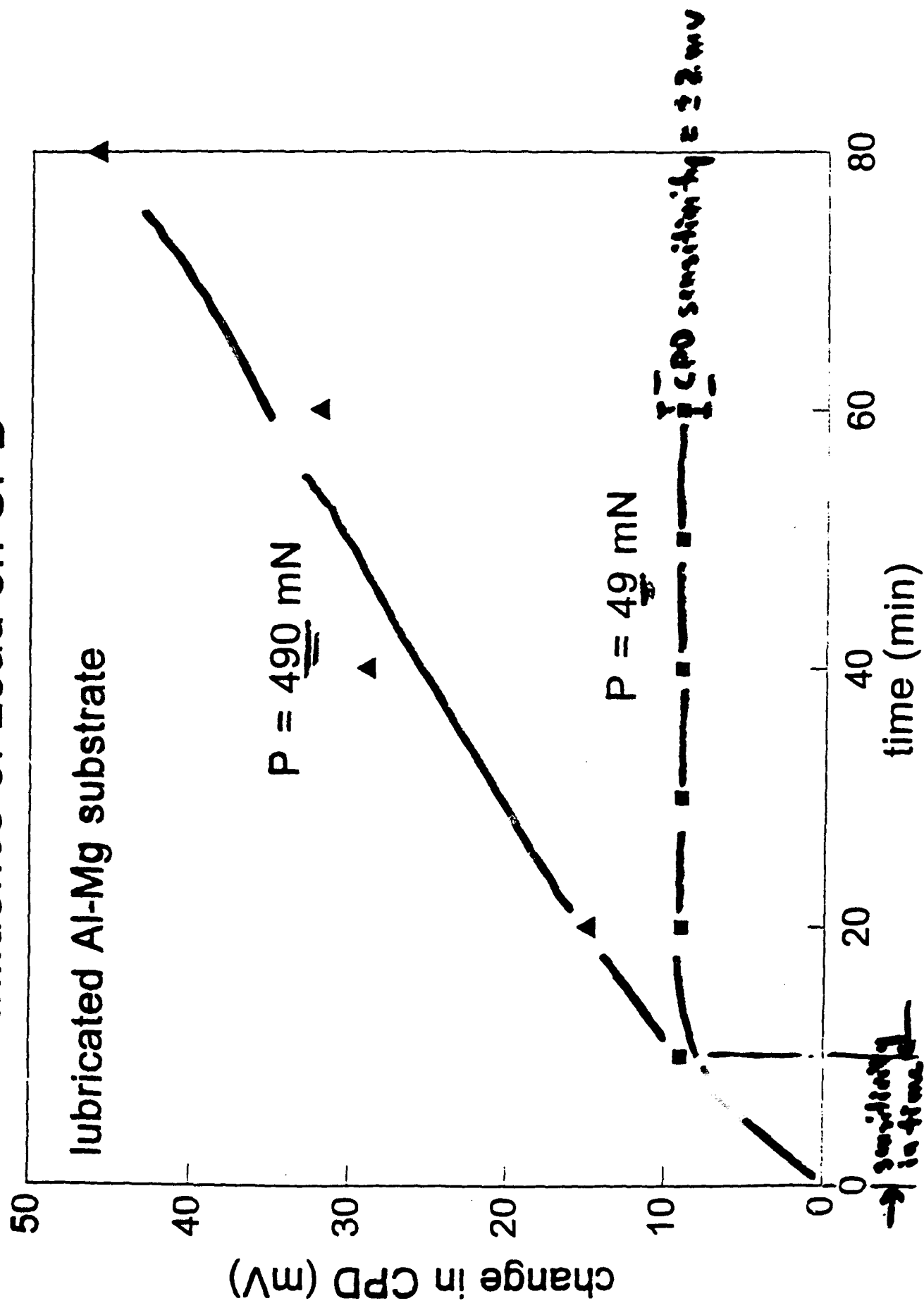
# Block Diagram of experimental Set-up



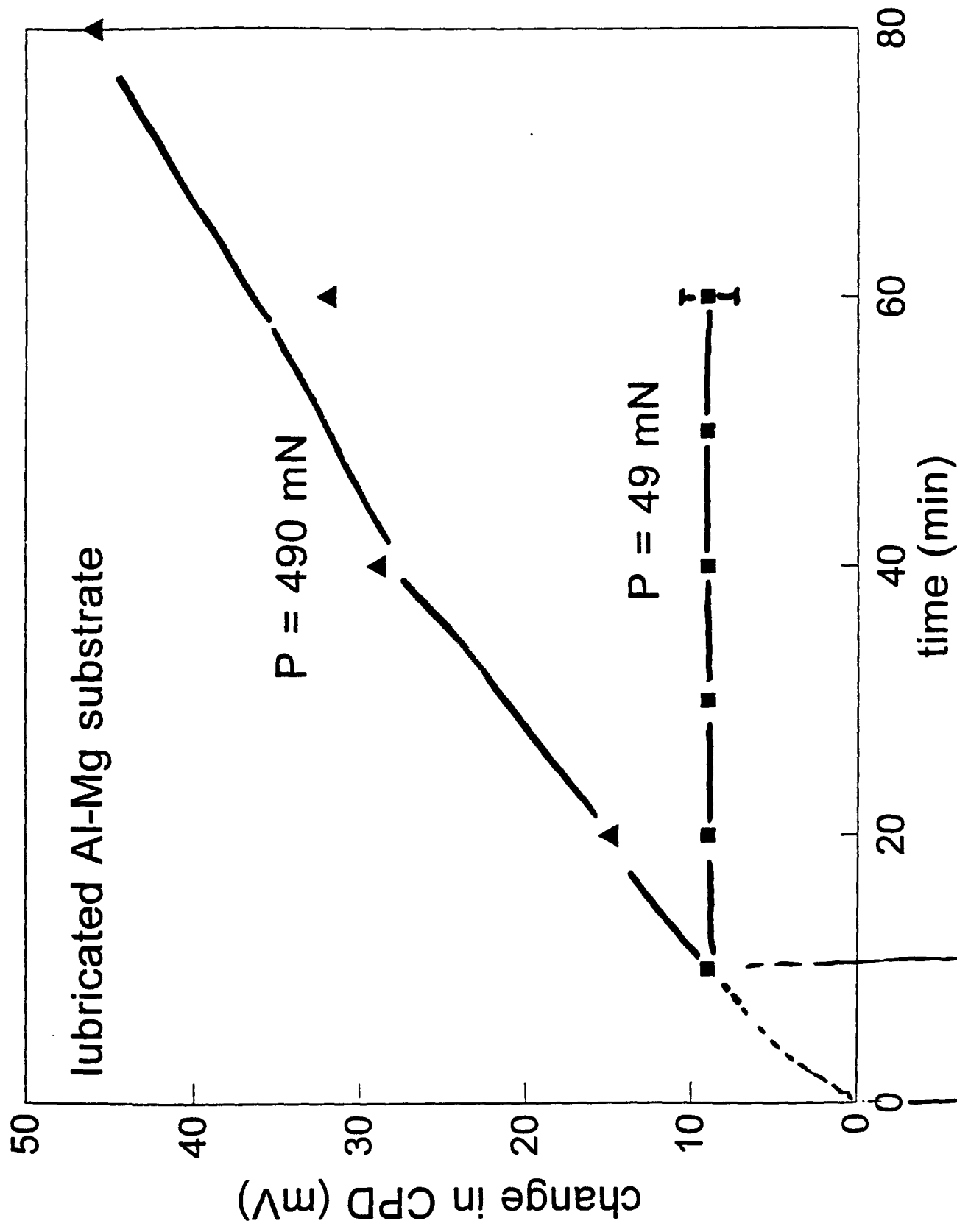




# Influence of Load on CPD

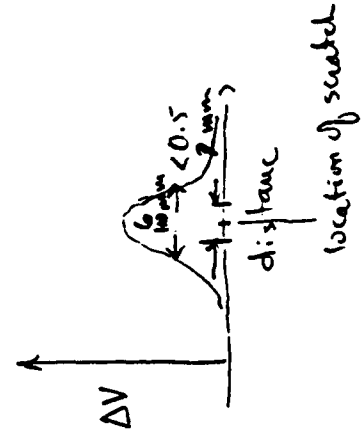
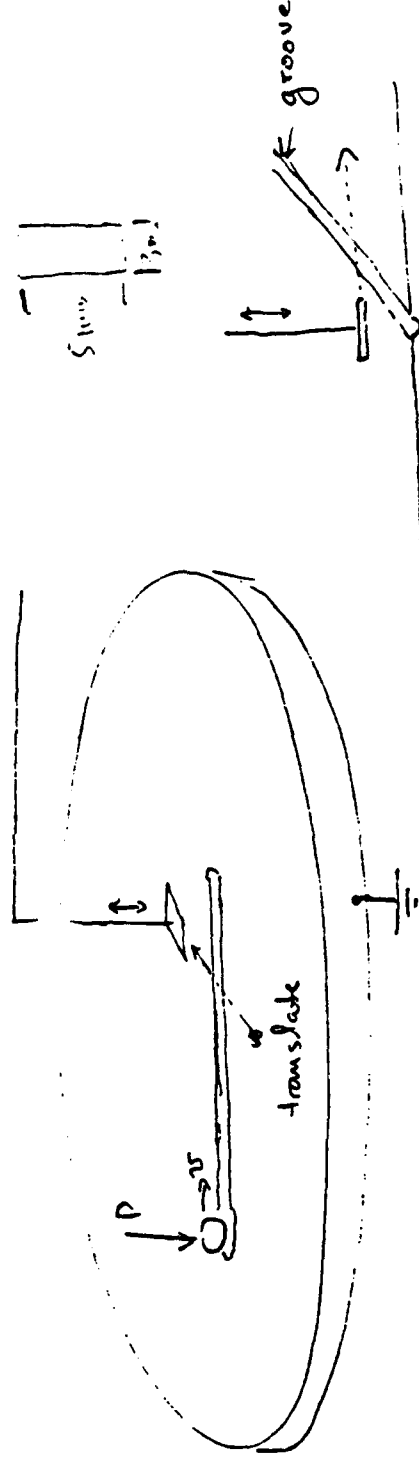


# Influence of Load on CPD

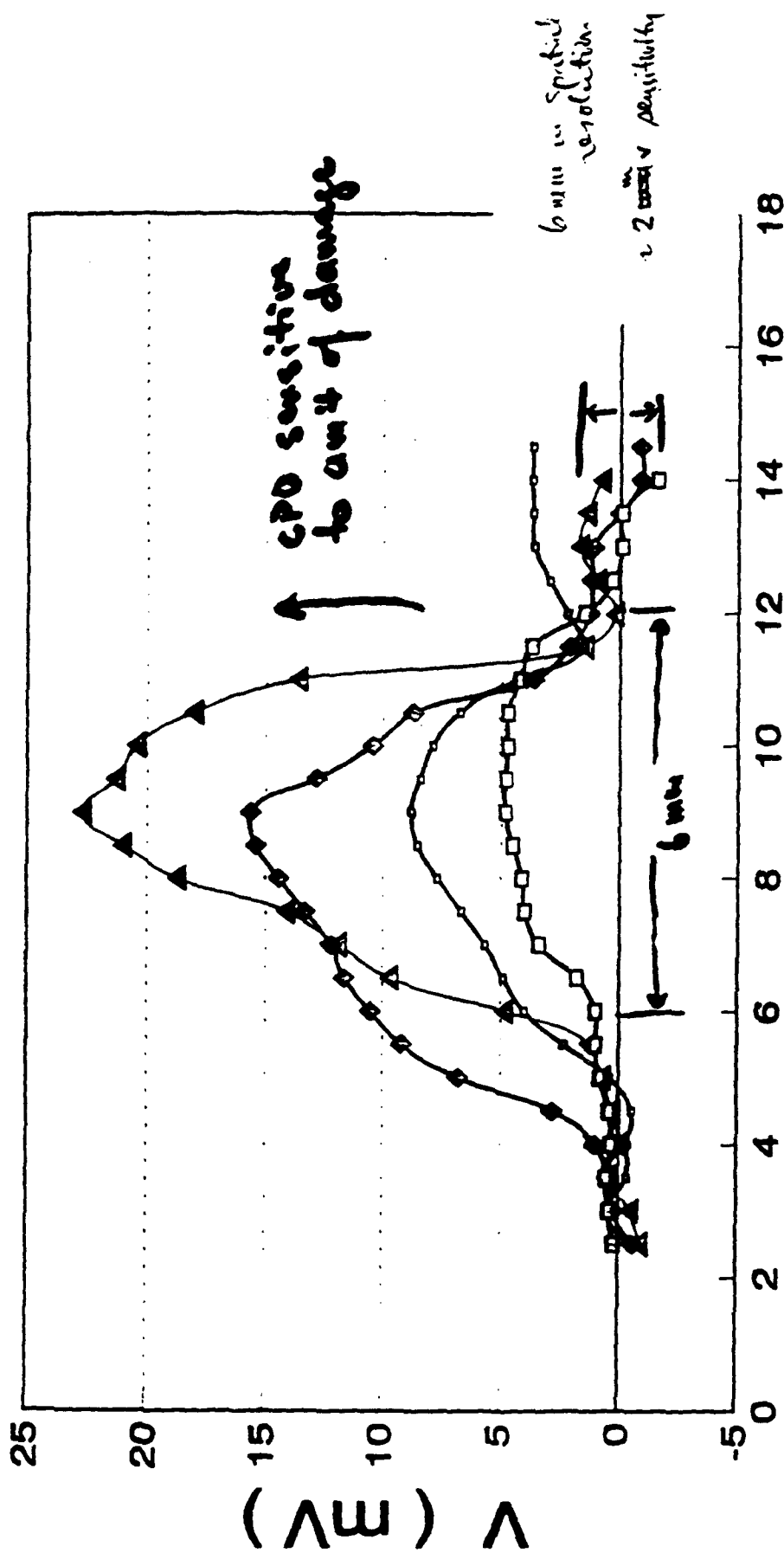




Sensitivity Study: linear ~~model~~ reciprocating scratches  
 Dia on ~~Si(100) or Si(111)~~ <sup>Si(100)</sup>;  $P \approx 0.1 \text{ N (50g)}$ ;  $v = 2 \text{ cm/min}$   
 laboratory air



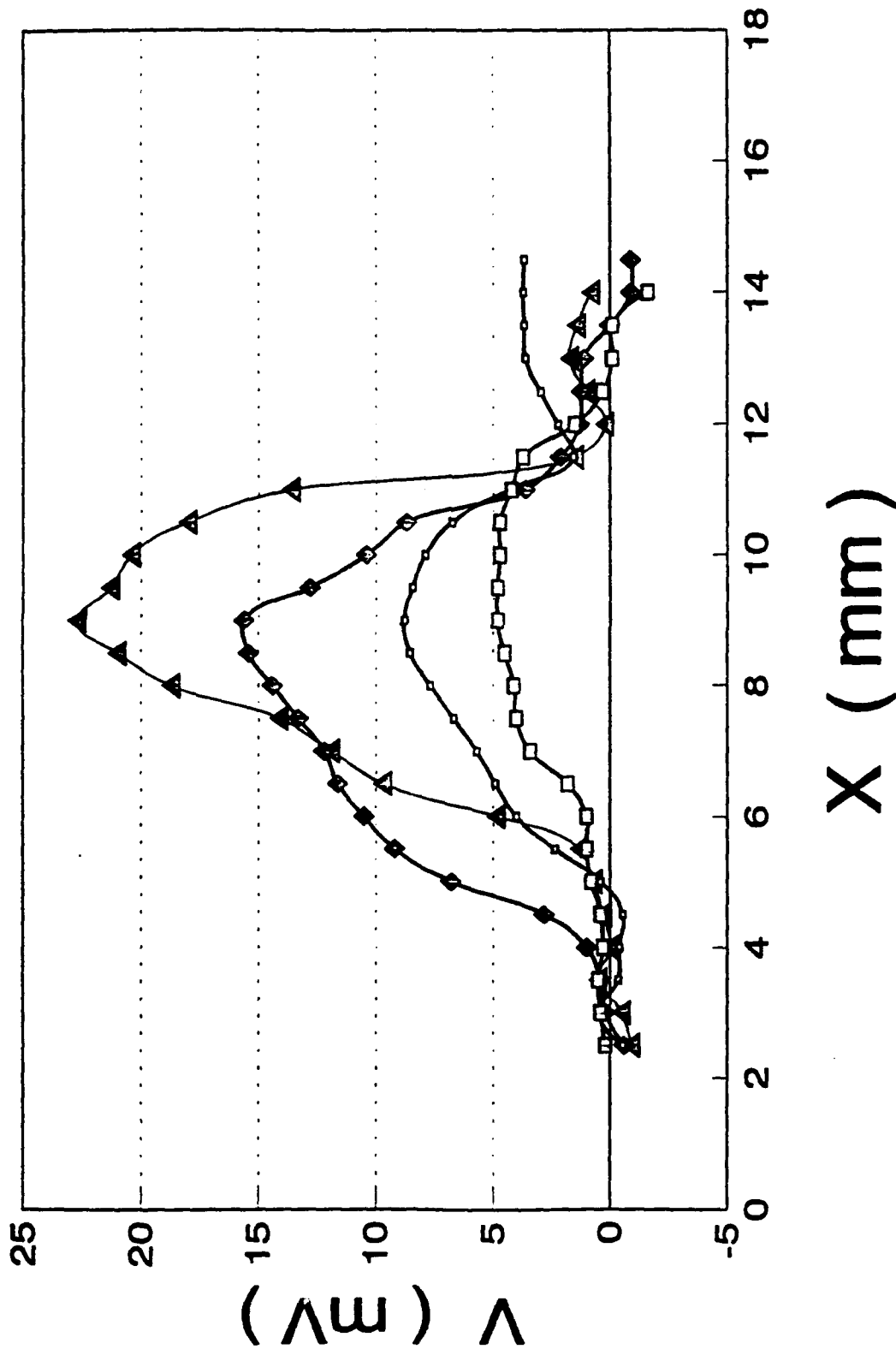
# CPD Change vs Position



X (mm)

○ 1 SCRATCH    □ 5 SCRATCHES    ♦ 10 SCRATCHES    ▲ 20 SCRATCHES

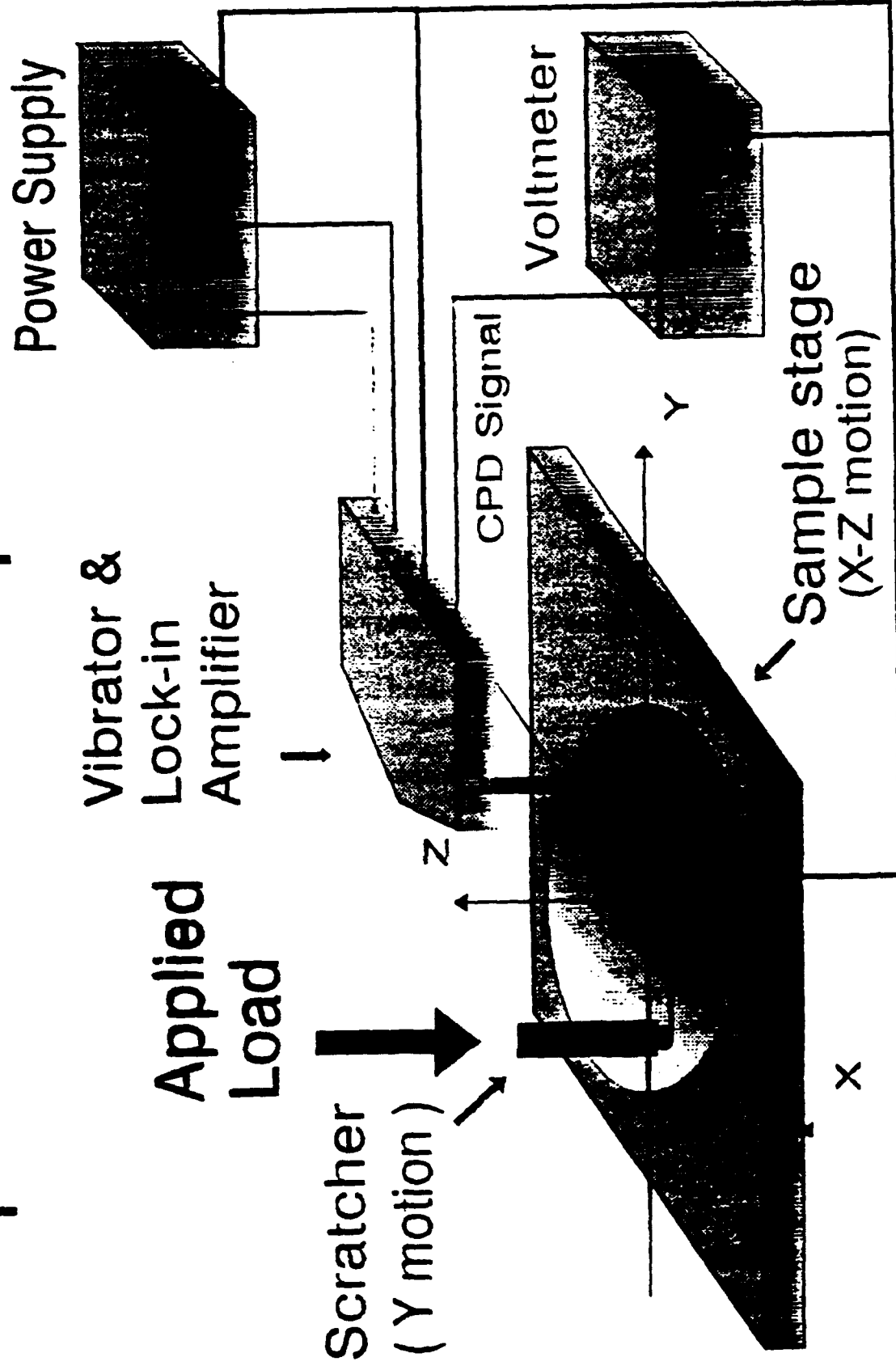
# CPD Change vs Position



□ 1 SCRATCH    ♦ 5 SCRATCHES    ◆ 10 SCRATCHES    ▲ 20 SCRATCHES

6 μm in spatial resolution  
2.2 μm in density

# Experimental Set-up



## Applications :

+ rotating machinery

NDT (contactless) probe

- rotor shafts
- seals

+ laboratory tool

convenient, easy-to-interpret,  
control of external variables

- lubricant interaction
- influence of T
- wear mechanisms
- spatial variability of wear



The Society shall not be responsible for statements or opinions advanced in papers or in discussion at meetings of the Society or of its Divisions or Sections, or printed in its publications. Discussion is printed only if the paper is published in an ASME Journal. Papers are available from ASME for fifteen months after the meeting.  
Printed in USA.

Scott Bair

Farrukh Qureshi

George W. Woodruff School  
of Mechanical Engineering,  
Georgia Institute of Technology,  
Atlanta, GA 30332

Michael Khonsari

Department of Mechanical Engineering,  
University of Pittsburgh,  
Pittsburgh, PA 15261

## Adiabatic Shear Localization in a Liquid Lubricant Under Pressure

*Experimental tests with a high-pressure flow visualization cell clearly reveal that the shear deformation in a lubricant film at elevated pressures can localize by a mechanism vastly different from previously reported mechanically-induced shear bands. Verification by numerical solution of the energy equation shows that for a stress-controlled experiment, provided that the Brinkman number is sufficiently large, the local temperature experiences a rapid rise. The rapid rise of temperature along with the local rate of shear favors an unstable temperature profile. The research provides valuable insight into the behavior of lubricants under extreme conditions since this phenomenon may be operating in the thermally dominated regime of EHD traction. Furthermore, the fact that the hot shear band is isolated from the metal boundaries by a cooler liquid, may confound recent attempts to infer the shear stress distribution in a concentrated contact from IR temperature measurement of the metal temperature distribution.*

### Introduction

The shear characterization of the thin high-pressure lubricant films in concentrated contact has been a challenge for at least three decades. The shear rheology of the liquid under elastohydrodynamic conditions displays several unique and interesting features: shear thinning is observed—even in relatively low molecular weight liquids (Bair and Winer, 1993). The response may be elastic for small strains (Barlow et al., 1972). The liquid may undergo a glass transition (Alsaad et al., 1978) and display essentially rate-independent behavior at a shear stress which is approximately proportional to pressure at high pressure (Bair and Winer, 1992a, 1979).

Recent experiments have revealed that the rate-independent behavior observed in high-pressure rheometers and disc machines results from intermittent slip within the liquid film along planes inclined to the principal shear direction, consistent with the Mohr-Coulomb failure criterion applied to an elastic liquid. Similar shear bands are observed during rate-insensitive deformation of amorphous polymers. These shear bands have been observed in a high-pressure flow visualization cell (Bair et al., 1992a, 1992b) and there is evidence that they exist in an operating EHD contact (Bair et al., 1992c). It, therefore, appears that continued development of rheological equations of state which consider the isothermal shear deformation to be homogeneous are not likely to result in significant advances in the field. A very different type of shear localization is the subject of this paper. We present the experimental observation and numerical simulation of a thermally driven localization similar to the "adiabatic shear bands" found during high rate deformation of metals (Bair and Dodd, 1992). We have adopted

the term "adiabatic" from the usage in plasticity literature, although the term is not strictly correct.

### Background

In 1967, Plint recognized that the inhomogeneous shear in an elastohydrodynamic film which exists due to viscous heating might localize at or near the mid-plane where the temperature is greatest. If the shear stress,  $\tau$ , is uniform across the film, the viscous dissipation will be approximately exponential with temperature. The lubricating film is generally a poor thermal conductor. Therefore, as the temperature,  $T$ , rises locally the dissipation which generates the temperature field rises rapidly with the local rate of shear,  $\dot{\gamma}$ , and conditions favor an unstable temperature profile.

The parameter which characterizes the thermal behavior of liquid films in plane Couette shear is the dimensionless Brinkman number (also known as Griffith or Nahme number)

$$B_r = \frac{\beta \tau^2 h^2}{\mu_0 k} \quad (1)$$

where  $h$  is the thickness of the film,  $\mu_0$  is the initial viscosity at  $T = T_0$ ,  $k$  is the thermal conductivity of the liquid, and  $\beta$  is the temperature-viscosity coefficient

$$\beta = \frac{-1}{\mu} \frac{\partial \mu}{\partial T} \quad (2)$$

Winter (1977) using time-temperature superposition showed that a generalized temperature-viscosity coefficient can be obtained by multiplying  $\beta$  by the strain-rate sensitivity coefficient,  $\partial \ln \tau / \partial \ln \dot{\gamma}$ . It has been long recognized in the rheology literature that a low value of  $B_r$  is a necessary condition to avoid the influence of viscous heating in continuous shear viscosity measurement (Walters, 1975). However, the significance of the Brinkman number is not well recognized in tribology. The Brinkman number appears as the coefficient of the dissipation

Contributed by the Tribology Division of THE AMERICAN SOCIETY OF MECHANICAL ENGINEERS for presentation at the STLE/ASME Tribology Conference, New Orleans, La., October 24-27, 1993. Manuscript received by the Tribology Division, January 29, 1993; revised manuscript received June 28, 1993. Paper No. 93-Trib-29. Associate Technical Editor: M. Godet.  
Copies will be available until March 25, 1993.

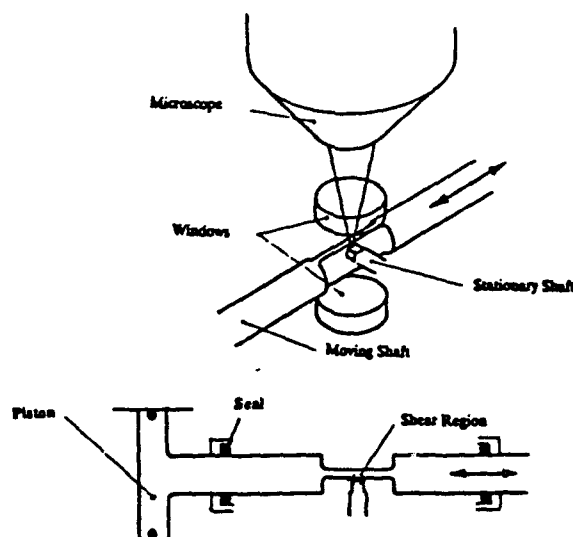


Fig. 1 Flow visualization configuration (illumination through lower window)

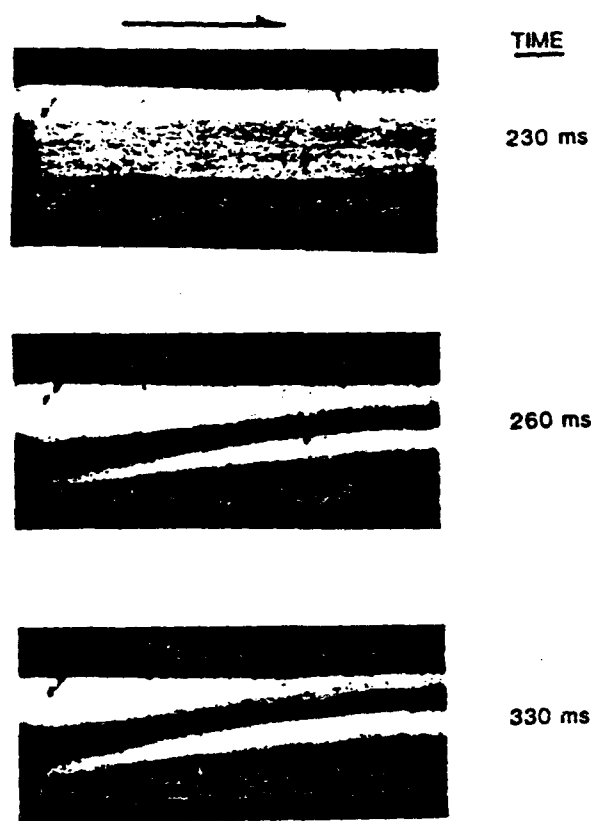
term in the dimensionless energy equation and its value represents the degree of coupling between the energy and momentum equations (Winter, 1977 and Tanner, 1985). A form of  $B$ , was used by Khonsari and Wang (1991) to analyze journal bearings. A steady-state solution to the energy equation exists for  $B_r < 3.51$  when the temperature-viscosity function is exponential (Poehlein, 1968) and for  $B_r < \pi^2$  when the viscosity varies linearly with temperature (Winter, 1971). Experimental investigations of lubricant constitutive behavior for EHD conditions which may be regarded as isothermal are performed at  $B_r < .3$  in high pressure rheometers (Bair and Winer, 1990 and 1993) and disc machines (Evans and Johnson, 1986). Thermal localization phenomena are expected to manifest at large ( $> 3.51$ ) values of  $B_r$ .

## Experiment

The High-Pressure Flow Visualization Cell has been described in detail elsewhere (Bair et al., 1992b). This device is shown schematically in Fig. 1. The liquid lubricant sample is sheared in the gap between a flat on a moving shaft and the end of a stationary shaft. The gap is illuminated and viewed in a direction perpendicular to the direction of motion and parallel to the plane of the bounding surfaces. The moving shaft is pushed/pulled by a gas actuated piston and this shaft must pass through high-pressure closure seals. Motion is not continuous reciprocation, but unidirectional for a given run.

For a shear rheological measurement during which rheological properties vary with time, one would choose to design the experiment following one of two idealizations (Tanner, 1985): 1. rate (of strain) control where the relative velocity is kept constant, or 2. force (stress) control where the average shear stress is imposed as constant. Whereas, it is known that rate control will not yield thermal runaway (Tanner, 1985), we intend to show that in a stress-controlled experiment localization can indeed take place. The device shown (a constant actuating gas pressure applied to the piston) would be ideal for force controlled experiments; however, there exists some friction in the high-pressure seals, which is known to have a viscous component.

The liquid lubricant chosen for this study is the five-ring polyphenyl ether, 5P4E for which there is probably the most high pressure property data available. The thermal properties,  $k = 0.15 \text{ W/m}^\circ\text{C}$  and  $\rho C = 1.85 \text{ MJ/m}^3^\circ\text{C}$ , of Richmond et al. (1984) and the rheological properties of Yasutomi et al. (1984) and Bair and Winer (1992a) were used. Refractive index was measured in a high pressure refractometer described by



5P4E, 22°C INITIAL TEMP, 172 MPa

Fig. 2 Visualization of an adiabatic shear bond. Time is elapsed from start to shear.

Bair (1993). In addition, the properties of this material have a great sensitivity to pressure so that, at relatively low pressure, behavior is observed which is representative of many materials at much greater pressure.

Regulated compressed nitrogen gas was applied to the left side of the piston in Fig. 1 with sufficient pressure (3 MPa) to develop an initial velocity of 0.75 mm/s. The sample pressure was 172 MPa and the initial temperature 22°C yielding a viscosity  $\mu_0 = 3 \text{ MPa}\cdot\text{s}$  and  $\beta = 0.6^\circ\text{C}^{-1}$ . Although the piston force was constant, the force contributed by the seals increased with sliding velocity so that the average stress applied at the shearing gap decreased with velocity (and time). A standard (30 frames/second) video camera recorded the video prints shown in time sequence in Fig. 2. The lower black object is the stationary boundary and the upper is the moving (left to right) boundary. The gap or clearance is 150  $\mu\text{m}$ , and  $\tau$  is obtained from the product of initial viscosity and the initial rate of shear, to give  $B_r = 6.75$ . The central one-third of the length (in the flow direction) is captured in each print.

The velocity history is shown by the points in Fig. 3—obtained by differentiating the signal from an LVDT on the moving shaft. Past 210 ms the velocity exceeded the measurement capability.

A striking feature in the sequence of images in Fig. 2 is the abrupt appearance of a dark band within the liquid film at 260 ms. In the previous frame at 230 ms the band is absent. However the interior of the film has begun to darken. In less than 30 ms a dark band has appeared. This feature faded and disappeared within 10s after the interruption of shear. We show in the next section that the dark band is consistent with the appearance of a hot liquid layer surrounded by cooler liquid. Light transmitted through the film should be refracted from

a hot region to cool regions. Effectively, two cool, viscous liquid films are sliding against a hot low viscosity film. The curvature of the band is apparently due to cool liquid being drawn into the shear gap by the moving shaft at the upper left of the prints in Fig. 2. That the band which suddenly appears represents shear localization will be shown by the analysis which follows.

### Thermal Analysis of Plane Couette Shear Under Stress-Controlled Conditions

The statement of the conservation of energy translates into the following commonly known as the energy equation

$$\rho c_p \frac{DT}{Dt} = (kT_j)_j + \phi, \quad (3)$$

where the left member of the above equation represents the energy transport by convection with  $D/Dt$  representing the material derivative and  $\rho c_p$ , the volume heat capacity. The first term on the right denotes the energy transfer by conduction followed by the viscous dissipation term which is

$$\phi = \tau \dot{\gamma}$$

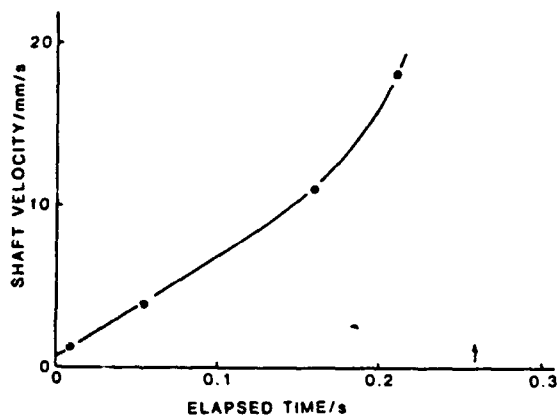


Fig. 3 Velocity history

For the geometry under consideration, the energy equation reduces to

$$\rho c_p \frac{\partial T}{\partial t} = k \frac{\partial^2 T}{\partial y^2} + \phi, \quad (4)$$

where  $y$  is the coordinate normal to the direction of motion in the direction of the film thickness.

If the Newtonian assumption is adopted, the viscous dissipation term becomes

$$\phi = \frac{\tau^2}{\mu}, \quad (5)$$

where the viscosity,  $\mu$ , varies exponentially with temperature (for small  $T - T_0$ ) prescribed as

$$\mu = \mu_0 e^{-\beta(T - T_0)}. \quad (6)$$

The dimensionless form of the Eq. (4) for a stress-controlled experiment takes on the form given below

$$\frac{1}{F_0} \frac{\partial \bar{T}}{\partial \bar{t}} = \frac{\partial^2 \bar{T}}{\partial \bar{y}^2} + B e^{\bar{T}}, \quad (7)$$

where  $F_0$  is the dimensionless Fourier number defined as

$$F_0 = \frac{k}{\rho c_p} \frac{t_{ob}}{h^2}$$

and

$$\bar{T} = (T - T_0)\beta, \quad \bar{t} = \frac{t}{t_{ob}}, \quad \bar{y} = \frac{y}{h}.$$

In defining the Fourier number above, the parameter  $t_{ob}$  represents an observation time.

Equation (7) was treated numerically using a marching technique. The initial and boundary conditions are maintained at  $\bar{T} = 0$ . The time history of the temperature distribution across the film is presented in Fig. 4 for  $B = 6.75$ . As shown, temperature rapidly rises in the center of the film at about 0.06s and becomes unbounded when  $t > 0.062$ s. The existence of hot center temperature surrounded by cooler liquid is indicative of the onset of localization. This is also apparent in the velocity profile at  $t = 0.062$ s shown in Fig. 4.

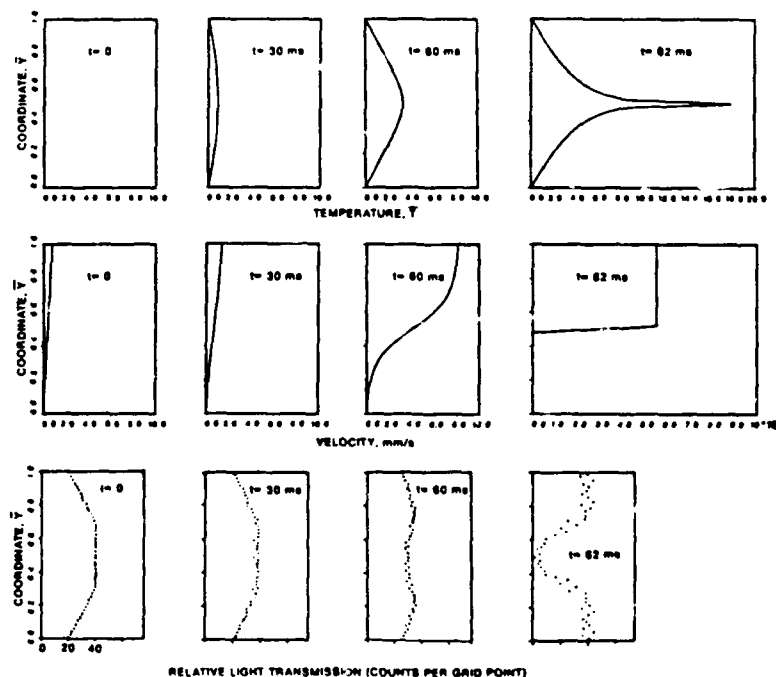


Fig. 4 Analytical results for  $B = 6.75$



## Optical Ray Tracing

It seems reasonable that the last temperature profile of Fig. 4 would result in the appearance of a dark band at the mid-plane. However, a calculation is in order, to show that the dark band accompanies localization and that the band will not appear earlier. The previous thermal analysis yielded temperatures at fifty equally spaced grid points within the liquid film. We assume that the temperature is uniform within strata centered at these points. Sources of light are placed at each grid point across the film at one edge of the liquid film where illumination enters. Forty rays originate from each source, equally distributed over an angular interval of  $\pm 0.05$  radian from the centerline of the stratum. Where a ray intersects the boundary between strata, Snell's Law is applied. Contact with a solid boundary surface absorbs a ray.

The refractive index,  $n_0$ , of the liquid at the test pressure and initial temperature,  $T_0$ , was measured in a high-pressure refractometer (Bair, 1993). The Lorenz-Lorentz equation can be manipulated to yield an expression for the refractive index,  $n$ , at other temperatures through the liquid density,  $\rho$ . The Lorenz-Lorentz equation (Poultier et al., 1932) reads

$$\frac{n^2 - 1}{n^2 + 2} \cdot \frac{1}{\rho} = \text{constant}$$

The thermal expansivity of the liquid lubricant was supplied by the manufacturer and corrected for elevated pressure from the results of Yasutomi et al. (1984).

The number of rays exiting the film gap within a stratum is considered a measure of the relative light transmission at the grid point associated with that stratum. These values are plotted in Fig. 4. It is clear that the dark band for which there is relatively little light transmission is not present at 60 ms but is fully developed at 62 ms and although it is a direct consequence of the temperature profile the band is associated with the extreme localization of shear as indicated by the velocity profile of Fig. 4.

## Discussion

Clearly, the dark band observed in the flow visualization experiment is due to a thin hot layer of liquid sandwiched between two cooler layers. This hot layer represents a region where the shear deformation is localized. The greatest part of the relative velocity is accommodated within a small fraction ( $\sim 5$  percent) of the film thickness. Notably, the localization occurs at shorter times than observed in experiments. We believe that this is due in most part to the inability of the experimental technique to achieve true stress control stemming from viscous seal friction which increases with sliding velocity and decreases with time of sliding or temperature.

The one-dimensional analysis presented here forces symmetry about the center of the film. The experimental geometry is finite in length in the flow direction with an inlet to the left in Fig. 2. The adiabatic shear band near the entrance is therefore displaced toward the hotter stationary boundary at the bottom of each print in Fig. 2 by the cooler liquid convected into the gap by the upper moving boundary. This accounts for the curvature of the band pictured in Fig. 2.

Lubricant resident times in EHD are typically about 1 ms or much less. In this simulation, localization occurs at longer times—on the order of 100 ms. However, in the dimensionless energy Eq. (7), time is scaled by  $h^2 \rho C_p / k$ . The film thickness,  $h$ , is at least 100 times thinner for a lubricated contact. Hence, the localization time would be of the order of 10  $\mu$ s which is in the realm of EHD.

## Conclusions

The shear deformation in a lubricant film at elevated pres-

sure can localize by a mechanism vastly different from previously reported mechanically induced shear bands. In a manner suggested by Plint (1967) and observed during high rate forming in metals, a shear band can form in liquid lubricants which possess a low thermal conductivity and a viscosity which falls exponentially with temperature. If the shear stress is uniform across the film, the dissipation will vary exponentially with temperature. Then as the temperature rises locally, the dissipation which generates the temperature rises rapidly with the local rate of shear and conditions favor an unstable temperature profile if the Brinkman number is sufficiently large. This phenomenon may be operating in the thermally dominated regime of EHD traction. Additionally, if the hot shear band is isolated from the metal boundaries by cooler liquid, this may confound recent attempts to infer the shear stress distribution in concentrated contact from IR temperature measurement of the metal temperature distribution.

## Acknowledgment

The work presented here was sponsored in part by the Office of Naval Research, Materials Division, and two of the authors (Bair and Qureshi) gratefully acknowledge this support.

## References

- Alsaad, M., Bair, S., Sanborn, D., and Winer, W. O., 1978, "Glass Transitions in Lubricants: Its Relation to EHD," *ASME JOURNAL OF LUBRICATION TECHNOLOGY*, Vol. 100, No. 2, pp. 404-417.
- Bair, Y., and Dodd, B., 1992, *Adiabatic Shear Localization*, Pergamon Press Oxford, p. 1.
- Bair, S., 1993, "An Experimental Verification of the Significance of the Reciprocal Asymptotic Pressure Coefficient," *STLE Tribology Transactions*, Vol. 36, No. 2, p. 156.
- Bair, S., and Winer, W. O., 1979, "Shear Strength Measurements at High Pressure," *ASME JOURNAL OF LUBRICATION TECHNOLOGY*, Vol. 101, No. 3, p. 255.
- Bair, S., and Winer, W. O., 1990, "The High Shear Stress Rheology of Liquid Lubricants at Pressures of 2 to 200 MPa," *ASME JOURNAL OF TRIBOLOGY*, Vol. 112, No. 2, pp. 246-253.
- Bair, S., and Winer, W. O., 1992, "The High-Pressure, High Shear Stress Rheology of Liquid Lubricants," *ASME JOURNAL OF TRIBOLOGY*, Vol. 114, No. 1, pp. 1-13.
- Bair, S., Winer, W. O., and Qureshi, F., 1992b, "Experimental Observation of Shear Localization in Liquid Lubricants Under Pressure," *Trans. ASME, Trib-3*.
- Bair, S., Winer, W. O., and Distin, K. W., 1992c, "Experimental Investigations into Shear Localization in an Operating EHD Contact," *Proceedings Leeds-Lyon Symposium*.
- Bair, S., and Winer, W. O., 1993, "A New High-Pressure, High-Shear Stress Viscometer and Results for Lubricants," *STLE Tribology Transactions*, Vol. 36, No. 4.
- Barlow, Harrison, Irving, Kim, Lamb and Pursley, 1972, "The Effect of Pressure on the Viscoelastic Properties of Liquids," *Proc. Royal Soc. London, Series A327*, pp. 403-412.
- Evans, C. R., and Johnson, K. L., 1986, "The Rheological Properties of EHD Lubricants," *Proc. Instn. Mech. Engrs.*, Vol. 200, No. C5, pp. 307-309.
- Khonsari, M. M., and Wang, S. H., 1991, "On the Maximum Temperature in Double Layered Journal Bearings," *ASME JOURNAL OF TRIBOLOGY*, Vol. 113, No. 3.
- Plint, M. A., 1967, "Traction in Elastohydrodynamic Contacts," *Proc. Instn. Mech. Engrs.*, Vol. 182, Pt. 1, No. 14.
- Poehlein, G., 1968, "Temperature Effects in Couette Viscometers," *Trans. Soc. Rheology*, Vol. 12, No. 2.
- Poultier, T. C., Ritchey, C., and Benz, C., 1932, "The Effect of Pressure on the Index of Refraction of Paraffin Oil and Glycerine," *Phys. Review*, Vol. 41, pp. 366-367.
- Richmond, J., Nilsson, O., and Sandberg, O., 1984, "Thermal Properties of Some Lubricants under Pressure," *J. Appl. Phys.*, Vol. 56, No. 7, pp. 2066-2067.
- Tanner, R. I., 1985, *Engineering Rheology*, Clarendon Press, Oxford, p. 365, 373.
- Walters, K., 1975, *Rheometry*, Wiley, New York, pp. 80-81.
- Winter, H. H., 1971, "The Unsteady Temperature Field in Plane Couette Flow," *Int. J. Heat Mass Transfer*, Vol. 14, pp. 1203-1212.
- Winter, H. H., 1977, "Viscous Dissipation in Flowing Molten Polymers," *Advances in Heat Transfer*, Vol. 13, p. 217.
- Yasutomi, S., Bair, S., and Winer, W. O., 1984, "An Application of a Free Volume Model to Lubricant Rheology," *ASME JOURNAL OF TRIBOLOGY*, Vol. 106, No. 2, pp. 304-312.

Printed in U.S.A.



The Society shall not be responsible for statements or opinions advanced in papers or in discussion at meetings of the Society or of its Divisions or Sections, or printed in its publications. Discussion is printed only if the paper is published in an ASME Journal. Papers are available from ASME for fifteen months after the meeting.  
Printed in USA.

S. Bair

Senior Research Engineer.

F. Qureshi

Graduate Research Assistant.

W. O. Winer

Regents' Professor and Director.

George W. Woodruff School of  
Mechanical Engineering,  
Georgia Institute of Technology,  
Atlanta, GA 30332

## Observations of Shear Localization in Liquid Lubricants Under Pressure

*A High Pressure Flow Visualization Cell has been designed and constructed to perform a fundamental investigation of the deformation behavior of liquid lubricants under lubricated concentrated contact conditions. A pressure of 0.3 GPa and a shear stress between parallel plates of about 25 MPa has been demonstrated. Time averaged velocity profiles show no continuous slip either in the bulk or at walls. Localized slip at shear bands inclined to the walls was demonstrated to occur during nonlinear shear response. The number of shear bands increases with shear rate (and shear stress) from as few as one at the onset of non-Newtonian flow until the shear region is essentially filled with bands with a spatial periodicity of 7  $\mu\text{m}$ . Bands are typically inclined 19 deg off the solid surfaces in a direction which reduces the compressive normal stress due to shear on the plane of the band.*

### 1 Introduction

The nature of traction behavior in the elastohydrodynamic (EHD) lubrication of concentrated contacts has been a vexing problem that has plagued researchers for years. Linear Newtonian behavior fails spectacularly in predicting EHD frictional traction. The fact that traction in EHD seldom exceeds one-tenth of the average pressure and that this could not be explained in terms of a Newtonian viscous fluid led Smith (1959) to propose a limiting shear stress for the lubricant. That is, that the lubricant flows as a plastic solid at some shear stress which varies with temperature and pressure. This concept has been supported by numerous primary high-pressure measurements (Bair and Winer, 1979 and 1990, and Ramesh and Clifton, 1987).

The transition from linear Newtonian behavior to rate-independent (plastic) behavior is illustrated by the steady shear flow curves in Fig. 1. Here, the logarithm of shear stress,  $\tau$ , is plotted versus logarithm of shear rate,  $\dot{\gamma}$ , for a polyphenyl ether (5P4E) and a mineral oil (N1). Shear stress is observed to increase first in proportion to shear rate (Newtonian)—then a nonlinear transition region occurs—followed by continuous shearing at a limiting stress,  $\tau_L$ . This limiting stress is approximately proportional to pressure. The data for the lowest pressure of Fig. 1 marked with (x) represent measurements with a new rotating concentric cylinder rheometer with greatly reduced instrument response time compared with results previously reported (Bair and Winer, 1990). These data confirm that the observed behavior is independent of time of shear.

An empirical law has been proposed, which in its simplest form is written

$$\dot{\gamma} = \frac{\tau_L}{\mu} \ln(1 - \tau/\tau_L) \quad (1)$$

Elastic effects are observed for transient loading in shear (Bair and Winer, 1979). The recoverable elastic strain is typically 0.02 to 0.03. Because the glass transition temperature increases with pressure, many liquid lubricants are below the glass transition temperature in concentrated contact (Alsaad et al., 1978). In Fig. 1,  $\hat{p}$  is the ratio of pressure to glass transition pressure.

As of this time the limiting shear stress concept lacks a firm theoretical foundation. Evans and Johnson (1986) proposed a mechanism by which the nonlinear transition is attributed to the thermal activation model of Eyring and the rate-independent behavior is explained by shear bands as occur in the deformation of solid polymers. Bair and Winer (1990) showed that the dislocation model of Gilman (1975) for amorphous metals predicts the pressure dependence of the limiting stress. Many have suggested wall slip and Kaneta et al. (1990) have presented an inconclusive argument based on EHD film thickness observations to support wall slip.

It is the objective of this paper to present a fundamental investigation of the shear deformation of liquid lubricant films at high-pressure to elucidate the flow mechanisms which produce the observed rheological behavior. Toward this end, flow visualization experiments have been designed and conducted.

### 2 Experimental

**2.1 Technique.** In order to visualize the shear deformation of liquid lubricant films at elevated pressure, a test cell must shear a liquid sample in such a manner that the sample may be illuminated and local displacements or velocities be

Contributed by the Tribology Division of THE AMERICAN SOCIETY OF MECHANICAL ENGINEERS for presentation at the ASME/STLE Tribology Conference, San Diego, CA, October 18-21, 1992. Manuscript received by the Tribology Division January 17, 1992; revised manuscript received May 1992. Paper No. 92-Trib-3. Associate Technical Editor: M. Godet.

This paper has been published, referenced as follows:

Bair, S., Qureshi, F., and Winer, W. O. (1993) "Observations of Shear Localization in Liquid Lubricants Under Pressure," *Trans. ASME, J. of Tribology* 115, No. 3, pp. 507-514.

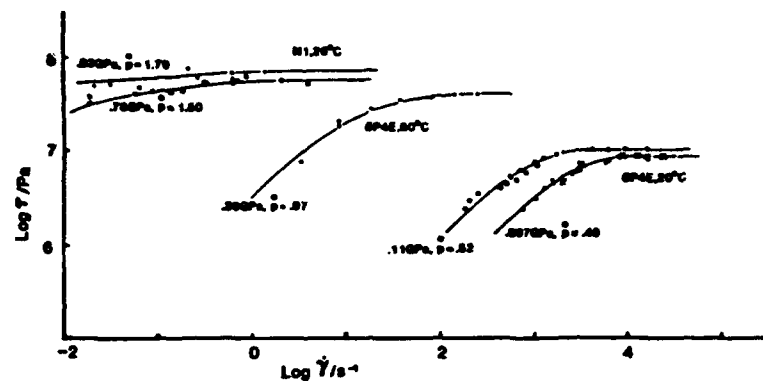


Fig. 1 The transition from Newtonian to plastic flow for various dimensionless pressures.  $\tau$  is shear stress and  $\dot{\gamma}$  shear rate.

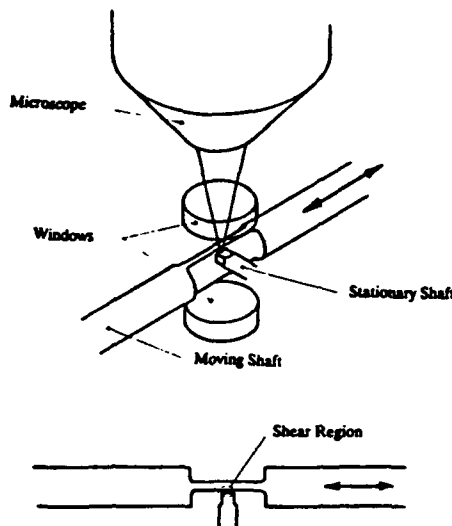


Fig. 2 Flow visualization configuration (illumination through lower window)

viewed and measured. To simplify interpretation of results, the parallel plate viscometer configuration was selected. A schematic drawing of the flow visualization configuration is given in Fig. 2. The liquid sample is sheared between the end of a stationary shaft (pin) and a flat on the side of a moving shaft. The moving shaft translates axially. Illumination and viewing are at right-angles to the axes of both shafts.

Two techniques for flow velocity measurement were considered: laser Doppler velocimetry and particle tracing. The former technique was rejected due to rather large (compared to the film thickness) spatial resolution. However, the present flow cell may be adaptable to other measurement techniques not yet considered.

Originally, carbon black with  $0.3 \mu\text{m}$  particle size was used as a tracer because of its opacity. This material agglomerates into larger particles of various sizes. It was quickly found that the larger of these particles could be seen far from the plane of focus of the microscope. Since it is imperative that only particles within the shearing gap be seen and preferable that only particles near the focal plane be visible, the smallest visible particle should be selected. Commercially available polystyrene tracer spheres with fluorescent dye were found to be soluble in some lubricants. Glass spheres of  $2 \mu\text{m}$  diameter were found to be visible in one of our model lubricants (SP4E)—apparently due to the difference in refractive index. These particles are not visible at more than  $0.1 \text{ mm}$  from the focal plane.

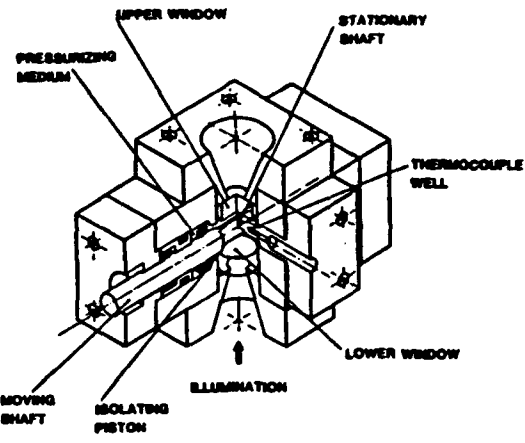


Fig. 3 High-pressure flow visualization cell

**2.2 Test Cell.** The final design of the High-Pressure Flow Visualization Cell is shown in Fig. 3 in cut-away. The internal components are symmetric about the cutting plane through the stationary shaft so that the entire cell interior need not be shown. The stationary shaft or pin is hollow to accept a thermocouple and is clamped to the pressure vessel. The moving shaft extends completely through the vessel to balance the hydrostatic force upon it. The shearing gap may be varied from  $0$  to  $200 \mu\text{m}$  by rotating the moving shaft, although the boundaries are only exactly parallel for one gap dimension. Illumination is usually through the lower window. A beam splitting prism in the optics allows illumination from above for finding the top of the gap.

The moving shaft passes through one isolating piston and one high-pressure seal at each end. The pressurizing medium, a diester, is admitted between the high-pressure seal and the isolating piston through a port in the back of the cell. The moving shaft is driven axially by a hydraulic cylinder (not shown in the figure) and positioned rotationally by a worm and gear (also not shown). The axial displacement of this shaft is measured by an LVDT external to the cell.

Windows are sapphire and are sealed to the closures by a lapped fit. Temperature of the cell is controlled by either a resistance heater or liquid nitrogen boil-off passing through an aluminum block which is fastened to the exterior of the cell. Temperature is measured at the thermocouple in the hollow stationary shaft (pin).

Initially, the moving shaft was driven hydraulically by kerosene from a variable displacement metering pump. It was soon found that the vibration of the pump motor caused the

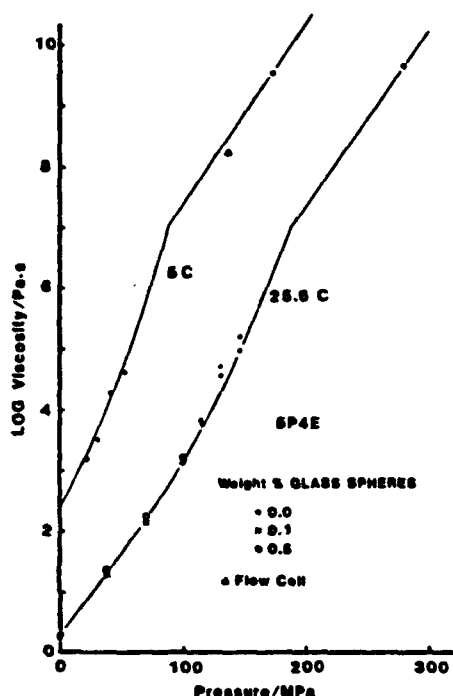


Fig. 4 Pressure-viscosity of SP4E and the effect of the 2  $\mu$ m tracer particles

small (2  $\mu$ m) tracer particles to disappear from view. Bottled gas was used thereafter in place of the pump.

The cell was pressure tested at 350 MPa and results have been obtained to 280 MPa.

**2.3 Optics.** A prerequisite for a microscope objective used to view material within a pressure cell is a long working distance to accommodate the thick pressure vessel walls. In this case, the minimum working distance is about 20 mm—longer if filters are placed between the cell and objective. Also a high magnification is required in order to keep the gap and tracer particles small. For these reasons, a reflecting objective (15X) was selected.

Illumination through the lower window is provided by a 150W incandescent variable source through a fiber optic bundle. A 50W incandescent source is provided for illumination from above in order to position the focal plane at the top of the shearing gap as seen in the upper view of Fig. 2. A dial indicator mounted to the microscope tube indicates the microscope objective relative working distance so that any position measured into the gap may be selected. However, there is a fundamental problem related to viewing the interior of a cavity with parallel walls in that material near the wall is obscured by the interference of the opaque wall with the acceptance cone of the objective. This effect is such that for each 100  $\mu$ m deeper one moves the focal plane into the gap, 5  $\mu$ m is obscured along the wall. A depth of 200–250  $\mu$ m into the gap was selected for viewing as a compromise between the conflicting requirements of viewing fully-developed flow and seeing material near the walls.

The microscope tube has been adapted to accept video cameras and a 35 mm film camera. A high-speed video system of up to 1000 frames per second was available.

**2.4 Experimental Liquid Lubricants.** For an exploratory study of lubricant shear rheology, it is advantageous to select as model liquids, materials which have seen application as EHD

lubricants and for which much data—both rheological and tribological—are available in the literature. Also, as the velocity measurement technique is limited to low shear rates of less than  $10s^{-1}$ , it is important that the viscosity be great enough to yield non-Newtonian flow at this shear rate. That is, a shear stress approximately equal to the limiting stress must be obtained at a shear rate of  $10s^{-1}$ .

The liquids selected are: a mineral oil—LV1 260 and two synthetic oils—SP4E, a polyphenyl ether and MCS 1218, a cycloaliphatic hydrocarbon. These have been characterized extensively in the literature (Johnson and Tevaarwerk, 1977; Bair and Winer, 1982 and 1990; Hutton, 1985; Alsaad et al., 1978).

As a guide in selecting experimental conditions and in interpreting the results, it was necessary to determine the pressure-viscosity characteristics of the experimental liquids. This was done to pressures above the glass transition by a method outlined by Bair and Winer, 1992. Results are shown in Fig. 4 for SP4E.

It is important to show that the tracer particles have negligible influence on the liquid rheology. This was demonstrated in the Newtonian regime by repeating some of the viscosity measurements with 2  $\mu$ m glass spheres dispersed in the liquid. Weight fractions of 0.1 and 0.5 percent were employed and are typical of concentrations used in the flow visualization experiments. (Volume fractions are 0.4 of these values.)

The viscosity,  $\mu$ , was found to be a function of temperature,  $T$ , and pressure,  $p$ , which could be described by a modified free volume model (Bair and Winer, 1991). The curves in Fig. 4 represent

$$\mu = \begin{cases} \mu_g e^{-2.3 \left[ \frac{C_1(T-T_g(p))F(p)}{C_2 + (T-T_g(p))F(p)} \right]}, & p \leq p_g \\ \mu_g e^{\alpha_g(p-p_g)}, & p > p_g \end{cases} \quad (2)$$

$$T_g = T_{g0} + A_1 \ln(1 + A_2 p)$$

$$F = 1 - B_1 \ln(1 + B_2 p)$$

The glass transition is assumed to be an isoviscous state with viscosity,  $\mu_g$ , at temperature  $T_g$ . Both  $T_g$  and the relative free volume expansivity,  $F$  vary with pressure. The conventional free volume relation fails above the glass transition pressure,  $p_g$  and is replaced by an exponential relation with a pressure viscosity coefficient,  $\alpha_g$ . This modification of the WLF equation is in general consistent with the recent results of Spathis et al. (1991).

### 3 Results

**3.1 Shear Force Measurement.** During preliminary measurements it was observed that the stationary shaft or pin deflected a small but measurable distance in the manner of a cantilever beam due to the shear stress at the shearing region and due to the drag of liquid flowing around the pin outside diameter. The relationship between pin deflection and a shear force at the end of the pin (stationary shaft) was calibrated and found to be linear. When the edge of the pin is in view (i.e., the entrance or exit to the shearing region) the shear force can be measured. Unfortunately, the pin deflection is not entirely due to the shear stress in the region of interest. Liquid must flow around the outside cylindrical surface of the pin when shearing is taking place in the gap. If the effective shear force from the drag of the flow around the pin varies linearly with moving shaft speed (and, therefore, with shear rate in the shear region) then, any nonlinearity in the steady shear force-shear rate response must be attributed to non-Newtonian flow in the shear region. This is reasonable because the Reynolds number for the external flow is very small ( $< 10^{-10}$ ).

For Fig. 5, the pin force is plotted versus shear rate (deter-

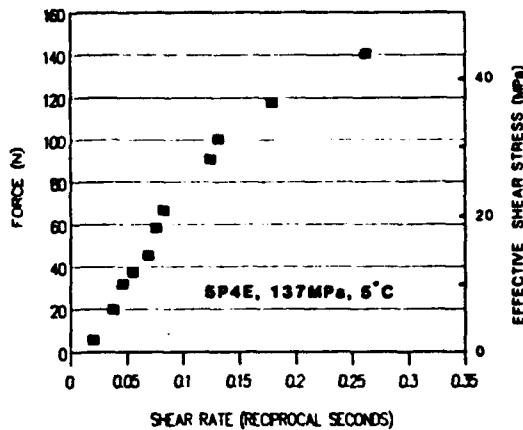


Fig. 5 Pin force versus overall shear rate

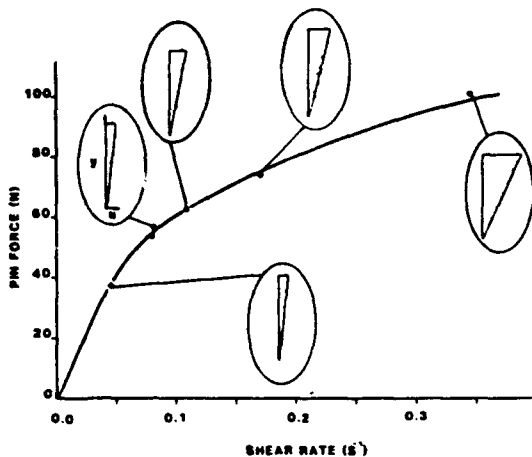


Fig. 6 Velocity profiles

mined from the moving shaft velocity divided by the gap which was  $150\text{ }\mu\text{m}$ ). A linear proportional behavior is observed up to a force of 100 N. If this force is converted to an effective shear stress by dividing the area of the pin end, the nonlinearity begins at about 30 MPa. The limiting shear stress at these conditions would be expected to be about 23 MPa from concentric cylinder rheometer measurements (Bair and Winer, 1990). In fact, if the last two measured points on Fig. 5 are assumed to represent rate-independent behavior in the shear region, the force due to free stream drag can be subtracted and a limiting shear stress of 21 MPa results. It may be concluded that a departure from linearity in the pin force/shear rate represents the transition between Newtonian to limiting stress behavior. The viscosity determined in this exercise is  $1.7 \times 10^8\text{ Pa}\cdot\text{s}$  which is in agreement with the viscosity measurements of Fig. 4 and is shown as the triangle in that figure.

**3.2 Velocity Profiling.** Local time averaged liquid velocities can be determined from the ratio of particle displacement to the time interval over which the displacement occurred (Muller-Mohnssen et al., 1990) assuming that the local particle velocity is identical to the local liquid velocity. Several commercial image analysis systems were utilized in an attempt to automate the particle tracing. All of these systems were found to be incapable of recognizing particles as small as  $2\text{ }\mu\text{m}$  and as explained previously we prefer not to use larger particles.

A typical set of time averaged velocity profiles is shown in Fig. 6 for the indicated shear rates. The gap measured  $127\text{ }\mu\text{m}$ . The local velocity,  $u$ , was found from the displacement of a tracer particle over a time which varied from one to two sec-

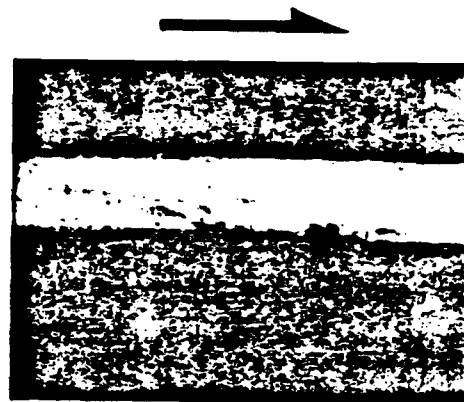


Fig. 7 Shear bands in 5P4E at 220 MPa, 22°C, and shear rate of  $0.25\text{ s}^{-1}$

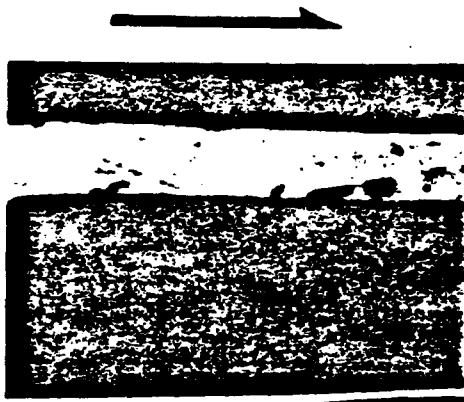


Fig. 8 Single shear band in 5P4E at 261 MPa, 22°C

onds. The velocity scale is not the same for all plotted profiles. Velocities are corrected for the deflection of the pin and the particle concentration was 0.1 percent by weight.

A total of about twenty-five velocity profiles have been obtained for the liquid 5P4E, for various temperatures, pressures and shear rates. These profiles, which were time averaged over several seconds, indicate a linear velocity variation across the gap. The velocities when extrapolated to the wall position are in good agreement with the wall velocities. (Note that approximately  $20\text{ }\mu\text{m}$  of liquid near the wall is obscured.) Then, if wall slip were occurring, it would necessarily be a very small fraction of the relative velocity of the boundary surfaces.

**3.3 Observation of Shear Bands** It was observed during

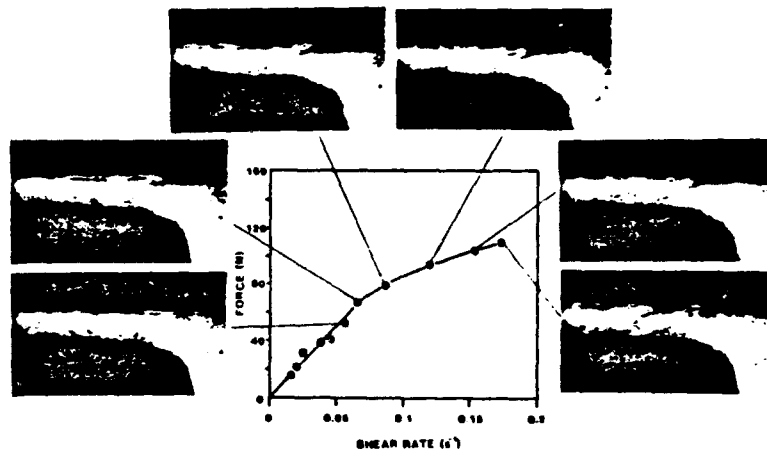


Fig. 9 Shear bands are associated with nonlinear behavior

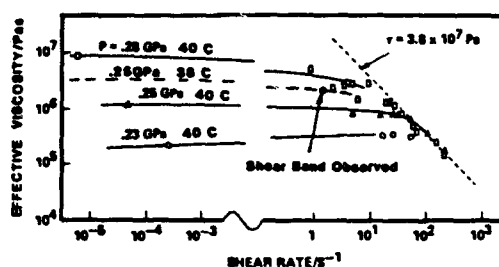


Fig. 10 Effective viscosity of 5P4E versus shear rate showing the limiting shear stress and the observation of shear bands

the velocity profiling that at the higher shear stresses visible artifacts appeared in the form of bands. When polarizing filters were placed between the light source and the cell and/or between the cell and the microscope, thick diffuse colored bands were observed along flow streamlines during stress transients. These are possibly due to birefringence from molecular alignment in shear. When no optical filters were employed and particularly for low tracer particle concentration very sharp bands were inclined to the liquid boundaries in the manner which has been observed for shear bands in solid polymers (Wu and Li, 1976). It is these sharp inclined shear bands that are of primary interest here and will be examined in more detail in what follows. It will be shown that slip or shear localization actually occurs along an individual band.

Multiple shear bands are shown in the two video prints in Fig. 7 along with the shearing direction. These bands appear at angle to the solid surfaces and oriented such that they lie in a plane of reduced normal stress due to shear. The inclination is 19 to 20 deg for 5P4E, about 23 deg for MCS 1218 and 16 to 19 deg for LVI 260. The conditions for Fig. 7 are 220 MPa, 22°C and a shear rate of 0.25 s<sup>-1</sup>. The material is 5P4E and the gap is 130 μm. When multiple bands form and fill a region, as in Fig. 7, a spatial periodicity is seen and the separation is about 7 μm measured perpendicular to the band. A single band is shown in Fig. 8 at higher pressure and much lower shear rate. Shear bands were observed in 5P4E at pressures of 125 to 280 MPa, temperatures of 5 to 40°C and for gaps of 47 to 220 μm and shear rates to 100 s<sup>-1</sup> and in LVI 260 (mineral oil) at a pressure of 270 MPa and 5°C and for MCS 1218 at 241 MPa and 15°C. Note that the 2 μm tracers are too small to be visible in these prints. Recall also that liquid very near the solid boundary is not visible in Fig. 8. Consideration of conservation requires that the shear band not intersect a wall. The band must terminate away from the wall.

The appearance of shear bands is associated with the onset

of nonlinear shear rheology as shown in Fig. 9. The first shear band is observed in the second video print from the left which corresponds to the first data point past the Newtonian regime as described in a previous section. The pressure is 220 MPa and the temperature is 22°C. This correlation was found at several temperature/pressure combinations. As the pin force (and shear stress) is increased the bands proliferate until they appear to fill the entire shearing region. The first band was always observed to occur very near the inlet to the shearing gap; possibly due to the corner of the pin acting as a stress concentration or possibly due to a lower temperature and, therefore, higher viscosity, hence higher stress at the inlet. This fact facilitated the study of individual shear bands in the next section.

Shear bands have been observed for conditions which overlap conditions for a previously measured flow curve (Bair and Winer, 1979b). The effective viscosity plotted in Fig. 10 was obtained in a high shear stress viscometer (Bair and Winer, 1979a). Shear bands were observed at the conditions indicated on the figure.

**3.4 Slip Measurement.** The tracer particles which were used to generate velocity profiles can be used to detect slip associated with a band. For this purpose it will be useful to find two particles near the midplane of the shearing region and nearly equidistant from the solid boundaries. The motion of this pair of particles without the influence of a shear band is shown in Fig. 11(a). Particles A and B move an equal distance in the shear direction over some time interval. If a shear band were operating between these particles, then the motion would be expected to be the same as in Fig. 11(a) except that a slip displacement aligned with the band would be added to the particle motion as shown in Fig. 11(b). Our ability to measure a particle position is limited to a resolution of about 0.5 μm and the video signal contains an electronic jitter; therefore, it is convenient to place a coordinate system, XY, on particle A as in Fig. 11(c). (Recall that these particles are equidistant from the boundaries.) Now, if there is no slip, the X and Y coordinates of B will not change over a time interval during which a band exists between A and B. If slip occurs, the total slip can be found from the change in X and Y during that time interval, ΔX and ΔY, respectively. Video tapes were reviewed to find pairs of particles which satisfied the above geometric requirements and for which a single shear band passed between. The displacement of B with respect to A is plotted for one such pair in 5P4E in Fig. 12. The displacement at the indicated time is relative to time zero. Straight lines were drawn between readings which were taken at 1, 2, and 3 seconds although the actual history between readings is not known. A shear band

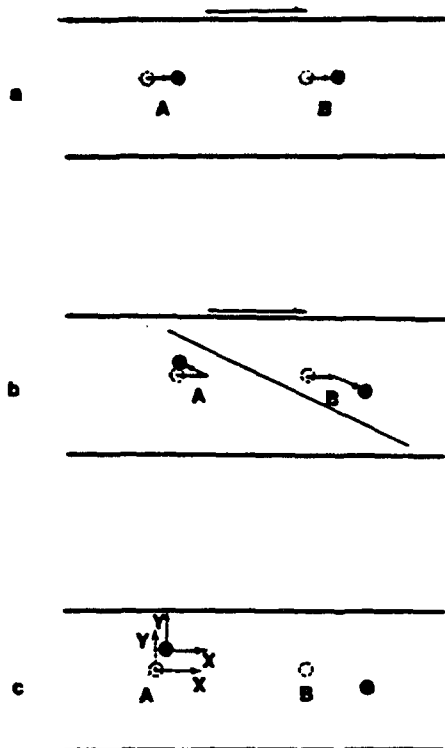


Fig. 11 Particle motion under influence of a shear band

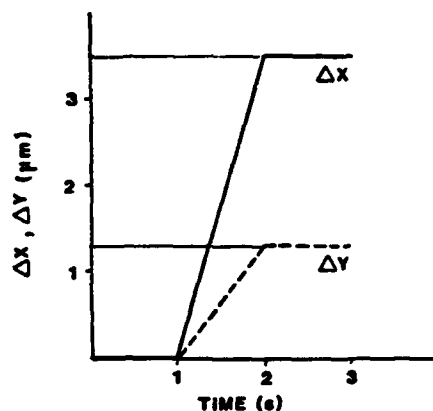


Fig. 12 Relative displacement of a pair of particles astride a shear band

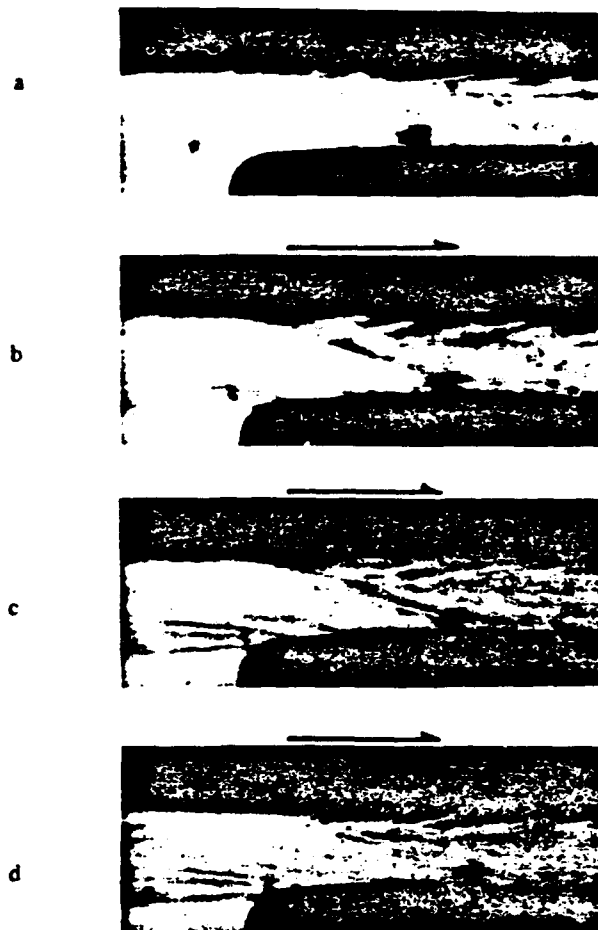
was visible for some time between 1 and 2 seconds and not for the previous and succeeding interval. The relative displacements are consistent with slip along the band.

The total slip,  $\sqrt{\Delta X^2 + \Delta Y^2}$  is tabulated along with the slip direction,  $\tan^{-1}(\Delta Y/\Delta X)$ , for three examples. The first entry in Table 1 is that of Fig. 12. Recalling that our resolution is  $0.5 \mu\text{m}$ , the slip direction is consistent with the observed band orientation.

The slip across a band is dramatically illustrated in Fig. 13 where a shear band intersects a large particle of extraneous material in 5P4E. The particle is visible near the stationary shaft in Fig. 13(a). A band passes through and cleaves the particle in Figs. 13(b) and (c). The particle pieces are seen to be shifted with respect to one another along the direction of the band and remain shifted after the band has disappeared in Fig. 13(d). The sense of the shift in cleaved particle pieces is consistent with the sense of shear of the bulk material.

Table 1 Relative displacements of particles astride shear bands

Pressure MPa	Temp. °C	Shear rate $s^{-1}$	5P4E	
			$\sqrt{\Delta X^2 + \Delta Y^2}$ $\mu\text{m}$	$\tan^{-1}\Delta Y/\Delta X$
130	5	0.12	3.9	19°
130	5	0.13	5.0	20°
130	5	0.14	5.9	29°



5P4E at 221 MPa, 23°C

Fig. 13 Interaction of a shear band with a large particle

**3.5 Shear Band Inclination.** An interesting and important aspect of shear bands is the nonzero angle of inclination,  $\theta$ , with the direction of principal shear. This angle of inclination is a clue to the mechanism (Bowden and Jukes, 1972) of shear localization and is expected from the pressure dependence of limiting shear stress. Our preliminary results suggest that  $\theta$  may be a material property, possibly related to the pressure-limiting stress coefficient  $\lambda$ . The ranking of shear band angle for the three materials is consistent with the ranking of the limiting shear stress (Bair and Winer, 1982).

In Fig. 14 are plotted inclination angles for 5P4E for various pressures. Within experimental error, the angle,  $\theta$ , appears to be independent of pressure. The glass transition pressure,  $p_g$ , is indicated. Note that our measurements bracket the glass transition.

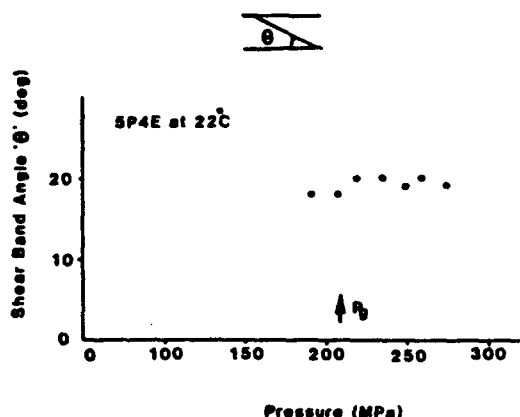


Fig. 14 Shear band inclination,  $\theta$ , versus pressure

The effect of shearing gap is investigated in Fig. 15 and the observed angles are independent of gap size.

**3.6 Shear Band Distribution.** A significant observation that deserves mention is that, aside from a preference toward the inlet to the gap for the initial appearance of a band, one can not predict beforehand the location of a shear band. This is particularly apparent at intermediate shear rates where bands appear in clusters with unaffected liquid in between (see Figs. 7 and 9). One may then conclude that a shear band will nucleate in a linear viscoelastic matrix when the shear stress reaches some critical value which exists at that location. This critical stress,  $\tau_c$ , is therefore statistically distributed within the material and the mean of that distribution is the limiting shear stress,  $\tau_L$ . We would expect that the functional form of Eq. (1) is a result of that distribution.

#### 4 Conclusion

A High Pressure Flow Visualization Cell has been designed and constructed to perform a fundamental investigation of the deformation behavior of liquid lubricants under lubricated concentrated contact conditions. A pressure of 0.3 GPa and a shear stress between parallel plates of about 25 MPa have been demonstrated. Time averaged velocity profiles show no continuous slip either in the bulk or at walls. Localized slip at shear bands inclined to the walls was demonstrated to occur during nonlinear shear response. The number of shear bands increases with shear rate (and shear stress) from as few as one at the onset of non-Newtonian flow until the shear region is essentially filled with bands with a spatial periodicity of 7  $\mu\text{m}$ . Bands are typically angled 16 to 23 deg off of the solid surfaces in a direction which reduces the compressive normal stress due to shear on the plane of the band. This angle may be a property of the material. Of course, conservation requires that slip not extend to the boundary. The shear band may turn tangent to the wall or end near the boundary. According to Haward (1973) shear bands may be wholly contained within the body accommodated by elastic deformation between the ends of the bands and the boundaries.

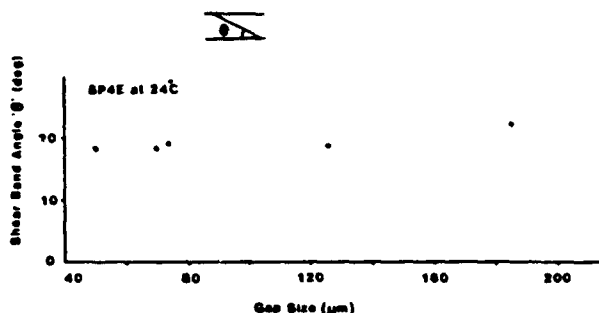


Fig. 15 Shear band inclination versus shearing gap

#### Acknowledgments

The authors are grateful for support from the Office of Naval Research, Materials Division.

#### References

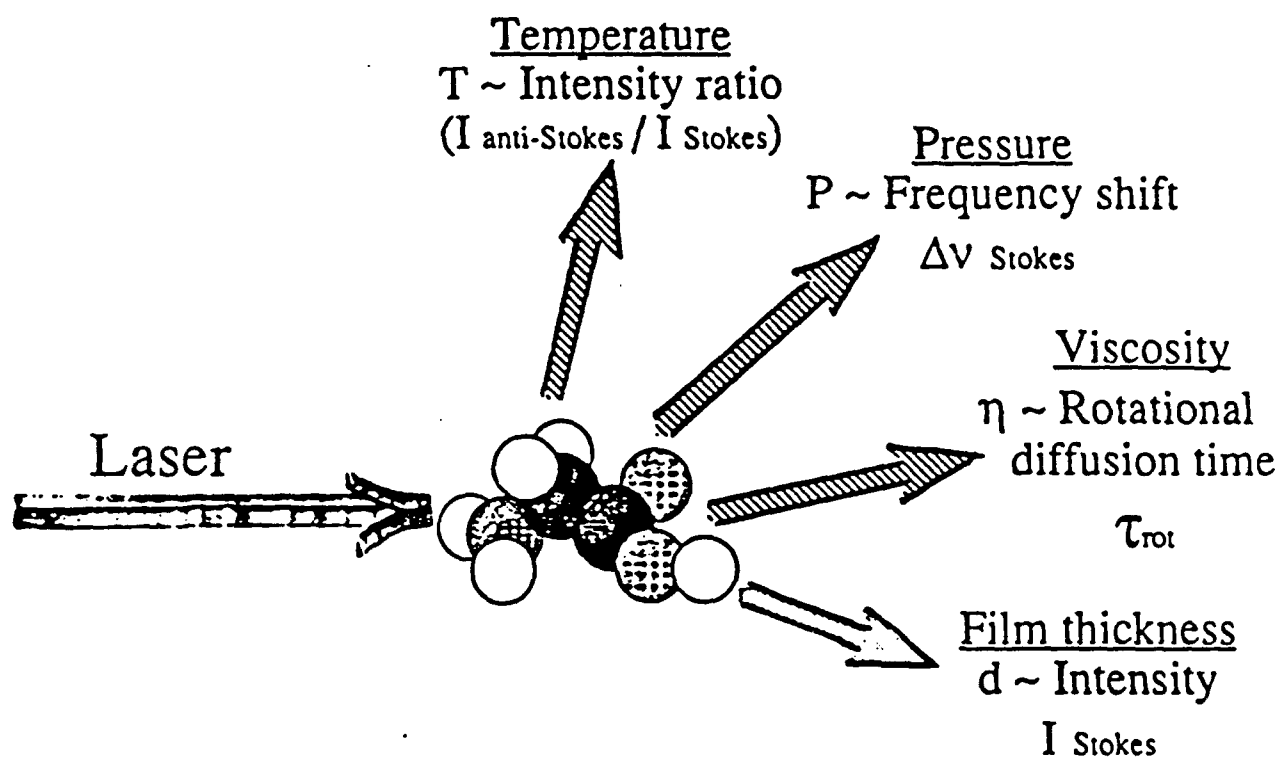
- Alsaad, M., Bair, S., Sanborn, D. M., and Winer, W. O., 1978, "Glass Transitions in Lubricants: Its Relation to EHD Lubrication," *ASME JOURNAL OF LUBRICATION TECHNOLOGY*, Vol. 100, No. 2, pp. 404-417.
- Bair, S., and Winer, W. O., 1979a, "Shear Strength Measurements at High Pressure," *ASME JOURNAL OF LUBRICATION TECHNOLOGY*, Vol. 101, No. 3, pp. 251-257.
- Bair, S., and Winer, W. O., 1979b, "A Rheological Model for Elastohydrodynamic Contacts Based on Primary Laboratory Data," *ASME JOURNAL OF LUBRICATION TECHNOLOGY*, Vol. 101, No. 3, pp. 258-265.
- Bair, S., and Winer, W. O., 1982, "Some Observations in High Pressure Rheology of Lubricants," *ASME JOURNAL OF LUBRICATION TECHNOLOGY*, Vol. 104, No. 3, pp. 382-386.
- Bair, S., and Winer, W. O., 1990, "The High Shear Stress Rheology of Liquid Lubricants at Pressures of 2 to 200 MPa," *ASME JOURNAL OF TRIBOLOGY*, Vol. 112, No. 2, pp. 246-253.
- Bair, S., and Winer, W. O., 1992, "The High Pressure High Shear Stress Rheology of Liquid Lubricants," *ASME JOURNAL OF TRIBOLOGY*, Vol. 114, No. 1, pp. 1-13.
- Bowden, P. B., and Jukes, J. A., 1972, "The Plastic Flow of Isotropic Polymers," *Journal of Materials Science*, Vol. 7, pp. 52-63.
- Evans, C. R., and Johnson, K. L., 1986, "The Rheological Properties of EHD Lubricants," *Proc. Instn. Mech. Engrs.*, Vol. 200, C5.
- Gilman, John J., 1975, "Mechanical Behavior of Metallic Glasses," *Journal of Applied Physics*, Vol. 46, No. 4, pp. 675-679.
- Haward, R. N., 1973, *The Physics of Glassy Polymers*, Wiley.
- Hutton, J. F., 1985, "Re-assessment of Rheological Properties of LV1 260," *ASME JOURNAL OF LUBRICATION TECHNOLOGY*, Vol. 106, No. 4, pp. 536-537.
- Muller-Mohnsen, H., Weiss, D., and Trippel, A., 1990, "Concentration Dependent Changes of Apparent Slip in Polymer Solution Flow," *Journal of Rheology*, Vol. 34, No. 2, p. 227.
- Johnson, K. L., and Tevaarwerk, J. L., 1977, "Shear Behavior of Elastohydrodynamic Oil Films," *Proc. Roy. Soc. of London, Series 365A*, pp. 215-236.
- Kaneta, M., Nishikawa, H., and Kameishi, K., 1990, "Observation of Wall Slip in Elastohydrodynamic Lubrication," *ASME JOURNAL OF TRIBOLOGY*, Vol. 112, pp. 447-452.
- Ramesh, K. T., and Clifton, R. J., 1987, "A Pressure Shear Plate Experiment for Studying the Rheology of Lubricants at High Pressures and High Shearing Rates," *ASME JOURNAL OF TRIBOLOGY*, Vol. 109, No. 2, pp. 215-222.
- Smith, F. W., 1959, "Lubricant Behavior in Concentrated Contact Systems—The Castor Oil-Steel System," *Wear*, Vol. 2, No. 4, pp. 260-263.
- Spathis, G., Kontou, E., and Bourkas, G., 1991, "A New Equation of the Relaxation Process in the Nonequilibrium State: Application to Creep and Dynamics Experiments in Epoxy Resins," *Journal of Rheology*, Vol. 35, No. 8, p. 1496.
- Wu, J. B. C., and Li, J. C. M., 1976, "Slip Processes in the Deformation of Polystyrene," *Journal of Materials Sci.*, Vol. 11, pp. 434-444.
- Yasutomi, S., Bair, S., and Winer, W. O., 1984, "An Application of a Free Volume Model to Lubricant Rheology," *ASME JOURNAL OF TRIBOLOGY*, Vol. 106, No. 2, pp. 304-312.



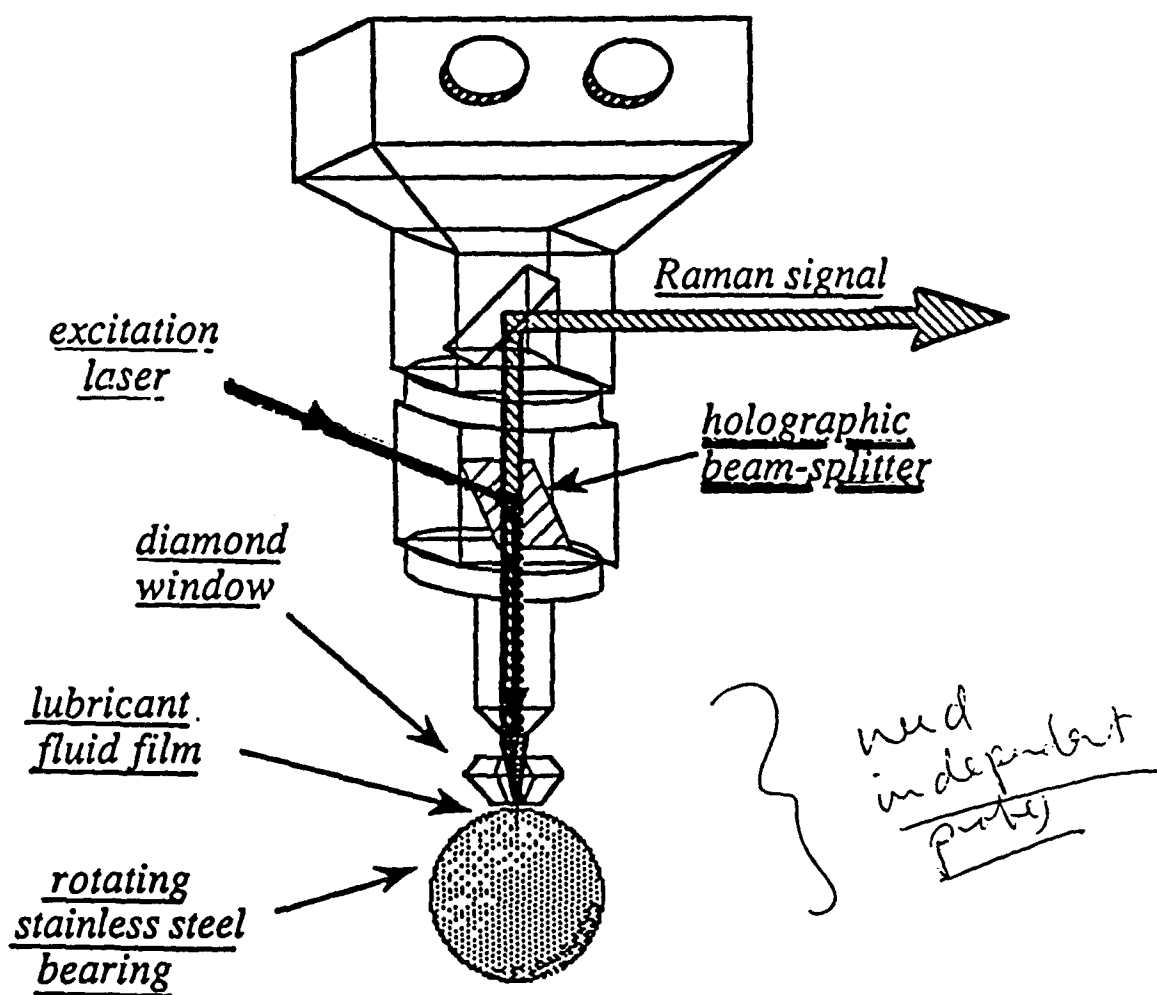
# SIKORSKY HUM FUNCTIONAL CAPABILITIES

AREA	INITIAL CAPABILITY	GROWTH
Gearboxes	Vibration	IDM
	Chip detection	Oil level
	Oil temperature	Filter pressure drop
	Oil pressure	
Rotors	Onboard tracker	Component diagnostics
	1 / MR tuning	Structural diagnostics
	1 / TR tuning	
	Power assurance	
Engines	Exceedances	EEMS™
	Vibration	IDM
	Chip detection	
	Vibration	
TDS support bearings	Temperature	
	Vibration	
	Structural usage	
	Usage	
Structure	Drain sump temperature	
		Cabin nR tuning
Operations Controls		Servo performance
		Drain flow rate
		Oil level
		Maintenance planning
Ground support station	Engineering analysis	
	Pilot actuated sampling	
Cockpit noise		

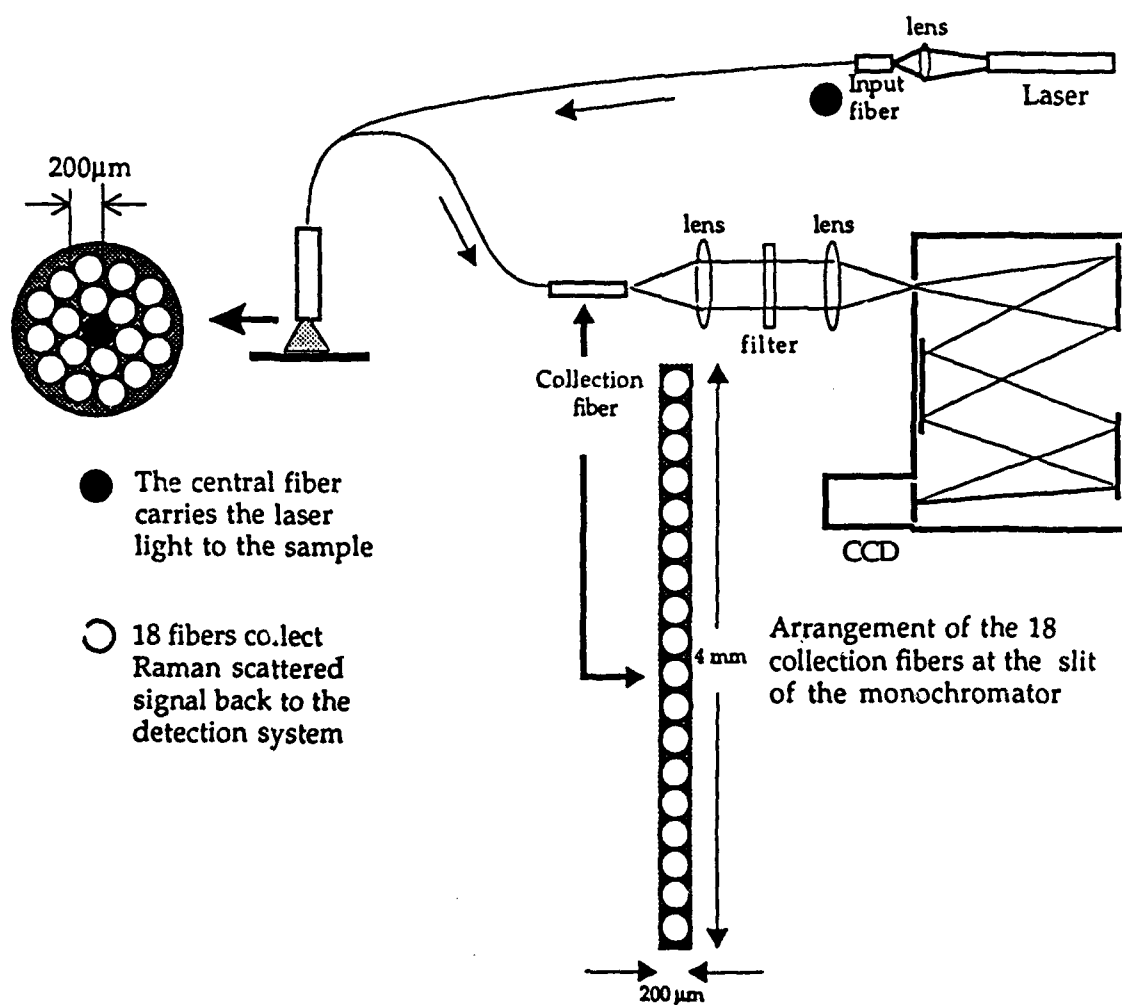
## Molecular Probes

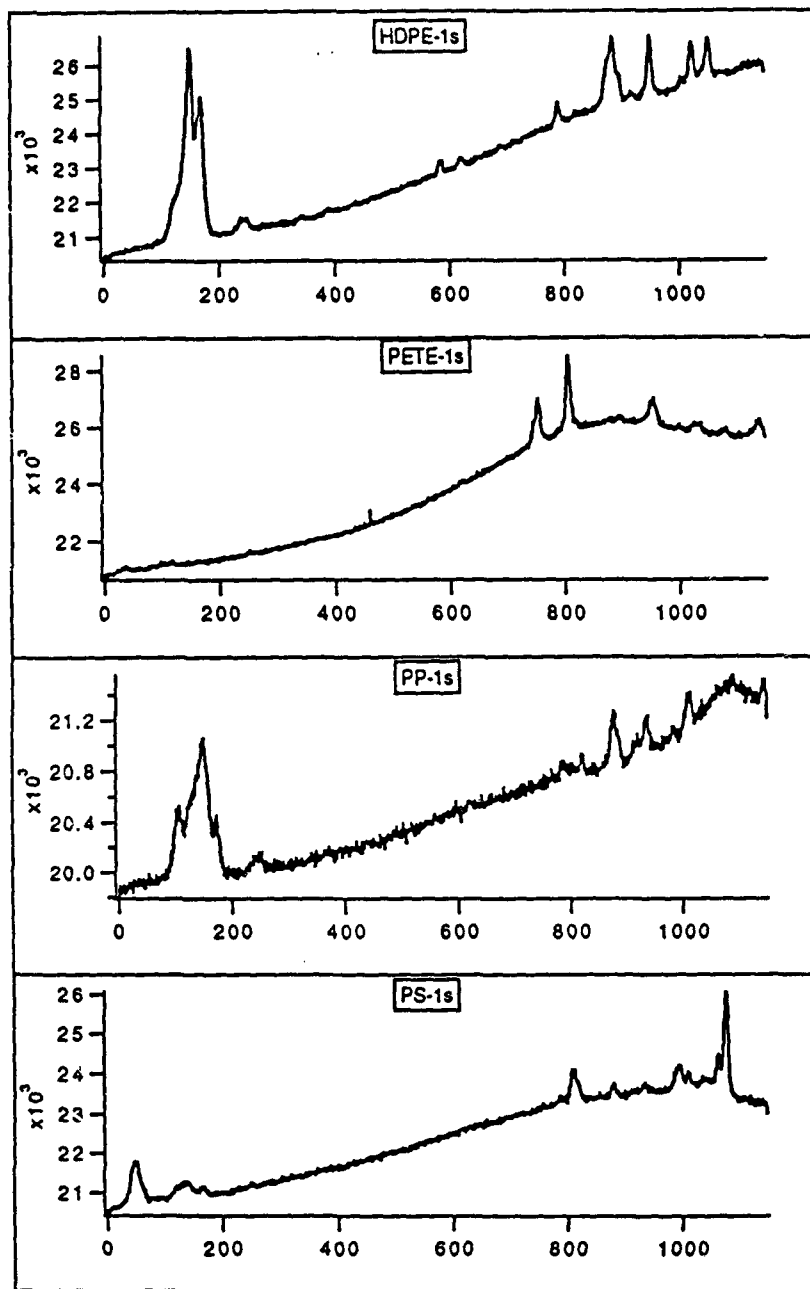


# Raman Microscope

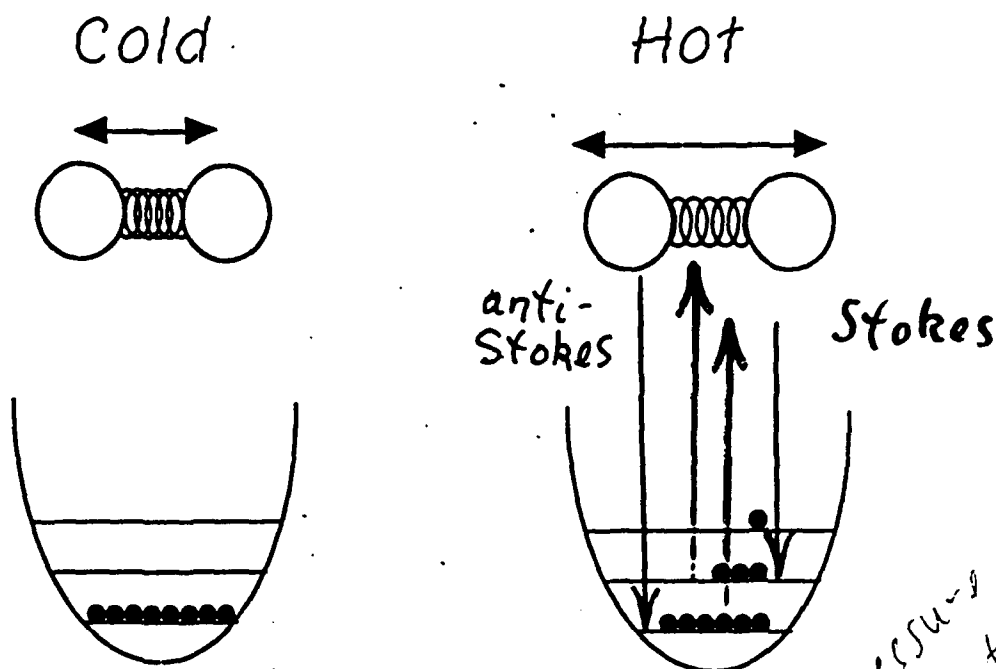


# Fiber Optic Probe

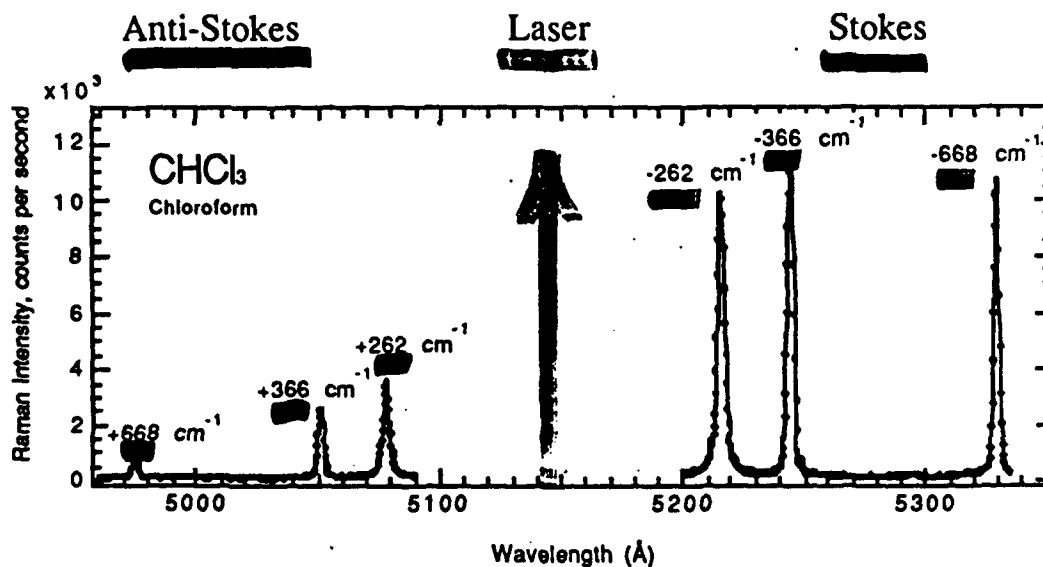




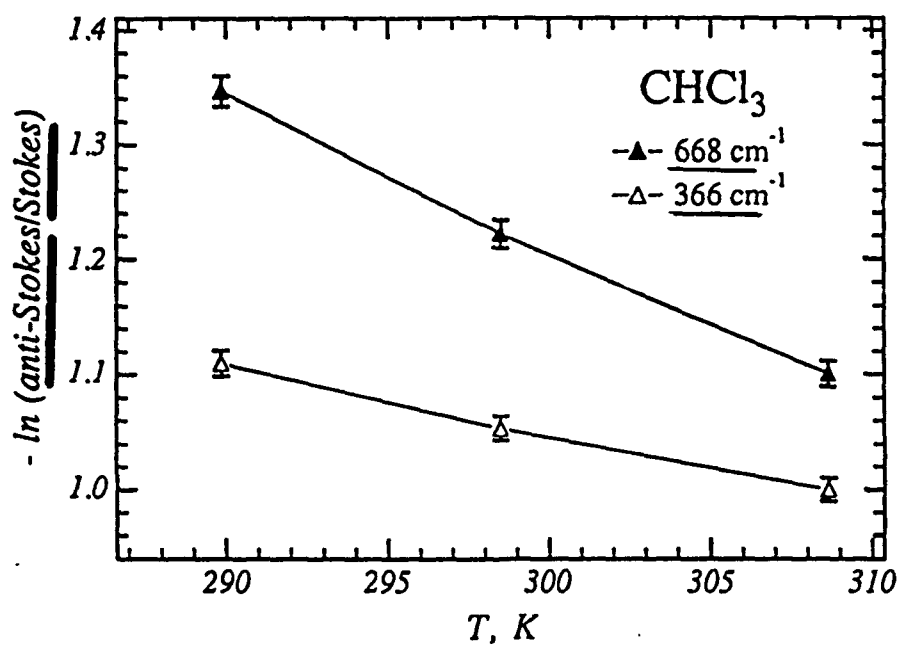
# Molecular Thermometer



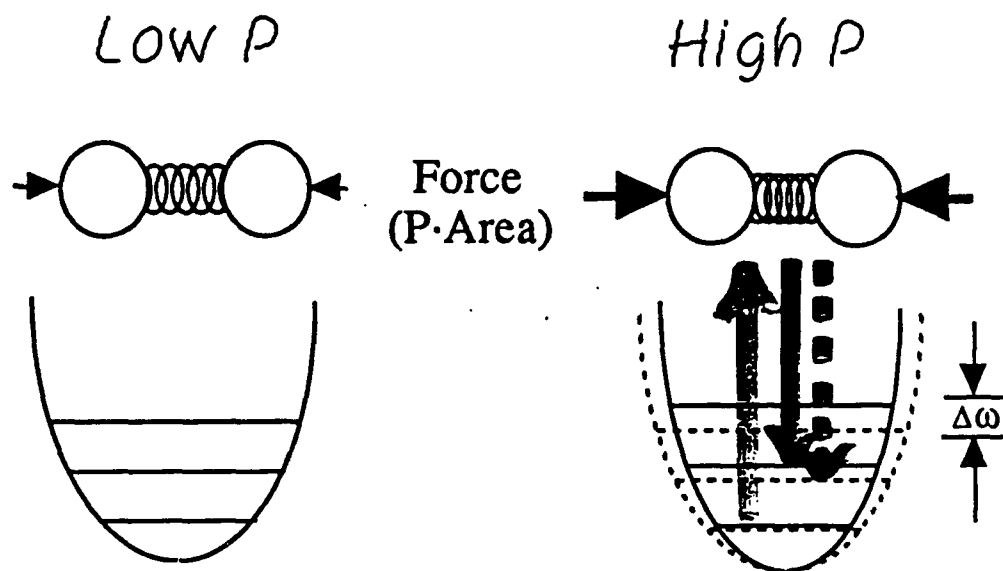
Boltzmann distribution,  $\frac{P_{v=1}}{P_{v=0}} \propto e^{-\Delta E/RT}$  *pressure independent*



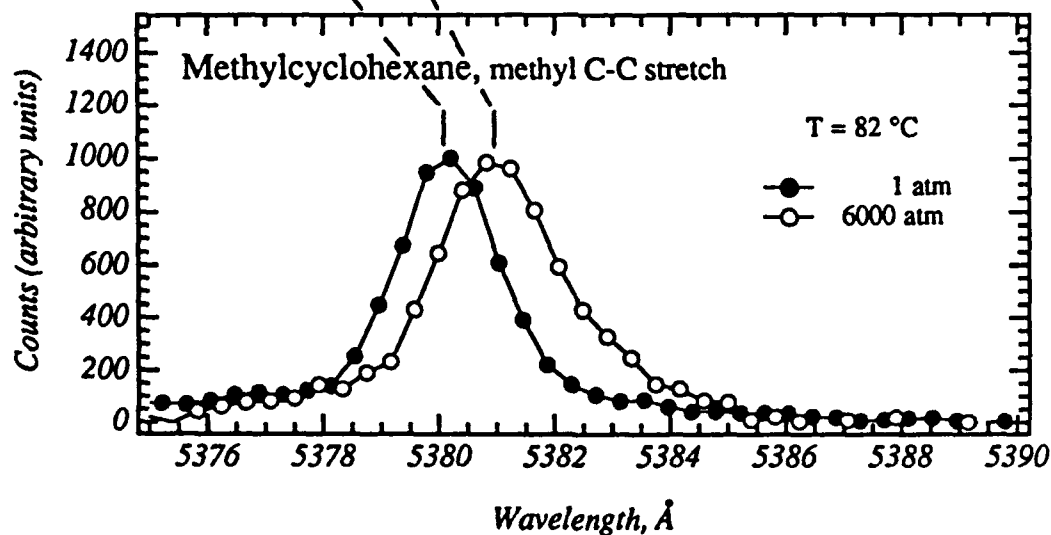
*go back to p-fluorocetyl polyethers*



# Molecular Barometer



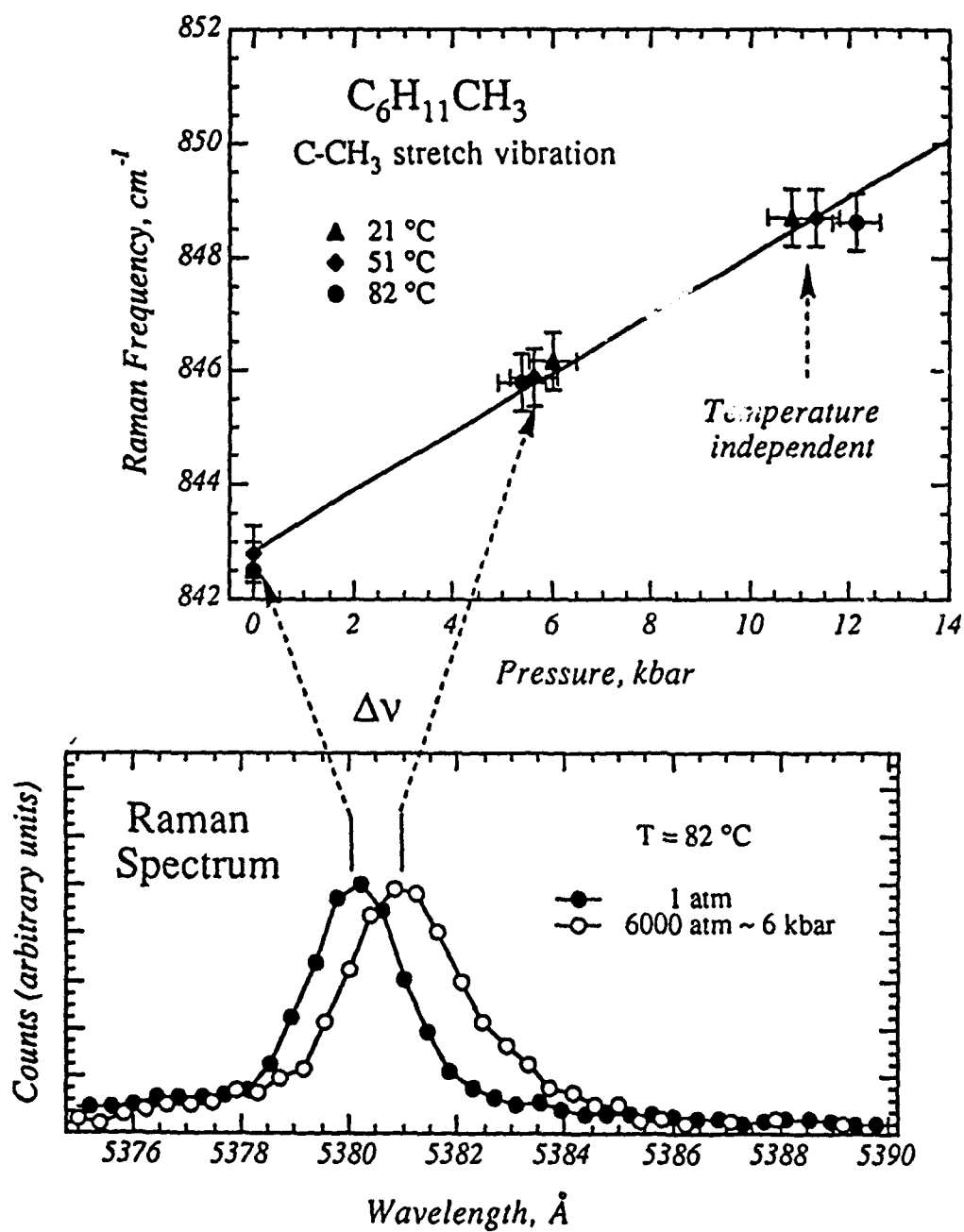
$$\Delta\omega_{\text{vib}} \propto \text{Force} \propto P$$





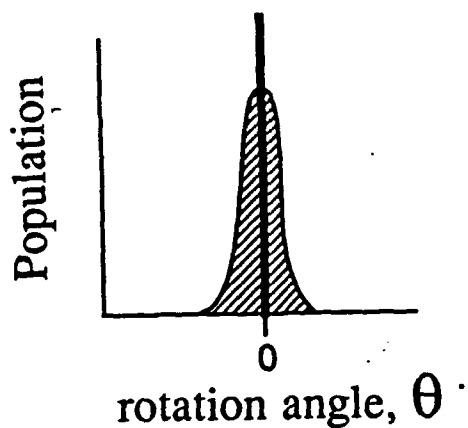
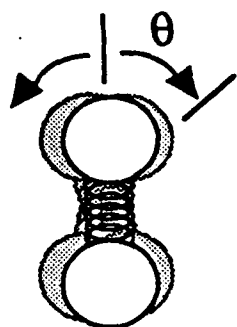
## Raman Barometer

Pressure,  $P \sim$  Raman Frequency shift,  $\Delta\nu$

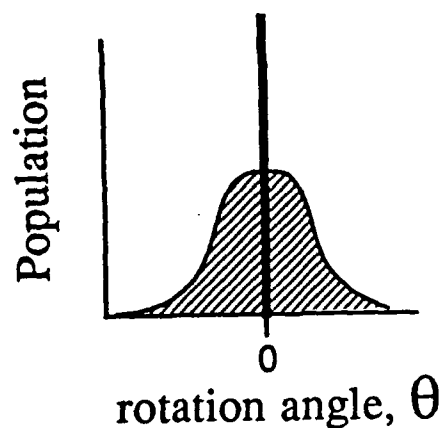
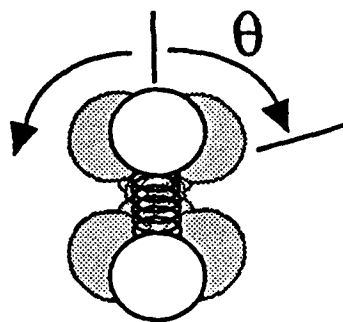


# Molecular Viscometer

High  
viscosity

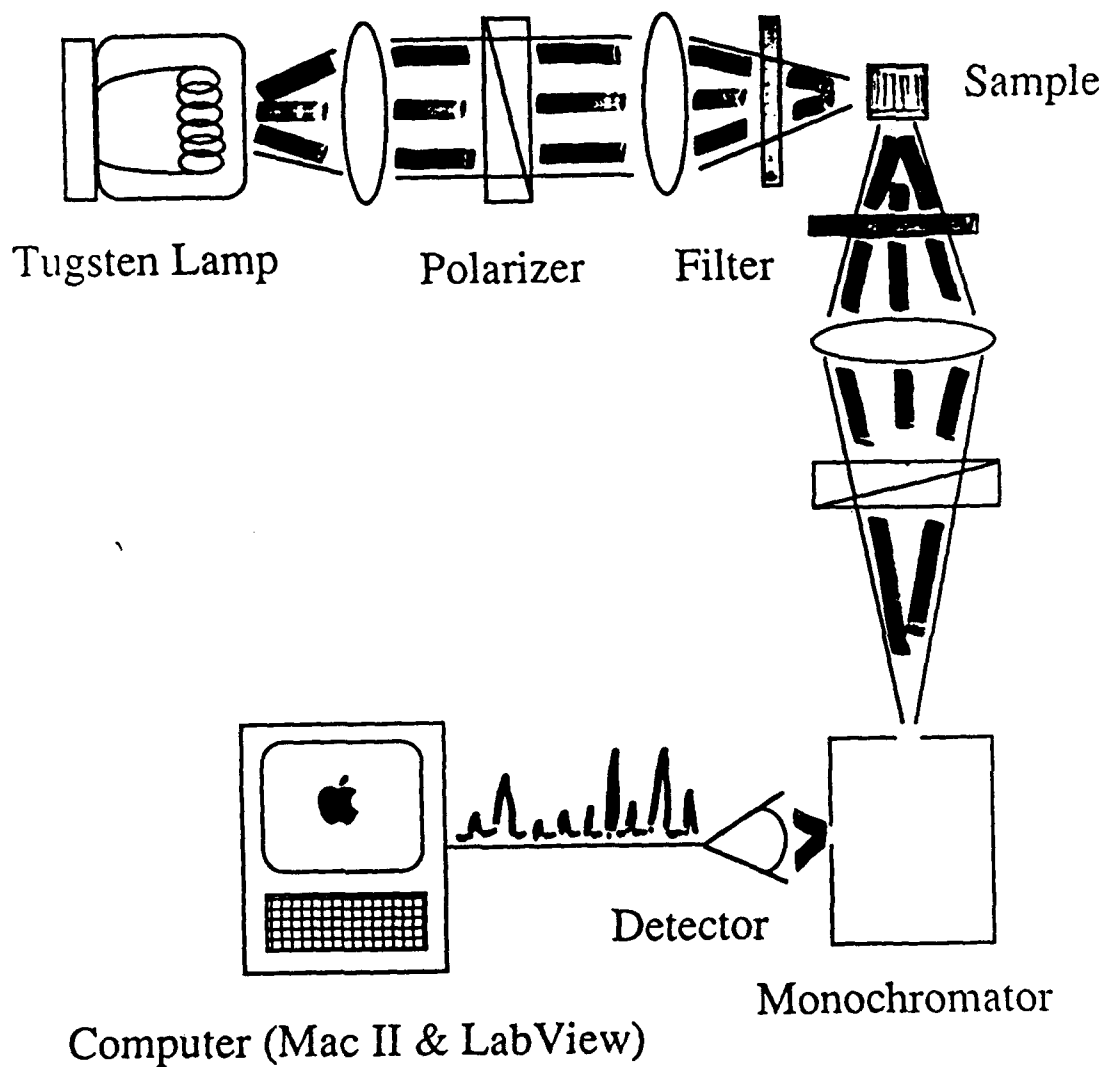


Low  
viscosity

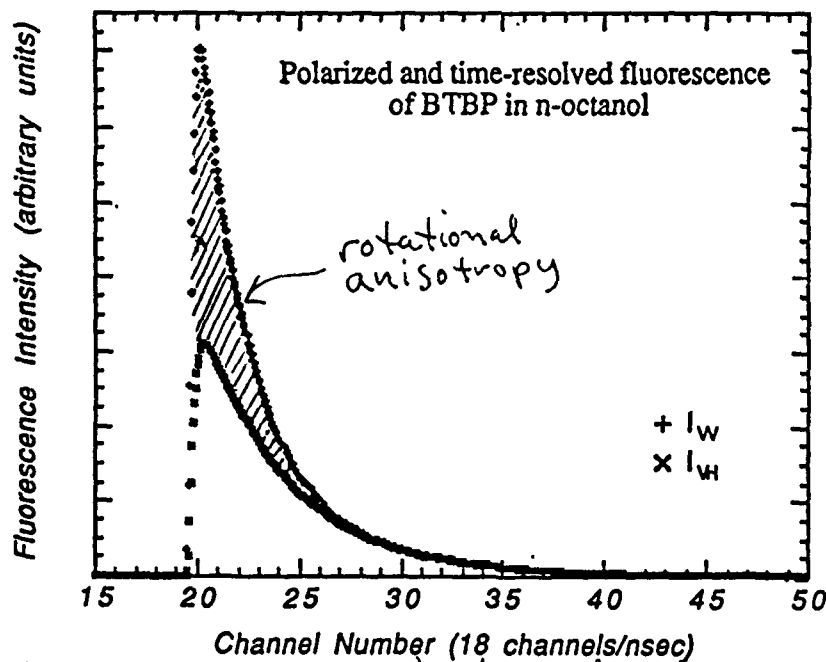
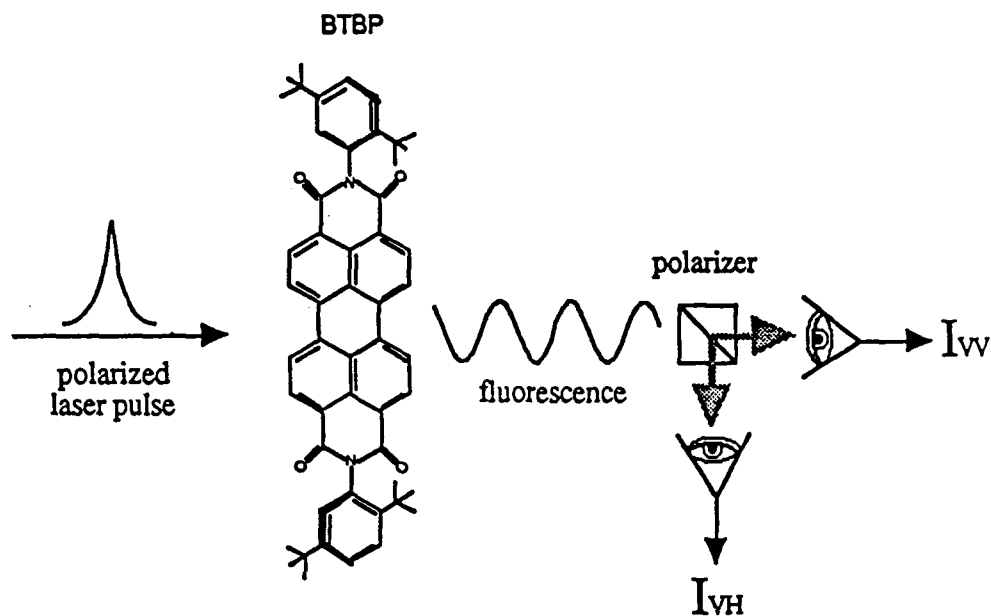


$$D_{\text{rot}} \approx \frac{k_B T}{\pi \sigma^3} \left( \frac{1}{\eta} \right)$$

# Fluorescence Depolarization Instrument

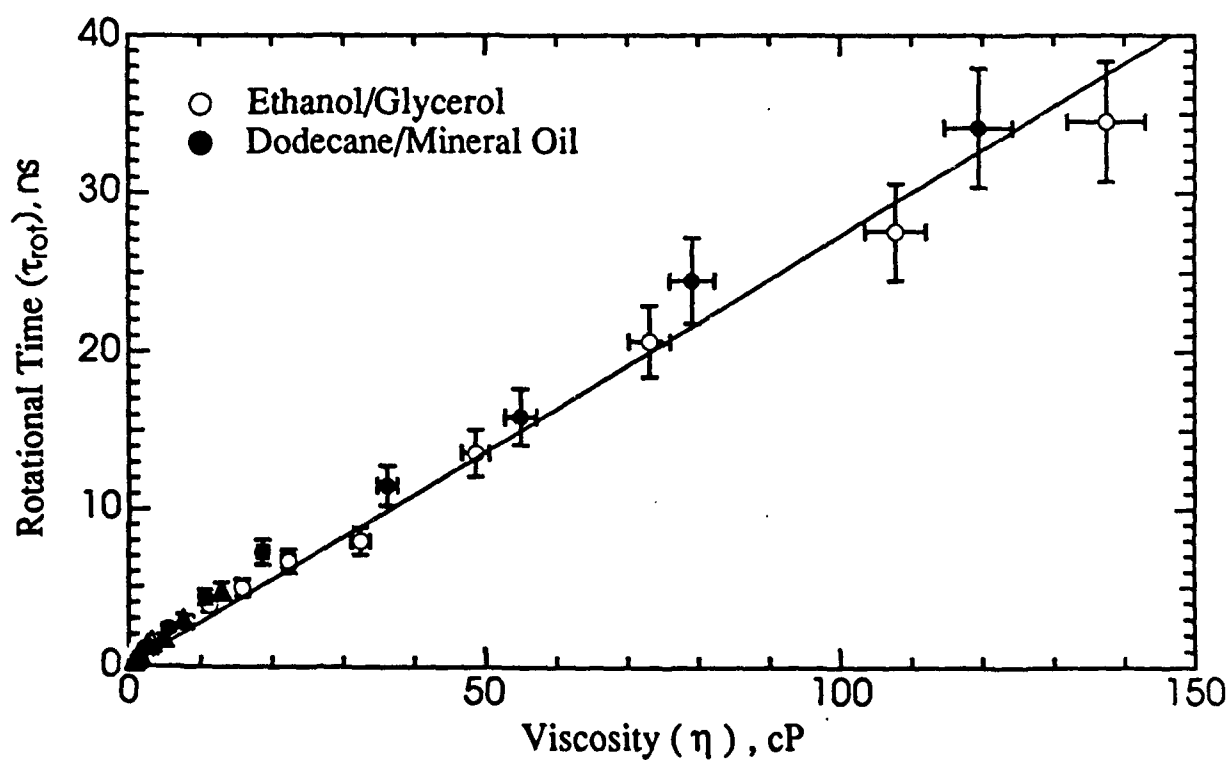
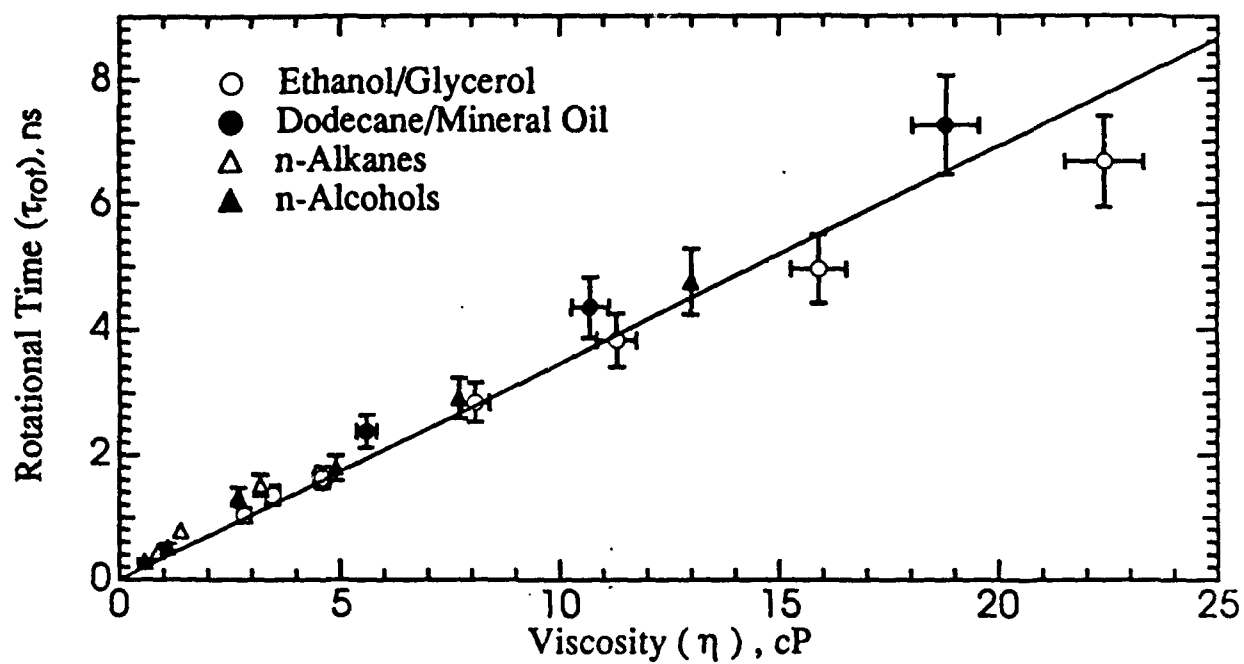


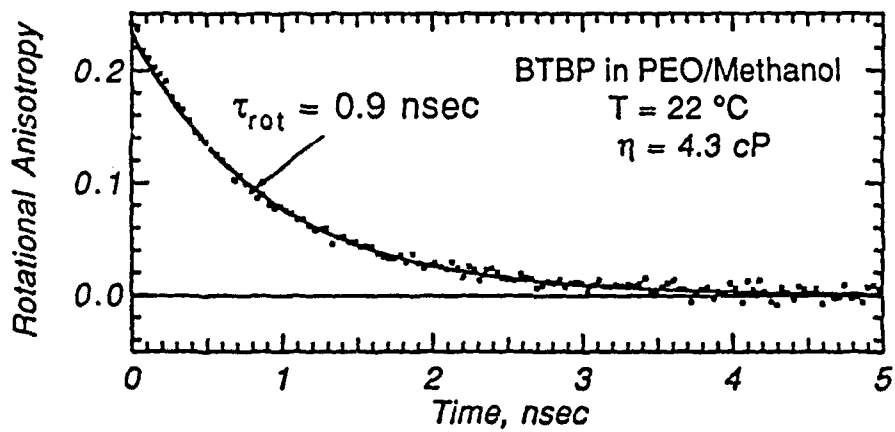
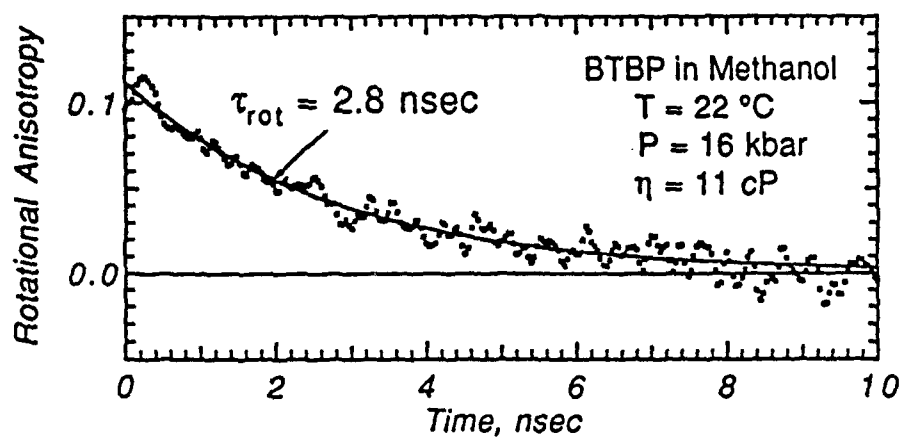
# Time-resolved fluorescence depolarization measurement of microscopic friction



want to understand: what molecular parameters  
determining the ~~time scale~~ magnitude of microscopic  
friction (time scale of rotational re-orientation)?  
a) substituent groups, charge, size, solvation

## Fluorescence Depolarization Viscometer Results





# **On-Line Diagnostics and Prognostics for Early Malfunction Alerting and Condition-Based Maintenance**

Contract N00014-93-C-0074  
Office of Naval Research

Thomas M. McKenna, Ph.D.  
Scientific Officer

Presented at the Workshop on Conditioned Based Maintenance  
15 – 17 November 1993

Roger L. Barron  
President and Senior Research Scientist

B. Eugene Parker, Jr., Ph.D.  
Research Scientist

Barron Associates, Inc.  
3046A Berkmar Drive  
Charlottesville, Virginia 22901  
(804) 973-1215

# Technical Objectives of SBIR Phase II Program on "Helicopter Transmission Diagnostics Using Vibration Signature Analysis"

---

- Develop algorithms for on-line vibration diagnostic system to detect, classify, and prognose faults in rotorcraft transmissions prior to failure
- Novelty detection is expected to be especially important in distinguishing normal vibration patterns from soft and hard faults
  - Can never be sure of having a "complete" catalog of faults with which to train classifiers
  - Data fusion approaches (including data reflecting flight regime) represent a luxury not part of present program
  - Per-cycle ensemble averaging works "for" us, pulling subtle fault signatures out of noisy background



# Abrupt Change Detection

---

- Suboptimal to do the obvious whitening operation, followed by level detection on innovation process
  - Detects only additive (deterministic) changes, not nonadditive (e.g., variance, spectrum) changes
- Use of multiple (accelerometer) information channels
  - Provides hypothesis testing with power that multivariate statistics has over univariate statistics
- Possible to perform adaptive beam forming to "listen" directionally within gearbox?
  - e.g., "cocktail-party" problem

# Signal Processing Steps

---

- Detection
- Preprocessing (e.g., feature extraction)
- Preclassification (data qualification)
- Classification (fault isolation)
- Estimation (prognostics, fault severity determination)
- Post-processing (e.g., multiple look, data fusion, etc.)

## Explicit Models

---

- Although it is desirable to have complete physical models that relate parameter values to components, which would allow prognostication through extrapolation, etc., physical modeling still a research topic
  - Problems:
    - Not a near-term solution
    - Analytic models generally require simplifying assumptions to make the mathematics tractable (e.g., neglect nonlinearities, cross-couplings, etc.)
    - Computationally intensive - is the computer power going to be available on-line for finite element methods?
    - May not be possible to fully relate parameters to components

$$\text{e.g., } \tau = RC, \quad \ddot{x} = -\frac{k}{m} x$$

The price for such observability is additional sensors

- Physical models not needed for optimal detection

## Implicit Models (Neural Networks)

---

- Nonlinearities, cross-couplings, and non-Gaussian statistics readily modeled
  - Baseball outfielder doesn't catch ball by solving equations of motion for ball
  - Ability learned inductively through association
  - Readily fuses with other information to improve process (e.g., sound made by "crack of the bat")
  - Popularity of kurtosis statistic (4th statistical moment) in vibration monitoring attests to presence of non-Gaussianity
- Natural for detection, isolation, and estimation (prognostication), as well as data fusion
  - Must exercise care in using neural networks; insert in right place (e.g., avoid using classifiers trained via supervised learning for detection)
- Fast computationally – inherently parallel
- Simple, adaptive, practical, affordable

## Technology Push vs. Requirements Pull

---

- What can be done reliably with existing signal processing techniques using sensors and other data that are available today?
  - No one knows since the data are not available for rigorous testing of algorithms
  - What if actual flight data could be recorded and used for this evaluation?

## Potential Phase II Data

---

- The following *seeded* fault data are being collected in analog form by Boeing Helicopters from CH-47D transmissions under an Army contract:
  - Engine transmission spiral bevel input pinion tooth root fault
  - Combiner transmission bevel collector gear tooth root fault
  - Forward transmission first stage planet gear tooth root fault
  - Forward transmission second stage planet gear post fault and a bevel tooth root fault
  - Aft transmission spiral bevel ring gear tooth fault and a second stage sun gear internal spline tooth root fault
  - Aft transmission first stage planet gear bore fault and a pinion shaft lube hole fault

## Phase II Data

---

- Under contract to Barron Associates, Inc., the following *unseeded* fault data from a CH-47D helicopter transmission, which was run in a test stand, will be provided by Boeing Helicopters in computer-readable digital format:
  - Accelerometer output signals from combiner transmission that developed a gear fatigue crack which propagated to failure and eventually destroyed the transmission
  - Stewart-Hughes Transmission Vibration Diagnostic System computer analyses (digital data sets and plots) previously analyzed and reported by H. J. Rose in "Vibration Signatures and Fatigue Crack Growth Analysis of a Gear Tooth Bending Fatigue Failure." (44th Meeting of Mechanical Failure Prevention Group, April 2-5, 1990)
- *Seeded* fault data collected in analog form by Westland in U.K. may become available in computer-readable digital format via NCCOSC/NRAD

**THIN-FILM FRICTION AND WEAR SENSORS  
FOR CONTINUOUS BEARING MONITORING**

A. W. Ruff and K. G. Kreider

Ceramics Division and Process Measurements Division

National Institute of Standards and Technology

Gaithersburg, MD 20899

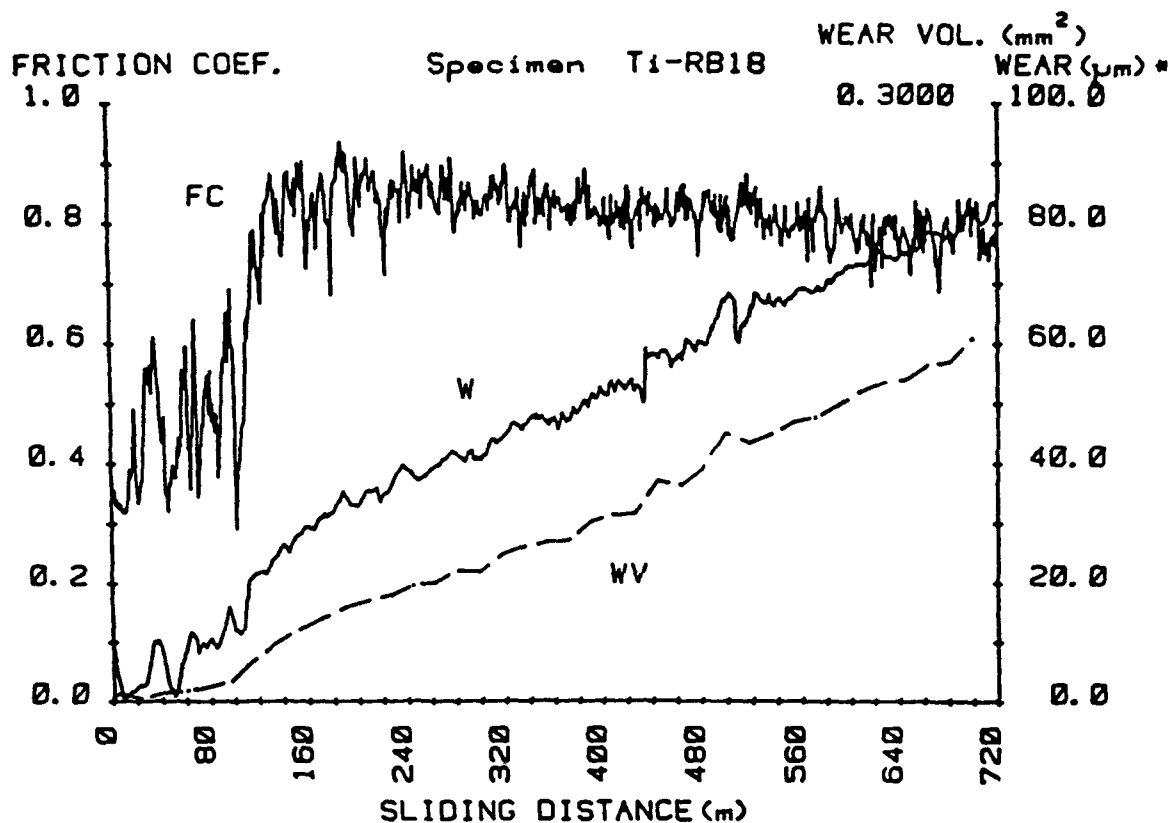


## **Need**

A bearing condition monitoring method that can be applied continuously in real-time on a variety of components regardless of size and complexity

## **Solution**

Develop thin-film sensors that can be incorporated into oil-lubricated bearing construction and that will respond accurately to friction and wear levels in a time-continuous manner



Test results for a titanium block sliding against 52100 steel ring in argon under 10N load show the variation in friction coefficient (FC), wear depth (W), and wear volume (WV) with sliding distance. Break-in occurs at about 120 meters of sliding; afterward the wear rate is constant.

1. General form of (linear) wear:  
(Archard's Eqn.)

$$W = K \frac{L \cdot N \cdot t}{H} \quad (\text{mm}^3)$$

where  $K, H$  are material dependent.

$$\therefore \frac{dW}{dt} = K \frac{L \cdot N}{H} = \text{const.} \equiv C_w$$

for steady-state conditions  
for one wear mechanism.

2. Mild wear ("zero-wear") regime:

$$N < \frac{2000}{1+\beta} \left( \gamma \frac{\sigma_y}{\sigma_{H\pm}} \right)^9 \quad (\text{cycles})$$

where  $\beta, \sigma_{H\pm}$  are test dependent

$\gamma, \sigma_y$  are material dependent.

## **Technical Approach**

- Develop thin film sensor designs to measure accurately wear and friction directly on bearing surfaces
- Develop thin film deposition techniques for locating multi-layer sensors on bearing contact surfaces
- Study sensitivity, durability, and compatibility of different thin-film sensor materials
- Work in later stages with commercial sources to fabricate prototype sensors for full-scale applications

## **Technical Approach (continued)**

- Evaluate friction and wear measurement capabilities of the sensors under controlled laboratory test conditions
- Compare sensor readings with independent direct measurements of friction and wear to verify accuracy
- Compare sensor measurements with analytical models of wear and friction for several contact geometries

## **Problems to Solve**

1. Development of fabrication processes for wear sensors to include multi-layer laminates with excellent adhesion to bearing steel and bronze, and with similar wear characteristics
2. Development of continuous thin-film insulators without flaws (pores, shorts, cracks, stresses, ..) as thin as possible
3. Development of thin-film sensor electrical connections compatible with bearing designs

## **Problems to Solve (continued)**

4. Development of thin-film strain gage rosettes for measuring friction (traction shears) under sliding and rolling conditions
5. Verification of sensor determination of wear and friction through direct post-test measurement of specimens
6. Comparison of sensor wear and friction data with analytical models predicting wear and friction for different geometries and test parameters



## **Tribological Models to Test**

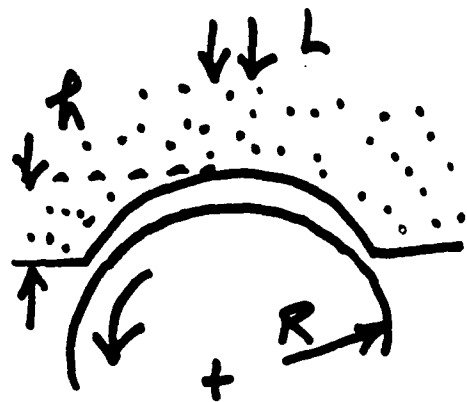
- Wear rate for block-on-ring test geometry  
(linear model ?; controlled by load or pressure ?)
- Wear rate for pin(sphere)-on-disk geometry  
(same ?; temperature effects ?)
- Wear rate for rolling ball contact  
(no general model; wear due to micro-slip and fatigue)
- Friction force for full fluid film  
(varies with fluid viscosity, load, surface roughness ?)
- Contact (surface) temperature  
(varies with speed, load, pressure ?)

1a. For block-on-ring geometry:

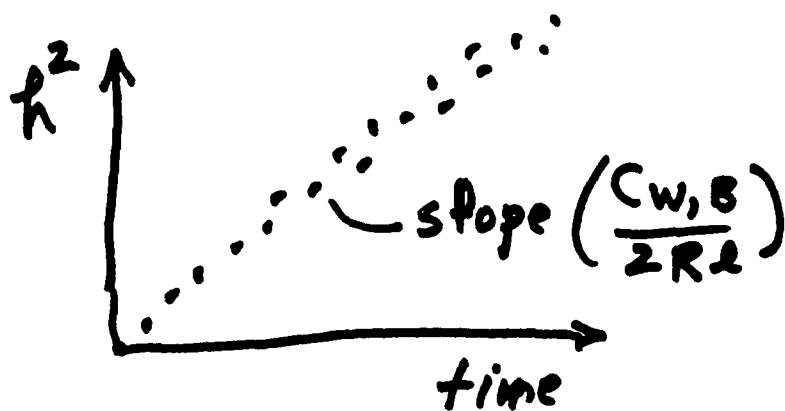
$$\frac{dW}{dt} \doteq \frac{d}{dt} (2R h^2 l)$$

$$= C_{W,B}$$

per unit length of  
contact

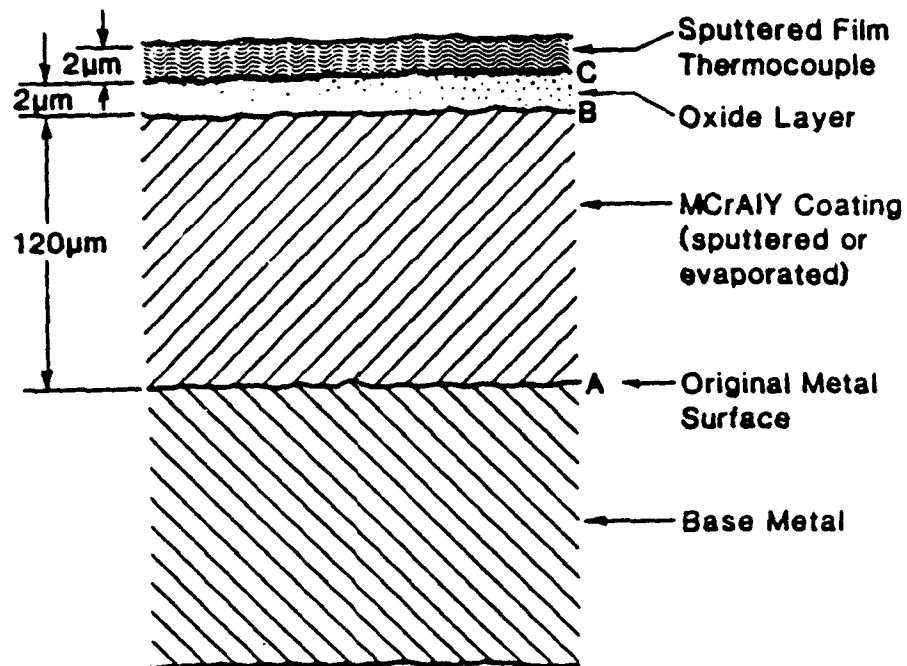


Plot:



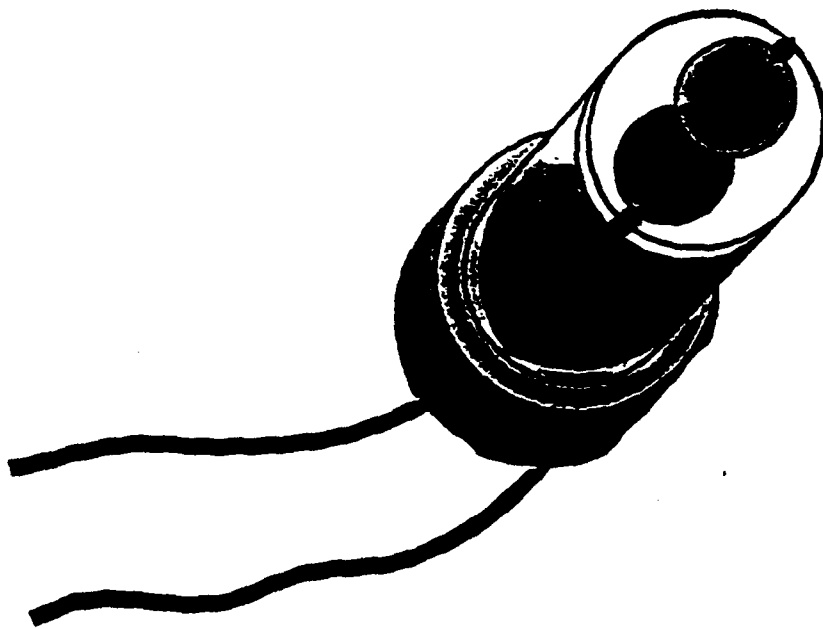
unless  $W$  (i.e.,  $K$ ) varies with  
contact size or pressure or mechanism  
change.

# Thin-film Thermocouple for Turbine Blade Leading Edge



- Low Profile -  $1\mu\text{m}$  - does not disturb gas stream
- Oxide insulation was critical problem

# Temperature Sensor for Diesel Engine



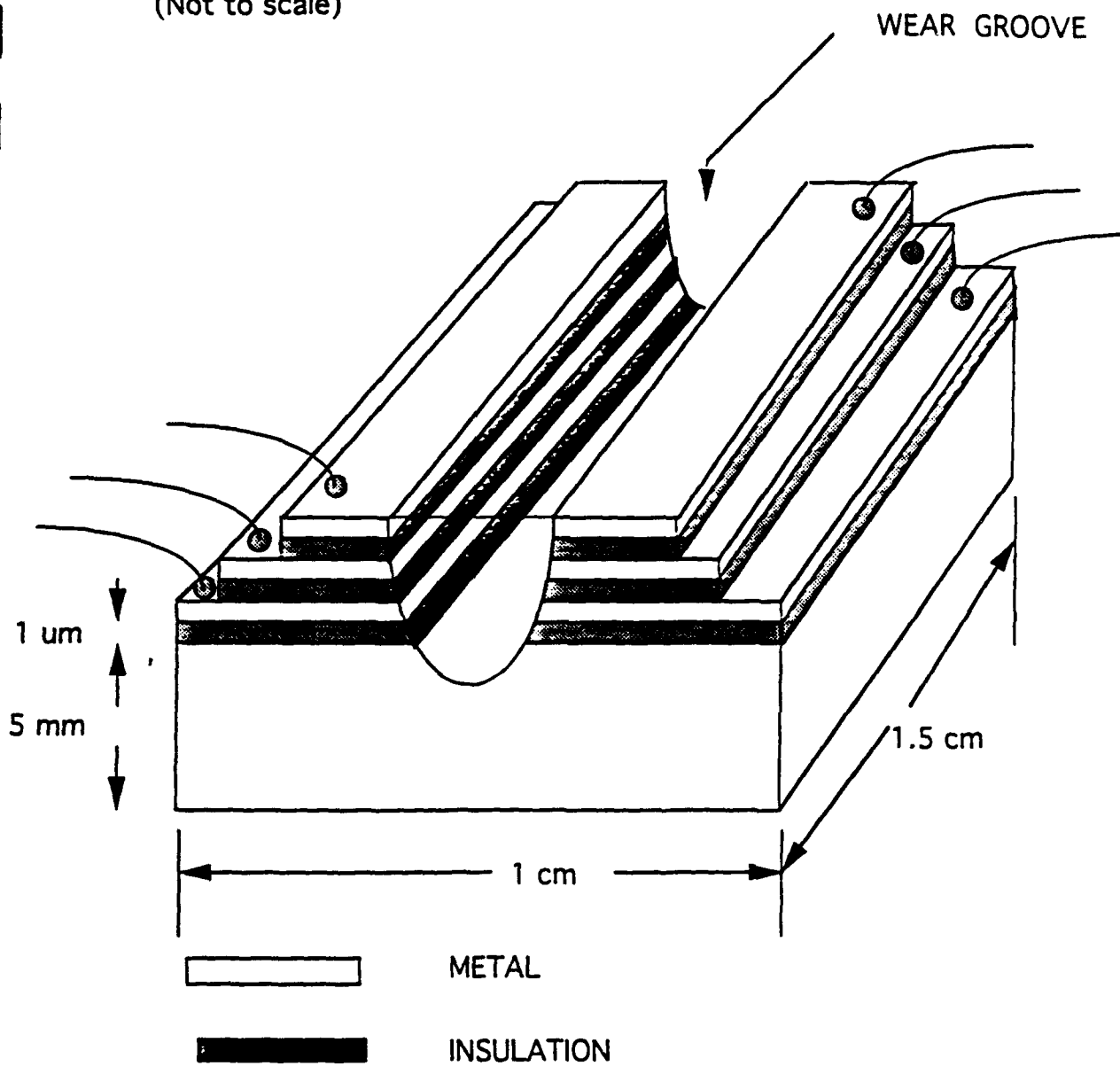
- Pt adherence was critical problem

## **Design Concepts of Thin-film Wear Sensors**

- Lamination of sputtered thin-film resistance elements with insulators directly on the metal bearing surfaces
- The laminated thin-film package would have similar wear behavior as the bearing material, and a small contact surface area conforming to the bearing contour
- Typical bearing wear of 1-4 micrometer (40-160 microinches) would be measured with 5-9 layer laminates of insulators and film resistors
- A thin-film thermocouple would be included within the gage to monitor surface temperature

# WEAR COUPON

(Not to scale)



## Surface Science, Tribology, and the NAVY's aging fleet.

Dr. Irwin L. Singer

How can surface science and tribology make an impact on condition-based maintenance (CBM)? One way is by developing microsensor technologies that evolve from proximal probe research. Proximal probes are the latest in a stable of surface-related techniques that have been used by tribologists over the past 30 years or so to get a closer look at the moving interface. By the mid-eighties, tools which read like an alphabet soup [X-ray Photoelectron Spectroscopy (XPS), Auger Electron Spectroscopy (AES), transmission electron microscopy (TEM),...] were able to identify compositions and structures with up to monolayer sensitivity and, thus, brought tribologists a step closer to understanding the interface chemistry and structure. However, most of these tools only provided ex-situ looks at surfaces; they were unable to give real-time views of the buried interface.

Today, tribologists are performing in-situ surface analysis and tribology at the atomic scale using proximal probes<sup>1</sup>. Proximal probes have developed over the past decade from a variety of experimental techniques, most notably from Scanning Tunneling Microscopy (STM)<sup>2</sup>. The most well known are Atomic Force Microscopy (AFM)<sup>3</sup> and its sliding companion Friction Force Microscopy, (FFM)<sup>4,5</sup>. These probes allow friction and wear to be studied with atomic resolution in all three dimensions. Another proximal probe, generically known as a Surface Force Apparatus (SFA), affords atomic resolution only in the vertical direction, but allows direct measurement and/or control of micrometer-sized areas of contact in the lateral direction<sup>6,7</sup>. A very recent technique, based on the Quartz Crystal Microbalance (QCM), permits sliding friction processes to be studied at the Ångström level and at time scales in the nanosecond range<sup>8,9</sup>.

These techniques offer new opportunities at three different levels. First, they are sensitive to events occurring at the atomic scale without regard to environment i.e., unlike the earlier group of surface techniques, the proximal probes NEED NOT BE used exclusively in vacuum. Secondly, they are mechanical as well as analytical and, therefore, capable of performing friction and wear tests as well as studying friction and wear. Thirdly, they are intrinsically microdevices and microsensors combined. They offer a rare combination of technique and technology, and suggest opportunities for turning nanoscale science into nanoscale technology (gigahertz accelerometers, picogram chemical microsensors,...).

The scientific opportunities can be seen in Fig. 1<sup>10</sup>. It highlights some of the newest issues that tribology must deal with to understand friction and wear at a fundamental level. The physics concept is simple: that of matching time and lengths scales in friction and wear studies. Of course, this has been accomplished at the macroscopic scale: thus, we are able to predict and calculate machine contacts, bearing, gear and hydrodynamic lubrication behavior. It is less successful at the mesoscopic (material microstructures, cracking, dislocation motion) and microscopic (gas/liquid/surface interactions, grain and crack-face boundaries,...) scales because the events take place over periods (< microseconds) shorter than most experimental techniques are capable of following. Only a handful of experiments have been performed at the short length and time scales of microscopic tribological processes; four of these, labeled 1 through 4 in the Fig. 1, are described briefly here:

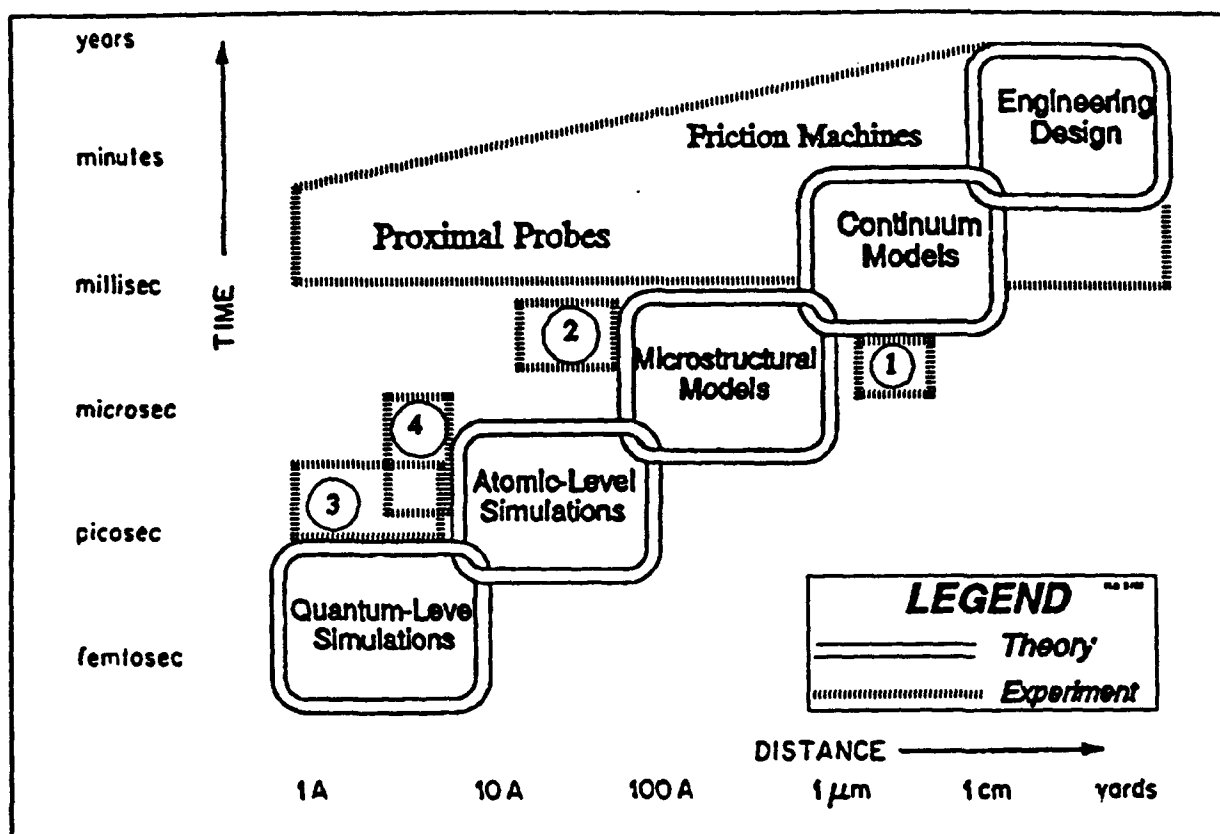


Fig. 1. Time and length scales of present-day models and experiments in Tribology.

1. Bair et al.<sup>11</sup> have used fast IR detectors to measure flash temperatures during high speed frictional contacts of asperities of length  $10\text{ }\mu\text{m}$  and greater, with time resolution of about  $20\text{ }\mu\text{sec}$ .
2. Spikes et al. have developed *real time* optical techniques for investigating the physical behavior of EHL films down to  $5\text{ nm}$  thick<sup>12</sup> and chemical processes occurring in contacts  $10\text{ }\mu\text{m}$  wide by  $80\text{ nm}$  thick.<sup>13</sup>
3. Krim et al.<sup>8,9</sup> have used the quartz crystal microbalance experiments (described earlier) for probing atomic vibrations amplitudes between  $0.1$  to  $10\text{ nm}$  and time scales from  $10^{-12}$  to  $10^{-8}\text{ sec}$ .
4. Hamers and Markert<sup>14</sup> have shown that STM images are sensitive to the recombination of photo-excited carriers whose lifetimes are in the picosecond range.

The technological opportunities are in the spin-offs in nanosensor technology that are derived from the nanoscience research. It isn't possible here to discuss or predict what sensors can be developed. However, it is possible to suggest how such opportunities can be opened up. It is first necessary that tribologists gather working groups of proximal-probe physicists and chemists and together work to design devices that can monitor changes in chemical and mechanical behavior of tribomaterials. Then engineers who have both active knowledge of the



nanotechnologies and collaborations with tribologists will extract the most promising technologies for CBM of aging fleet components.

## REFERENCES

1. Fundamentals of Friction edited by I.L. Singer and H.M. Pollock (Kluwer Academic Publishers, Dordrecht, 1992).
2. G. Binnig, H. Rohrer, Ch. Gerber and E. Weibel, Phys. Rev. Lett. 49 (1982) 57; Phys. Rev. Lett., 50 (1983) 120.
3. G. Binnig, C.F. Quate and Ch. Gerber, Phys. Rev. Lett., 56 (1986) 930.
4. C.M. Mate, G.M. McClelland, R. Erlandsson and S. Chiang, Phys. Rev. Lett., 59 (1987) 1942.
5. E. Meyer, R. Overney, L. Howald, D. Brodbeck, R. Lüthi and H.-J. Güntherodt, in Ref. 1, p. 427.
6. J.N. Israelachvili, P.M. McGuiggan and A.M. Homola, Science, 240 (1988) 189; A.M. Homola, J.N. Israelachvili, P.M. McGuiggan, and M. L. Gee, Wear, 136 (1990) 65; also, J.N. Israelachvili, in Ref. 1, p. 351.
7. A. Tonck, J.M. Georges and J.L. Loubet, J. Colloid Interface Sci., 126 (1988) 150; also in Ref. 1, p. 263.
8. J. Krim and A. Widom, Phys. Rev., B38 (1988) 12184.
9. J. Krim, D.H. Solina and R. Chiarello, Phys. Rev. Lett., 66 (1991) 181.
10. I.L. Singer and H.M. Pollock, in Ref. 1, p. 569.
11. S. Bair, I. Green and B. Bhushan, J. Tribology, 113 (1991) 547.
12. G.J. Johnston, R. Wayte and H.A. Spikes, Tribology Transactions, 34 (1991) 187.
13. P.M. Cann and H.A. Spikes, Tribology Transactions, 34 (1991) 248.
14. R.J. Hamers and K. Markert, Phys. Rev. Lett., 64 (1990) 1051.

RESEARCH RELATED TO THE DEVELOPMENT OF  
IN-SITU TRIBOLOGICAL SENSORS

at

THAYER SCHOOL OF ENGINEERING  
DARTMOUTH COLLEGE  
HANOVER, NH 03755

IN-SITU FLUORESCENCE PROBE  
OF TRIBOLOGICAL CONDITIONS

URSULA GIBSON

THIN FILM THERMOCOUPLES FOR  
SURFACE TEMPERATURE MEASUREMENT

FRANCIS KENNEDY and ALBERT HENNING

## OBJECTIVES

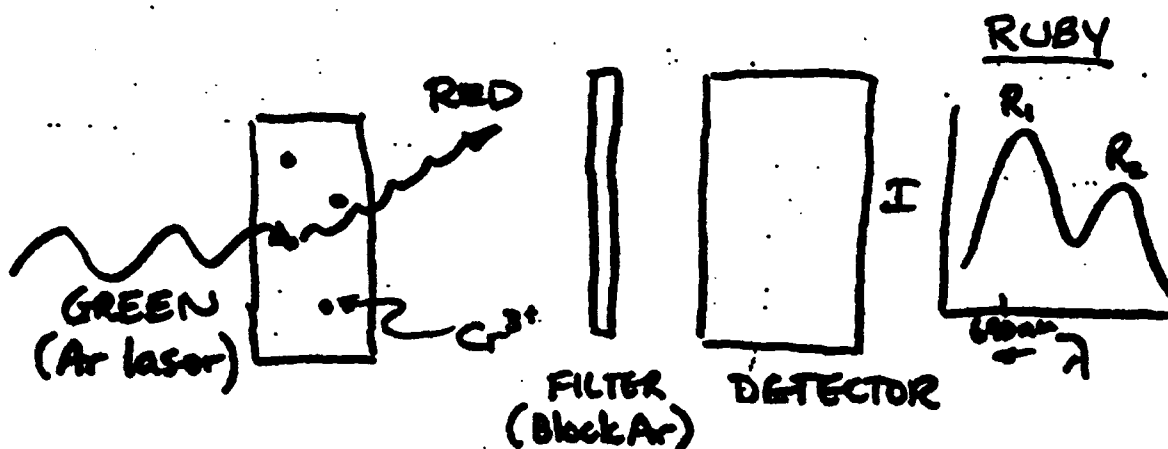
- DEVELOP NEW IN-SITU SENSORS FOR CONTACT TEMPERATURE MEASUREMENT (ALSO USEFUL FOR CONTACT PRESSURE AND CONTACT AREA MEASUREMENT)
- STUDY USE OF SENSORS IN DETECTING ONSET OF TRIBOLOGICAL FAILURE

## IN-SITU FLUORESCENCE PROBE

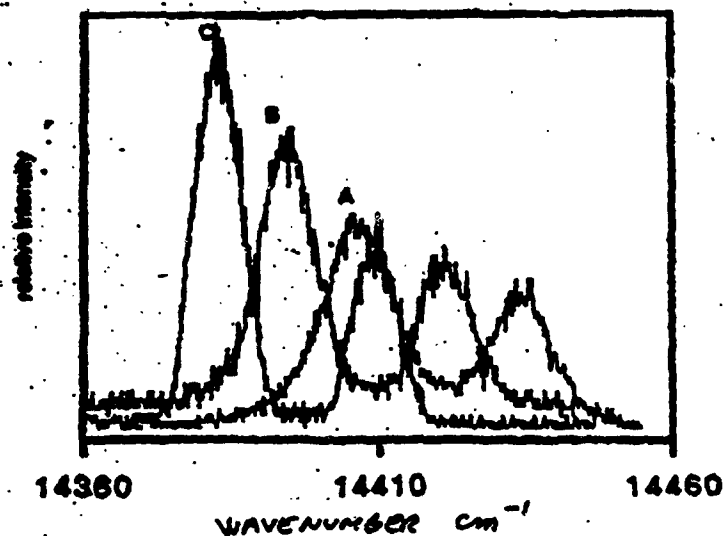
GOALS: FUNDAMENTAL CHARACTERIZATION  
DETERMINATION OF DEGRADATION

FLUORESCENCE:  
EMISSION OF WAVELENGTH-SHIFTED LIGHT  
DUE TO IMPURITIES

e.g., RUBY =  $\text{Al}_2\text{O}_3:\text{Cr}^{3+}$



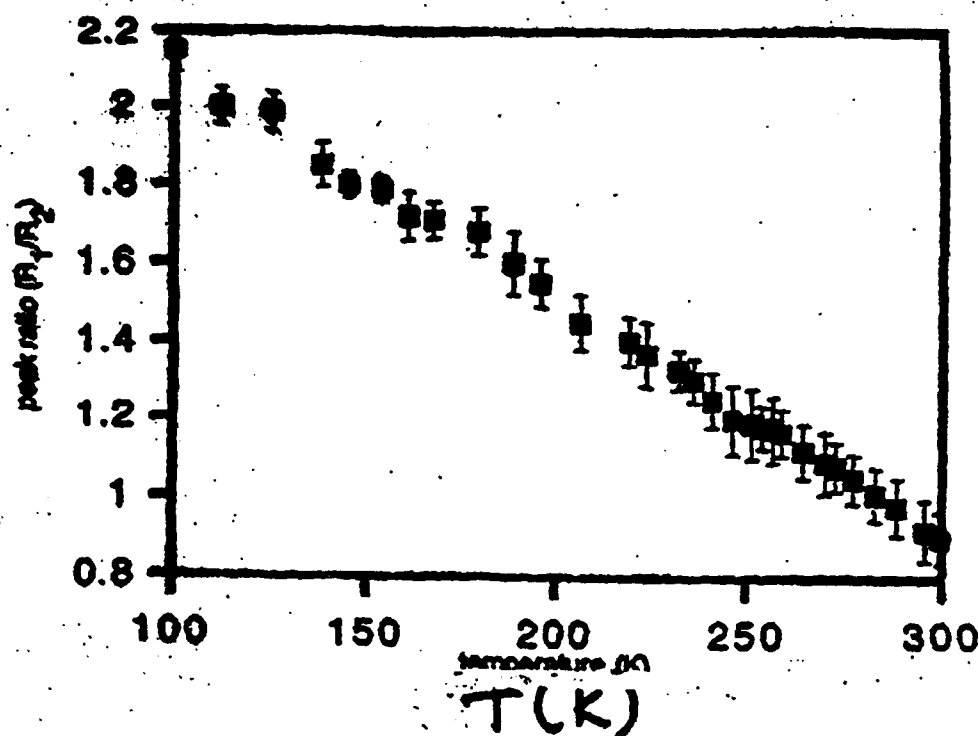
SEPARABLE { FLUORESCENCE PEAKS SHIFT WITH  
 $\Delta$  PRESSURE  
 PEAKS SHIFT, AND  $\frac{I(R_1)}{I(R_2)}$  changes WITH  
 $\Delta$  TEMPERATURE



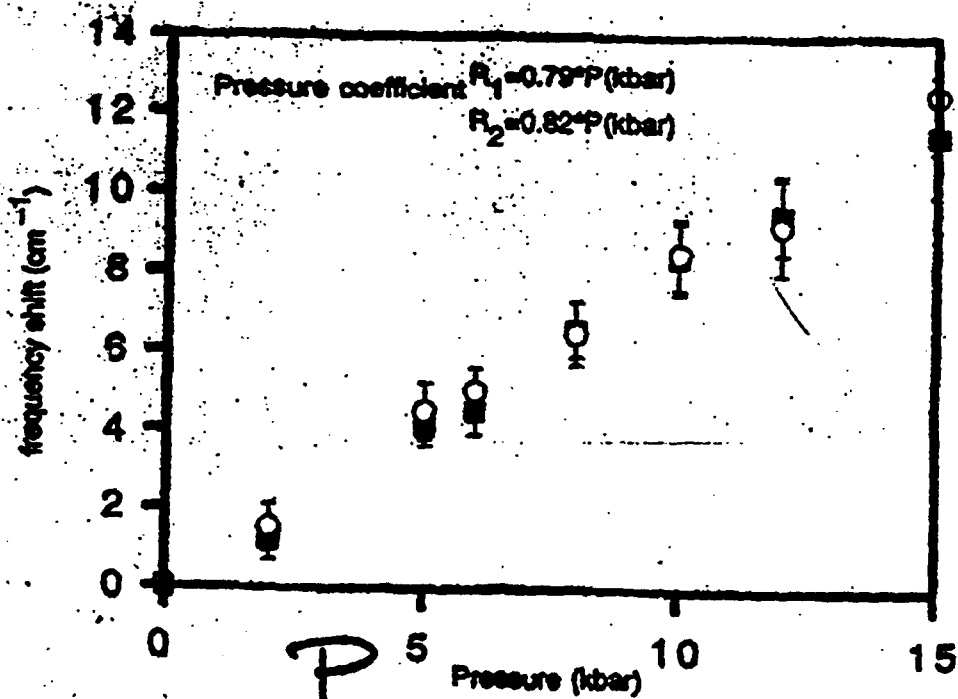
Fluorescence spectra at zero pressure:

A, room temperature; B, 200K and C, 100K.

REL. PEAK HEIGHT



PEAK SHIFT

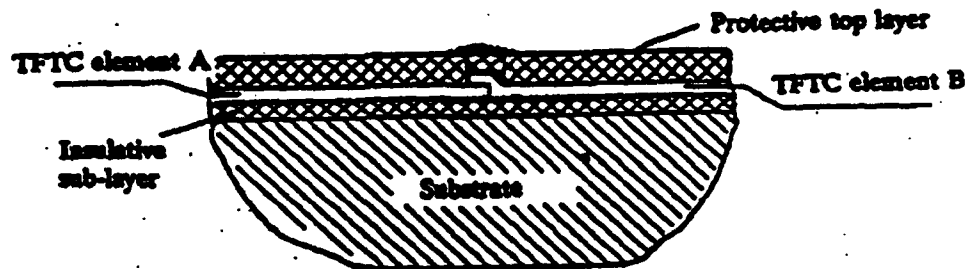


## THIN FILM THERMOCOUPLES

DEPOSITED ON SURFACE OF SLIDING  
COMPONENT

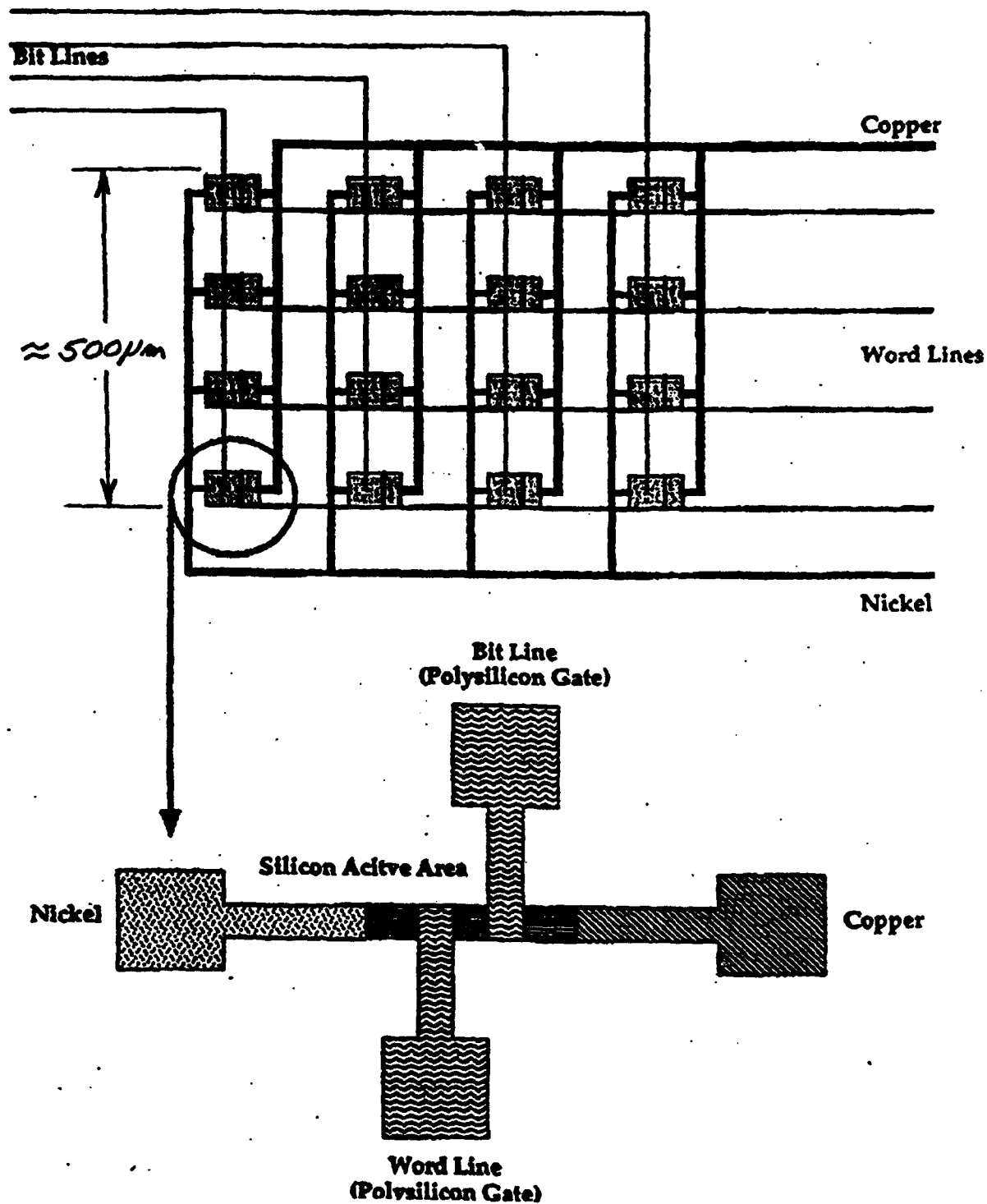
VERY SMALL JUNCTIONS (10 - 100  $\mu\text{m}$  SQUARE,  
 $<0.5 \mu\text{m}$  THICK)

RAPID RESPONSE (CAPABLE OF MEASURING  
FLASH TEMPERATURE RISES)



Schematic cross-section of thin film thermocouple.

**ARRAYS OF THIN FILM THERMOCOUPLES**  
**INCLUDES INTEGRATED SWITCHING ELEMENTS**





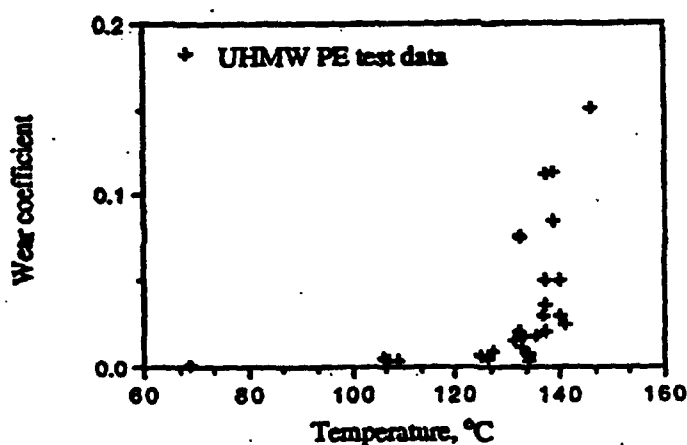
## APPLICATION OF THIN FILM THERMOCOUPLES

USED TO MEASURE TRANSITIONS IN WEAR AND  
FRICTION OF MATERIALS AS FUNCTION OF  
SURFACE TEMPERATURE

PARTICULAR APPLICATION: WEAR OF  
THERMOPLASTIC BEARING MATERIALS  
IN OSCILLATORY SLIDING

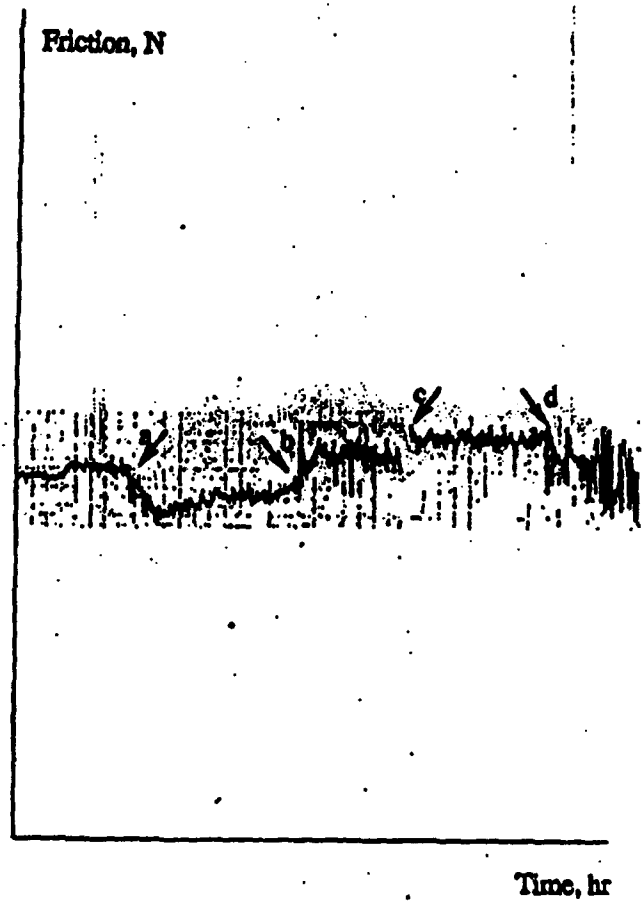
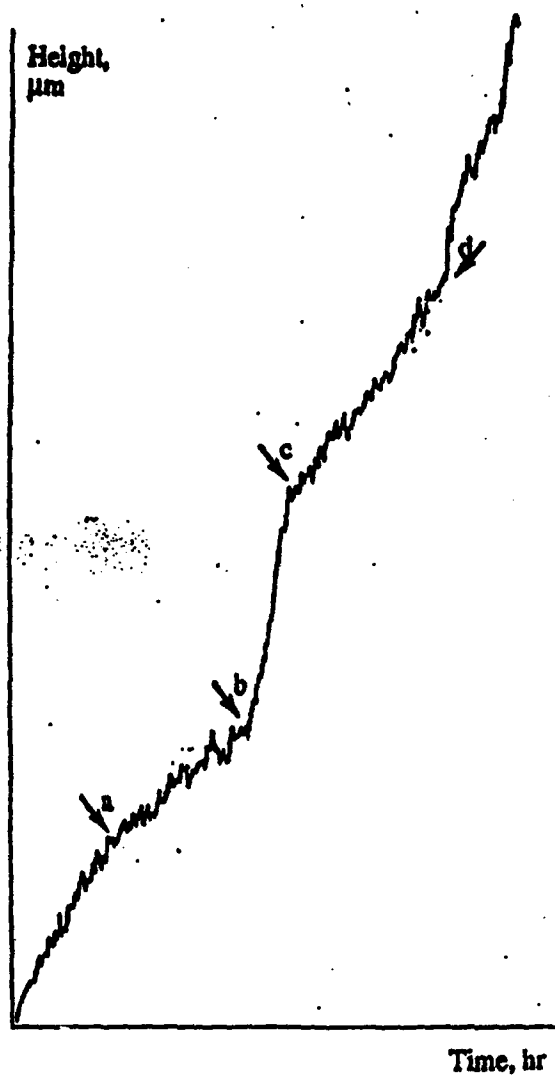
### WEAR DATA

WEAR COEFFICIENT = VOLUME LOST / SLIDING DISTANCE \* LOAD



CRITICAL TEMPERATURE FOR UHMWPE ~ 137°C  
( $T_{\text{melt}} = 138^{\circ}\text{C}$ )

VARIATION OF WEAR RATE AND FRICTION  
PMMA PIN  
AMPLITUDE = 4 mm, LOAD = 9.8 N



< a,  $T_{\text{back}} = 48^\circ\text{C}$ ,  $f = 9.3 \text{ Hz}$ ; a > b,  $T_{\text{back}} = 36^\circ\text{C}$ ,  $f = 9.3 \text{ Hz}$ ;  
b > c  $T_{\text{back}} = 53^\circ\text{C}$ ,  $f = 9.3 \text{ Hz}$ ; c > d,  $T_{\text{back}} = 48^\circ\text{C}$ ,  $f = 9.3 \text{ Hz}$ ;  
d <,  $T_{\text{back}} = 36^\circ\text{C}$ ,  $f = 12 \text{ Hz}$

## Abstract

Successful Boundary lubrication is essential in the design and operation of many mechanical components. The lubrication process is complex and it involves contact mechanics, fluid mechanics, tribochemistry, and material deformation and fracture. Two schools of thought have emerged over the years in examining the mechanisms and modelling of boundary lubrication. The chemical school believes that chemical reactions at the rubbing surfaces control the efficacy of the lubrication process. The mechanical school believes that while chemistry is a factor, hydrodynamics, elastohydrodynamics, (EHD), and micro-EHD can account for most of the load-bearing mechanisms, so at least in design, they are the principal issues. This paper attempts to bring the two schools together to examine a common set of experimental data.

The experiments involve running wear tests on a four-ball wear tester using micro-liters of lubricant until seizure. Lubricant degradation and breakdown are therefore a factor in the wear test. Eventually we would like to compare the chemical kinetic model with the mechanical contact model in describing and predicting the effectiveness of the lubrication process, i.e. the time to seizure. The chemical kinetics model assumes that oxygen consumption by the lubricant to make "friction polymers" control the process. The mechanical model suggests that if temperatures in the contact exceed a certain limit, scuffing will occur. The key to both models is the temperatures in the contact. This paper describes the two models and focuses on the temperatures in the contact.

The temperatures calculated from the two models differ significantly. The temperatures predicted by chemical kinetics are about 100°C higher than the mechanical model. The identification of the discrepancy and the magnitude of the difference highlight the difference between the two approaches. It is hoped that this paper will bring forth further research effort to this critical issue. Various possible explanations were offered for the temperature difference. A plausible explanation was proposed and initial calculations suggest that by taking into account of the wear process, the temperatures calculated by the mechanical model can reach the temperatures estimated by the chemical model.

## A Mechano-Chemical Model: Reaction Temperatures in a Concentrated Contact

S. M. Hsu<sup>1</sup>, M. C. Shen<sup>1</sup>, E. E. Klaus<sup>2</sup>, H. S. Cheng<sup>3</sup>, and P. I. Lacey<sup>1</sup>

Surface Properties Group<sup>1</sup>  
National Institute of Standards and Technology  
Gaithersburg, MD 20899

Department of Chemical Engineering<sup>2</sup>  
The Pennsylvania State University  
University Park, PA 16802

Center for Engineering Tribology<sup>3</sup>  
Northwestern University  
Evanston, IL 60208

September, 1993

For: Issue of WEAR to Honor the Retirement of Duncan Dowson

## Introduction

Boundary lubrication effectiveness has long been considered to be essential in modern machine designs for proper operation. As the demands for better energy efficiency, tighter tolerances, and the availability of new materials, the need to understand and predict lubrication effectiveness in this regime soars. This effort attempts to model a simple system in this regime to elucidate the various aspects of the lubrication process.

In concentrated contacts, lubricants are to protect the contacting surfaces and reduce friction and wear. Various mechanisms have been shown to contribute to the lubrication process as a function of contact severity defined by the load, speed, temperature, surface roughness, etc. Hsu et al. [1] listed the various lines of defenses against wear: hydrodynamic,

elastohydrodynamic (EHD), micro-EHD, chemical film, oxide film, and finally materials themselves. The full-film lubrication condition, where the protection is provided by hydrodynamic and/or EHD films, is desirable as it renders low friction and almost no wear. With increasing contact severity, the lubrication condition changes from full-film lubrication to boundary lubrication, where the protection mechanism changes from hydrodynamic/EHD films to surface films such as chemical and oxide films. Significant increase in friction, wear, and contact temperature results under boundary lubrication conditions. In this regime, the surfaces are separated by a thin lubricating film oftentimes thinner than the surface roughness. In real machinery, it may be debatable whether pure boundary lubrication conditions exist at all, most researchers acknowledge that a mixed lubrication condition probably is a more reasonable reality. The majority of the applied load will be supported by asperity contacts. Depending on the surface roughness, some of the asperities may undergo plastic deformation [2] leading to wear [3,4]. Some surface asperities are probably supported by micro-EHD, some asperities are elastically deformed. Meanwhile, localized temperature build-up may also occur due to the asperity contacts. The extreme pressure and temperatures localized to asperities disrupt the surface structures and chemical reactions between the lubricant and the surface occur. As early as 1958, Hermance and Egan [5] noted that the lubrication of metallic surfaces was often accompanied by opaque organic deposits. The

reaction products form a surface layer to help to redistribute the contact stresses and aid the lubrication process. Under this set of complex phenomena, failure sometimes occurs.

Although the increased friction and wear and the potential failure are undesirable, boundary lubrication has become unavoidable due to increasingly stringent service conditions. A better understanding of the characteristics of boundary lubrication is therefore critically needed for engineering designs to provide effective lubrication and prevent failure.

Historically, two schools of thought have prevailed in examining the boundary lubrication mechanisms. One is chemical; researchers in this school concentrate on the chemical film formation rate and the depletion rate associated with the lubricant degradation. If the chemical film fails, the lubrication process fails. The other is mechanical; researchers focus on the load support mechanisms and the elastohydrodynamic support afforded by the fluid film. Very sophisticated models were developed to describe scuffing and wear taking into account such factors such as heat transfer rates, surface roughness, contact mechanics, and fluid mechanics. While each school acknowledges the existence of the other, research continues in two independent paths. This paper brings the two schools together in an attempt to define the issues and promote future collaborative efforts in this important area.

## Approach

To test the two schools of thought, we selected a simple experiment on a four-ball wear test. The chemistry of the lubricant was kept simple by using a purified paraffinic base oil which has extensive data base and prior experience. A micro-sample test procedure was used to allow maximum lubricant degradation. The composition of the lubricant during and after the test was carefully analyzed so that adequate information was available for modelling. Given the amount of products generated during the wear test, and knowing the chemical kinetics of the reactions, the temperatures in the contact can be calculated. The temperatures can also be estimated by using a mechanical contact model given the surface roughness, material properties, and physical properties of the lubricant. These two temperatures can then be compared.

### Wear Tests

Wear tests were conducted on a four-ball wear tester using the following test specimens and conditions:

Table 1: Specifications of Test Samples

Test Specimen Material:	ALSI E-52100 (Grade 25 EP)
	12.7 mm dia. spherical balls
R <sub>a</sub> Hardness:	64 to 66
Initial Surface Roughness:	0.034 $\mu\text{m}$ (CLA)

Table 2: Experimental Conditions

Lubricant:	Purified Paraffin Oil
Speed:	0.23 m/s (600 rpm)
Applied Load:	40 kg
Ambient Temperature:	20 °C
Atmosphere:	0.25 L/min dry air

Before the wear test, the ball samples were preworn under 40 kg and 0.23 m/s by using 10 mL white oil for 60 minutes. The wear scars on the lower balls after this procedure were measured to be 0.6 - 0.62 mm in diameter. The radius of curvature of the wear scars was approximately 8.7 mm. Then the whole ball assembly was rigorously cleaned to remove the oil lubricant before the subsequent wear test. The wear tests used were similar to the one

developed by Gates and Zeng [6]. It is a micro-sample wear test procedure in which only microliters of lubricant are used over the three contact points. The test continues until high friction occurs and the test terminates. This time to seizure then measures the wear and the life of the lubricant. The deposits formed around the wear scars by lubricant degradation at the conclusion of the test were measured using Gel Permeation Chromatography (GPC). The running time to failure for 1  $\mu\text{l}$  of lubricant using this technique was 50 minutes and GPC analysis of the polymer deposits indicates that 10% of the lubricant was oxidized when failure occurred [7]. A model is developed in the following section which predicts the contact temperature required to produce this level of degradation.

### Chemical Model

Under boundary lubrication conditions, complicated physical and chemical processes occurring at the asperity tip contacts. Organic polymers containing iron have also been found in four-ball wear tests, suggesting that a reaction occurs between the lubricant film and the iron surface [8]. This film is likely to be composed of frictional polymers (organometallic compounds) adsorbed on the asperity tips, which provide lubrication by forming an easily shearable layer on the rubbing surfaces. Subsequent work in this area [9] showed that the frictional polymers are formed by the reaction of the lubricant with oxygen in the presence of metals. For the majority of contact configurations, the oxidation is believed to occur with minimum or no limitations from oxygen diffusion within the liquid system. After the initial oxidation process, further reaction of the surface layers then takes place, forming insoluble high-molecular-weight deposits, which play a part in the lubrication process. As the lubricant is depleted by oxidation and degradation, protection afforded by the continually forming chemical film ceases to exist, hence wear occurs. Since the chemical reactions are strongly dependent upon the temperature, the temperatures within the contact zone appear to be critical parameters to control the effectiveness of boundary lubrication.

Klaus et al. [10] demonstrated that conditions within a thin-film micro-oxidation test closely

resemble those within a sliding contact. This test uses a thin lubricant film on a metal catalyst cup in a nitrogen-oxygen mixture, thus both temperature and oxygen availability may be controlled. Subsequent work [11,12] demonstrated that the oxidation reaction for a variety of lubricants is of the Arrhenius type. The equation has the form:

$$k = m e^{-E/RT}$$

where,

T = Temperature

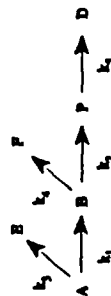
m = A coefficient

E = Activation energy

R = Gas constant

This relationship has been shown to hold true for a variety of organic esters, mineral oils, and synthetic hydrocarbons over a wide range of temperatures.

Naidu et al. [13] described a global rate model based on the consumption of lubricant within a micro-oxidation test, subjected to conditions similar to those encountered in a sliding contact. The model describes the primary oxidation step as well as the subsequent condensation polymerization step, which results in lubricant viscosity increase and insoluble sludge formation. These reactions can be described as follows:



where,

A = Original oil

E = Evaporated original oil

B = Low molecular weight oxidation products

F = Evaporated low molecular weight products

P = High molecular weight liquid polymerization products

D = Insoluble deposits

The constants k are reaction rate constants

Klaus et al. [7] used gel permeation chromatography (GPC) to determine the molecular weight distribution of the liquid lubricant remaining after the conclusion of the wear test. Results showed that under wear testing condition high molecular weight products are dominant. Because of the short duration of the flash temperature experienced by the lubricant in the contact, evaporation can be neglected from the micro-oxidative model. The primary oxidation products, once formed, proceed to form high molecular weight polymers and deposit, so  $k_1$  is the rate limiting step in the degradation process ( $k_1 < k_2$ ). As the formation of the primary oxidation product (B) is the rate limiting step, the polymerization of B appears to continue at the same rate to produce the polymer (P) and the deposit (D). Therefore, the model can be simplified to:



Since the reaction rate is an exponential function of temperature, the temperature in the contact controls the rate of oxidation and polymerization of the lubricating oil. An accurate estimation of the thin oil film temperature generated by inter-asperity contact is therefore essential for any predictive model.

#### Calculation of Contact Temperature Using Chemical Reaction Kinetics

During a micro-sample four-ball wear test the bulk of the lubricant forms three reservoirs, one around each point contact, and the remainder of the lubricant is spread around the wear halo on the rotating ball as illustrated in Fig. 1. As the upper ball rotates, a portion of the lubricant is entrained within the contact conjunction formed with each of the three lower balls. The total volume of oil available for oxidation in each revolution (V) may be calculated by considering the swept area of the wear halo on the rotating ball and the mean separation between the opposing surfaces. The results of these calculations are given in

column 2 in Table 3. From this information the total period of time each lubricant molecule is likely to remain within the contact may be easily calculated. To determine the effect of film thickness on temperature, a range of interfacial distances between 0.005 to 1  $\mu\text{m}$  (50-10,000 Å) were considered. A separation of 0.005  $\mu\text{m}$  corresponds to the molecular dimensions of a layer of mineral oil and represents the minimum separation possible between the opposing surfaces. 1  $\mu\text{m}$  is the upper bound for the film thickness and is equivalent to four to five times the length of the oil soluble condensation polymers formed by the oxidation of mineral oil, as measured by adsorption on the wall of a nucleopore filter capillary [14]. Finally, the total period of time each oil molecule is likely to remain within the contact during the course of a 50 minute test is given below in Table 3:

Table 3: Time an average molecule remains within the contact conjunction during a 50 minute four-ball wear test.

Film Thickness (nm)	Film Volume ( $\mu\text{L}$ )	Time (s)
5	$1.61 \times 10^{-4}$	$1.1 \times 10^{-2}$
10	$3.22 \times 10^{-4}$	$2.1 \times 10^{-2}$
50	$1.61 \times 10^{-3}$	$1.1 \times 10^{-1}$
100	$3.22 \times 10^{-3}$	$2.1 \times 10^{-1}$
200	$6.21 \times 10^{-3}$	$4.2 \times 10^{-1}$
400	$1.24 \times 10^{-2}$	$8.7 \times 10^{-1}$
1000	$3.22 \times 10^{-2}$	2.1

Based on the kinematic reaction model by Naidu et al, the theoretical period of time required for 10% oxidation to occur was calculated, as a function of temperature. These calculations assume, that evaporation of both the original oil and low molecular weight liquid phase oxidation products is negligible. It is also assumed that there is no oxygen diffusion limitation within the oil film. The results are presented in Table 4 below.

Table 4: Theoretical time required for 10% lubricant oxidation

Time (sec- $\bar{f}$ )	Temperature ( $^{\circ}\text{C}$ )
2400	200
600	225
150	250
37	275
9	300
2.3	325
0.6	350
0.13	375
0.03	400
0.01	425
0.0023	450
0.0006	475
0.0001	500

The estimated contact temperature required to produce polymerization in 10% of the total lubricant volume is shown in Fig. 2, as a function of film thickness. As the mean separation between the opposing surfaces decreases, the theoretical oil temperature increases exponentially, as less oil is able to enter the contact junction.

The mean boundary film thickness between the opposing surfaces is approximately 0.06  $\mu\text{m}$  (600 Å), as calculated from the asperity contact model detailed in the following section. The required film temperature at this separation is 375 $^{\circ}\text{C}$ . Figure 3 shows the calculated lubricant life at this temperature as a function of lubricant volume, along with experimentally determined values for comparison. As may be seen, the predicted values are in general agreement with the experimental data.

#### Mechanical Model

In the present work, the asperity temperatures within the contact zone of two rough surfaces

were calculated using the model developed by Lee [2]. The input data include two groups:

1) experimental conditions such as sample geometries, load, speed, material's elastic constants, and lubricant properties and 2) measured data such as friction and surface roughness profiles of the worn samples. Given roughness profiles of the opposing surfaces, the calculations include three sequential steps: 1) contact modeling to determine the relationship between average contact pressure and the average distance (gap) between the two surfaces, 2) rough-EHD analysis to calculate the average film thickness and the load distribution between hydrodynamic film support and asperity contacts, and 3) temperature calculation to determine the asperity temperature distribution within the contact zone.

To model two surfaces in contact, one has to describe the surface roughness and simulate the contact geometry under static load mathematically. The contact model employed in this study assumes that both surfaces have longitudinal roughness. The validity of this assumption has been demonstrated in recent studies [15, 16] for wear scars formed after a four-ball wear test. Fig. 4 shows the surface roughness profiles taken from the top ball (inverted) and the lower balls after the prewear test. These profiles were measured perpendicular to the sliding direction. To ensure accurate representation of the wear scar on the top ball, its roughness trace was determined by averaging digitized profiles in three angular directions ( $\theta=0^\circ$ ,  $\theta=120^\circ$ ,  $\theta=240^\circ$ ). An average trace for the lower balls was similarly determined, one profile being taken from each of the lower balls. Subsequently, the profiles from the top ball and the lower balls were combined, by subtraction, to form a composite profile, denoted as "relative" trace in Fig. 4. The contact between the top ball and the lower balls was then simulated by analyzing the contact between the composite profile and a rigid plane. Taking into account of the elastic deformation, the local high spots (asperities) of the composite profile would deform and become flattened when the profile is pressed against the rigid plane. The distance measured from the rigid plane to the mean line (plane) of the deformed composite profile defines the average gap between the mean lines (planes) of the two rough surfaces under the same load. Meanwhile, the average pressure of those deformed asperities defines the average contact pressure. By increasing the severity of loading, the average gap becomes smaller, while the contact pressures of the individual

asperities increase. Depending on the local geometries, some of the asperities may yield as the contact severity increases. When this happens, the model assumes that the contact pressure stays at the yield pressure and does not increase further. If one varies the loading mathematically, one could determine the relationship between the average contact pressure and the average gap, as illustrated in Fig. 5. For this particular simulation, since the balls are preworn, the maximum Hertzian pressure under an applied load of 40 kg is estimated to be 0.847 GPa. The average gap in the central portion of the contact is about 0.06  $\mu\text{m}$ , according to Fig. 5. The r.m.s. value of the "relative" roughness shown in Fig. 4 is 0.23  $\mu\text{m}$ . After the relationship between average contact pressure and average gap has been determined, the rough-EHD analysis was then carried out.

In the rough-EHD analysis, a line-contact between two rough cylinders is assumed, and only the inlet half of the contact is analyzed [2]. The pressure along the centerline of the line contact is assumed to be the same as the maximum Hertzian pressure determined by considering the pre-worn geometry. The film thickness solution of the rough-EHD analysis is based on the average gap. Since the analysis is based on two rough surfaces in contact, the two cylinders are subjected to two types of pressures; one from hydrodynamic lift, the other from asperity contact pressures. The relationship between average contact pressure and average gap determined in the contact simulation previously is therefore utilized in the calculation of the overall pressure distribution of the contact. Figure 6 illustrates the load-sharing characteristics between asperity contact and hydrodynamic lift, as a function of the normalized distance from the center of the contact. The parameter  $b$  is the Hertzian contact radius. Clearly, asperity contacts carry most of the normal load, thus, sliding friction between the opposing asperity contacts will be responsible for most of the heat generated. Besides the pressure estimations, the rough-EHD analysis also calculates the average friction coefficient from the asperity contacts based on the measured friction value [2]. In this case, the measured friction coefficient was 0.11, and the average asperity contact friction was determined to be 0.112.

From the rough-EHD calculations, the size and shape of the asperities within the contact



zone can be determined. Each asperity contact forms roughly an elongated ellipse, with its major axis orientated in the sliding direction. Also, the pressure distribution on each asperity as a function of distance from the contact centerline can be determined. Before the temperature calculations are performed based on Jaeger's work [17], some further simplifications are taken. Each asperity contact is approximated to be rectangular, and its average contact pressure is used for temperature calculations. Frictional heating is considered as the heat source, which includes both the average asperity contact friction and the hydrodynamic film friction. The resulting temperature within each asperity contact is a function of the location measured from the centerline of the nominal contact zone. The maximum temperature of each asperity contact is sought and will be considered as the representative temperature for that asperity. Fig. 7 shows the cumulative temperature distribution under the conditions included in Fig. 4. The highest temperature attainable is approximately 220 °C covering about 3% of the nominal area. These results also reveal that the asperity contacts cover approximately 45% of the nominal area and the bulk temperature is ~ 150 °C.

The results of the temperature analysis show that the temperatures within the contact zone are in the range of 150 - 220 °C. This is in general agreement with other continuum models [18,19], which, for the present test conditions, predict the maximum contact temperature to be 157°C and 160°C, respectively. By using the current model, the considerations of asperity contacts, thus local high contact pressures, and a slightly higher average friction than the measured overall friction appear to have already increased the temperature estimates. However, the reaction kinetics model estimates an average temperature of 375°C in the lubricant film is necessary to degrade 10% of the total lubricant. Also, measurements carried out by Bos [20] under slightly more severe conditions using a subsurface thermocouple, demonstrated that the true surface temperatures during a four-ball wear test are in excess of 300°C. Clearly, the predicted contact temperatures based on the current mechanical model are considerably lower than that required by the oxidation process. The discrepancy is large enough to be significant.

## Discussion

By estimating the temperatures in the contact zone, it brings to focus the differences the two schools. From the chemical school, the protection against failure is thought to be afforded by the lubricant molecules via the formation of easily shearable chemical films underneath asperities. The formation rate and depletion rate of such films are associated with lubricant degradation process, which is a strong function of temperature. From the mechanical school, the micro-EHD films underneath asperities are thought to support the load, thus separating the two contacting surfaces. When the asperity temperature exceeds a certain level, the micro-EHD films would collapse leading to failure. These two schools of thought apparently represent two separate and distinct ideas. However, the temperatures within the contact zone appear to be the common parameter to both for predicting the effectiveness of boundary lubrication.

From the chemical model presented previously, an average film temperature of 375 °C was predicted by counting the total reaction products at the end of test. The model assumes all reactions occur in the contact using the nominal contact area, and wear particles are not reactive to significantly change the rate. This means one reactor at a uniform temperature of 375 °C to deplete 10% of the original lubricant molecules. However, the presence of "hot-spots" inside rough contacts, observed experimentally [21] as well as predicted numerically [22], suggests that there may be many hot spots with different temperatures inside the contact. Since the oxidation rate is an exponential function of temperature, it stands to reason that some spots will be at higher temperatures than 375 °C. Based on these arguments, one may conclude that the temperature estimate offered by the chemical model is an average integral of time and temperature, and may be conservative in its estimate of maximum temperatures.

The mechanical model has taken into account the asperity contacts. The load-supporting characteristics are rearranged such that the majority of the applied load is concentrated on the asperities which cover only ~45% of the nominal area. By such consideration, the predicted

asperity temperatures are in the range of 150 - 220 °C. The lower end of those temperatures agree well with predictions by using other continuum models [18,19], which do not include considerations of local contacts by asperities. The higher end of those temperatures show noticeably higher temperatures, concentrated on more localized areas, than those earlier models. However, the asperity temperatures predicted by the mechanical model are still significantly lower than 375 °C predicted by the chemical model. Following the discussions in the previous paragraph, 10% depletion of the original lubricant molecules at the end of test would not be possible at the temperatures predicted by the mechanical model.

One uncertainty in the mechanical temperature analysis is the bulk temperature of the upper ball. In the present study, this was assumed to be 75°C. This estimate is based on an earlier analysis of steady-state temperatures in a four-ball apparatus [23]. The previous analysis concluded that the bulk temperature of the upper ball is sensitive to the thermal resistance between the ball holder and the shaft. An underestimate of the thermal resistance can result in a low estimate of the temperature for the upper specimen. It is conceivable that the bulk temperature of the upper ball may be slightly higher than 75°C. However, it is unlikely that it would exceed 110°C, which was the experimentally measured temperature at the same speed (600 rpm), but at 80 kg, which is twice the present load [20]. Another uncertainty is that the temperature in the fluid film underneath asperity contact may be higher, if a temperature gradient exists within the lubricant film, similar to that within the bearing surface. One can take a 0.1 µm thick insulating polymeric layer with a thermal conductivity comparable to mineral oil and assumes it adhere to the solid surfaces. Then, the mid-film temperature can be estimated to be ~ 17 °C higher than the surface temperature by considering heat conduction through this film. This temperature increment is still inadequate to resolve the discrepancy. Although one may argue that the thermal properties of a monomolecular layer adsorbed onto the metal surface may be significantly altered by thin film effect, the thermal conductivity of condensed polymer has not been accurately quantified so far.

The above two effects may alter the estimated lubricant film temperature by no more than

40-50°C, which is still far from that required to achieve the experimentally measured level of oxidation. A third possibility to reconcile the temperature discrepancy may be that the average film temperature within the contact is likely to be less important than isolated areas of high temperature, at which almost instantaneous oxidation will take place. However, it has been demonstrated previously that the opposing profiles formed during a four-ball wear test are alike [15]. The magnitude of the "relative" roughness between the opposing profiles (normal to the sliding direction) is often similar to that measured in the sliding direction. For this reason, undisturbed reservoirs of oil are unlikely to persist within the surface roughness. Rather, the fluid will be regularly forced around areas of intersparsity contact and high temperature. Therefore, the discrepancy still remains unresolved.

Besides the attempts discussed previously, the unavoidable wear events in boundary lubrication may present additional possibility to reconcile the temperature discrepancy. In a recent report [24], an asperity friction coefficient of at least 0.4 is shown to be required for the formation of a wear particle. Less severe asperity contacts with lower friction coefficients merely produce a combination of elastic and plastic deformation. Clearly, this would produce abnormally high flash temperature in that region. Furthermore, Hsu and Klaus [25] demonstrated that the reaction rates between an oxide covered surface and a freshly worn surface are only slightly different, accounting for about 20°C difference. Meanwhile, each wear particle will contain some energy, imparted to it during asperity deformation, immediately after its formation. This energy will be released to the surrounding lubricant film as heat. Hsu and Klaus [23] utilized experimental data by Bos [20] to demonstrate that the surface area of the wear debris formed during a four-ball wear test is of the order of 1000 mm<sup>2</sup>. Hence, even a thin film of oxidized lubricant formed on the surface of the wear debris would have an appreciable effect on the overall level of lubricant degradation. From these studies, a slight redistribution of the energy within the contact zone to account for the disruptions due to wear appears to be capable of producing high temperature spots locally. Subsequently, the formation of wear debris may also increase the amount of reaction products.

The effect of wear on the temperature prediction has not been included in either chemical model or mechanical model. The temperature predicted by the chemical model was asserted previously to be a conservative measure because the effect of localized hot-spots is not considered. Such an assertion seems to be reasonable based on the effect of wear events discussed. However, wear may be considered incidental for the chemical model at the current moment simply because the estimation of the average film temperature is already rather high compared to the predictions by continuum models. On the other hand, the significantly low estimates predicted by the mechanical model appear to present a more serious inconsistency. In the following, we present a modified mechanical model to account for the effect of wear on local temperatures.

#### Modified Temperature Model

To incorporate wear process in the temperature calculation, localized disruptions due to wear need to be modeled. To achieve this goal, the plastically yielded asperities are assumed to be the sources of wear. Also, higher friction is to be associated with those plastically deformed asperities. From the contact simulation [2], the asperity contacts can be separated into two groups, elastically deformed and plastically yielded. The relative amount of each group in the overall contact is dependent upon the surface roughness profiles. The friction coefficients of the two groups of asperity contacts are then modified as follows,

$$\beta W_{yield} + \alpha W_{elastic} = \mu W_{app} \quad (1)$$

where  $\beta$  = friction coefficient on plastically yielded asperities  
 $W_{app}$  = total load on yielded asperities  
 $\alpha$  = friction coefficient on elastically deformed asperities  
 $W_{elastic}$  = total load on elastically deformed asperities  
 $\mu$  = average asperity contact friction determined from rough-EHD analysis  
 $W_{app}$  = total load on asperity contacts

The above equation is to redistribute the asperity friction according to the types of deformation and not to violate the total asperity contact friction estimated by the rough-EHD analysis. By increasing the friction on plastically deformed asperities, the friction on elastically deformed asperities will be lowered. The no wear condition is a special case where  $\beta = \alpha = \mu$ . Considering the random nature of the asperity contacts, the left-hand terms in the equation (1) may be best represented by summations over all the asperities within the individual groups. Specifically, the plastically deformed asperities do not always provide wear particles. Therefore, it would be more reasonable to assume different degrees of high friction for those asperities. However, this will make the model extremely complex, and thus is omitted in this study.

With the modification of asperity friction outlined in equation (1), the temperature distribution shown in Fig. 7 is recalculated. Before the temperature calculations are performed, the types of deformation on the asperities are identified. Fig. 8 shows the original roughness profile and the deformed profile at the centerline of the contact, determined by rough-EHD analysis. Most of the asperities are flattened near the centerline, but not all of them are subjected to plastic yielding. The plastically deformed asperities are labeled by open circles. The total number of plastically deformed asperities is three under an average pressure  $\sim 0.847$  GPa. To simplify the calculation, only, one  $\beta$  value and one  $\alpha$  value are considered in equation (1). Fig. 9 shows the temperature results by varying the friction on plastically yielded asperities,  $\beta$ , from 0.15 to 0.4. The no wear case is also included, where the average asperity friction  $\mu$  determined from rough-EHD analysis was 0.112. After the friction modification, the temperature level and its distribution over the entire asperity junctions are significantly changed. As the  $\beta$  value increases, high temperatures are concentrated in the plastically yielded contacts, which cover  $\sim 7\%$  of the nominal area. The  $\beta$  value appears to have an upper bound around 0.4. When  $\beta = 0.4$ ,  $\alpha$  becomes negative, suggesting that the redistribution of asperity friction apparently reaches its physical limit. The maximum attainable temperature can reach the level of  $410^\circ\text{C}$  when  $\beta = 0.38$ . Meanwhile, the temperatures on the elastically deformed asperities remain largely at the bulk temperature level.

By examining the resulting temperature levels shown in Fig. 9, the goal to reconcile the temperature difference between chemical model and mechanical model appears to be achievable. Especially, even higher temperatures may be reached if one assumes only one of the three plastically deformed asperities is producing wear debris. Under such assumption, the largest  $\beta$  value may go beyond 0.4 without violating the limitation set by equation (1). At any rate, these results clearly confirm the need of reconsidering the energy distribution within the contact zone in modeling boundary lubrication.

Following the assumption of high friction being associated with the wear event in the modified temperature model, the high temperature, e.g. 410 °C when  $\beta=0.38$ , is not expected to last for the entire test duration. The asperity should be worn off producing wear particle. Recalling the discussion in the previous section on wear debris, such wear particles would also increase the amount of reaction products. Meanwhile, the reaction rate in the area surrounding the "hot" asperities would produce more reaction products. Therefore, it is conceivable that more reaction products may be produced as a net result of having such high temperature junctions. As sliding continues, other asperities may become plastically deformed, causing localized high temperature rise and eventually wearing off.

The results shown in Fig 9 are encouraging. The modification is strongly dependent upon the surface roughness features, since it follows the plastically yielded asperities. Changes in the surface roughness may alter the number as well as the size of the plastically yielded zones. Consequently, the maximum attainable temperature and the temperature distribution within the contact zone may also be changed.

#### Conclusions

Boundary lubrication is a complicated process. Historically, the two schools of thought, chemical and mechanical, have examined the boundary lubrication mechanisms independently. The approaches are different and distinct. Taking the same system of a

simple micro-sample four-ball wear test and estimating the temperatures within the contact zone, the similarity and differences by the two approaches have been highlighted.

By modeling the chemical kinetics and counting the overall depletion of the original lubricant molecules, an average film temperature required for lubricant degradation during sliding contact was estimated. The asperity temperatures within the contact zone were also predicted by using a mechanical model which includes the effects of asperity contacts. The average film temperature obtained from the chemical model is significantly higher than the asperity temperatures predicted by the mechanical model. The significant discrepancy reveals inconsistency between the two approaches.

Discussions of the possibilities to reconcile the discrepancy suggested that a slight redistribution of the energy within the contact zone would be required to reconcile the two approaches. Subsequently, a modified mechanical model was tested to incorporate local disruptions caused by wear in the temperature calculations. By redistributing the energy within the contact zone to reflect the wearing events, the resulting asperity temperatures could be increased adequately to match with the temperature required for the lubricant degradation process. The success of the modified mechanical model confirmed the need to redistribute the energy within the contact zone. Further research into this area is needed.

#### Acknowledgment

The authors wish to acknowledge the lubricant life data gathered by Dr. K. K. Chao. Partial support from the Tribology Program, Office of Transportation Materials, Department of Energy is also gratefully acknowledged.

# REFERENCES

- [1] S. M. Hsu, E. E. Klaus, and H. S. Cheng, A Mechano-Chemical Descriptive Model for Wear Under Mixed Lubrication Conditions, *Wear*, 128 (1988) 307.
- [2] S. C. Lee, *Scuffing Modeling and Experiments for Heavily Loaded Elastohydrodynamic Lubrication Contacts*, PhD. Thesis, Northwestern University, Evanston, IL (1989).
- [3] S. Jahanmir, N. P. Suh, and E. P. Abrahamson II, The Delamination Theory of Wear and the Wear of A Composite Surface, *Wear*, 32 (1975) 33.
- [4] K. Komvopoulos, N. P. Suh, and N. Sata, Wear of Boundary-Lubricated Metal Surfaces, *Wear*, 107 (1986) 107.
- [5] H. W. Hermance and T. F. Egan, Organic Deposits on Precious Metal Contacts, *Bell System Tech. J.*, 27 (1958) 739.
- [6] R. S. Gates and S. M. Hsu, Development of an Oxidation - Wear - Coupled Test for the Evaluation of Lubricants, *ASLE Lubrication Engineering*, 40 (1) (1984) 27.
- [7] E. E. Klaus, J. L. Duda, and K. K. Chao, A Study of Wear Chemistry Using a Micro Sample Four-Ball Wear Test, *STLE Tribology Trans.*, 34 (3) (1991) 426.
- [8] G. Bryan, *The Effects of Metal Surfaces on Chemical Reactions in Boundary Lubrication*, M.S. Thesis, The Pennsylvania State University, University Park, PA (1976).
- [9] R. S. Gates, K. L. Jewett, and S. M. Hsu, A Study on the Nature of Boundary Lubricating Film: Analytical Method Development, *STLE Tribology Trans.*, 32 (4) (1989) 423.
- [10] E. E. Klaus, V. Krishnamachar, and H. Dang, Evaluation of Basestock and Formulated Lubes Using the Penn State Micro-oxidation Test, *Proceedings of the Conference on Measurements and Standards for Recycled Oil*, NBS Special Pub. 584 (1980) 285.
- [11] E. E. Klaus, P. Shah, and V. Krishnamachar, Development and use of the Micro-Oxidation Test with Crankcase Oils, *Proceedings of the Conference on Measurements and Standards for Recycled Oil*, National Bureau of Standards, September (1982).
- [12] D. B. Clark, E. E. Klaus, and S. M. Hsu, The Role of Iron and Copper in the Oxidative Degradation of Lubricating Oils, *STLE Lubrication Engineering*, 41 (5) (1985) 280.
- [13] S. K. Naidu, E. E. Klaus, and J. L. Duda, Kinetic Model for High-Temperature Oxidation of Lubricants, *Ind. Eng. Chem. Prod. Res. Dev.*, 25 (1986) 566.
- [14] E. E. Klaus, R. Nagarajan, J. L. Duda, and K. M. Shah, The Adsorption of Tribochemical Reaction Products at Solid Surfaces, *Friction and Wear - 50 Years on*, Proc. Inst. Mech. Eng. International Conference on Tribology (1987) 370.
- [15] F. X. Wang, P. I. Lacey, R. S. Gates, and S. M. Hsu, A Study of the Relative Surface Conformity Between Two Surfaces in Sliding Contact, *ASME J. of Tribology*, 113 (1991) 755.
- [16] J. Sugimura and Y. Kimura, Characterization of Topographical Changes During Lubricated Wear, *Wear*, 98 (1984) 101.
- [17] J. D. Jaeger, Moving Sources of Heat and the Temperature at Sliding Contacts, *Proc. Roy. Soc. London, N.S.W.*, 56 (1942) 203.
- [18] H. A. Francis, Interfacial Temperature Distribution within a Sliding Hertzian Contact, *ASLE Trans.*, 14 (1970) 41.
- [19] R. S. Fein, Transition Temperatures with Four-Ball Machine, *ASLE Trans.*, 3 (1960) 34.
- [20] A. Bos, The Temperature at the Wear Scars of the Four-Ball Apparatus, *Wear*, 31 (1975) 17.
- [21] T. F. J. Quinn and W. O. Winer, An Experimental Study of the 'Hot-Spots' Occurring During the Oxidational Wear of Tool Steel on Sapphire, *ASME J. of Tribology*, 109 (2) (1987) 315.
- [22] H. S. Kong and M. F. Ashby, Friction-Heating Maps and their Applications, *MRS Bulletin*, 16 (10) (1991) 41.
- [23] S. M. Hsu and E. E. Klaus, Estimation of Molecular Junction Temperatures in a Four-Ball Wear Contact by Chemical Reaction Rate Studies, *ASLE Trans.*, 21 (3) (1978) 201.
- [24] T. N. Ying and S. M. Hsu, Asperity-Asperity Contact Mechanisms Simulated by a Two-ball Collision Apparatus, *Proceeding of the First International Workshop on Micro-Tribology*, edited by R. Kaneko and Y. Enomoto, Morioka, Japan, (1992) 298.
- [25] S. M. Hsu and E. E. Klaus, Some Chemical Effects in Boundary Lubrication Part I: Base Oil-Metal Interaction, *ASLE Trans*, 22 (2) (1979) 135.

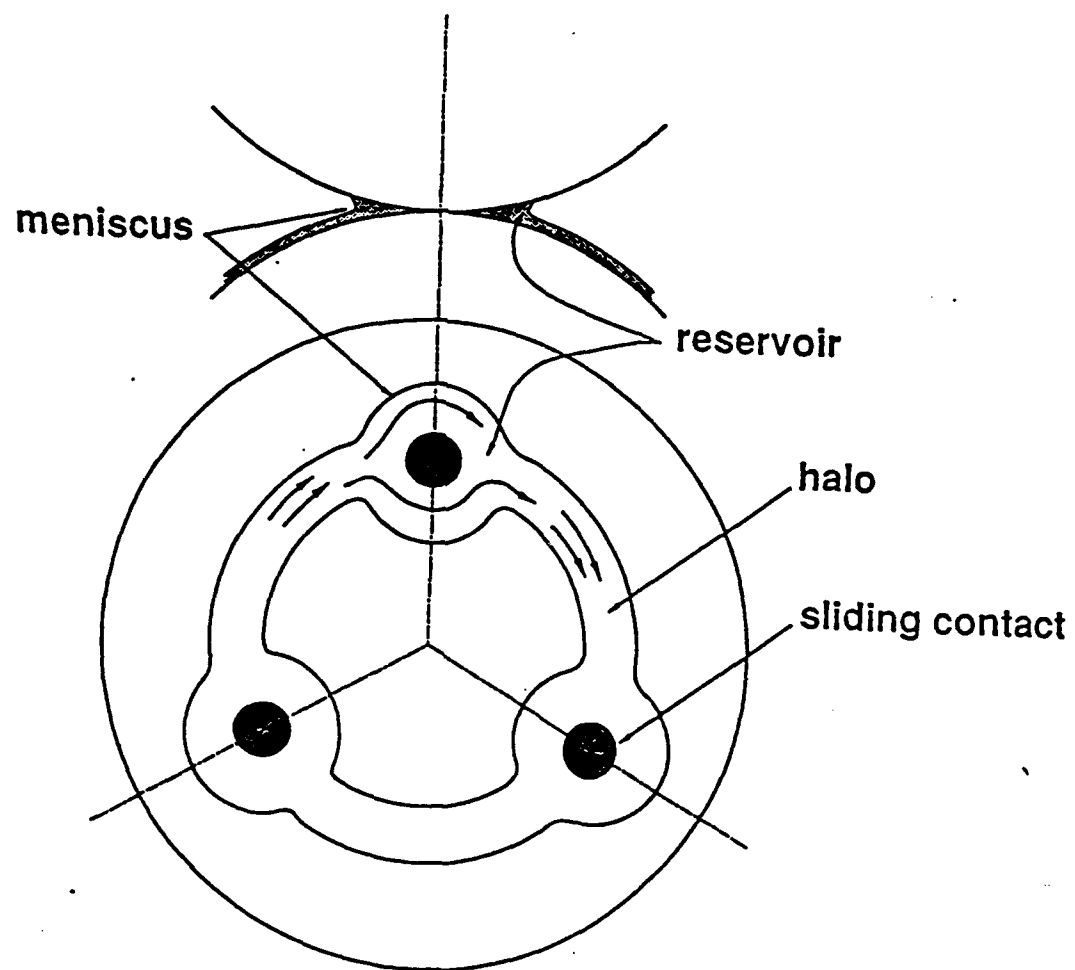


Fig. 1

Hsu et al.

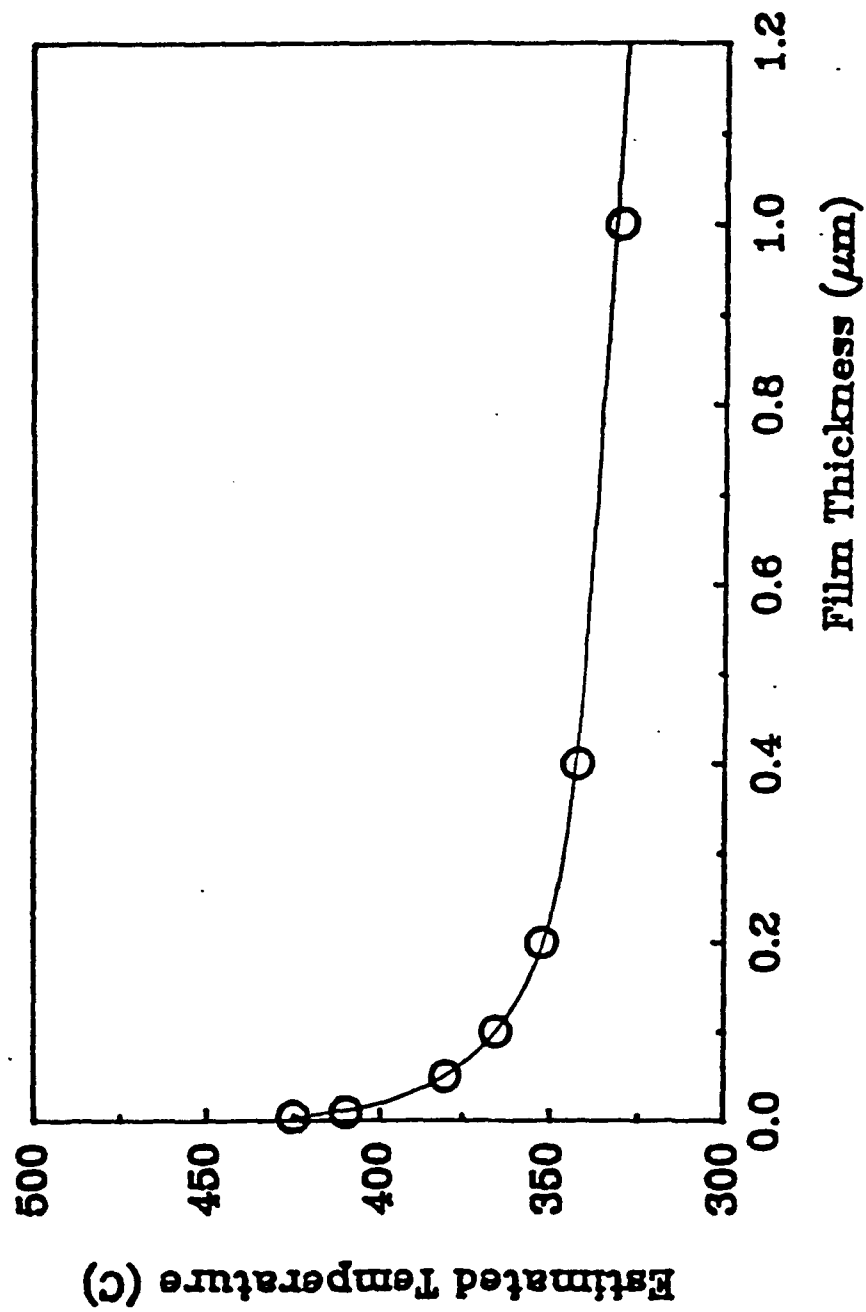


Fig. 2  
Hsu et al.

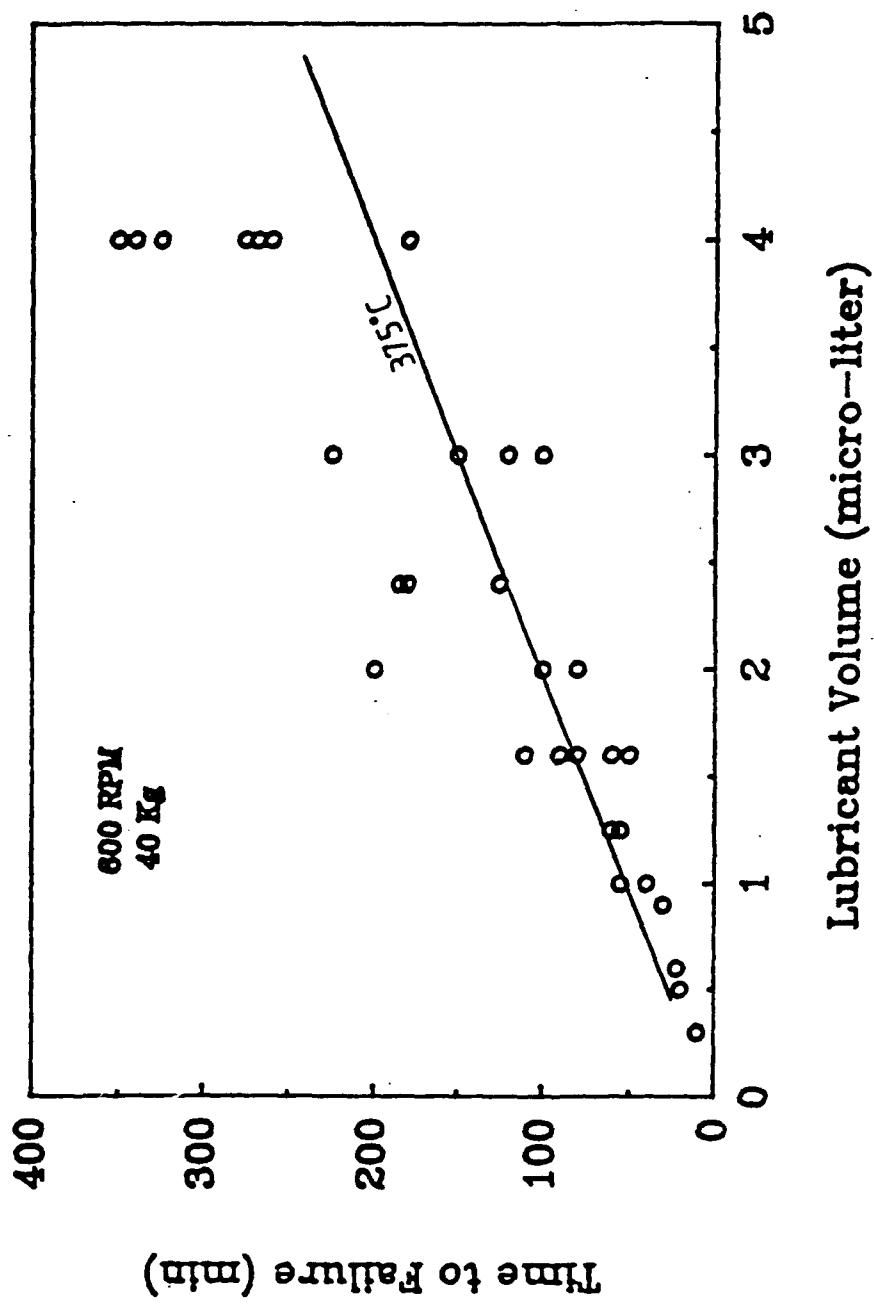


Fig. 3  
Hsu et al.



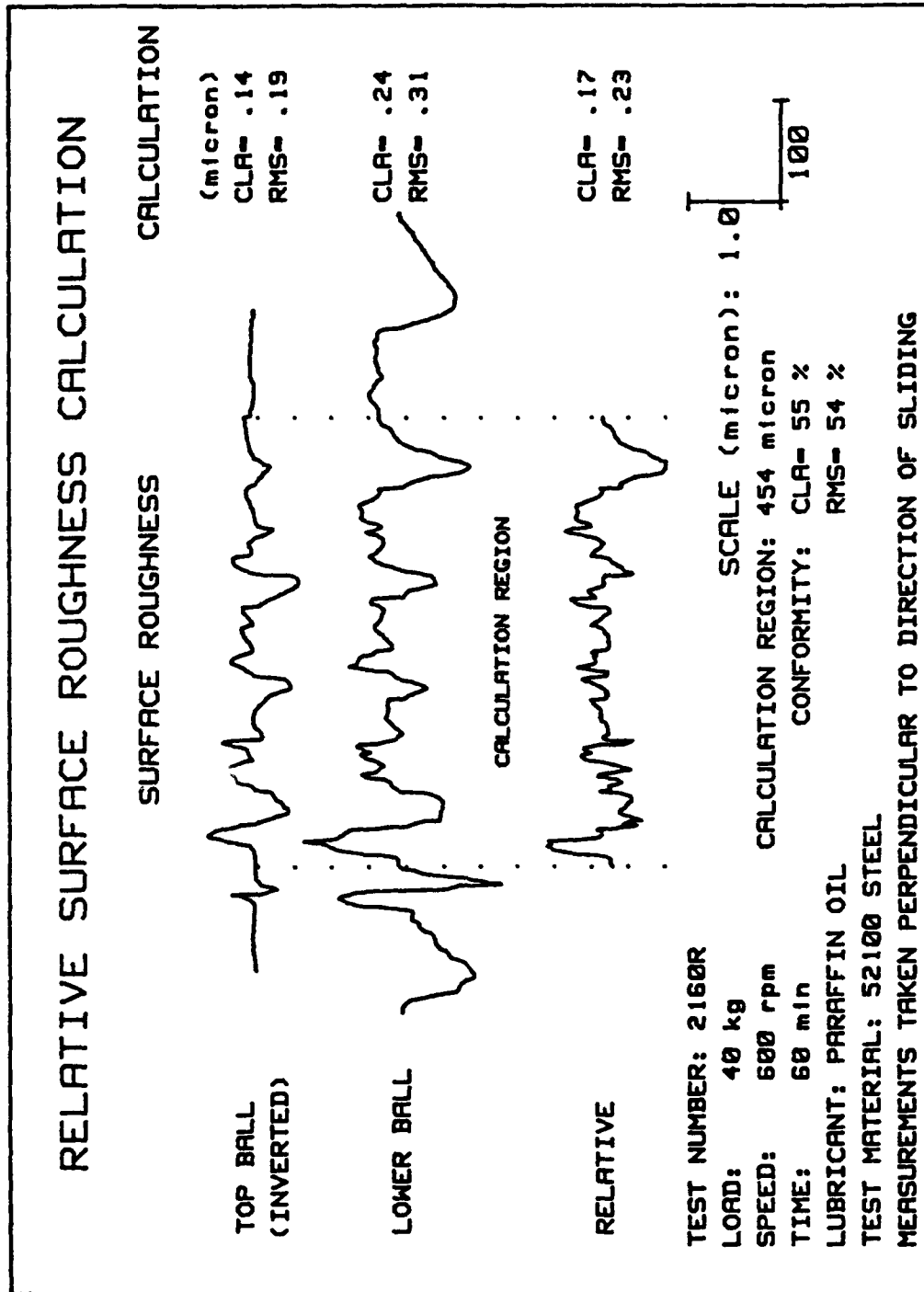


Fig. 4  
Hsu et al.

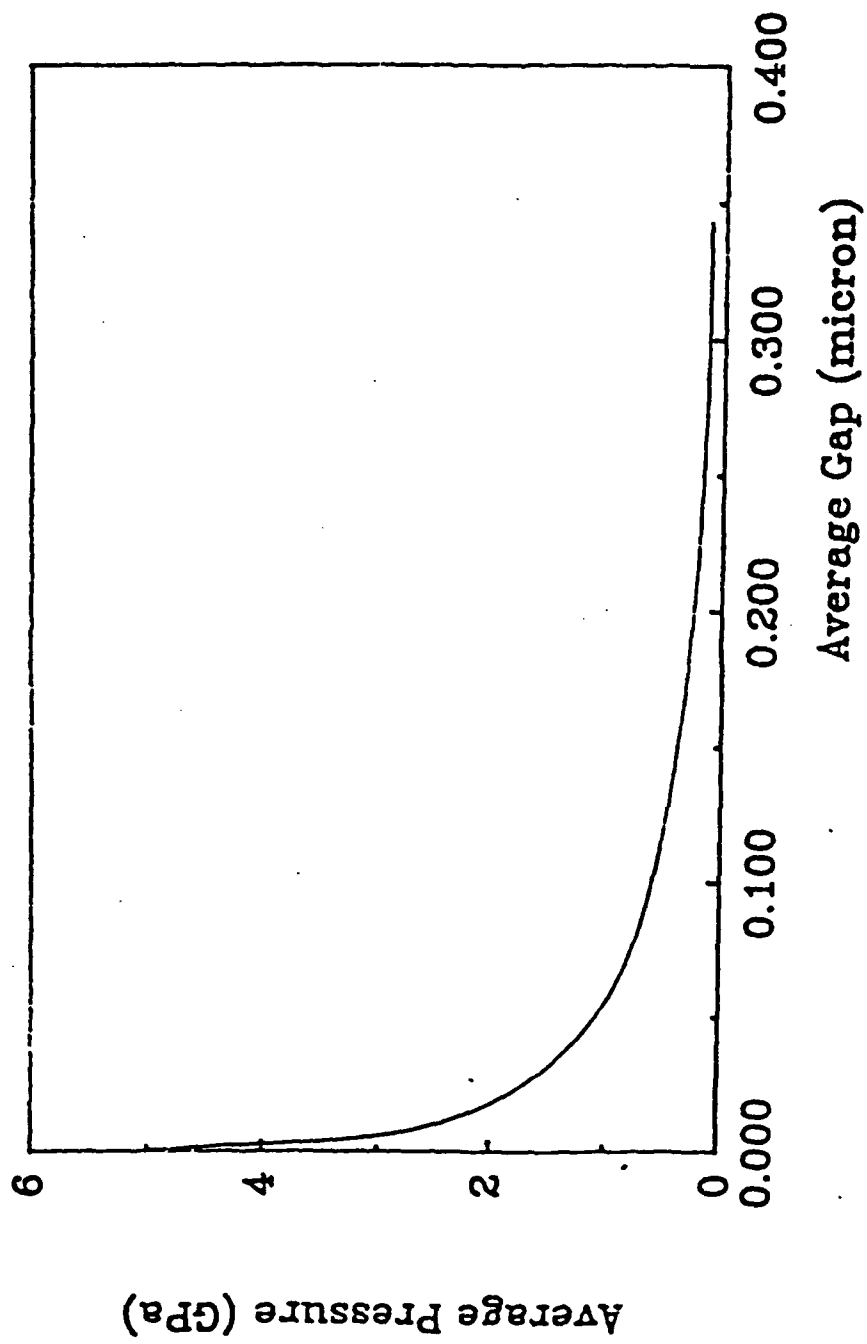


Fig. 5  
Hsu et al.

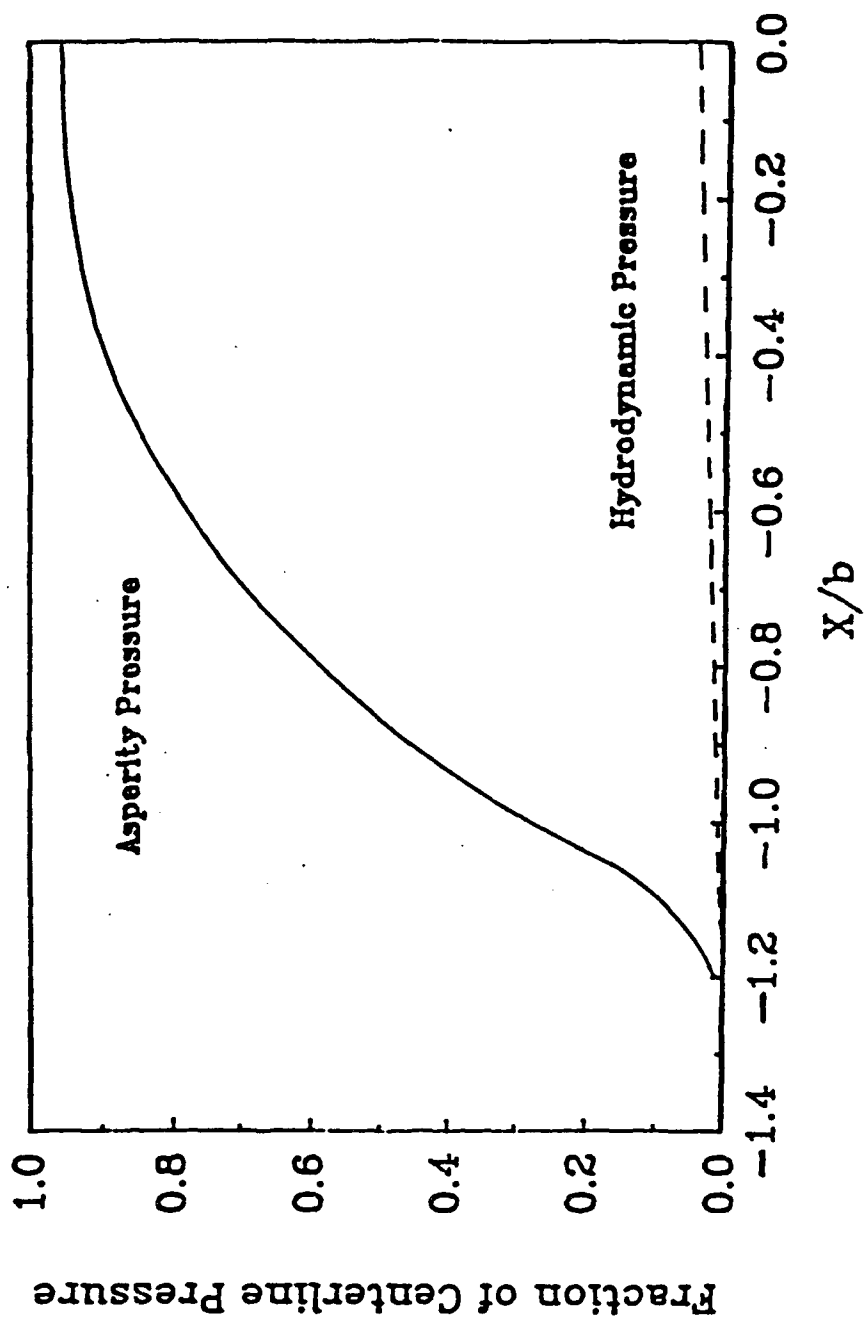


Fig. 6  
Hsu et al.

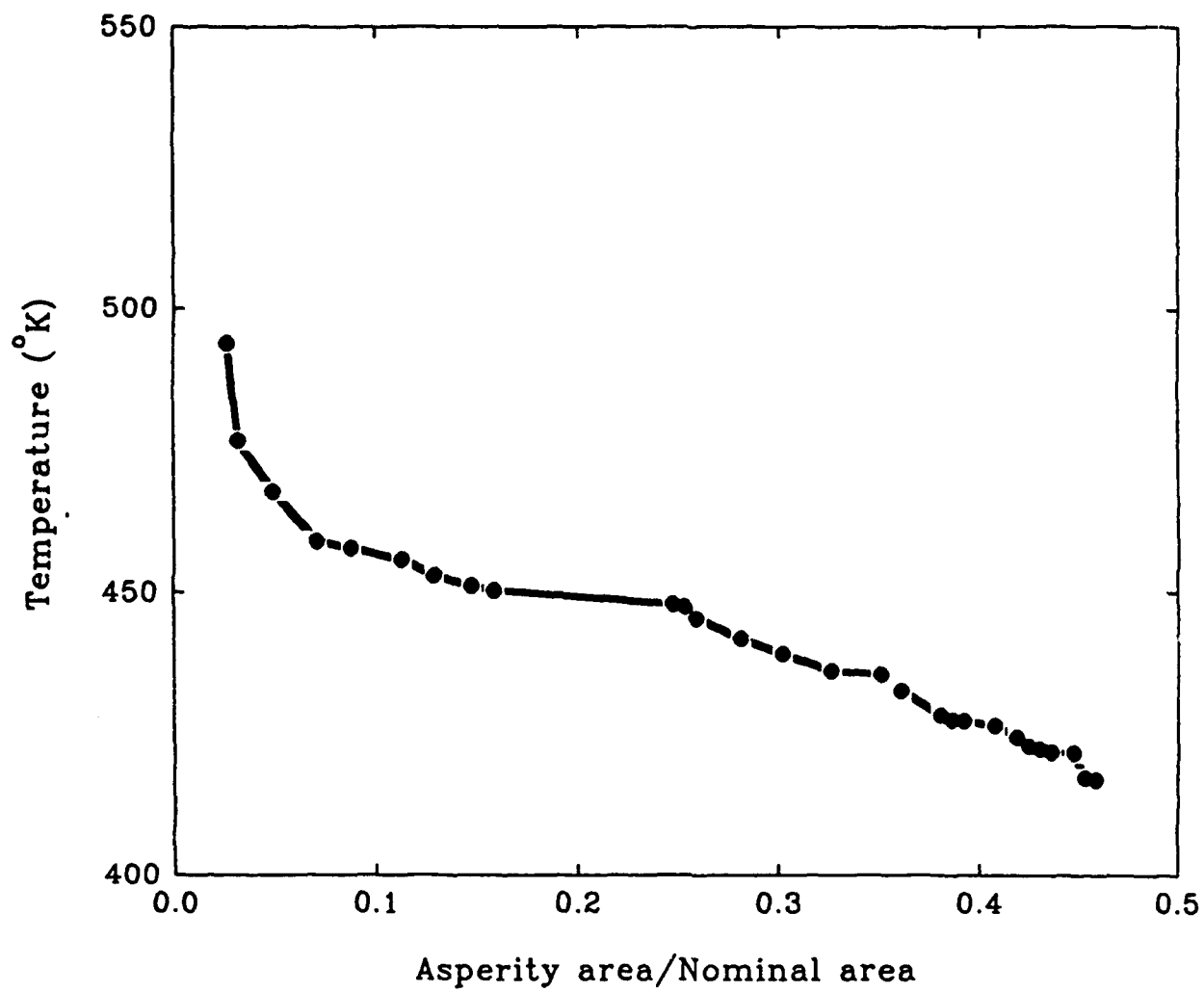


Fig. 7

Hsu et al.

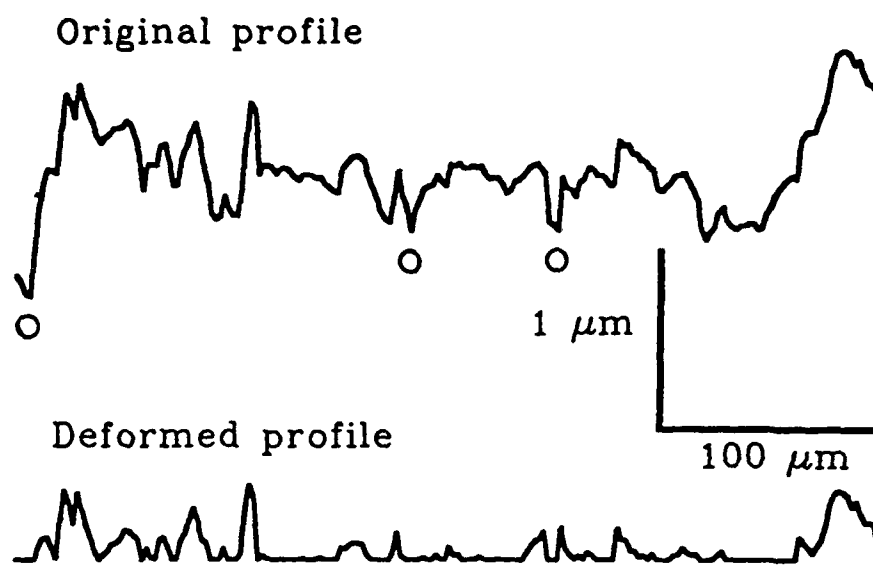


Fig. 8

Hsu et al.

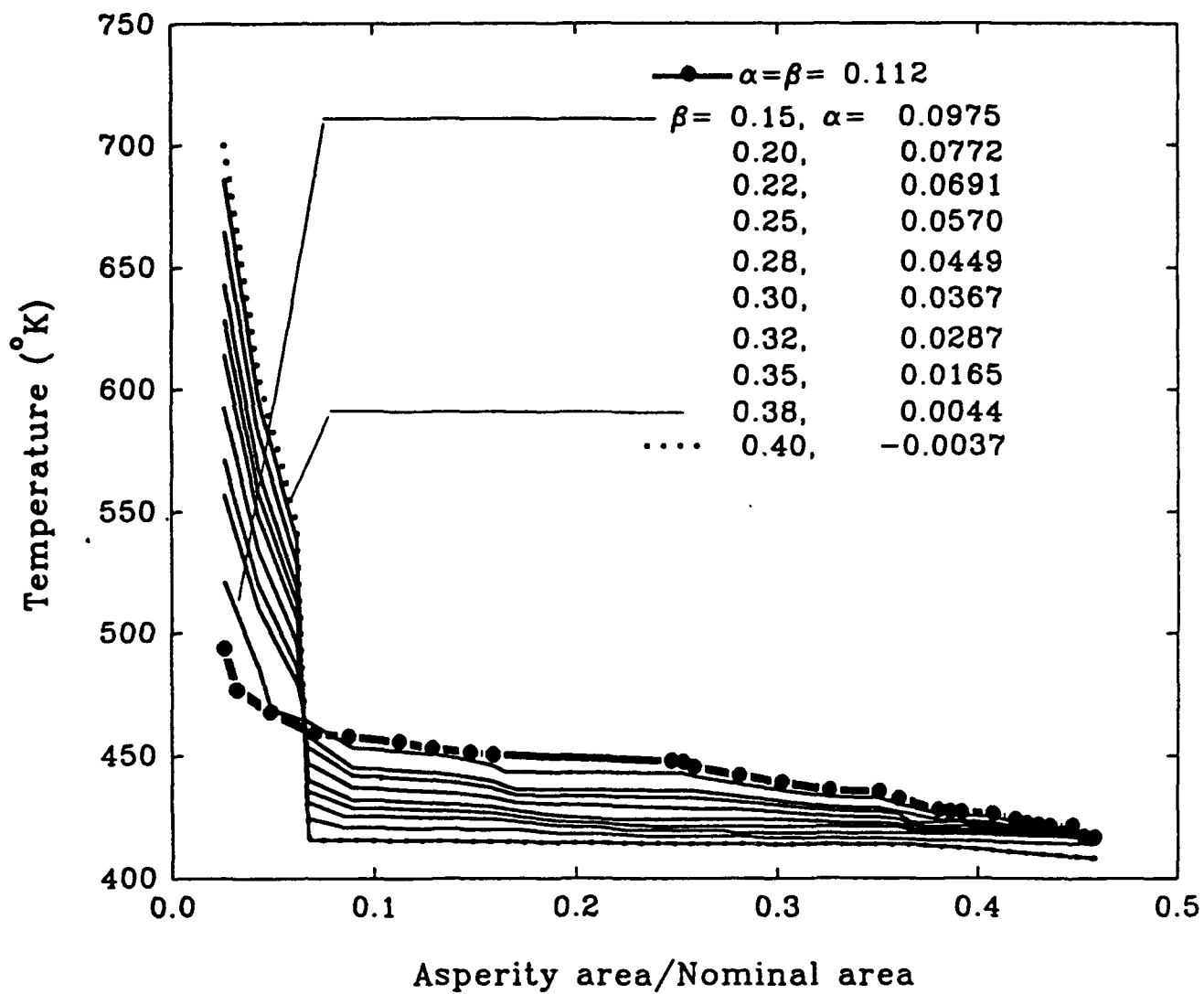


Fig. 9

Hsu et al.

**PENNSSTATE**



**Applied Research Laboratory**

# **Condition-Based Maintenance Initiatives**

**Bill Nickerson  
NCAGMT  
410-479-4781  
INTERNET: BNickerson@aol.com**

\*\*\*\*\* Bill Nickerson, "Initiatives In Conditioned Based Maintenance" \*\*\*\*\*

# **Presentation Topics -**

- Background
- Planning Process
- CBM Initiative Functions
- Objectives and Implementation
- Summary



# **Background -**

- Increasing Importance of Maintenance Costs
- U.S. Does Not Have a Leadership Position in Mechanical Diagnostics
- Negative Impact on U.S. Business Sectors
- Recommendation that Penn State Consider a Broad-Based CBM Initiative
- Planning Process for CBM Initiative Complete

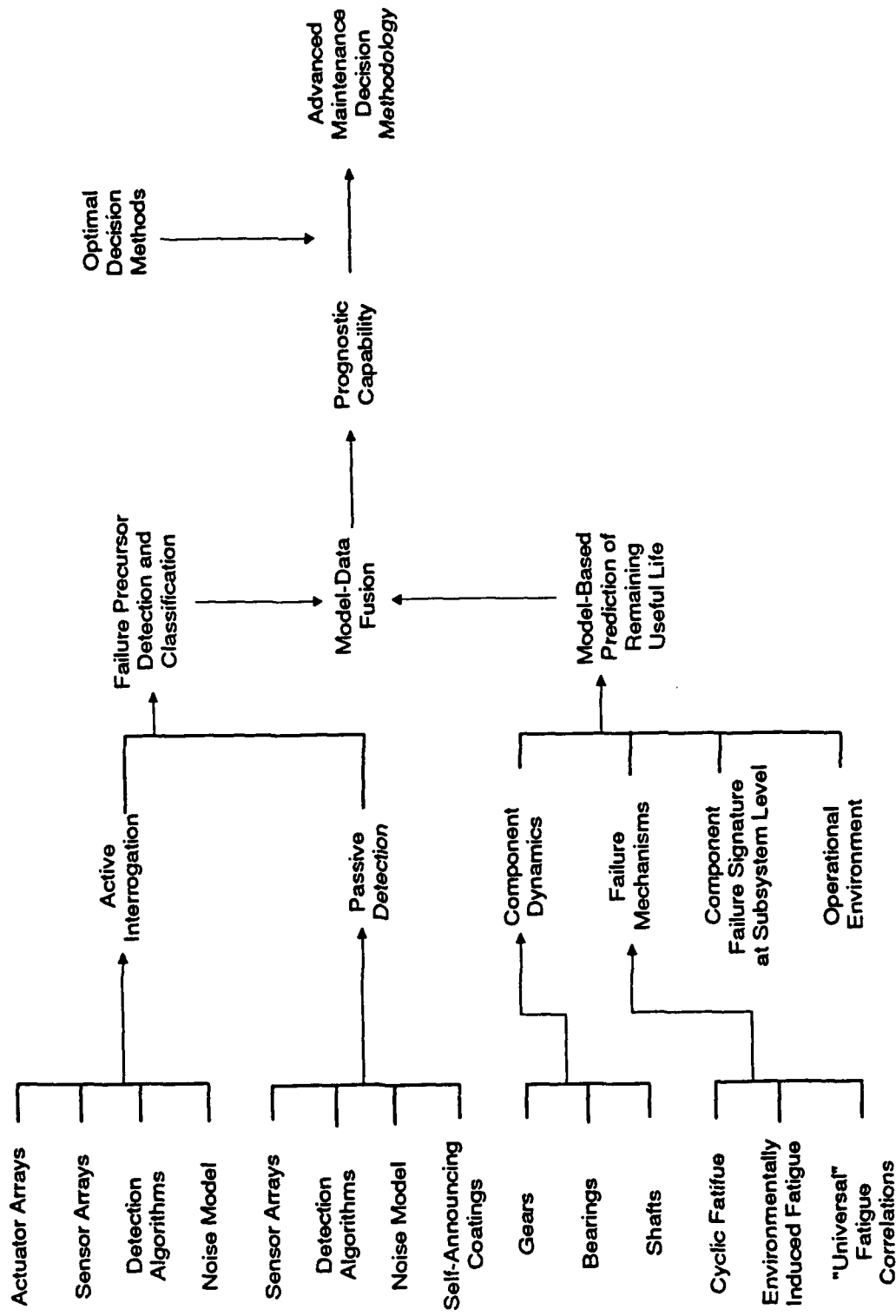
# Participants -

Prof. J. P. Cusumano	Nonlinear Dynamics in Mechanical Failure
Dr. D. L. Hall	Data Fusion & Decision Methodologies
Prof. T. A. Harris	Bearing Failure Simulation/Information System Architecture
Prof. G. H. Koopman	Improved Sensors for Failure Precursor Detection
Prof. S. K. Kurtz	Advanced Materials for Failure Reporting
Mr. A. J. Lemanski	Condition Monitoring System Architecture
Prof. G. A. Lesieutre	Relationship of Failure Mechanisms to Observables
Dr. W. D. Mark	Gear System Dynamic Failure Modeling
Mr. G. W. Nickerson	Program Formulation & Leadership
Dr. S. B. Rao	Advanced Gear Manufacturing Technology
Dr. D. C. Swanson	Active Fault Identification
Dr. R. K. Young	Improved Algorithms for Failure Precursor Detection

# **Strategic Technical Objectives -**

- Develop a Robust Prognostic Capability
  - Remaining Useful Life
  - Cause of Imminent Failure
  - Remedial Actions to Extend
- Mature Technologies for Application to New Materials and Processing
  - Failure Mechanisms
  - Sensing Methodologies
  - Failure Precursors

# Prognostics Development Roadmap-



# **CBM Initiative -**

- Pre-competitive, Generic R&D
  - Diagnostics
  - Prognostics
- Non-vested Testing at Realistic Scales
- Broad-based Educational Program
- Formation & Leadership of Consortia
  - Government
  - Industry
  - University

# **Pre-Competitive Generic R&D -**

- Technology Gaps Identified
  - Corporate
  - Government
  - Academic
- Strategic R&D Thrusts Identified
- Team formed to Conduct Necessary Work
  - ARL
  - Other Units of Penn State
  - Other Organizations as Appropriate

# **Non-Vested Testing -**

- Alpha Test Facility to Evaluate Concepts
  - Realistic Scale (e.g. High Speed Gearbox)
- Side-by-Side with Most Extensive Materials Testing in U.S. Universities
- Basis for Subsequent Design of Beta Test Facility

# **Education in Diagnostics/Prognostics -**

- Introduce Concepts in Undergraduate Engineering Curriculum
- Graduate Level Courses & Multi-Disciplinary Specialization
- Credit Courses for Practicing Engineers at Remote Sites
- Short Courses
- National Seminar Series



# **Consortia Formation & Leadership -**

- Address Specific Diagnostic Requirements
  - New Weapons Systems
  - Upgrades
  - Civil Sector Implementation
- Teams Formed from Industry & University - Expertise & Interest
- Management to Meet Customer Requirements

# Summary -

- University Community Can Make Major Contributions
  - Strategic R&D
  - Non-vested validation of concepts
  - Educational Initiatives
- Penn State is Positioned to Provide These Services

planetary sun gear, and associated bearings. Sensor number 1, mounted on the forward bolt circle of the gearbox at the 9 o'clock position (Figure 4), was in the best position to monitor the planetary gear system and the propeller shaft support bearings.

The stress wave data were acquired using a SWAN-100 BEARING/GEAR ANALYZER and a Digital Audio Tape (DAT) data recorder. The SWAN-100 filtered out background noise and vibration signal components to provide a Stress Wave Pulse Train (SWPT) analog output that represented a time history of friction and shock events generated by the gearbox internal components. The SWAN-100 also computed the Stress Wave Energy (SWE), which is a quantitative measure of friction and shock, at each sensor location. The Stress Wave Pulse Train was recorded on the DAT recorder and then played back for post flight analysis by a System 3000 Stress Wave Analyzer.

The System 3000 produced Stress Wave Amplitude Histograms (SWAHs) that show the statistical distribution of stress wave peak amplitudes. The System 3000 was also used to perform spectral analysis of the SWPT and plot Stress Wave Power Spectral Density (SWPSD) data. The Stress Wave Amplitude Histograms are most useful in detection of aperiodic events frequently associated with lubrication problems such as fluid or particulate contamination or skidding between bearing rolling elements and races. The Stress Wave Power Spectral Density data are most useful in isolating the source of elevated SWE readings caused by periodic friction or shock events associated with localized surface damage to gears and bearings. These three types of stress wave data; SWE, SWAH, and SWPSD are presented in this analysis of the C-130 Engine Gearbox.

The first set of stress wave data (Figures 5, 6, and 7) show the effects of gearbox load on stress wave energy, amplitude distribution, and power spectral density. All data were taken from sensor location 1 at a low load condition of High Speed Ground Idle (HSGI); a medium torque level of 7000 in-lbs; and a high load level of 19,600 in-lbs. Figure 5 shows a smoothly increasing amount of frictional energy generation as a function of increasing load. This is typical of constant speed, variable torque (load) machinery.

Figure 6 shows the sensitivity of stress wave amplitude distribution to changes in operating torque. The medium load condition shows a statistically "normal" distribution with a relatively small standard deviation. The HSGI condition shows a "log-normal" statistical distribution, while the high load condition is only slightly biased towards a log normal distribution, but with a notably larger standard deviation than at 7000 in-lbs. The normal distribution with a relatively small

standard deviation is typically indicative of smooth running, properly aligned, well lubricated gears and bearings. The spuriously high rates, at two stress wave peak amplitudes in each of these distributions, are indicative of periodic friction or shock events at two relatively constant amplitudes during the 15 second data frame.

Figure 7 shows the frequencies of these periodic events at each of the three load conditions. The dissimilarity in the frequencies of the significant spectral lines ( $>10$  dB above background levels) indicates significant changes in dynamic contact stresses as a function of load. This is markedly different from what would be expected from localized gear or bearing surface damage in a constant speed machine, which would cause a fixed set of spectral lines of varying amplitude as a function of load.

The second set of stress wave data (Figures 8, 9, and 10) show the effects of gearbox oil temperature on stress wave energy, amplitude distribution, and power spectral density. All data were taken from sensor location 2 at a low load condition of High Speed Ground Idle. Figure 8 clearly demonstrates the ability of the SWE parameter to measure changes in friction levels associated with changes in lubricant temperature. The amplitude distribution histograms also show the effect of elevated temperature on lubrication efficiency. At the higher temperature, the mean amplitude of friction events is only slightly higher, but the occurrence of more high amplitude pulses increases the standard deviation and slightly biases the distribution towards a log normal shape. The spectral data show no significant change as a function of temperature, thus indicating that the changes in SWE and SWAH are due to randomly occurring, aperiodic events.

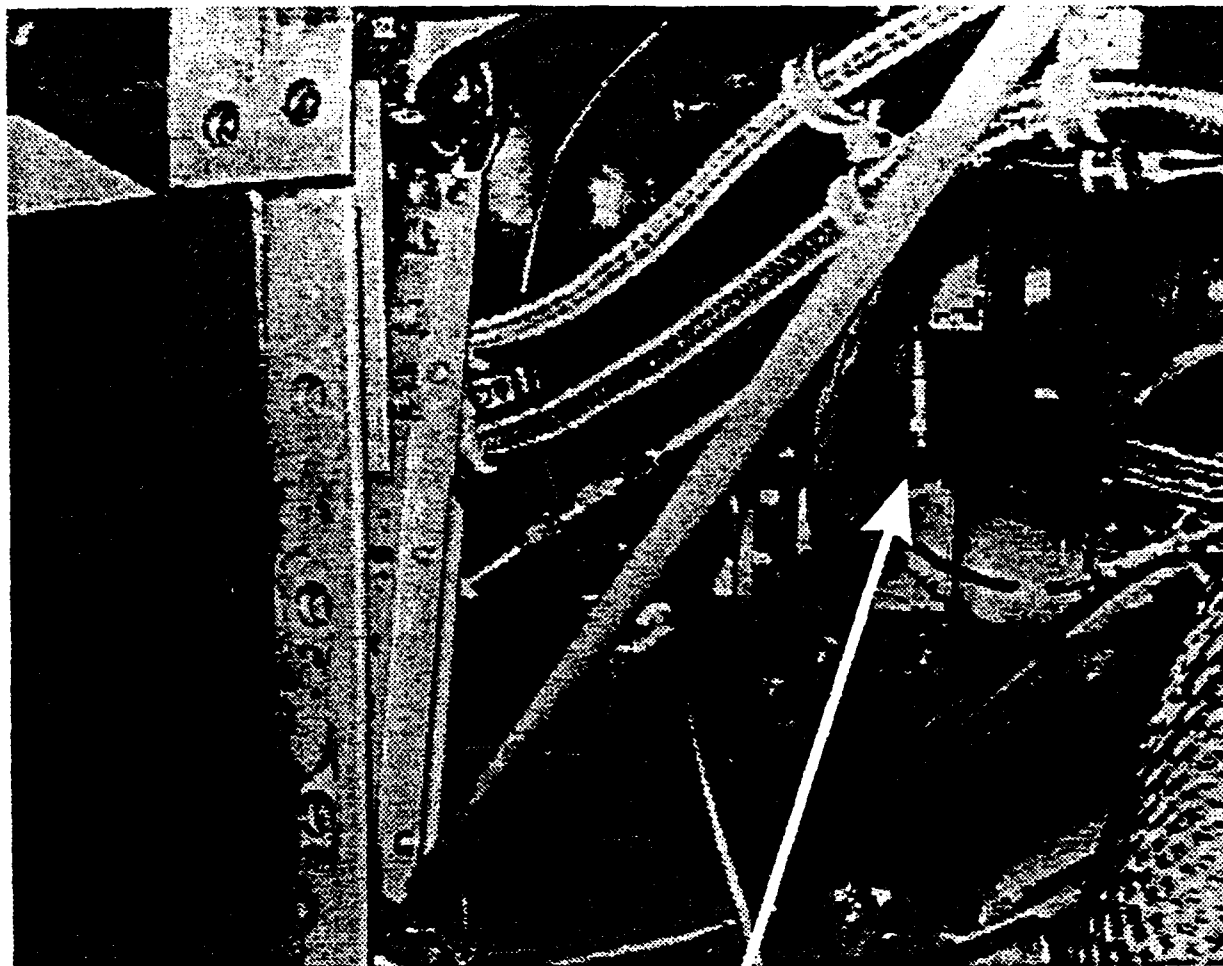
The third set of data illustrate what can be "seen" through stress wave analysis at each of the three gearbox sensor locations. Figure 11 shows the measured levels of SWE over a three minute period of steady state operation at a maximum power level of 19,600 in.-lbs. of torque. It is important to note the stability of the SWE readings under steady state operating conditions, since this is an important factor in the ability to set limits for early detection of discrepant parts and trending damage progression for planned corrective maintenance. The standard deviation of the SWE readings is within a range of 4% to 6% of the mean of all the SWE measurements at each sensor location. There is a slight upward trend to the readings obtained from sensor #2, which is due to the fact that the oil temperature was increasing from 73°C to 80°C while this series of measurements was being made. (In combination with the data in figures 8 through 10,

this also illustrates the ability of SWAN to detect changes in lubrication efficiency over a broad range of loads.)

The amplitude distribution histograms (Figure 12) for all three sensor locations have bell shaped normal distributions. It is interesting to note that although the #1 sensor distribution has the highest mean amplitude, the total stress wave energy is highest at sensor location #2. This illustrates the uniqueness of these two forms of SWAN. Part of the explanation for this lies in the spectral data of Figure 13 that show more spectral lines characteristic of periodic friction and shock events in the data from sensor #2. Another reason for the increased SWE at location #2 is the shape (amplitude versus time) of the stress wave pulses from this sensor location. There are two significant spectral lines, 67.8 Hz and 73.7 Hz, that are apparent in each of the three sensor spectra of Figure 13. The 67.8 Hz line is the 4/rev of the output shaft on which is mounted the 4 blade propeller. The 73.7 Hz line is the 1/rev of the main reduction bull gear and the planetary sun gear (which are on the same shaft).

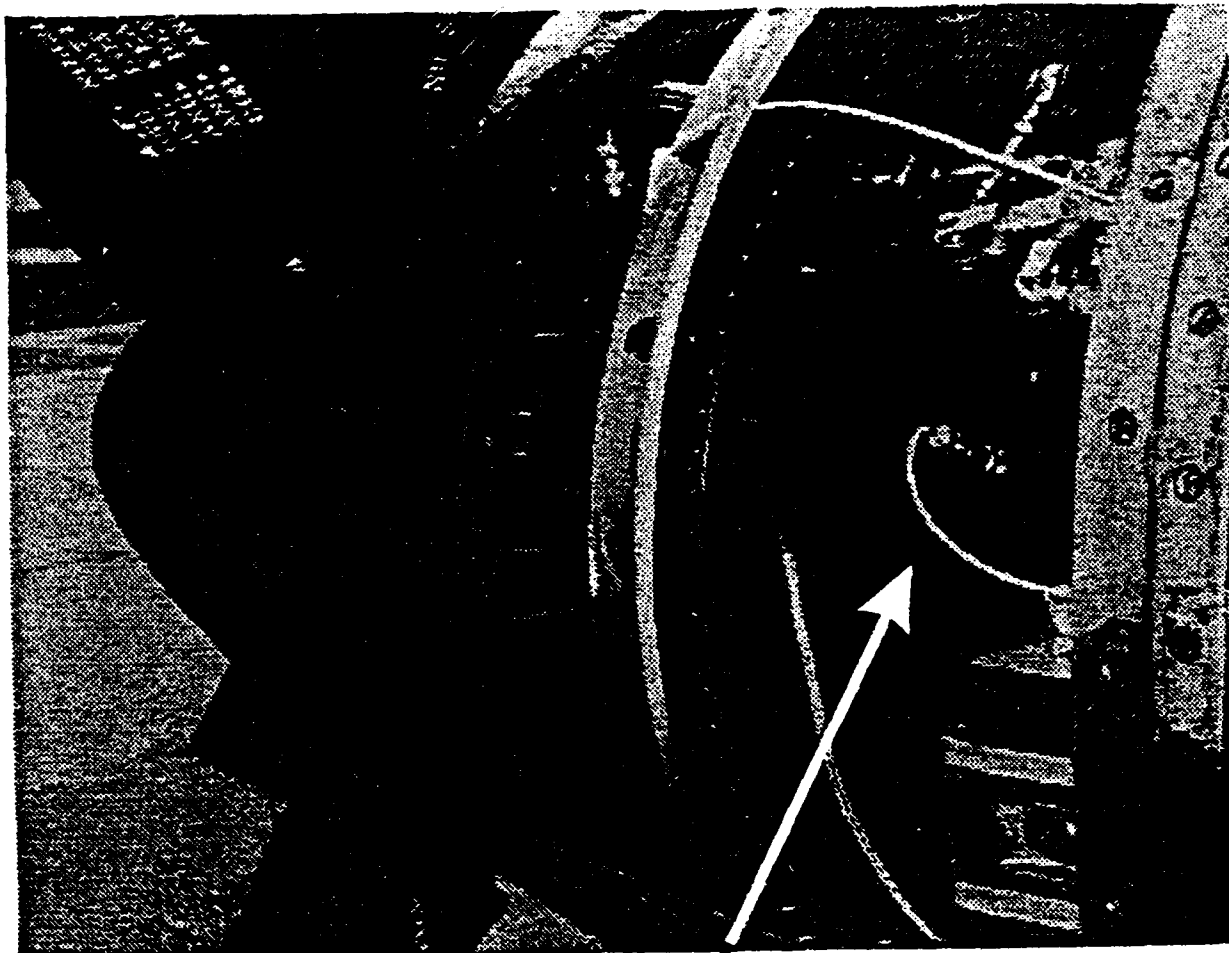
Although there are not sufficient data from this one SWAN "snapshot" of one gearbox to make a high level of confidence diagnosis of it's current condition or prognosis of future condition, some significant observations can be made:

1. All three basic stress wave analysis techniques (SWE, amplitude distribution, and power spectral density) are sufficiently sensitive to detect changes in frictional energy released by dynamic contact stresses as a function of operating torque level in the C-130 engine reduction gearbox.
2. There are significant changes to both the amplitude distribution and energy content of stress waves as a function of changes in lubrication properties associated with bulk oil temperature (indicating that local oil temperatures may vary more dramatically than bulk oil temperature).
3. SWE levels are very consistent under steady state operating conditions. This factor, in combination with the sensitivity to measure the friction associated with changes in load and lubricant temperature, indicate that alarm limits can be set which will maximize the probability of detecting discrepant parts early in the failure process while minimizing the probability of false alarms.



**Sensor No. 3**

Figure 2. Number 3 Sensor Located on Upper Rear bold of Torque Meter Sensor



**Sensor No. 2**

Figure 3. Number 2 Sensor Located on the Gear Box at the 9 O'clock Position

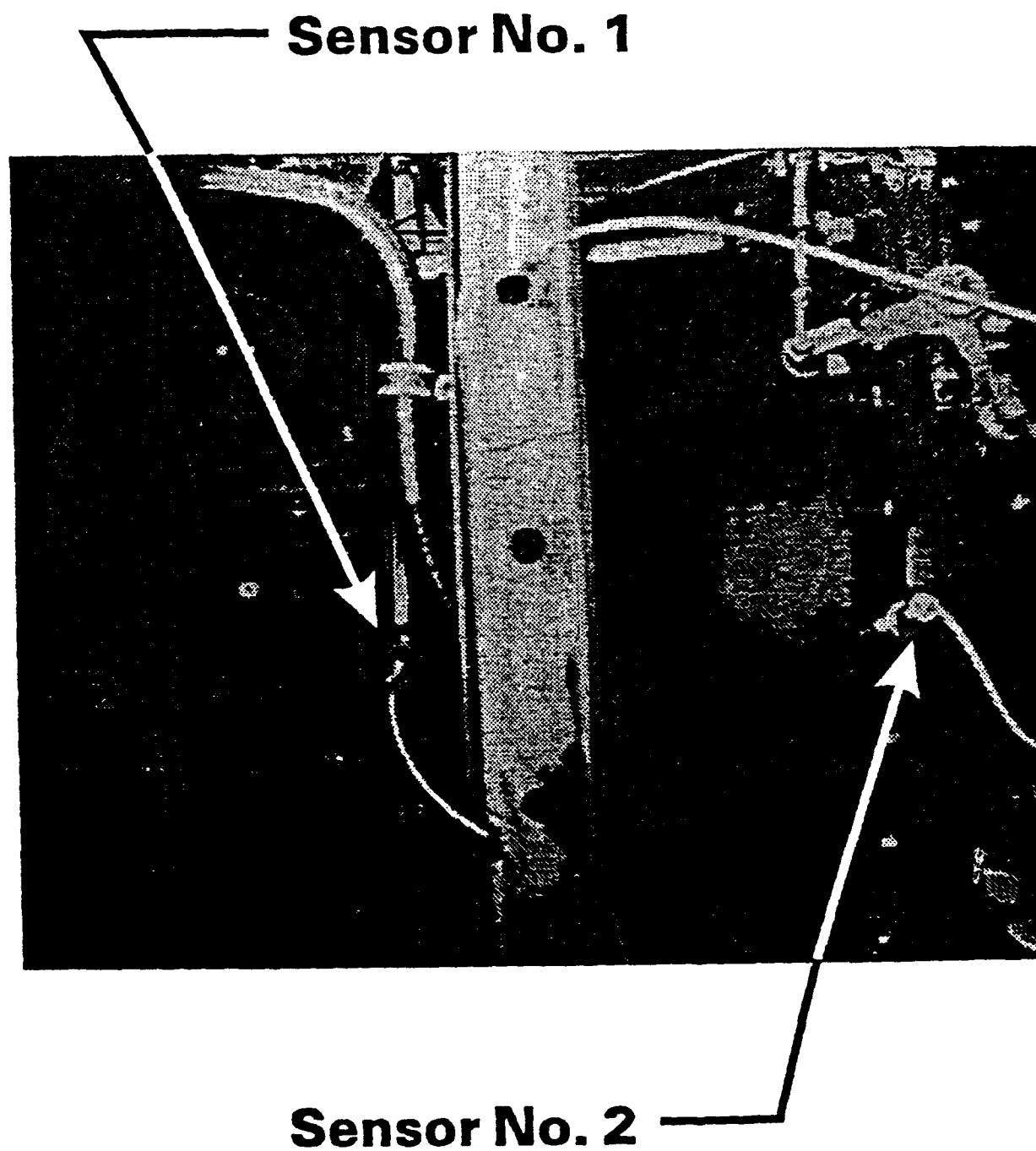


Figure 4. Sensor Number 1 Located on the Forward Bolt Circle of the Gearbox



## STRESS WAVE ENERGY READINGS

SENSOR 1, GAIN "B"

C-130 ENGINE #4, A/C 806

1/9/92

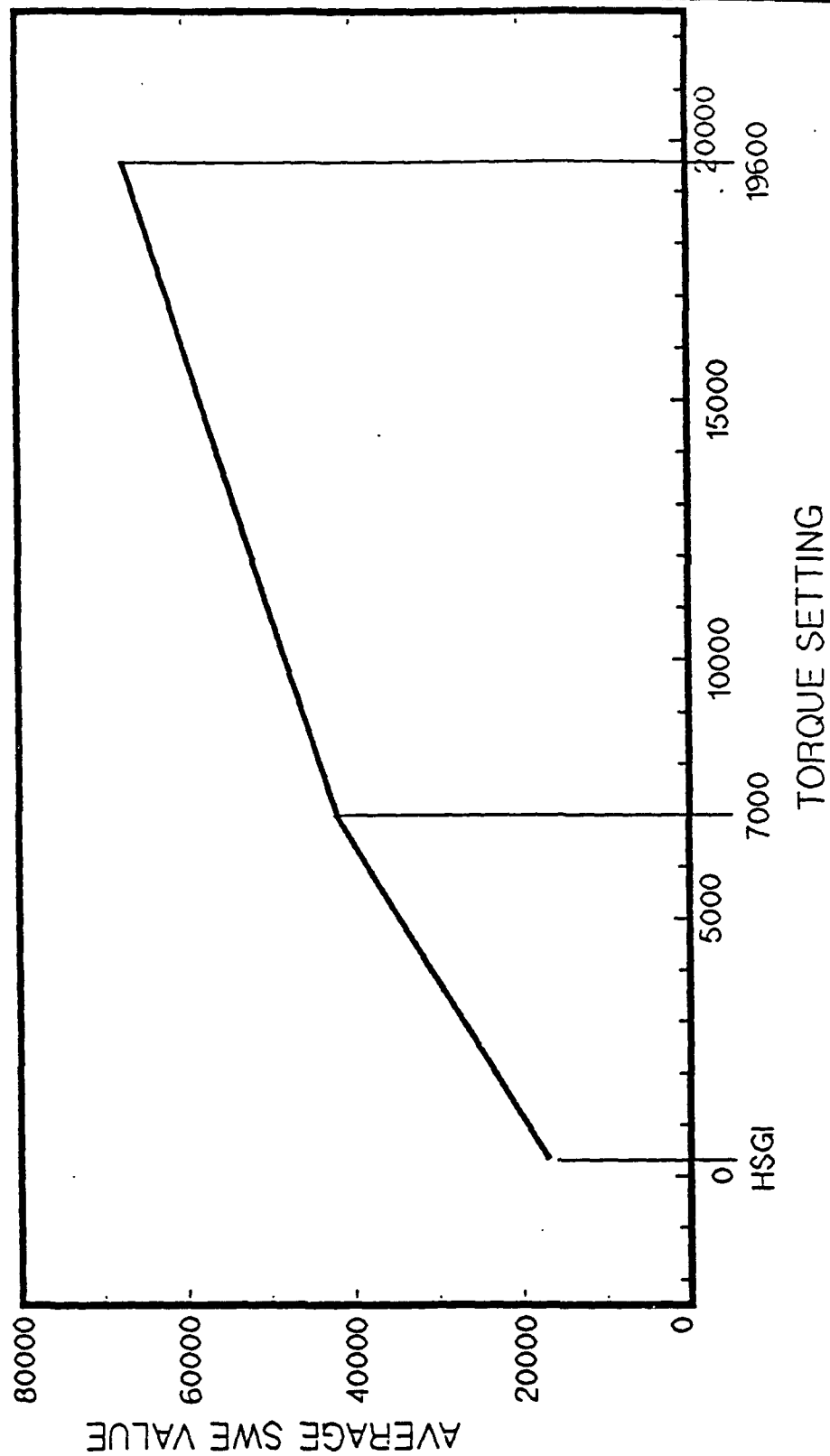
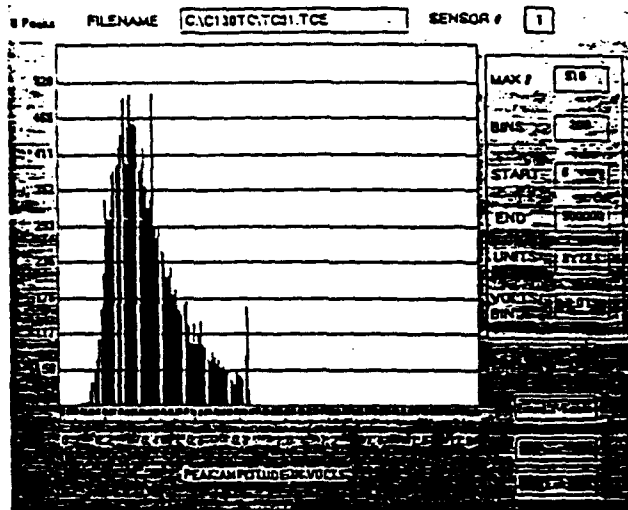
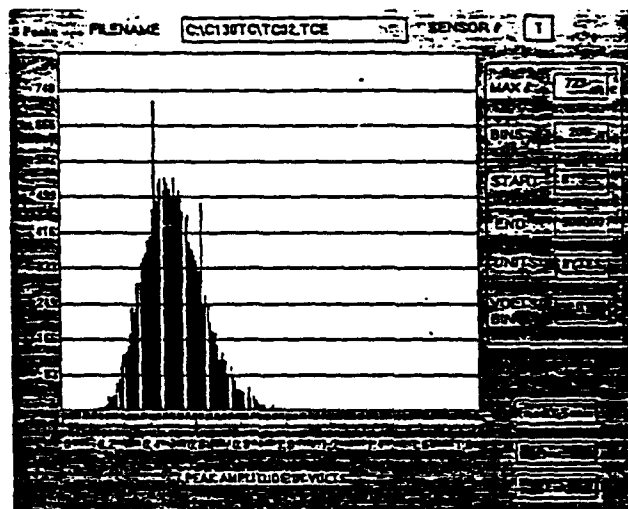


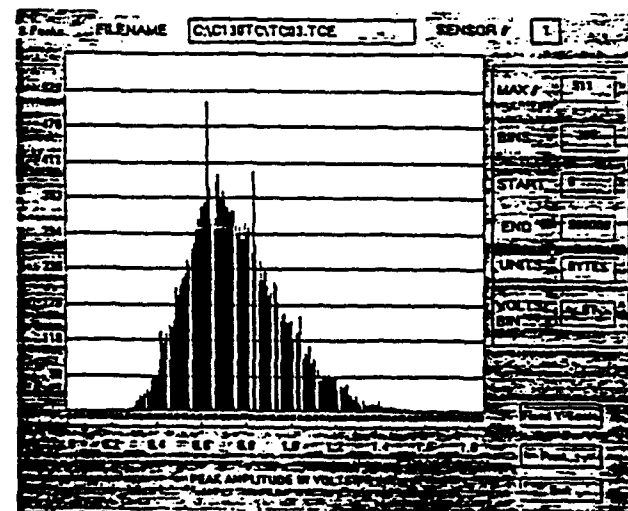
Figure 5. Stress Wave Energy Readings at Sensor 1 at High Speed Ground Idle, 7000 in-pounds of torque and 19,600 in-pounds of torque.



HSGI, XDCR #1

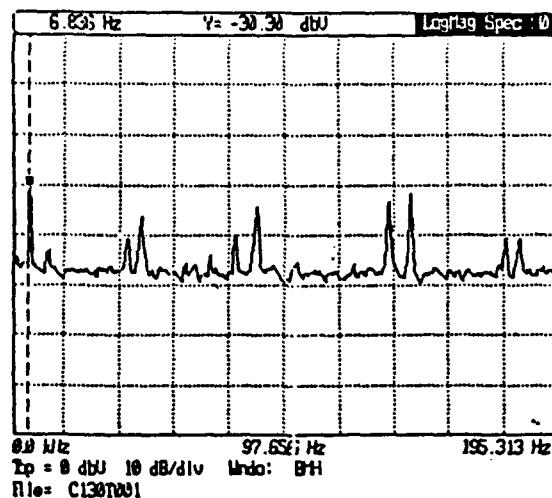


7000 IN-LBS., XDCR #1

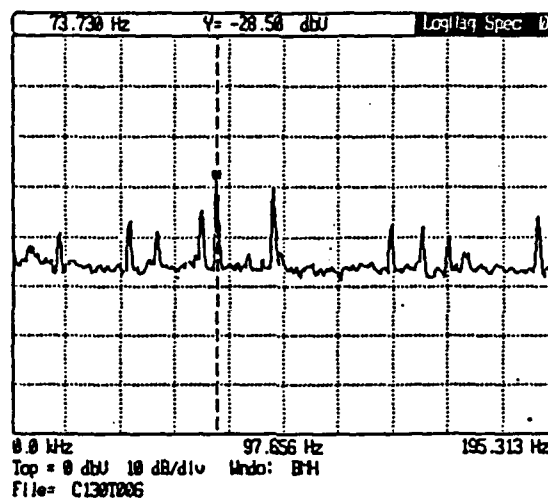


19,600 IN-LBS., XDCR #1

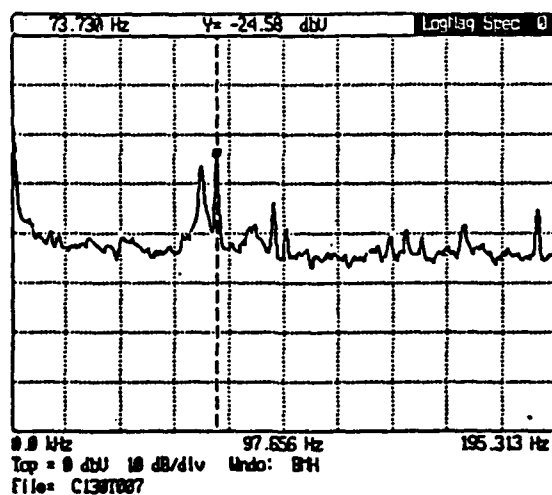
Figure 6. Stress Wave Amplitude Distribution as a Function of Load for Sensor 1



HSGI, XDCR #1



7000 in.-lb, XDCR #1



19,600 in.-lb XDCR #1

Figure 7. Stress Wave Power Spectral Density as a Function of Load for Sensor 1

## STRESS WAVE ENERGY READINGS

HSGI SENSOR LOCATION: 2

C-130 ENGINE #4, A/C 806

1/9/92

GAIN "C"

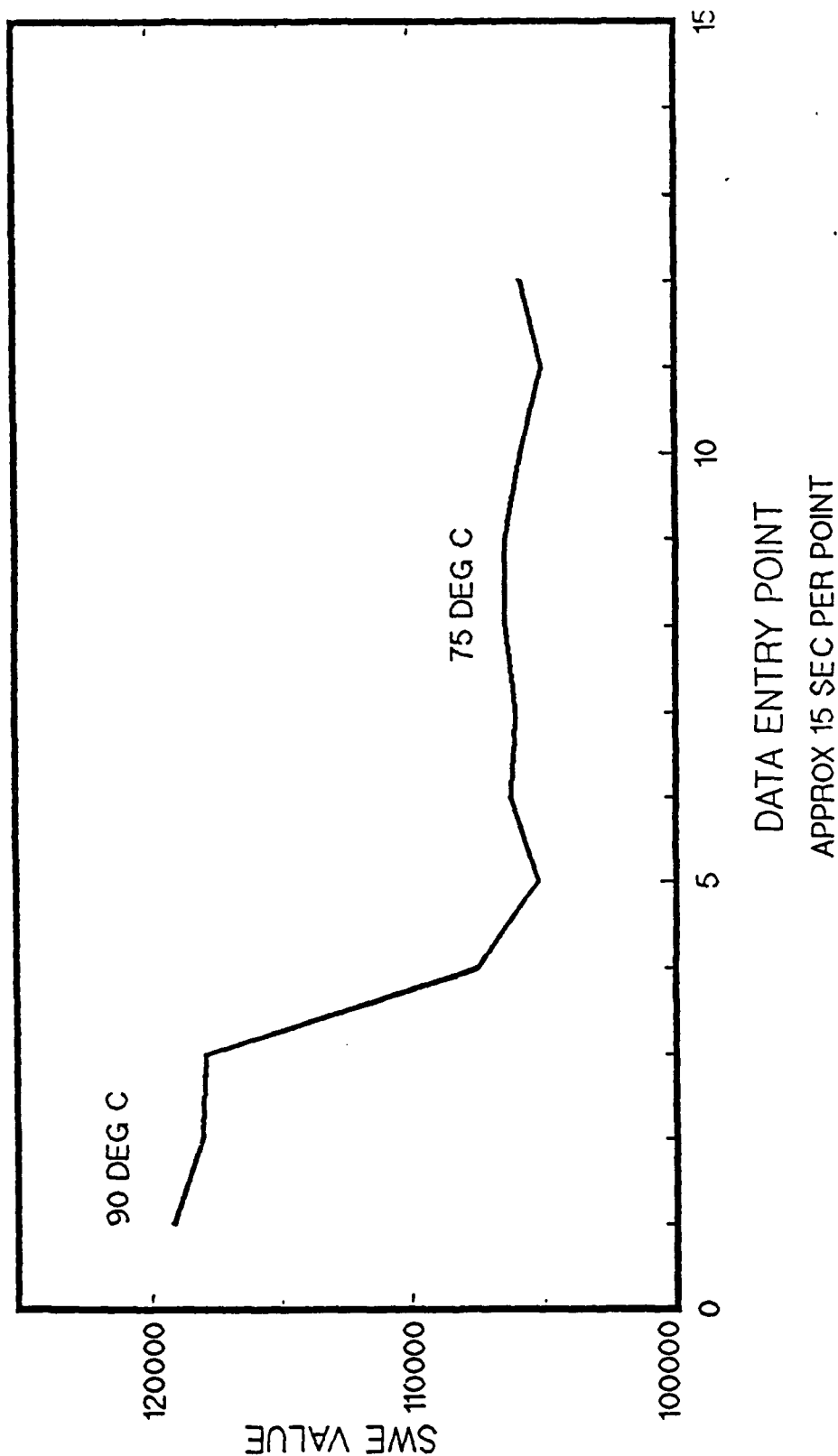


Figure 8. Stress Wave Energy Readings for Sensor 2 at Different Oil Temperatures

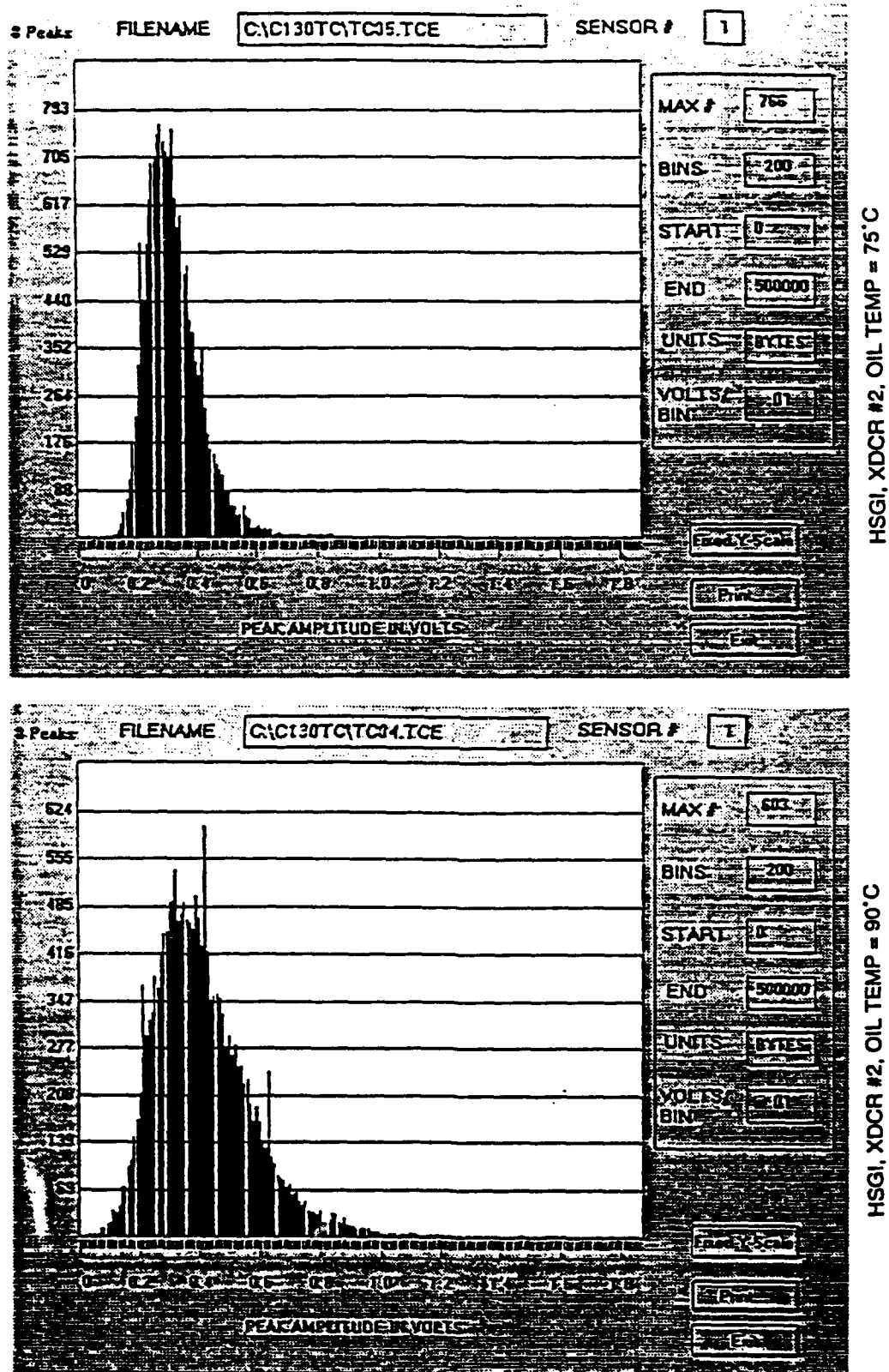
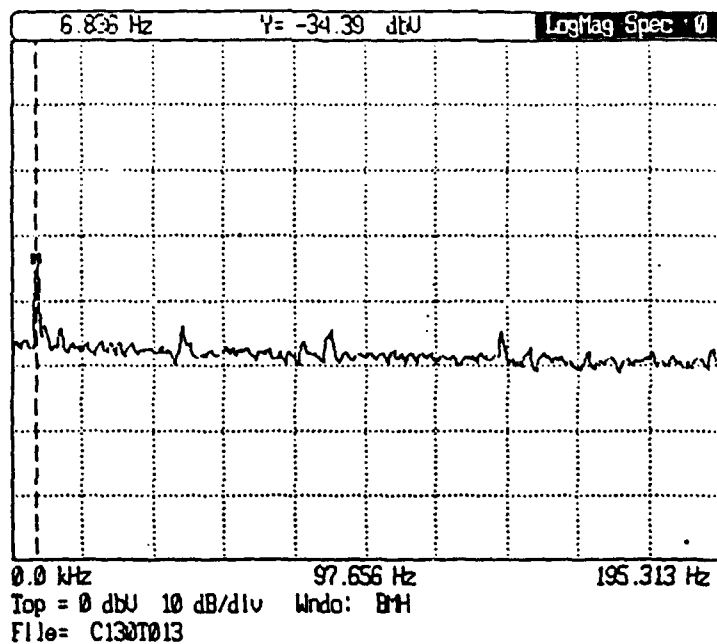
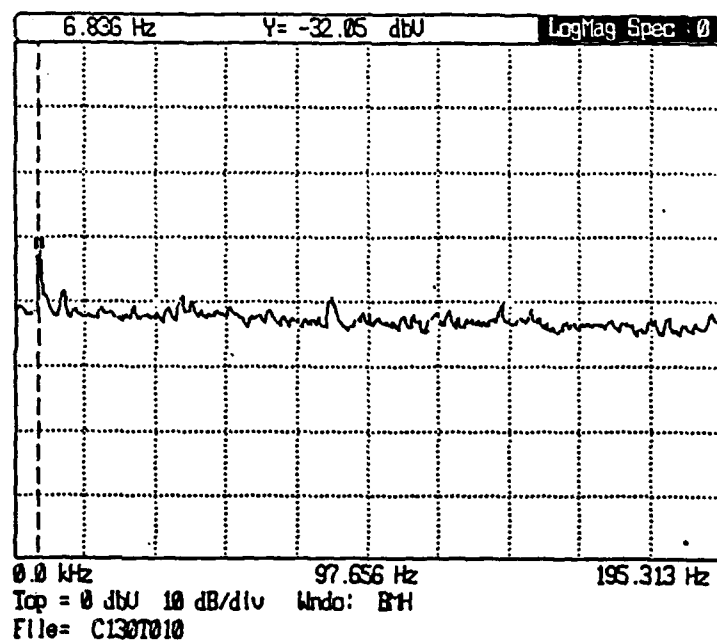


Figure 9. Stress Wave Amplitude Distribution as a Function of Oil Temperature



HSGI, XDCR #2, Oil Temperature = 75°



HSGI, XDCR #2, Oil Temperature = 90°

Figure 10. Stress Wave Power Spectral Density as a Function of Oil Temperature

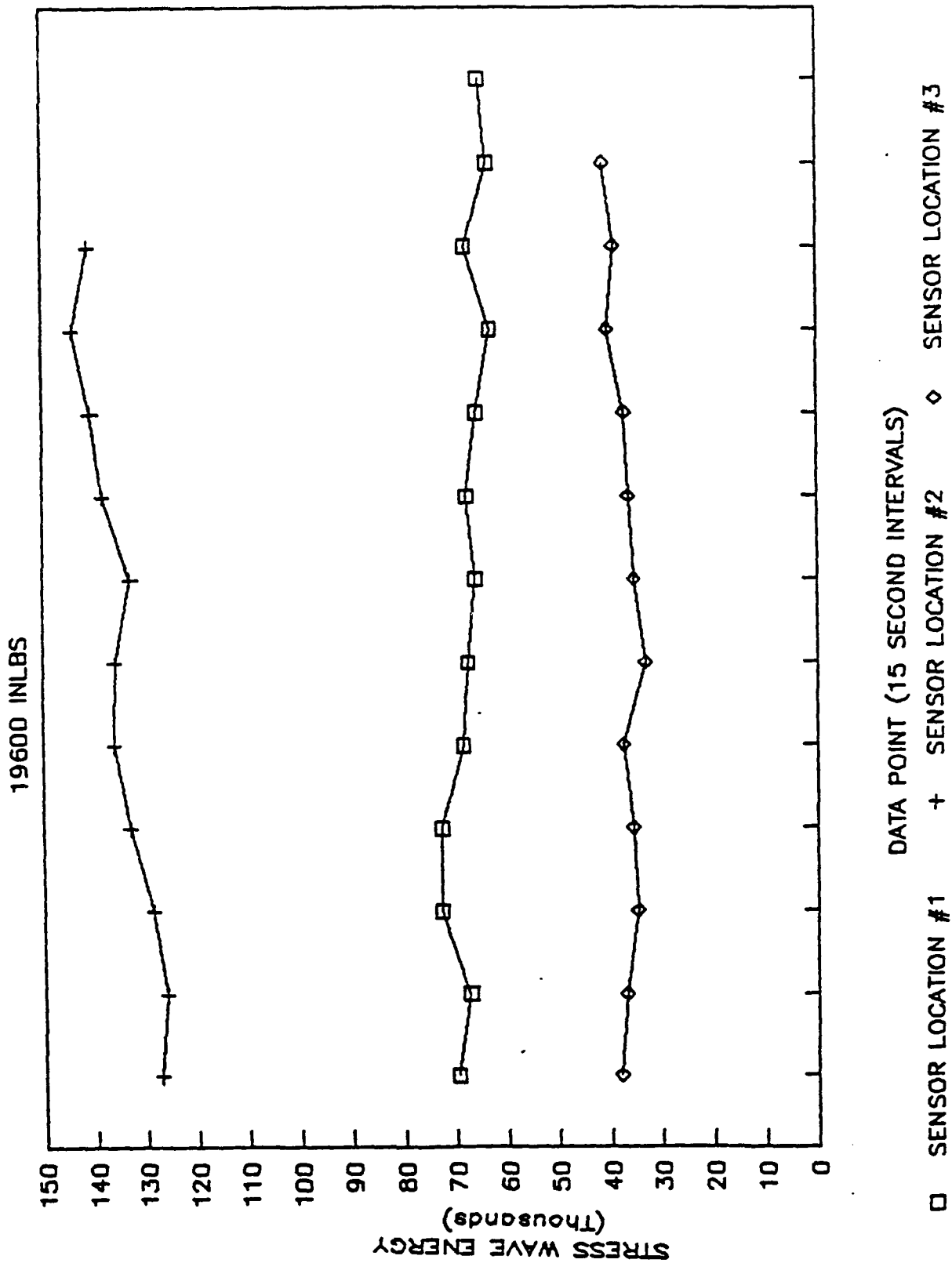
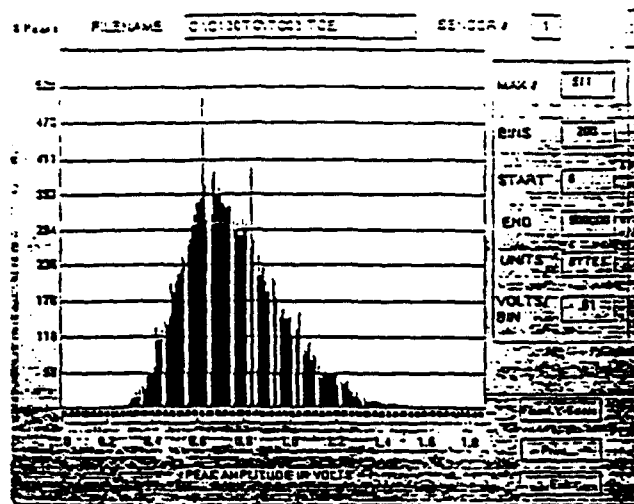
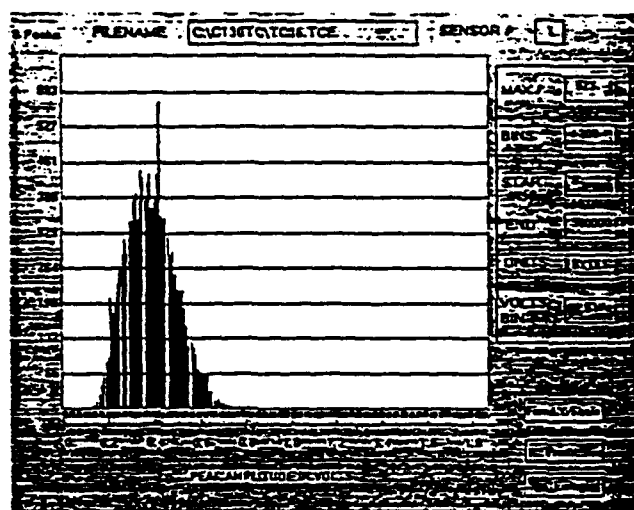


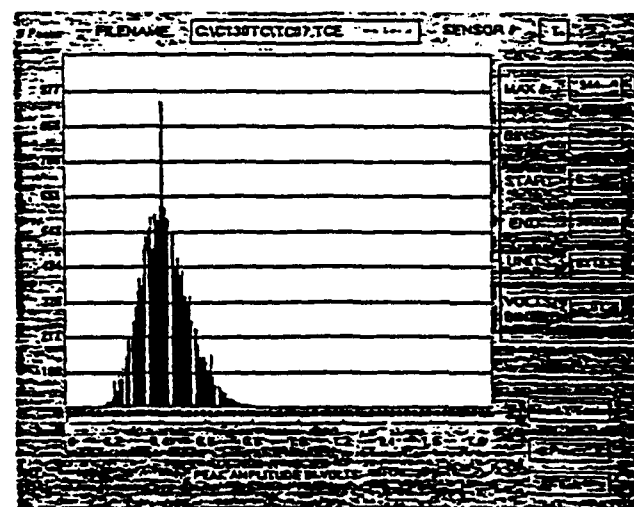
Figure 11. Stress Wave Energy at Three Sensor Locations at 19,600 in.-pounds of Torque Over Three Minutes Continuous Operation



19,600 IN-LBS, XDCR #1



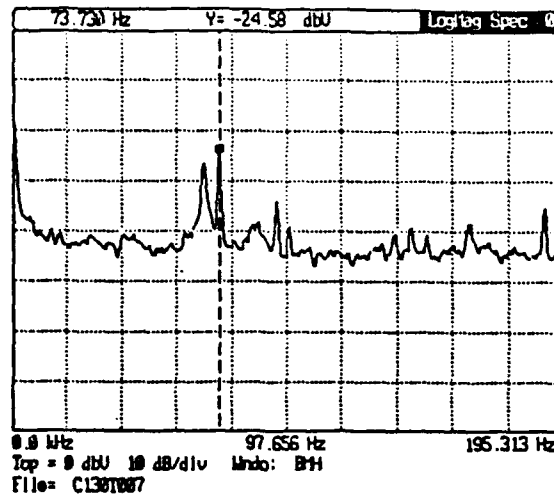
19,600 IN-LBS, XDCR #2



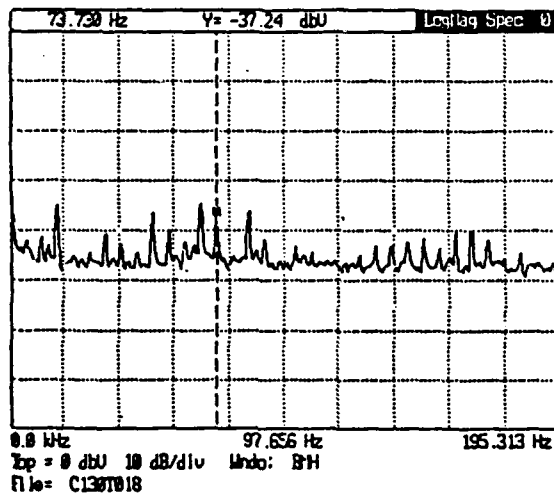
19,600 IN-LBS, XDCR #3

Figure 12. Stress Wave Amplitude Distribution at C-130 Gearbox Sensor Location

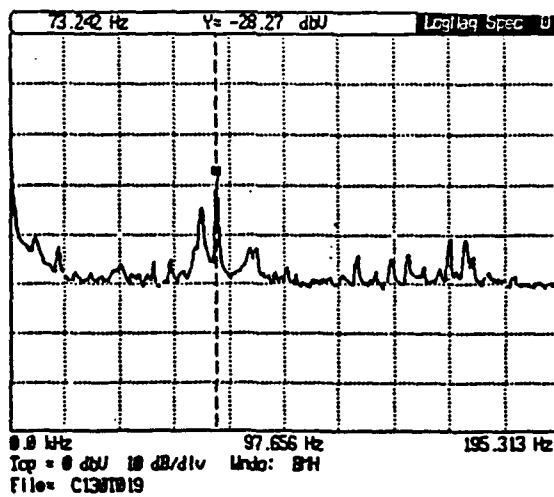




19,600 in.-lb XDCR #1



19,600 in.-lb XDCR #2



19,600 in.-lb XDCR #3

Figure 13. Stress Wave Power Spectral Density by C-130 Gearbox Sensor Location

# Chaos in a high speed gearbox

Ted Frison

Randle, Inc.  
P.O. Box 1010, Great Falls, Virginia 22066  
(703) 759-5257

## ABSTRACT

We use the methods reviewed by Professor Abarbanel<sup>1</sup> to show that accelerometer data from a gearbox are chaotic. These data have broad-band Fourier components and a natural question arises as to whether these data are chaotic. The requirements for chaos are that:

The Fourier spectrum is broad-band,  
There is a non-integer fractal dimension,  
There is at least one positive Lyapunov exponent.

These analyses are a prelude to fault prediction and analysis. In this paper we present the results of our studies on a healthy high-speed gearbox. That is, the gearbox was known to contain no faults.

## 2. INTRODUCTION

Predictive fault analysis of rotating machinery has proven to be a difficult problem. Before taking on the problem of fault prediction and analysis, however, there is a natural curiosity about the nature of these systems and their signals. The insights derived from the analysis of baseline data provide guidance for the future development of maintenance tools.

The methods are reviewed in detail in [1]. The general idea is to reconstruct the signal's underlying attractor using phase space reconstruction<sup>2</sup>. Once the attractor has been reconstructed, its invariant geometric and information propagating properties are used to classify and analyze the behavior of the system.

The configuration of the gearbox is shown in figure 1. The input spur pinion driven by a high-speed turbine. For this test, the developmental gearbox was statically mounted on a test bench. The signal trace of an accelerometer mounted on the case is shown in figure 2, along with its FFT. The sensor, an accelerometer, was sampled at 320 khz and low-pass filtered at 80 khz. The data were stored on a modified video recorder. These data are especially interesting because they were collected under circumstances similar to the shop conditions that will exist for the final application. Thus, they contain all the artifacts that one would expect from real data.

## 3. CHAOTIC CHARACTERISTICS OF A HIGH-SPEED GEARBOX

The main menu for the chaotic signal processing ("CSP") system used in these studies is shown in figure 3. The modules that perform the calculations are platform independent and run on Sun workstations, Apple Quadras, Cray supercomputers, and even an occasional IBM PC. The status windows for four processes running in the background are in the upper left corner.

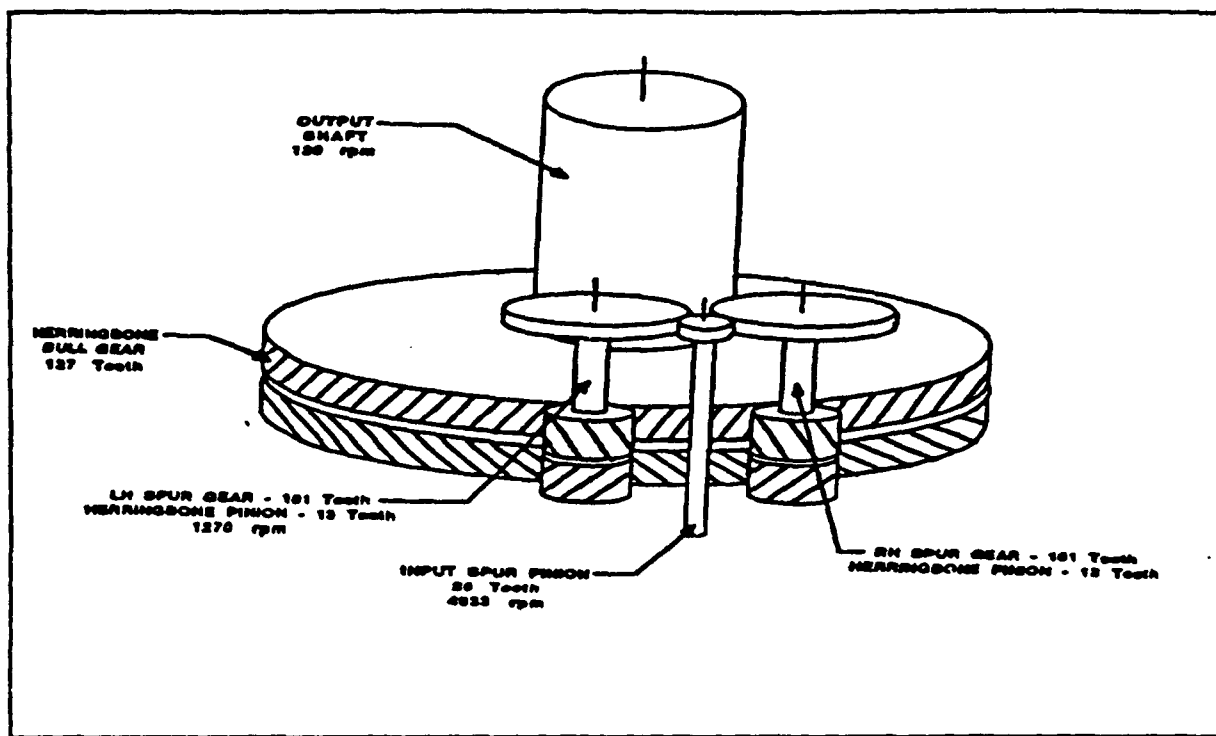


Figure 1. Schematic of gearbox.

### 3.1. Find the time delay for phase space reconstruction.

Average mutual information,  $I(T)$ , is a prescription for selecting an appropriate time delay interval ( $T$ ) for reconstruction of the attractor<sup>3</sup> and is the amount of knowledge (expressed as bits) that one can derive about two datums separated by the time delay,  $T$ . It is defined in two dimensions as the joint probabilities of the two datums:

$$I_{AB}(T) = \sum P_{A,B}(a,b) \log_2 \left[ \frac{P_{A,B}(a,b)}{P_A(a)P_B(b)} \right]$$

The determination of the time lag,  $T$ , is important because an optimum selection of  $T$  gives best separation of neighboring trajectories within the minimum embedding space. This is important because calculation of the Lyapunov exponents relies on solving a matrix that is comprised of descriptions of how close trajectories diverge. If the trajectories are not separated, then the matrix will be ill conditioned and may not be solvable.

In the reconstructed attractor, if the time delay is too small, there is little new information contained in each subsequent datum. If  $T$  is too large,  $x(n)$  and  $x(n+T)$  will appear to be random with respect to each other for a chaotic system. The first local minimum of  $I(T)$  determines an optimum value of  $T$ . Past this point in a chaotic system, ambiguities in the correlation between  $x(n)$  and  $x(n+T)$  arise -- they start to appear random with respect to each other. The state space portrait begins to lose resolution and the fractal nature of the attractor starts to become blurred.

The average mutual information for the baseline (known good) gearbox data is shown in figure 4. The first

local minima, at sample 6 ( $1.875 \times 10^{-5}$  sec), is a shallow minima. The higher peaks correspond to events that are occurring on an average of 149.7 samples. These events are the engagements of the input spur pinion and the intermediate spur gears. The rate of engagement is 2,137.66 meshings per second. These artifacts are evident across the entire data collection, as are the lower mesh rates from the teeth on the other gears.

### 3.2. Find the minimum embedding dimension.

The full behavior of a system described by  $n$  independent variables can be observed in an  $n$  dimensional "state" space. However, the attractor of the system may be contained in a subset of the state space with dimension  $d_A$ , and may be described in a state space,  $d$ , that is much smaller than  $n$ . This minimum embedding dimension  $d_E$  is, at most, the first integer greater than  $2d_A$  (the correlation dimension); it may be less.

Determination of the minimum embedding dimension,  $d_E$ , is of practical interest because the computation burden rises dramatically as dimension increases. Further, noise fills all dimensions, so computations carried out in a higher-than-necessary dimension will be corrupted by noise. If  $d_E$  is too small, the trajectory may cross itself. Neighbors near the crossing may be indistinguishable in lower dimensions.

*An easy method of determining minimum embedding dimension* is used in our processor<sup>4</sup>. As dimension is increased, attractors "unfold." Points on trajectories that appear close in dimension  $d$  may move to a distant region of the attractor in dimension  $d+1$ . These are "false" neighbors in  $d$  and the method measures the percentage of false neighbors as  $d$  increases. Trajectories that are close in  $d$  are tallied, and the number of these trajectories that become widely separated in  $d+1$  are calculated. Over the data set one tallies

$$\left[ \frac{R_{d+1}^2(n, r) - R_d^2(n, r)}{R_d^2(n, r)} \right] = \frac{|x(n+Td) - x^{(r)}(n+Td)|}{R_d(n, r)} > R_{tol}$$

where  $R_d$  is the Euclidian distance between a point and its nearest neighbor and  $R_{tol}$  is the criteria for declaring whether the neighbors that are close in  $d$  are distant in  $d+1$ .

A second criteria is necessary because the nearest neighbor is not necessarily "close." If the nearest neighbor to a point is false but not close, then the Euclidian distance in going to  $d+1$  will be  $\approx 2R_d$ . So, the second criteria is

$$\frac{R_{d+1}(n)}{R_d} > R_{tol}$$

where

$$R_d^2 = \frac{1}{N} \sum_{n=1}^N [x(n) - \bar{x}]^2$$

A nearest neighbor is false if either test fails.

Figure 5 shows the global false nearest neighbor calculations for these data. The data are clearly higher dimension, which is not surprising considering that the accelerometer is capturing multipath signals from six gears with 381 teeth. The teeth on the input spur pinion are engaging at a rate of 2,138 engagements per second. The bull gear mesh rate is only 275 engagements per second on each of the two pinions, but it takes almost a half a second for one complete revolution. It would appear that the global embedding dimension for this signal is at least 12, but could be higher.

### 3.3. Compute the correlation dimension of the attractor.

The fractal dimension of the attractor<sup>5</sup>,  $d_a$ , provides information on how much of the state space is filled by the system. One interpretation of  $d_a$  is that it measures how many degrees of freedom are significant. Another interpretation of the fractal dimension is that it provides a measure of how an object's bulk scales with its size: bulk = size <sup>$d_a$</sup> . Bulk that can be associated with volume and size is then interpreted as Euclidean distance. A plane, for example, has dimension two because the area =  $d^2$ . The fractal dimension of the attractor,  $d_a$ , may be estimated using Ruelle's approach by calculating the number of spheres or boxes,  $N(r)$ , of size  $r$  that capture all points as  $r$  approaches zero:

$$d_a = \frac{\log(N(r))}{\log(1/r)} \quad \text{as } r \rightarrow 0$$

Grassberger and Procaccia<sup>6</sup> defined a relatively easy approximation, the correlation dimension, that may be done on a PC for high SNR signals. One major issue is the sensitivity of these calculations to signal SNR. The amount of data required to do the calculations may dramatically increase as SNR decreases.

Using 120,000 samples (a little less than 1/2 second) the attractor is shown to be well populated by the histogram of  $N(r)$  -- the top curves in figure 6. The bottom curves in figure 6 are the estimates of  $d_a$  for all locations along the top curves. The pointer shows where the final estimates are selected, and presented in figure 7. The final estimate of  $d_a = 5.9$  is consistent with the estimate of  $d_e \approx 12$ .

### 3.5. Compute the Lyapunov exponents.

The Lyapunov exponents describe the rate at which close points in the state space diverge. There is one exponent for each dimension. If the Lyapunov exponents are all zero or negative, the trajectories do not diverge and the system is stable. If one or more Lyapunov exponents is positive, the system is chaotic<sup>7</sup>. The Lyapunov exponents are invariant with respect to initial conditions. Therefore, they are another way of classifying a chaotic system. The more exponents one can correctly find, the more accurate predictions of system behavior will be<sup>8</sup>.

All the Lyapunov exponents may be calculated from the Jacobian of the map by the QR decomposition technique discussed by "EKRC."<sup>9</sup>

As defined above, Lyapunov exponents are a global invariant because they describe the effect of infinitesimal perturbations over infinite time. Recent approaches examine how perturbations grow in finite time<sup>10</sup> and how these local Lyapunov exponents relate to predictability<sup>11</sup>. The local Lyapunov exponents measure the divergence of trajectories in different regions of state space.

Our calculations of the global Lyapunov exponents in twelve dimensions show that there are several positive exponents. The numeric results of these calculations are questionable due to the amount of data that would be required in such high dimension and other algorithmic issues. But, the sign of each exponent is believable and the presence of at least one positive exponent is sufficient for our purposes.

## 4. CONCLUSION

These data meet the rigorous definition of chaos: broad-band spectra, a non-integer correlation dimension  $d_a < d_e$  and at least one positive Lyapunov exponent. Our curiosity about the global nature of this physical system is satisfied. The next challenge is to translate this knowledge into methods for fault prediction.

## 5. ACKNOWLEDGMENTS

This work was performed as part of ongoing joint research between Randle, Inc., the Institute for Nonlinear Science, University of California (San Diego), and the gearbox developer. The author thanks Henry Abarbanel for his advice and encouragement.

## 6. REFERENCES

1. Henry D. I. Abarbanel, Reggie Brown, J.J. Sidorowich, and Lev. Sh. Tsimring, "The analysis of observed chaotic data in physical systems," accepted, *Reviews of Modern Physics*.
2. Eckmann, J.-P. and D. Ruelle, "Ergodic theory of chaotic and strange attractors", *Rev. Mod. Phys.* **57** 3, pp. 617-656, 1985.
3. A. M. Fraser and H. L. Swinney. "Independent coordinates for strange attractors from mutual information," *Phys. Rev. A*, **33**:1134-1140, Feb. 1986.
4. Kennel, Matthew B., R. Brown, and H. D. I. Abarbanel, "Determining embedding dimension for phase-space reconstruction using a geometrical construction," *Phy. Rev. A* **45** pp. 3403-3411, 15 March 1992.
5. Hausdorff, "Dimension and ausseres Mass," *Math. Annalen*, vol 79, pp. 157-179, 1918.
6. P. Grassberger and I. Procaccia, "Measuring the Strangeness of Strange Attractors", *Physica* **9D**, pp. 189-208, 1983.
7. J.-P. Eckmann and D. Ruelle, *Rev. Mod. Phys.* **57**, 617 (1985).
8. Abarbanel, Henry D. I., "Determining the Lyapunov Spectrum of a Dynamical System from Observed Data", Presented at the SIAM Conference on Dynamical Systems, Orlando, Florida, 8 May 1990.
9. Eckmann, J.P., S.O. Kamphorst, D. Ruelle, and S. Ciliberto, *Phys. Rev.* **A34**, 4971 (1986).
10. Abarbanel, H. D. I., R. Brown, and Matthew Kennel, "Variation of Lyapunov Exponents on a Strange Attractor", *Journal of Nonlinear Science*, **1**, pp. 175-199, 1991.
11. Abarbanel, H. D. I., R. Brown, and Matthew Kennel, "Local Lyapunov Exponents Computed from Observed Data", *Journal of Nonlinear Science*, Vol 2, pp. 343-365, Sept. 1992.

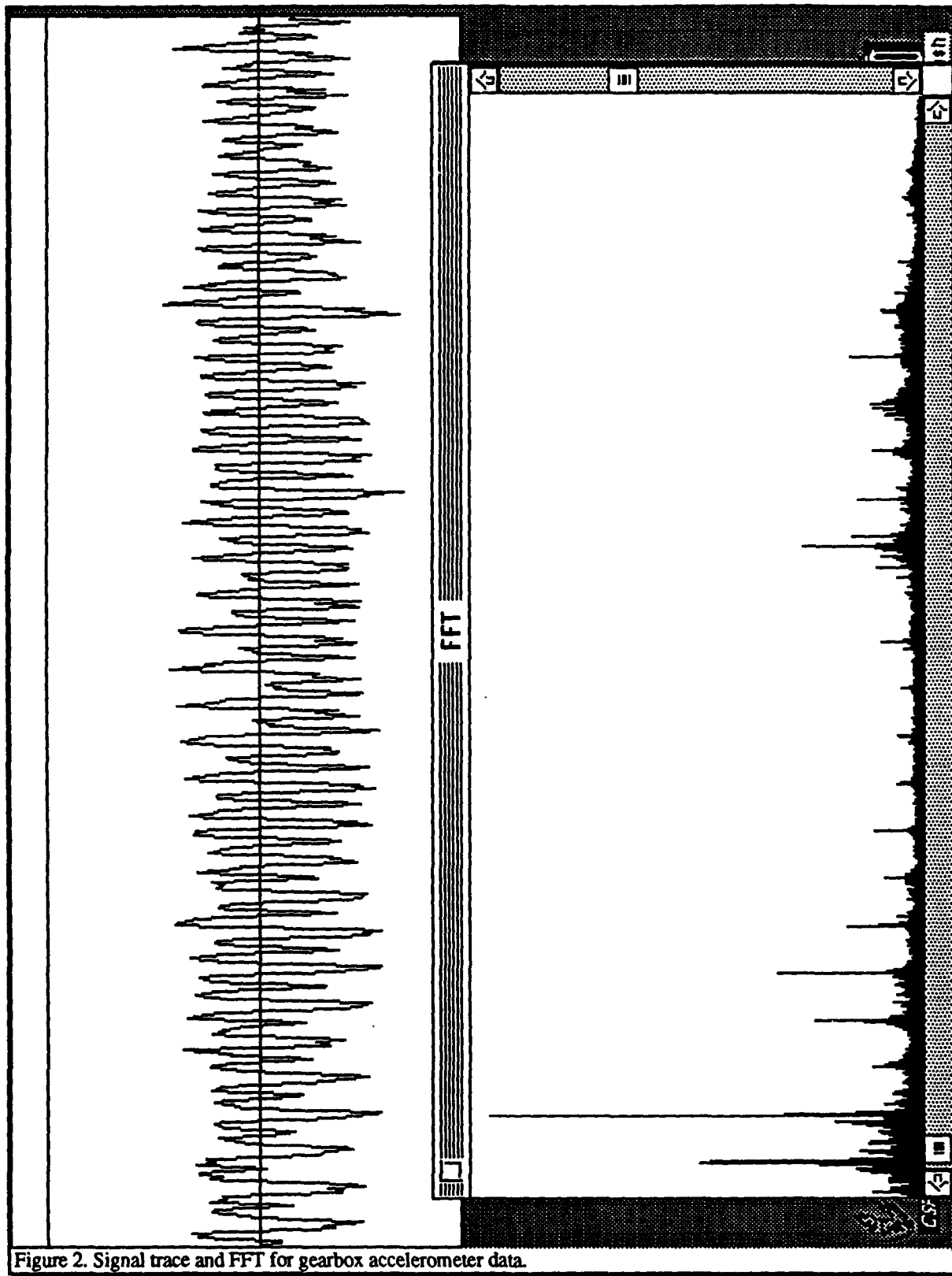


Figure 2. Signal trace and FFT for gearbox accelerometer data.

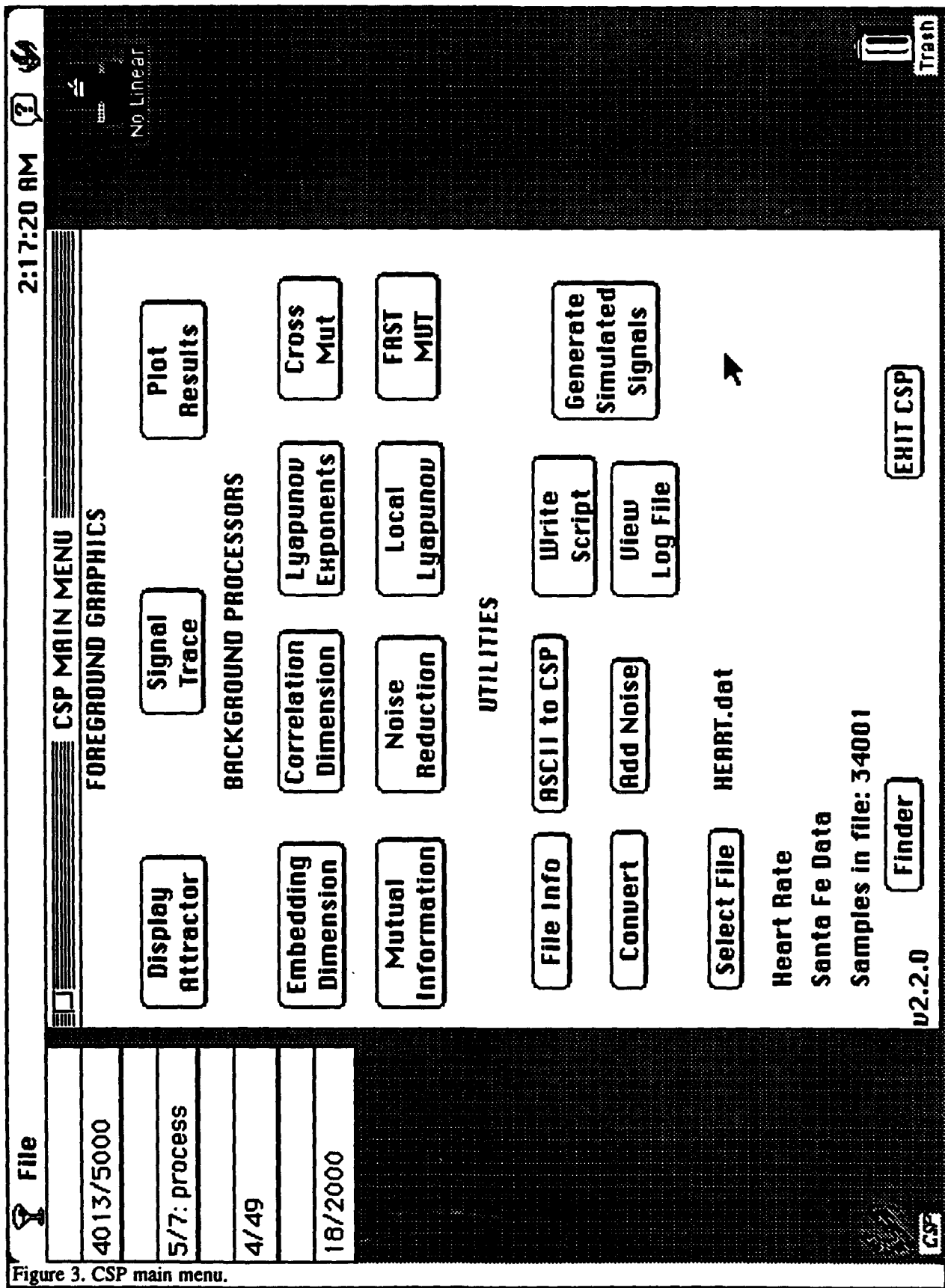
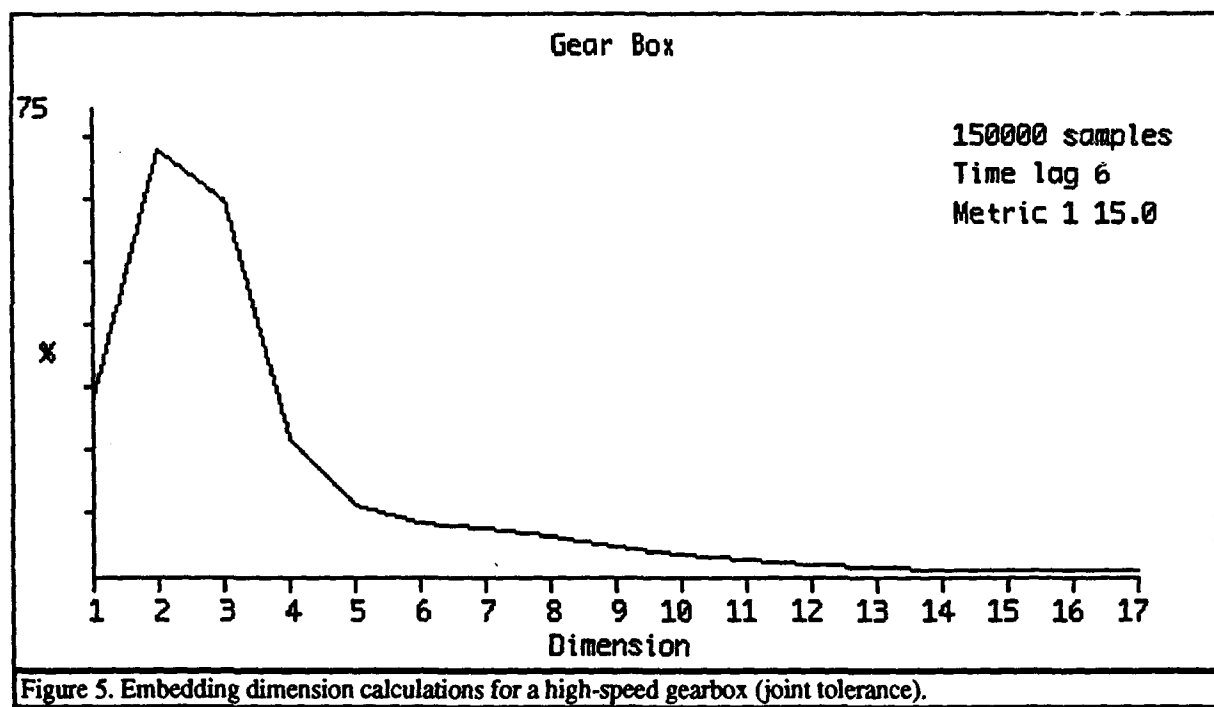
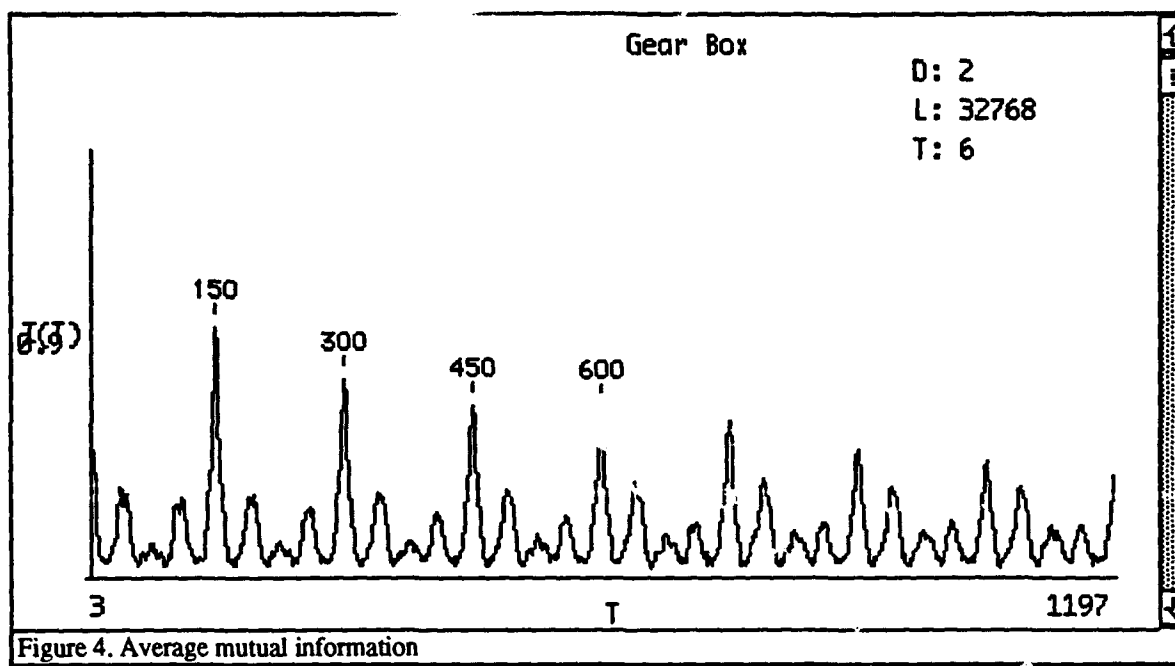


Figure 3. CSP main menu.





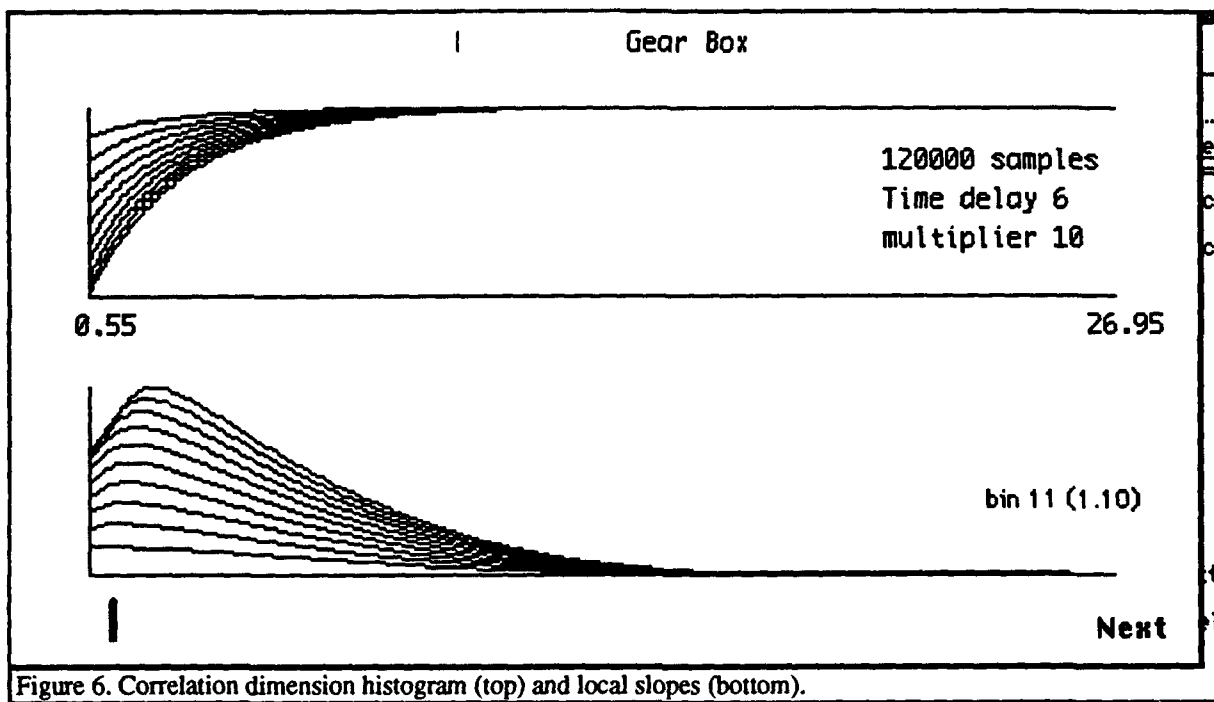


Figure 6. Correlation dimension histogram (top) and local slopes (bottom).

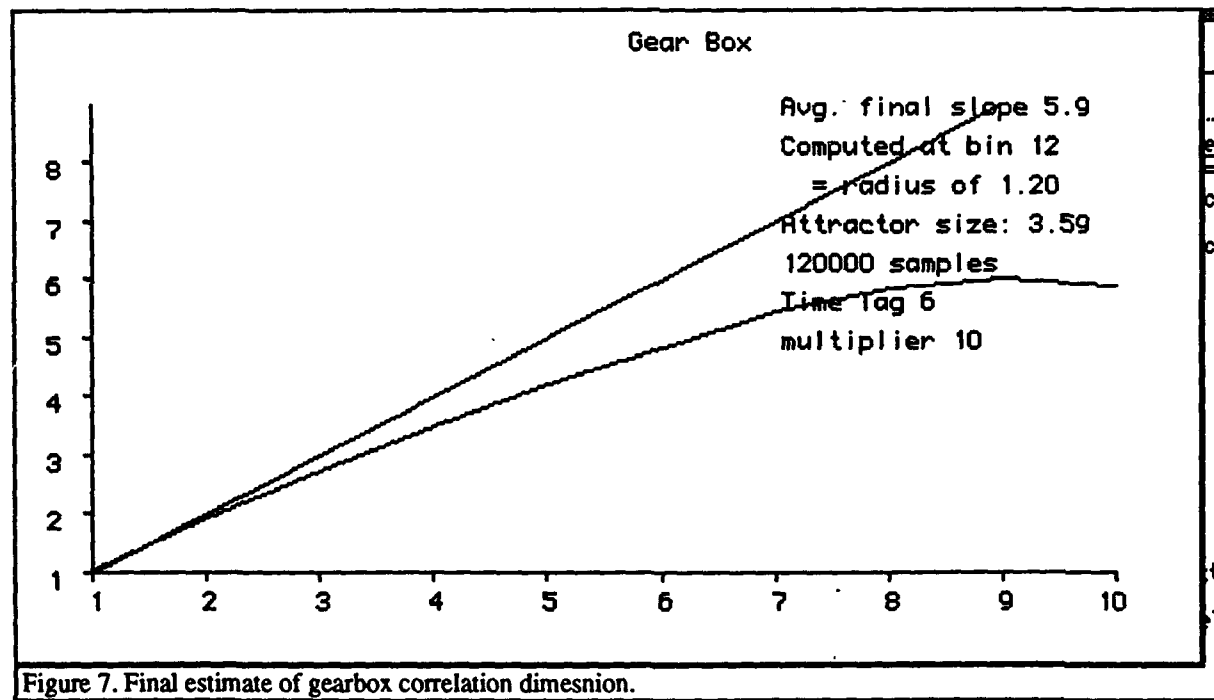


Figure 7. Final estimate of gearbox correlation dimesnion.

# CHAOS IN A HIGH SPEED GEARBOX

Ted W. Frison  
Randle, Inc.  
P.O. Box 587  
Great Falls, VA 22066  
(703) 759-5257

## Application:

Health and maintenance monitoring (HMM)

Improve safety on a single point of failure device

Affects safety, effectiveness, affordability

Reduction in maintenance costs

Reduction in replacement costs

## Issues:

Global vice local anomalies

"Economically useful" advance warning

Incipient fault warning (a binary alarm) is  
different than specific diagnostics

## Stressing issues:

High sample rate

Large number of samples

Multipath effects

Computation efficiency

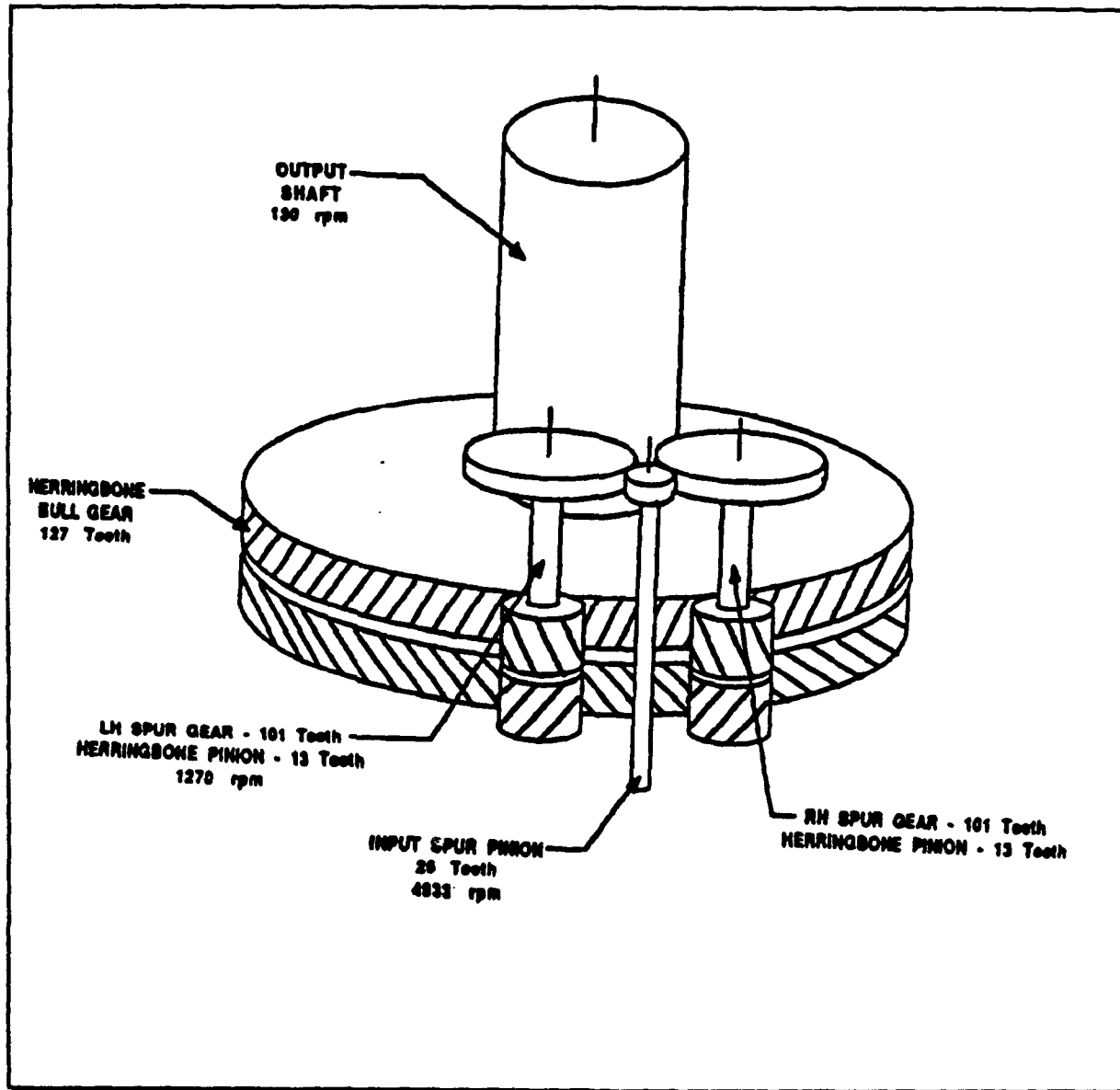
## Related research:

Acoustic emissions

Biological HMM

Other types of rotating machinery

## A HIGH SPEED GEARBOX



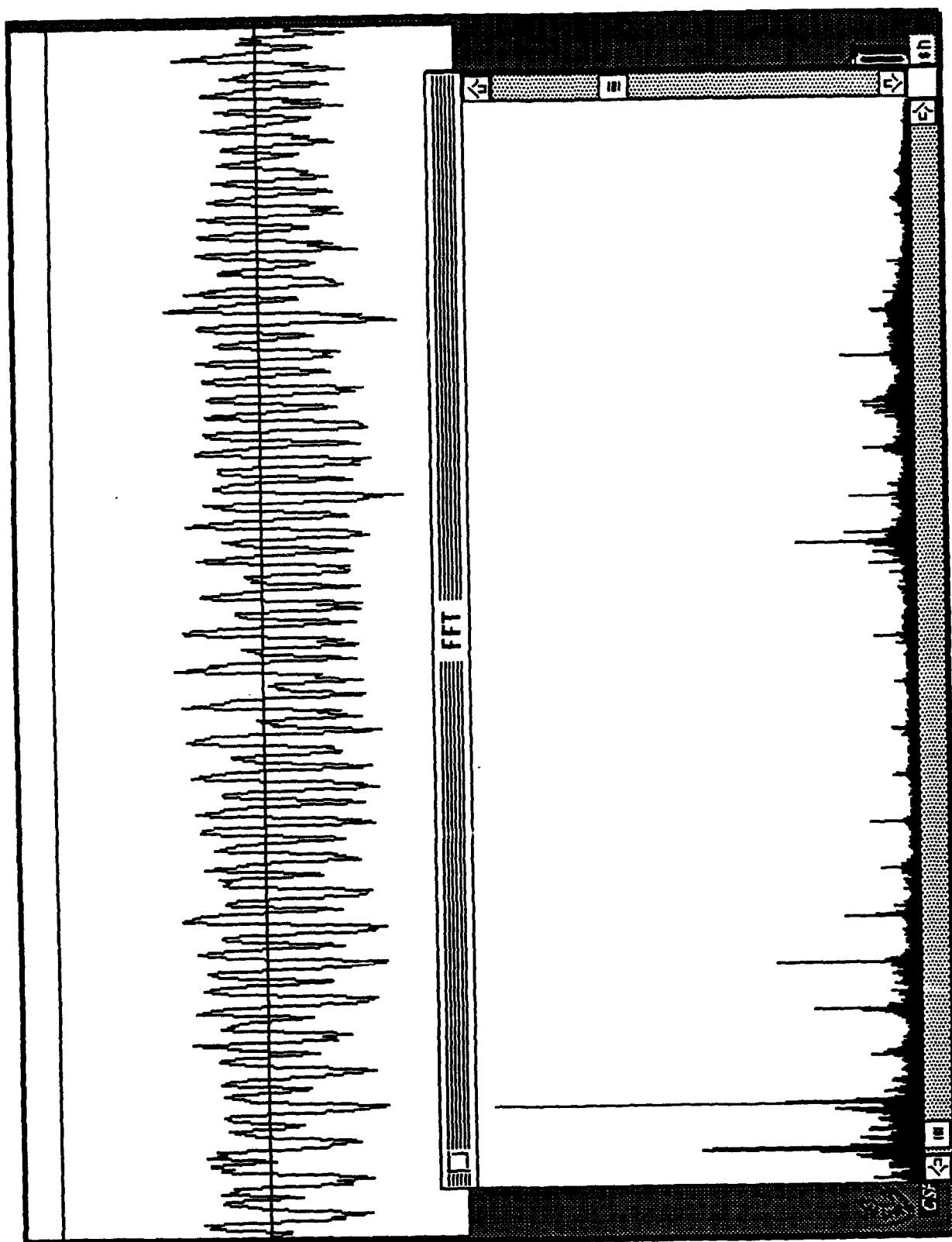
## EVENT RATE

### GEARS

Gear	RPM	rpm (sec)	Samples
Input spur pinion	4,933 rpm	82.2 (.0122)	3,892 samples
Spur	1,270 rpm	21.2 (.0472)	15,118 samples
Herringbone Bull	130 rpm	2.16 (.461)	147,692 samples

### TOOTH RATES

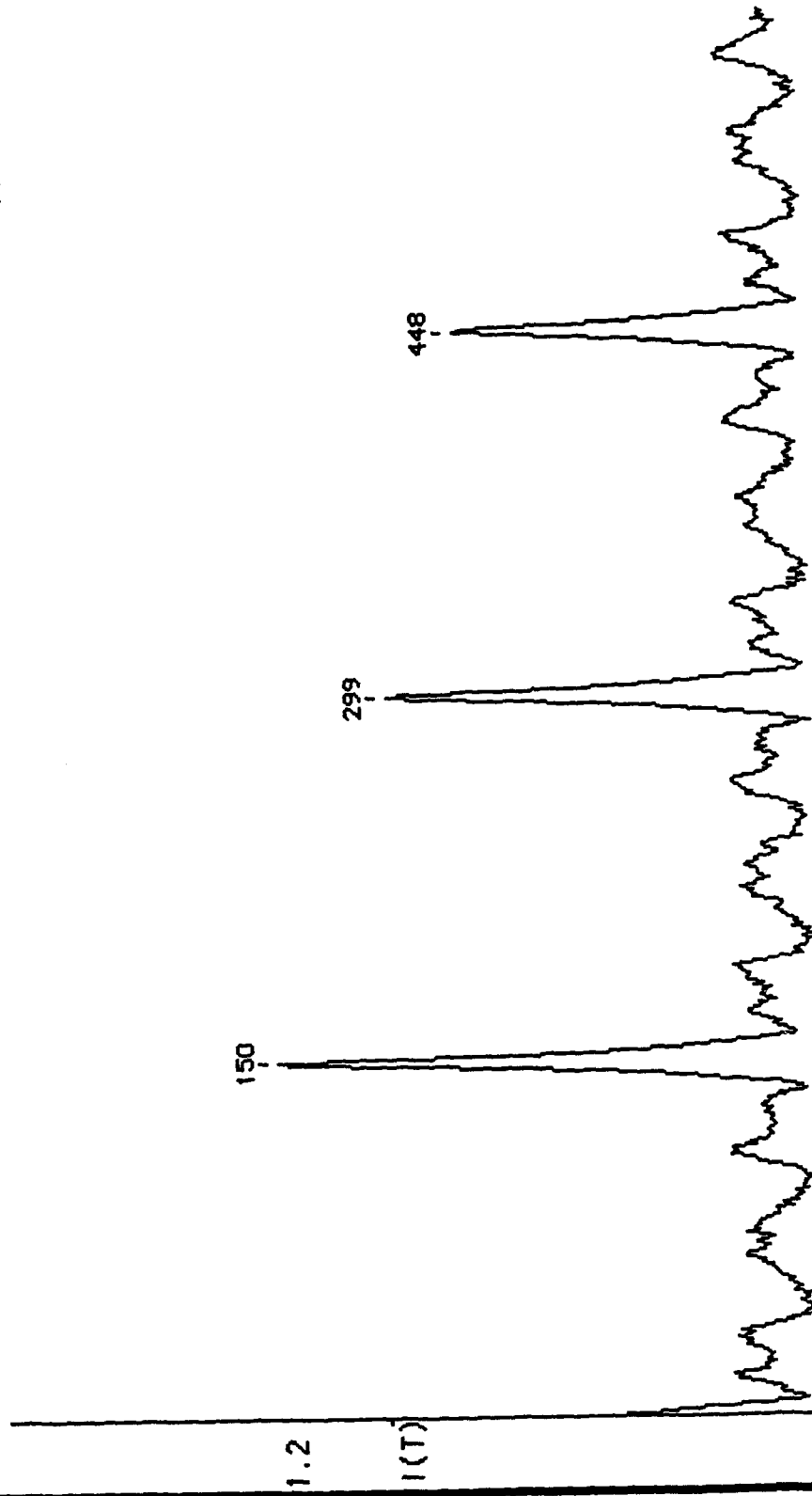
Gears	Mesh rate (/sec)	samples between
Input/Spur	2,137.6	149.69
Spur/Bull	275.16	1,162.9



Mutual Information - t37c22d16.mut

Gearbox

D: 2  
L: 16384  
T: 11



579

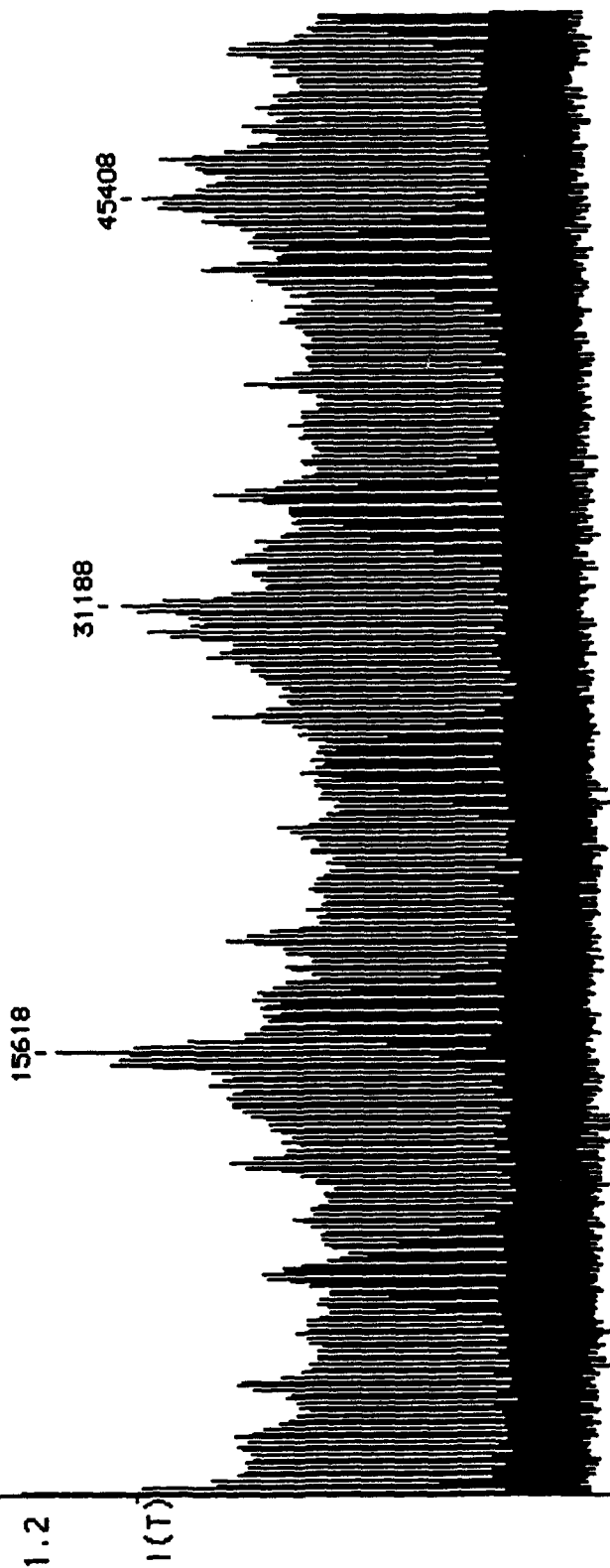
T

3

Mutual Information - t37c22d16.mut

Gearbox

D: 2  
L: 16384  
T: 11



51843

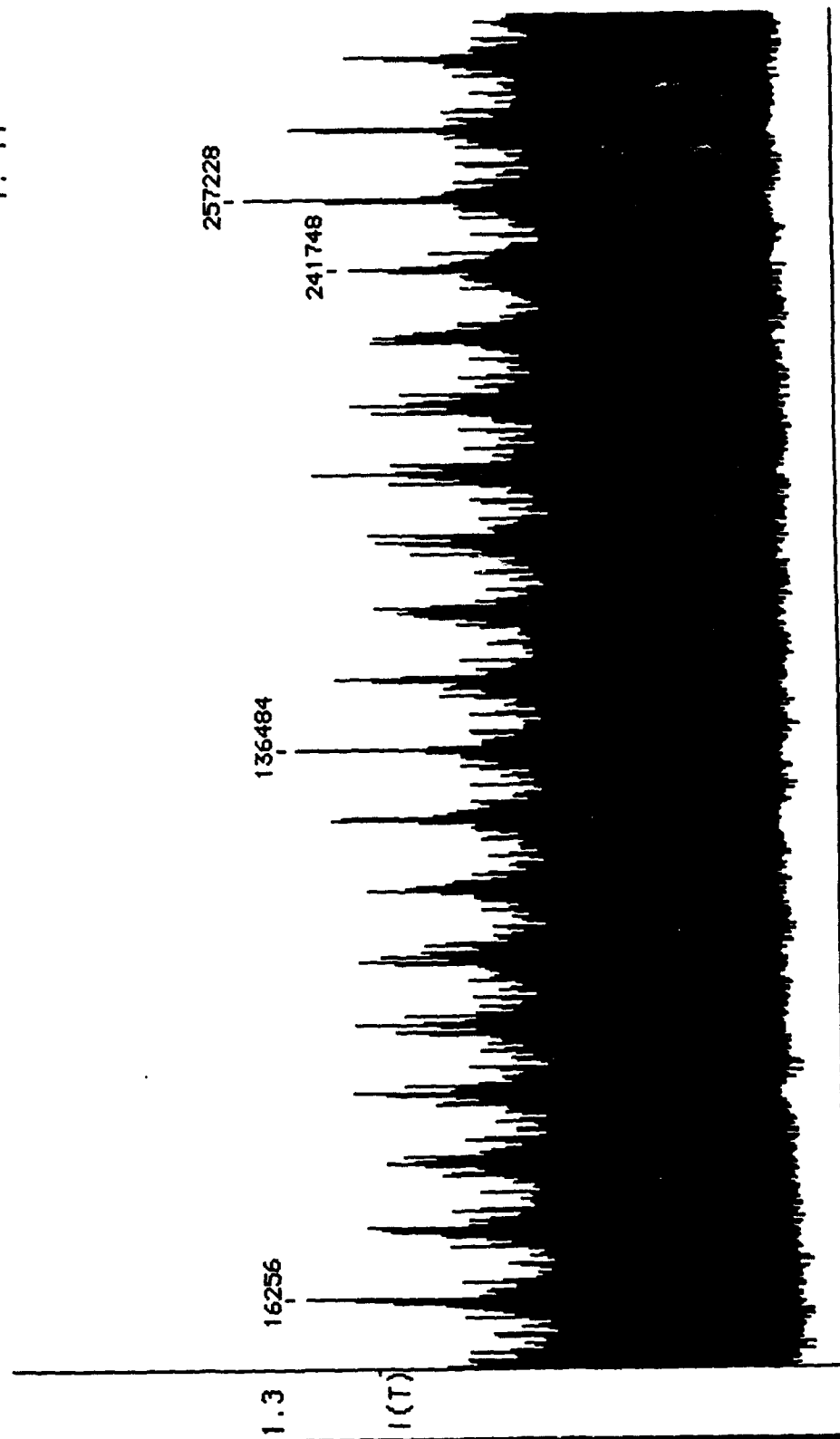
T



Mutual Information - t37c22d16.mut

Gearbox

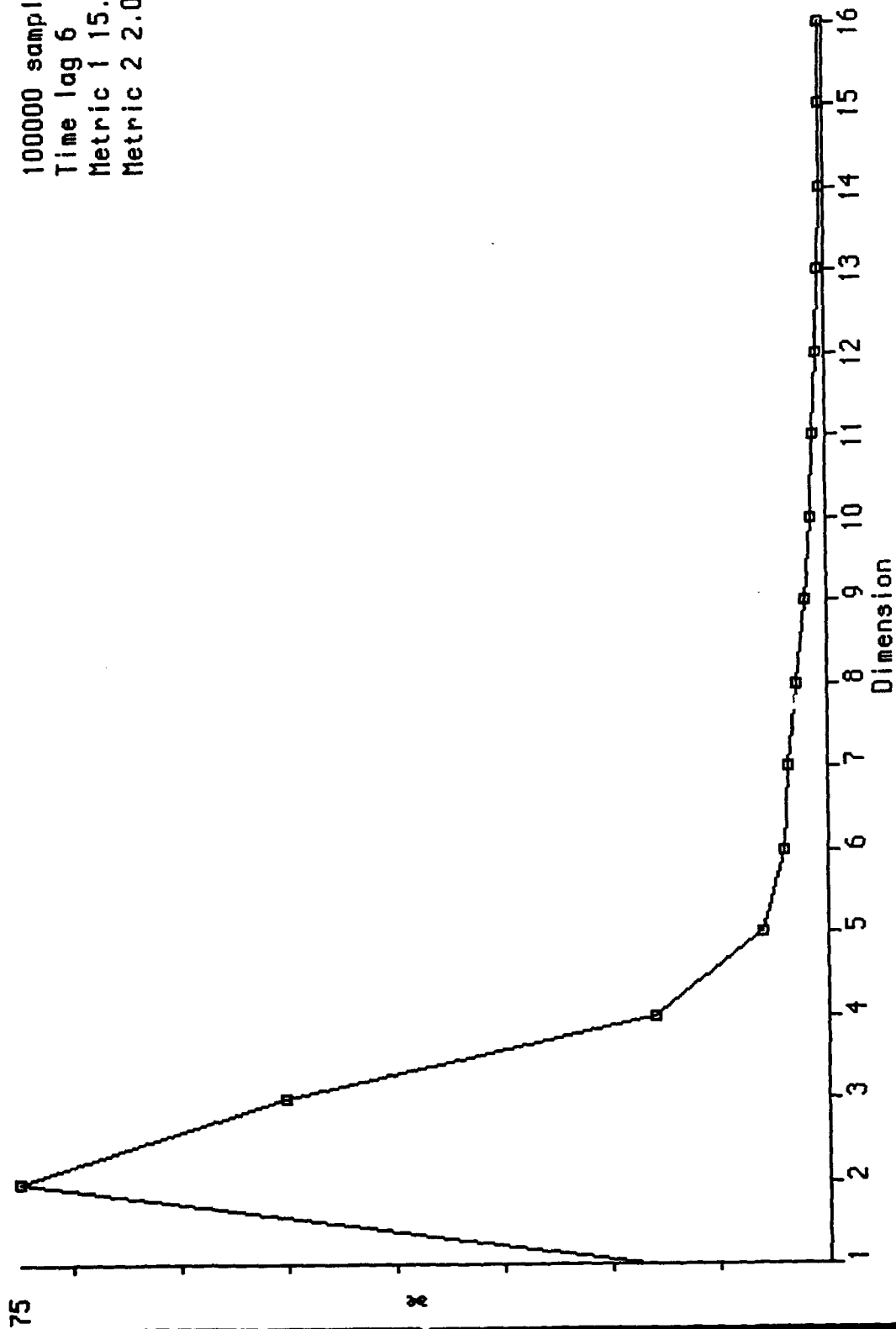
D: 2  
L: 16384  
T: 11



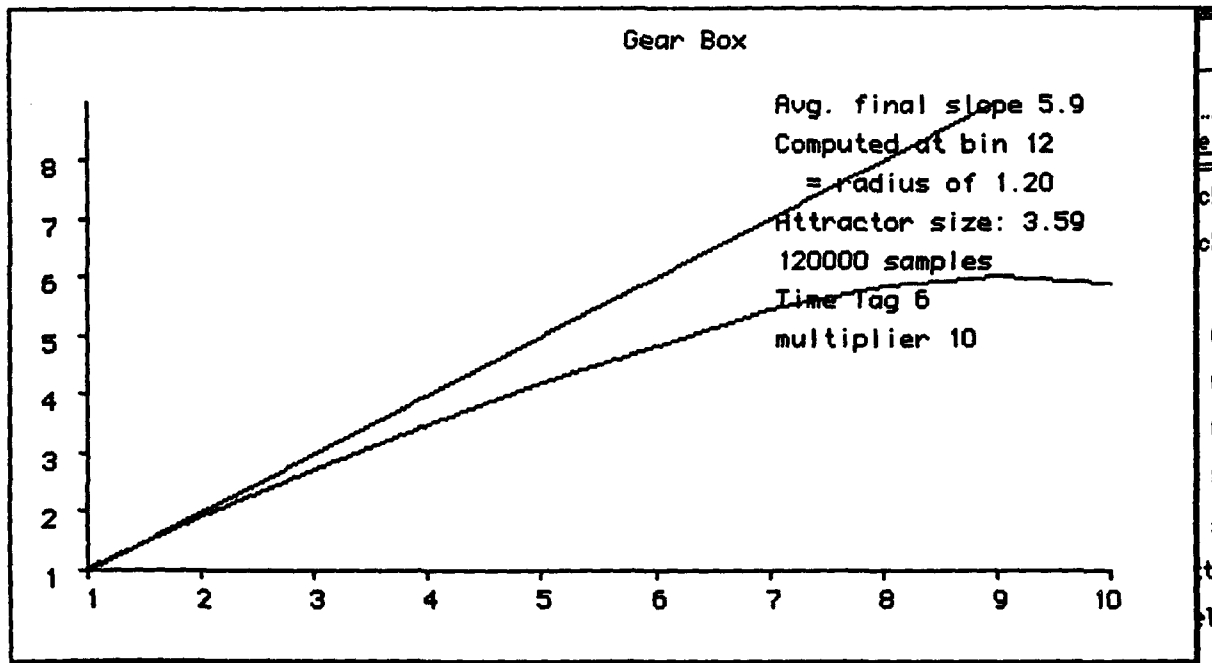
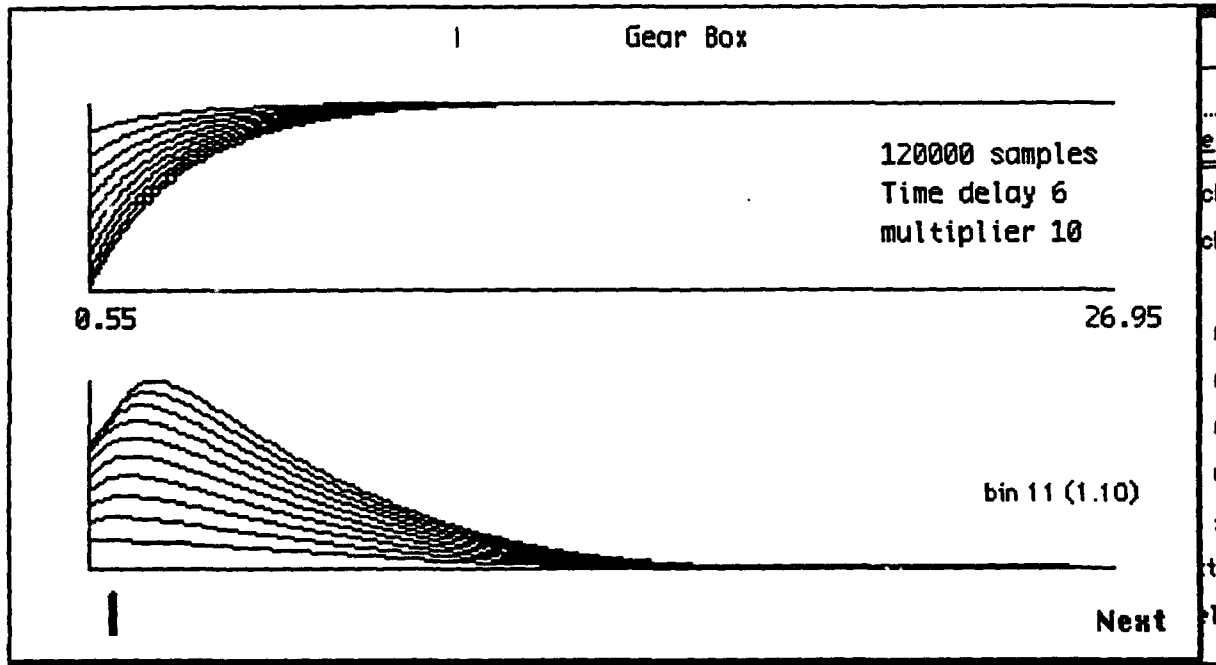
# False Nearest Neighbor - gears.emb

Gear Box

100000 samples  
Time lag 6  
Metric 1 15.0  
Metric 2 2.0



# CORRELATION DIMENSION



PLENARY SESSION  
Subgroup Report  
**CRITICAL EQUIPMENT FAILURES AND MAINTENANCE ISSUES**

17 November, 1993

John Bowen  
Brian O'Connor  
Ellick Wilson  
Joe Marciano  
John Mason  
Paul Fitzgerald

Applied Research Laboratories, UT  
Lubrizol  
NADep, Cherry Point, NC  
Sikorsky Aircraft  
NADep, Cherry Point, NC  
NADep, Cherry Point, NC

Our group meet to discuss and define issues related to **CRITICAL EQUIPMENT FAILURES AND MAINTENANCE ISSUES**. Our methodology was to combine broad definitions with specific examples to generate a list of specific recommendations for future investigation.

Our topic area begs a definition of some terms. The following general definitions were developed:

a. A **CRITICAL FAILURE** is one that results in any of the following:

- 1) A loss of the platform.
- 2) A loss of life or serious injury.
- 3) Significant financial impact

No attempt to further define items such as 'serious injury' or 'significant financial impact' was made by the group, these can be filled in by the appropriate medical and comptroller personnel.

b. A **CRITICAL SYSTEM OR COMPONENT** is one in which - if failure of the system or component were to occur - would result in a **CRITICAL FAILURE**. Further break down to identify the specific system or component would need to be done at the platform level based on the guidance given by the cognizant system directorate.

The group then shifted to specific failures related to the H-46 helicopter. A list of 176 critical failures in 12 separate components of the rotor and drive system components was provided by Ellick Wilson from NADep Cherry Point. This list covered the period generally from 1990 to 1993 and involved equipment failures found during inspections at time intervals less than the then expected lifetime expectancy of the individual components. Some aircraft were lost, but most of the failures were found during depot level inspection. The current corrective actions consist of increasing the inspection frequency and/or tightening the inspection criteria to tighter than the original design specification. Most of the failures involved fatigue cracks in forged components. The failures were repeatedly found in the same locations and, in retrospect, the location could have been implied from the original design to be susceptible to failure.

\*\*\*\*\*Plenary Session, "Critical Equipment Failure/Maintenance Issues"\*\*\*\*\*

The most limiting operational item on the list was the Pitch Shaft. This component allows the individual rotor blade to change pitch and absorbs the forces and moments to connect the blade to the rotor assembly. Due to the short interval between the initial detectable fault and ultimate failure, this component requires an inspection after every two hours of operation. The steps formulated were then generalized to be applicable to other platforms.

The first step in formulating this monitoring process is to identify the failure mechanism. In this case, the Pitch Shaft failure mechanism is due to a combination of corrosion and fatigue induced cracking. In the more generalized case, this information may not be known and would require investigation to determine the cause of failure.

The second step is to identify any detectable or characteristic indicators of the inception of the fault or failure mechanism. This should not preclude the pre existing fault that escaped the initial manufacturing process. The initial detection would imply the first detection of a crack or crack propagation. The underlying assumption being that if the condition passed the initial manufacturing criteria, it was acceptable for service.

The third step is to identify the sensor(s) and the locations to detect the characteristic indicators of the fault. Additionally, the transmission path for the detected characteristic indicator(s) may need to be identified. In the case of the Pitch Shaft, the sensor would probably have to be on the rotating portion of the H-46 rotor assembly.

The fourth step is to analyze the sensor(s) output(s) for the characteristic failure signature to classify and confirm the detection of the failure. This process used to classify the failure would depend on the sensor(s) used and the characteristics to be detected. To preassign an analysis regime would limit the effectiveness of the first three steps. Pitch Shaft and the process as a whole. The process hardware will need to withstand adverse operational environment and weather.

The fifth step is to generate an output identifying the detected fault to the appropriate location. Since this is the Pitch Shaft and an identified critical part for the H-46, the pilot should get the real time indication of each detected fault. Only one detected fault is a different circumstance from multiple fault detections and this information would be needed by the pilot. The detection event(s) should be recorded for down loading to maintenance personnel at the end of the flight. The monitoring process should yield a positive indication of fault inception or growth with a high probability of detection and a low probability of false alarm.

The above situation was for a pre existing platform such as the H-46. For platforms in the initial design phase, the designation of critical systems and components, identification of failure locations and mechanisms with the characteristic detectable parameters should be accomplished in the design phase. Sensor(s), processing techniques, etc. can be incorporated up front at reduced cost and afford greater utility to the operator and the maintenance activities.

For routine maintenance the need exists for improved inspection techniques. Improvements in the sensitivity, ease of conducting the inspection, decreasing the skill level of the inspector and improving the ruggedness of the inspection device all would make the inspection functional and meaningful at the lowest organizational level feasible. This would require systems with built in expertise and integration with the training pipelines for the various maintenance personnel.

In addition, for routine maintenance inspections that can not be covered by other means but require some tear down to gain access to the inspection site by the inspector and/or the instrument, installation of devices to facilitate the inspections would save the tear down time and costs. Such devices as remote or imbedded sensors, remote calibration capabilities or even the simple expedience of an access plate can save hours and dollars in the maintenance area.

The last two items in the routine maintenance category are more programmatic than technical. First, the timely analysis of the maintenance data for the whole fleet (of aircraft, ship Pitch Shaft, trucks, etc.) should be conducted to identify repeated failures and systems or components that need to be re engineered. This is a case where the design did not meet the functional demands of the platform and the design should be modified. Secondly, an analysis of the operational data should be conducted routinely - on a fleet wide basis - to see if the platform, system or component is living within the design operating profile. Excessive operating demands (that have not yet caused failure) should be identified and over stressed systems or components should be re engineered in advance to preclude future failures.

None of the above specifically calls for a prediction of the remaining life in a platform, system or component. Such a forward looking device is warranted to allow the scheduling and coordinating of maintenance efforts and to insure that proper support is available from supply and personnel are available to effect the repair in a timely manner. The recording of operational or life cycle data and the systematic (religious) determination of life remaining before failure is a desired goal. The actions recommended above would lead to that end. For existing platforms (e.g. the H-46 which has probably exceeded its designers wildest expectations) this is a difficult to impossible task since the life time may have been already exceeded. For individual components within these platforms, this may be an approachable goal. Certainly in new acquisition platforms, this should be an attainable goal.

### Recommendations

Recommend that the methodologies indicated above be implemented to improve the reliability of the Navy's maintenance system. Specifically recommend the following methodology for in service platforms:

- First: Identify the failure mechanism.
- Second: Identify any detectable or characteristic indicators of the inception of the fault or failure mechanism.
- Third: Identify the sensor(s) and the location(s) to detect the characteristic indicators of the fault. Additionally, the transmission path for the detected characteristic indicator(s) may need to be identified.
- Fourth: Analyze the sensor(s) output(s) for the characteristic failure signature to classify and confirm the detection of the failure. This process used to classify the failure would depend on the sensor(s) used and the characteristics to be detected.
- Fifth: Generate an output identifying the detected fault to the appropriate location.
- Sixth: Identify remaining service life

While the implementation of these stePitch Shaft may be a daunting task for a complete platform, the implementation on selected components or systems should be a feasible goal for a trial on an aircraft, ship or land platform. For a pre construction platform or weapon system, these stePitch Shaft should be done in the design stage.

For routine maintenance, recommend the following:

- First: Improved inspection techniques to make the inspection functional and meaningful at the lowest organizational level feasible.
- Second: Installation of devices to facilitate the inspections, remote or imbedded sensors, remote calibration capabilities to obviate the need for tear downs and rebuilds merely for access
- Third: Timely analysis of the maintenance data for the whole fleet to identify repeated failures and systems or components that need to be re engineered.
- Fourth: Analysis of the operational data to identify excessive operating demands should identify over stressed systems or components that require re engineering to preclude future failures.

PLENARY SESSION  
Subgroup Report  
FAILURE MODELS

17 November, 1993

Bill A. Glaeser, Group Leader  
Lavern D. Wedeven, Recorder

**Introduction**

The issue of understanding "failure mechanisms" seems to have surfaced from almost every group addressing the issues of condition based monitoring (CBM). Failure mechanisms undergird the whole concept of CBM in the following ways:

- Intelligent use of current condition monitoring technology
- Required for the development of new sensors and monitoring technology, including basic decisions to make CBM work.

Failure mechanisms were subdivided into two categories - **TRIBOLOGICAL** and **STRUCTURAL**. The category of structural includes bearing and gear structural parts like rolling elements, rings, gear teeth, etc. Tribology deals with load carrying surfaces and lubricating materials.

Approximately 8 people participated in this group. Unfortunately, the distribution of disciplines was very heavily weighted on the tribology side. For this reason, the report does not do justice to the very important structural failure mechanisms.

**TRIBOLOGICAL FAILURE MECHANISMS**

Almost all oil wetted parts are critical components in power transmitting systems. The lubricating fluid is an integral part of the mechanistic process. Because of this mechanistic studies and modeling should include both oil supply attributes and mechanistic processes that are connected to oil analysis.



## **Supply Attributes**

With extended operation, there is greater concern for oil coking of passage-ways in hot sections (potential engine problem). A least one engine company has discussed the possible use of sensors in areas known to give problems. There are no known sensors for coking. Currently, oil suppliers are working on what some call "third generation" oils which tend to be somewhat "cleaner" with regard to deposits. The fact that there is action in this area is an indicator that there is some concern.

Marginal oil supply, oil interruption and oil-off conditions are critical events for lubrication and cooling. There is little understanding of the tribological progression of events in real hardware, or even simple bench tests, that would allow prognosis of running time to failure or remaining life following recovery.

## **Oil Analysis**

It is relatively easy to monitor oil condition for total acid number (TAN), change in viscosity and other attributes routinely provided in programs like SOAP. Whether on-line or off-line, the results of oil analysis are not entirely clear with regard to the precise location of a problem and decisions on maintenance or remaining life. In addition, oils become contaminated and suffer from additive depletion. There is a need to address the impact of this on the tribological mechanisms that relate to performance and remaining life.

## **Lubricating Film Formation Mechanisms**

Mechanisms associated with the formation of lubricating films are generally understood. These include:

- hydrodynamic
- elastohydrodynamic (EHL or EHD)
- boundary film

The first two are used in design by way of the "lambda ratio ( $h/\sigma$ ) which allows a calculated oil film thickness ( $h$ ) to be judged in relationship to surface finish ( $\sigma$ ). There is no profitable reason for CBM to focus on subtle features associated with hydrodynamic or EHD mechanisms.

The formation of boundary films are much more mysterious. Designers and users know that they can push there performance limits further with, for example, certain types of oils such as DOD-L-85734 vs MIL-L-23699 due to the added chemistry. In any case, the mechanisms of film formation are much better understood the mechanisms of failure.

## Lubricating Film Failure Mechanisms

Life for very small ( $h/\sigma$ ) has many pathways. It is recognized that these conditions produce many competitive tribological processes. Some of these are identified below:

### *Sub-surface Fatigue*

Crack initiation and propagation below the surface due to cyclic stresses can lead to spalling. With much improved bearing and gear materials, the frequency of sub-surface initiated fatigue has been mostly eliminated. Most spalling fatigue appears to be due to surface initiated phenomena to be discussed below. Yet, sub-surface fatigue is an issue, not only for tribological surfaces but for structural failure mechanisms. There is a need for capturing some kind of precursor to the initiation of a subsurface crack. This is particularly important for failure mechanisms where crack initiation is more important than crack propagation.

### *Surface initiated Failure*

The CBM needs associated with surface initiated failure mechanisms can be divided into singular defects and low ( $h/\sigma$ ) operation.

*Singular defects* - These include nicks, scratches, corrosion pits and dents caused by third body particles (hard or soft). These defects cause local stress risers which can lead to crack initiation and pitting or spalling. These defects also cause local loss of lubricating films which may be an initiating site for progressive wear or scuffing. Large singular defects cause vibration signatures. There is a need for modeling the impact of surface defect size and shape or third body morphology on life and tribological performance. At overhaul there are inspection criteria and tooling for rejection due to surface defects. However, the impact of defect size is now known to be relative to component size (radius of curvature) and lubrication. It is possible that too many parts are scrapped. It is also possible that overhauled parts should not have been returned to service.

*Low ( $h/\sigma$ ) operation* - Many oil wetted components operate under these conditions due to one, or a combination of, low speed, high temperature and rough surfaces. With regard to mechanistic understanding for CBM, the difficulty is that the tribological processes can follow many pathways and the rate of events can be from benign to catastrophic. Some surface descriptive features are listed below:

run-in	polishing wear	scuffing (light, mild, heavy)
	scratches (score marks)	severe wear
	peeling	
	smearing	

The tribological processes associated with the items in the middle column are very common in hardware and are likely to be precursors to more catastrophic failure. The debris from these processes is very small and not easily collected with debris monitoring equipment. Also, typical tribological bench tests for wear go well beyond these mechanisms where the wear coefficient is very small. There is a need for better understanding of these wear modes and how they relate to satisfactory lubrication and also how they progress to more advanced forms of surface deterioration. A "neural network" of features associated with wear, fracture and oil attributes as sketched together by Bill Ruff is attached.

With regard to surface initiated failure mechanisms two general needs can be identified:

- Identification of tribological pathways in critical hardware and their connection to operating conditions.
- Development of tribological models for low ( $h/\sigma$ ) operation and laboratory simulation of hardware conditions to find indicators for life prognosis (remaining life).

<enrdbm>

## CONCLUSIONS AND RECOMMENDATIONS

The deliberations of the group were based on the premise that *what we don't know* should be explored. Three subjects about which there is a critical gap in understanding were selected as priority items for new research programs:

- Lubricated wear
- Contact Fatigue Precursors
- Structural Fatigue Precursors

*Specific concerns for the above candidates:*

### Lubricated Wear

Lubricated wear can occur in thin film hydrodynamic contacts and in so-called boundary lubricated contacts. In the former, the lubricating film supports the contact load by self-generated film pressure. The thickness of the film and the pressure distribution in the film can be calculated. In boundary lubrication, on the other hand, there is no hydrodynamic factor relying on viscosity to support load. Currently there is no useful analytical approach for modeling boundary lubrication. All models depend on empirical data. *NOTE: Any models that are developed for lubricated wear must recognize that it takes many pathways - some to thin film break down failure - others do not result in failure.*

For thin film, hydrodynamic wear, we can estimate film thickness and relate it to the surface roughness (heights of asperities). This approach is used in the design of bearings and gears. However, there is no way of determining what film break down and subsequent release of wear debris or scuffing is. The factors which lead to film break down are not known to the extent that they could be used in a failure model. It is quite possible that when the supporting lubricant film becomes so thin that some asperities contact, boundary lubrication takes over.

New research is needed, therefore, to develop a film break down model. The model should define film break down and find conditions that lead to it. Detection of incipient film break down should then be a product of this research.

### Boundary Lubrication

Boundary lubrication has been left to empirical studies for half a century. In the meantime, hydrodynamics and EHL have been developed into elegant mathematical models. It is time that the dynamics of boundary lubrication be investigated and subjected to modeling.

For the Navy's concerns, some aspects of boundary lubrication demand attention:

What properties are required to develop an effective boundary film?

Substrate bonding

Reaction process in the contact region

Degradation process (how does it wear away)

Effect of contact pressure and shear rate

Structure

What can poison a boundary film reaction

It is suggested that new surface analytical techniques may be useful in the study of the above boundary film mechanisms. It appears that techniques being developed will enable study of chemical processes within the contact zone during lubricated wear for study of the basic mechanisms of boundary lubrication and wear.

### Contact Fatigue

Since subsurface generated contact fatigue is less likely owing to development of improved materials, surface generated contact fatigue should be concentrated on. In particular, the effect of surface defects on the fatigue process needs to be addressed. If those surface defects that lead to fatigue can be classified so that they can be detected nondestructively, considerable savings in replacement of parts in low supply can be achieved. It is hoped that those surface defects that are benign can be characterized so that they can be confidently ignored.

Defects include dents, scratches, scuffing, fretting and corrosion.

Some suggested characteristics to be investigated include:

- Morphology

The shape, size and stress raiser features of defects will influence the probability of initiating a crack.

- Orientation

In rolling contact bearings, the orientation of defects to the rolling direction will influence the disruption of the EHL film.

- Surface chemistry

Local polarity of critical surface areas can lead to galvanic effects. Segregation of alloy constituents caused by contact stress can lead to pitting. Corrosion pitting can act as sites for crack initiation.

- Dents and nicks can produce near surface residual stresses that can increase the likelihood of or inhibit crack generation.

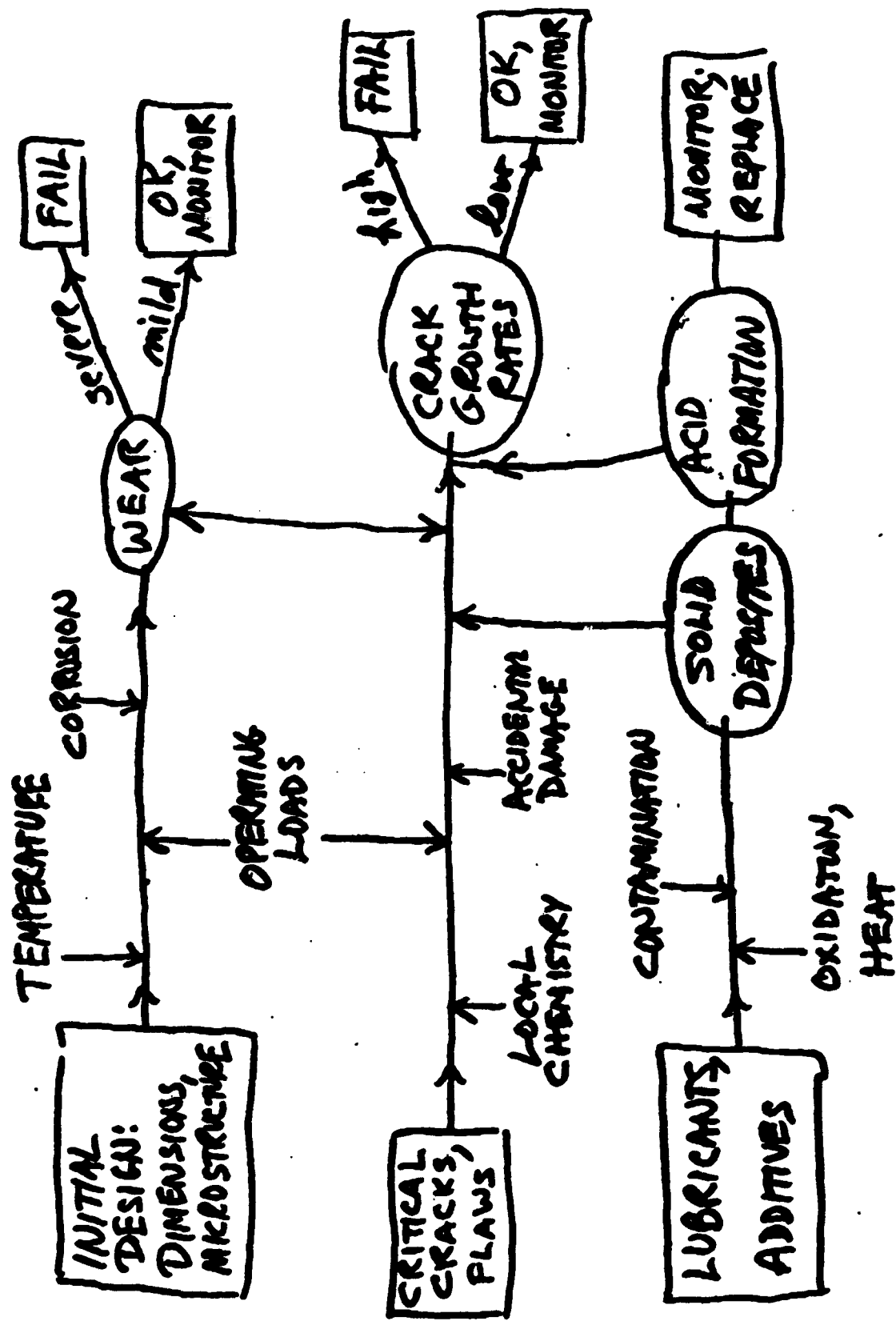
The above characteristics and their interaction with the contact fatigue process should be modeled so that the probability of damaging fatigue from defects or combination of defects can be confidently predicted. The model should enable establishment of criteria for detecting critical defects.

### Structural Fatigue

The effect of surface defects on structural fatigue should also be illuminated by the research on basics of surface defects on contact fatigue.

**ISSUE: FAILURE MECHANISMS - Modeling**

Visuals used at meeting





## ISSUE: FAILURE MECHANISMS - Modelling

Why? Undergirds concept of CBM

- \* intelligent use of current condition monitoring technology.

- \* development of new sensor and monitoring tech. incl CBM decisions

Categories: TRIBOLOGICAL STRUCTURAL

### TRIBOLOGICAL



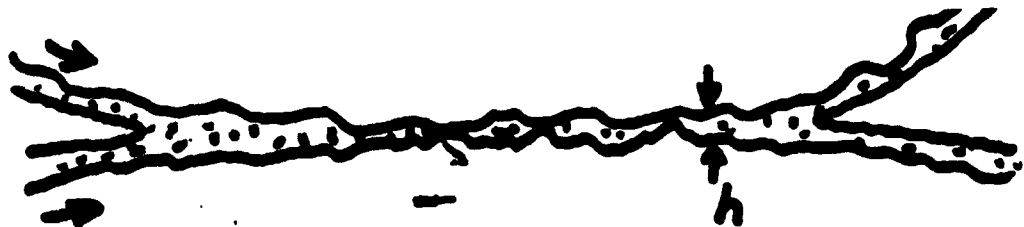
Oil integral part  
of mechanistic  
process

Modelling should incl.

- \* Supply Attributes re: cooling, lubr.

- Coking w extended operation, SENSOR?

- Impact of marginal lubr. & oil-off  
(safe operating time)



Film formation mechanisms - OK

- hydrodynamic
  - EHD
  - Boundary
- } h/lr used in design,  
responsible for life  
and reliability

Film failure mechanisms - Not OK

- \* Life beyond small  $h/lr$  has many pathways
  - \* Competitive processes:
  - \* Sub-surface fatigue
    - Less important w good mat'ls
    - Can detect when failure (spalling) is evident, but need precursor
  - \* Surface initiated failure
    - Singular defects  
dents, nicks, scratches  
corrosion pits, 3rd body contaminants
- Need model for impact on life  
critical defect size and inspection  
criteria & tooling
- false indicators of faults?
  - scrap too many parts?

- Low  $h/\sigma$  operation { high temp  
rough surf
- Prob. - many possible pathways; specific to hwre and its operation.

RUN-IN      polishing wear  
                 scratches  
                 peeling      scuffing { slight  
                 smearing      severe wear { mild  
                 { heavy  
                 }  
                 } → debris  
                 low wear coeff. region

**NEED:**

1. Identify pathway in critical hardware and relate to operating conditions
2. Tribo-models and laboratory simulations to find indicators for life prognosis.

PLENARY SESSION  
Subgroup Report  
SENSORS

17 November, 1993

Steve Shaffer, Group Leader

We recognize the urgent need to develop advanced sensors for machinery and structures on ageing aircraft, ships and land vehicles which exhibit the characteristics of reliability over the life of the machine or structure, low life cycle cost, reduced or eliminated calibration, and local intelligence.

We recommend a two-pronged approach: (1) to initiate projects for the near term, which would lead to improved sensors to be incorporated into critical areas of existing equipment; (2) to launch projects, for the long term, which would lead to complete retrofit in existing platforms or future new ones.

The approach that we suggest for the near term program is to modify and integrate existing sensors into retrofitable or replaceable parts that can be introduced directly into existing systems. This may be accomplished through the development of a family of *in situ* microsensors for primary parameters including pressure, temperature, vibration, acoustic emission, viscosity, strain, shear forces, wear debris, and lubricant contamination. The long term approach is likely to involve the development of new sensor strategies, including sensors that are compatible with fiber optic transmission systems and central array processing as well as decentralized "smart" sensors which incorporate both transducer and processing capability on a single chip, and sensors which are integrated directly into critical machine components. The fiber optic system anticipates the upgrade of on-board signal transmission systems, in an effort to avoid problems associated with hostile environments, such as temperature, shock, dirt and electro-magnetic interference.

These efforts will require further research at a basic level in areas such as corrosion and wear processes and their relation to crack initiation and growth, and chemistry at the interface of lubricated contacts. These processes must be studied to determine what metrics may be the most important for future development.

PLENARY SESSION  
Subgroup Report  
SIGNAL ANALYSIS

17 November, 1993

Tom McKenna, Group Leader

Our initial discussion revealed that the participants had different views of what a model should encompass. Roger Barron presented his typology of four kinds of models: (1) Phenomenological Models, eg. simple fault propagation models, (2) S-R (Stimulus Response) Models relate the output to input parameters such as load, (3) Inverse Models of Explanation Type predict outcomes, but also reveal what inputs were critical, which leads to explanations of the model predictions, and (4) Inverse Model of Control Actions generates suitable control actions. One example would be a reconfigurable flight control. Models of this fourth type would be suitable where analytical models are intractable (such as time-varying nonlinear systems). Paradoxically, this type of model may be easier to defend than the third type, which permits explicit explanation of performance, since the criteria or rules then become subject to oversight.

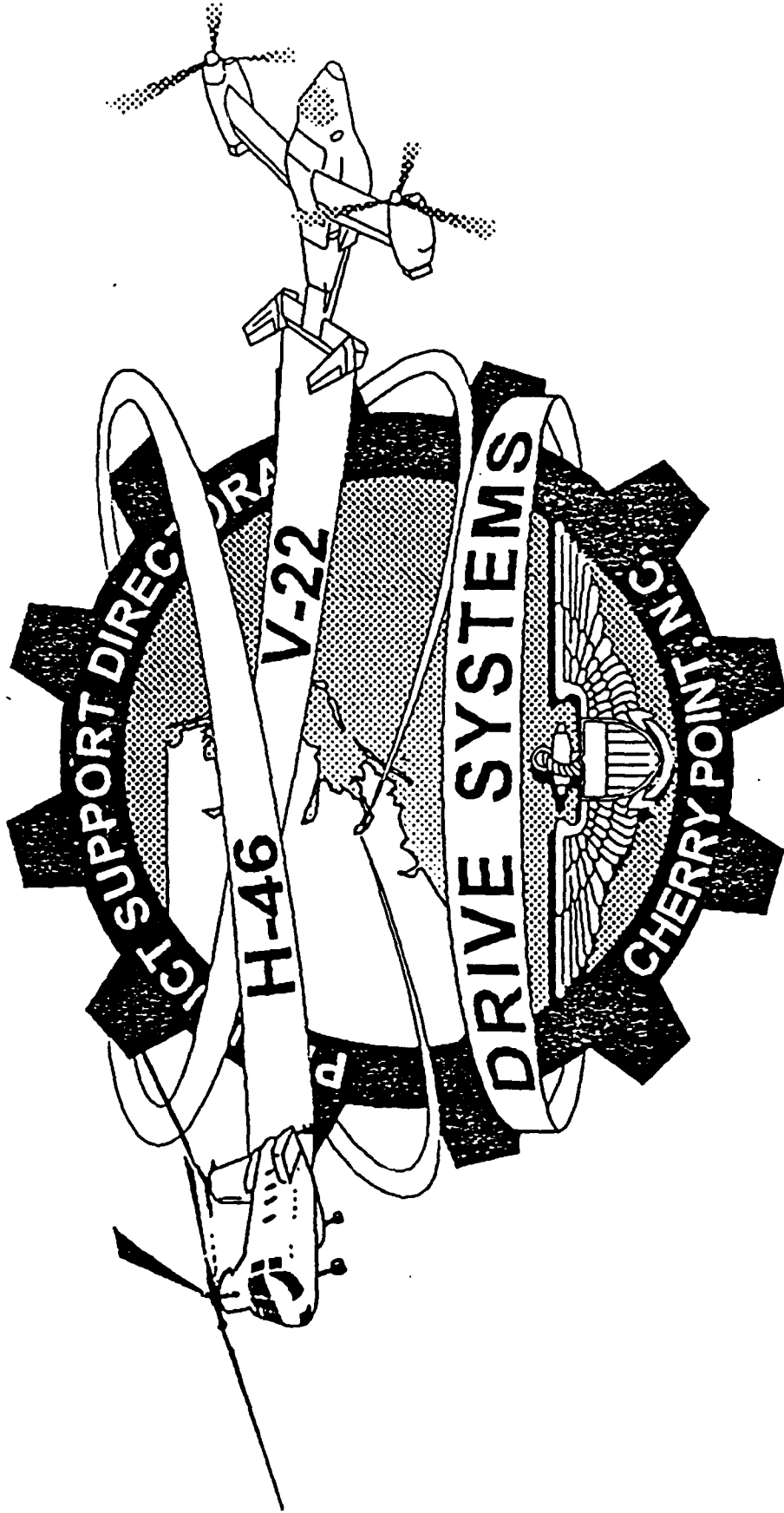
In the context of mechanical diagnostics, different types of models are appropriate for different parts of the task. For example in the system design phase (diagnostic system) a model "A" that predicts signals emitted by a fault, and the site of emission would be used to select sensors and locations. An example is provided by CAD design programs such as gear mesh models that predict vibration spectra and noise produced by cracks. Such models can operate off-line with extensive computer resources, permit many "what if" experiments, and permit details to be added, such as local surface interactions. The actual real-time diagnostic system, would consist of two integrated components, an automatic fault detection and classification system (which could consist of spectral decomposition, feature extraction/reduction, and neural network classifier) and a model "B" to track the fault and make prognosis of time to component and/or system failure. The fault detection/classifier component would flag signals of faults or fault inception, would be on-board, and would process more than one sensor type. Signal paths from different sensors or sensor types would maintain parallel paths until independent calls could be made and an arbitration technique used to interpret divergent calls. If the model "B" component was statistical or a simple neural network it would require the availability of an adequate data sample, which might be expensive and difficult to obtain. However, if this model incorporated an adaptive representation of the physical failure process, this requirement might be relaxed. This model should be environmentally and regime sensitive.

Both the "A" and "B" models would require validation and updating. We recommend that a simple mechanical system be selected and physically built and modeled. Possible mechanical systems include a set of four right angle gears, with variable torque and internal control, or a simplified rotor head. The physical model could be replicated for use in more than one laboratory, and embedded sensors placed within it. Parts could be run to failure routinely, without the danger associated with large mechanical systems. Problems which emerge in field systems could be analyzed at different stages of the failure process, such as cracks developing on gear teeth. Such testbeds would be important for model validation, sensor development, and advancing the understanding of the failure process of materials as components.

Some of the scientific and engineering approaches we see as critical include: (1) developing hybrid systems that combine inductive processors (eg. neural nets) with deductive methods (eg. expert systems, physical models), (2) Creating software tools based on real data and knowledge of the failure process, (3) fully characterizing simple mechanical models, eg. simple gearbox (4) characterizing the critical steps in mechanical failure, (5) developing that target performance of a diagnostic system, based on cost/benefit analysis of the entire

maintenance process, (6) specify a hardware implementation path of the diagnostic system, (7) specify the sensors and signals required, and the data path of the system, (8) Develop models that predict signals of failure and anomalous conditions (eg. state variable distributions) consistent with data obtained on physical systems, (9) integrate the diagnostic system with HUMS (health and usage monitoring system), and (10) recommend changes in fleet procedures pertaining to logging problems, maintenance records, and recorded data to produce a richer audit trail of the development of mechanical failures.

The technology goal of S&T research should be the develop a system that accurately predicts the remaining useful life of machine components under specified conditions.



# MATERIAL FACTOR MISHAPS/INDICATORS

## MISHAPS

MAY 90 29 PALMS CA H-46E: LOST DRIVE TO AFT ROTOR.  
AFT TRANSMISSION QUILL SHAFT FATIGUE FAILURE.  
MULTIPLE INJURIES. NO FATALITIES. STRIKEN  
AIRCRAFT.

JUN 90 OFFSHORE NORFOLK VA H-46D: ROTOR SYSTEM  
FAILURE IN FLIGHT (ROTOR PITCH SHAFT).  
FOUR FATALITIES. STRIKEN AIRCRAFT.

JUL 92 CHERRY PT NC H-46E: FLIGHT CONTROL SYSTEM FAILURE  
IN FLIGHT (UPPER BOOST ACTUATOR). NO FATALITIES.  
STRIKEN AIRCRAFT.

## MATERIALS INDICATORS

MAY 88 H-46E: ROTOR TIE BAR DEGRADATION DISCOVERED.

JAN 89 INCREASE IN FREQUENCY OF ROTOR HUB CRACKS DOCUMENTED.

MAY 90 CRACK DISCOVERED IN ROTOR CONNECTING LINK.

JAN 91 CRACK DISCOVERED IN PITCH HOUSING.

MAR 91 SECOND OCCURRENCE OF A FORWARD ROTOR SHAFT CRACK  
(PLANET CARRIER) NOTED.

JUN 91 IMPROVED TIE BAR FOUND DEGRADATED IN SERVICE.

JUL 91 ROTOR BLADE ATTACHMENT FITTING CRACK DISCOVERED.

AUG 92 AFT ROTOR SHAFT FOUND WITH CIRCUMFERENTIAL CRACK.

JUL 93 SEALED PITCH SHAFT FOUND CRACKED IN SERVICE.





# Summary of Cracked Rotor and Drive

## System Components

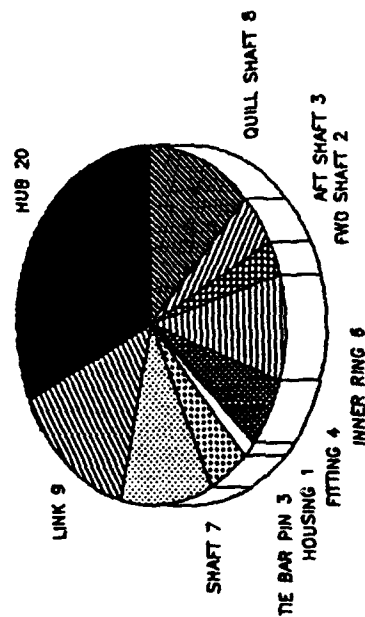
H-46 AIRCRAFT

Component	Nr Cracked
Rotor Hubs	19
Connecting Links	15
Pitch Shafts	9
-2 Tie Bar Assy	104
Tie Bar Pin	3
Pitch Housing (Barrel)	3
Blade Attachment Fitting	11
Inner ring	8
Forward Rotor Shaft	2
Aft Rotor Shaft	8
Quill Shaft	8
Input Pinion Adapter	1

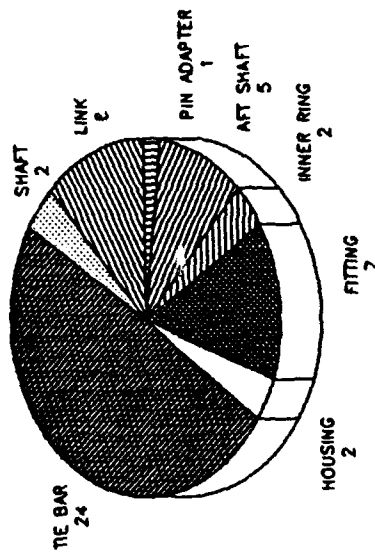
July 29, 1993



# CRACK DETECTION ACTIVITY



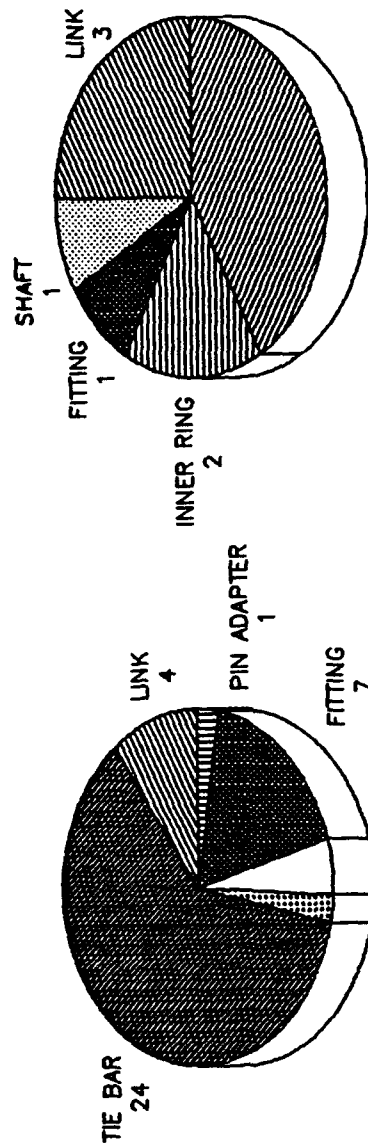
DEPOT (56%)



FLEET (44%)

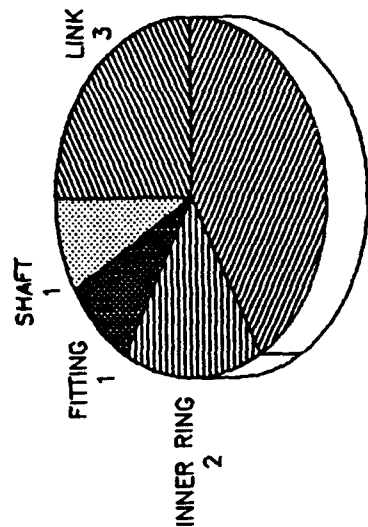
JULY 1993

# FLEET DETECTION METHOD



SHAFT 1  
HOUSING 2

VISUAL INSPECTION  
(76%)

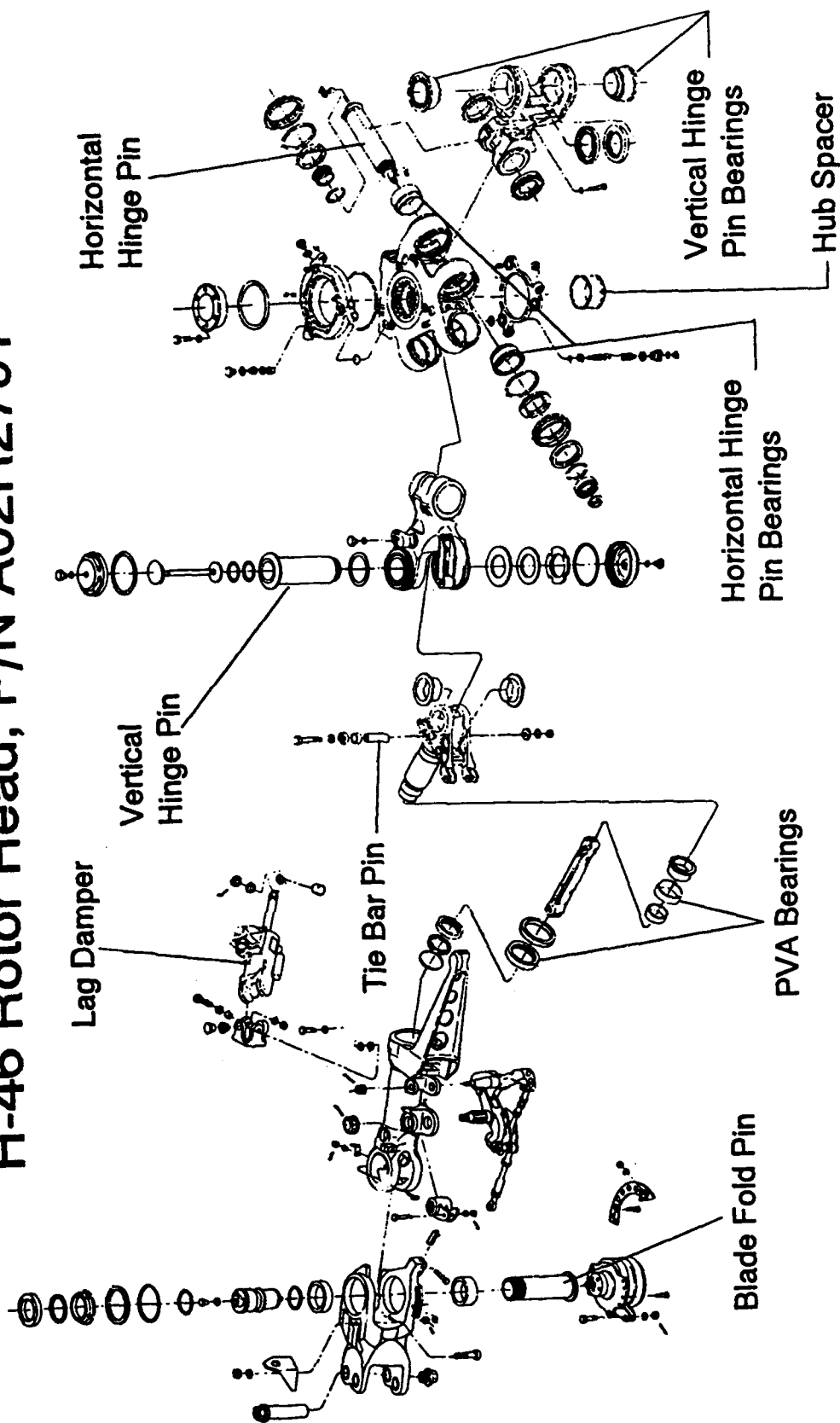


AFT SHAFT 5

NDI TECHNIQUE  
(24%)

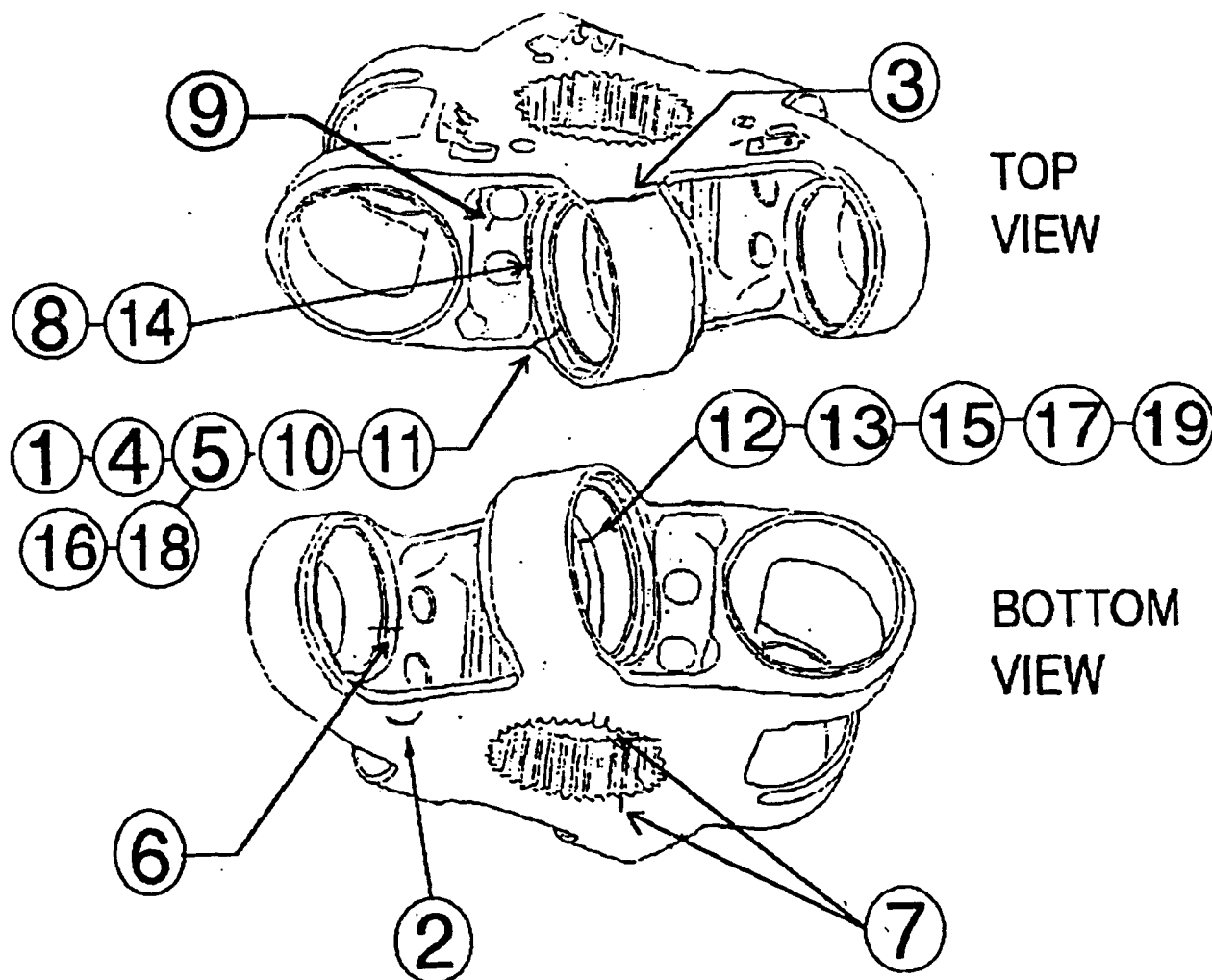
JULY 1993

# H-46 Rotor Head, P/N A02R2701



# H-46 ROTOR HUB, P/N A02R2550

## CRACK LOCATIONS



Handwritten text: 200-100-0000000000

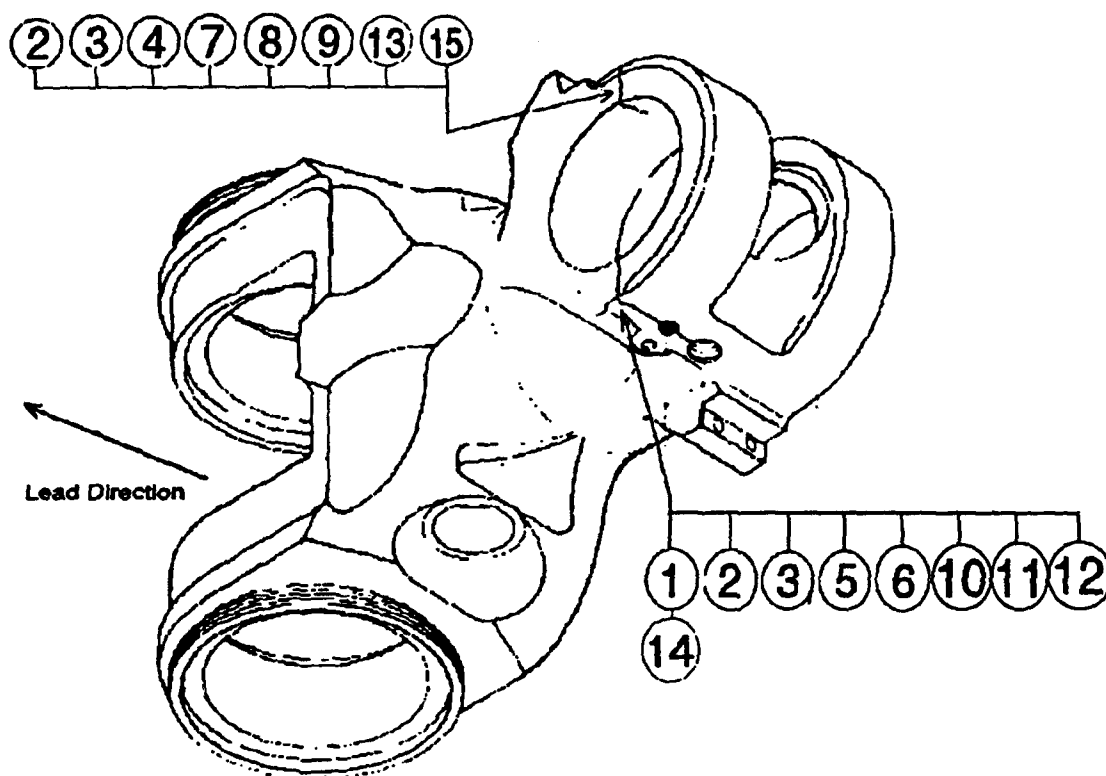
# H-46 ROTOR HUB FAILURE LOCATIONS DEPOT LEVEL PROCESSING

NR	DATE FOUND	DEFECT	PROGRESSION
1	Feb-69	GOUGE	YES, 1.5*
2	Feb-83	STOP IMPACT	NONE
3	Aug-83	GRIND CRACKS	YES, 2.0*
4	May-86	GOUGE	YES, 1.0*
5	May-87	GOUGE	YES, 0.9*
6	Aug-87	NICKED	YES, 2.0*
7	Feb-88	CORR. PIT	YES, 0.4*
8	Dec-88	GRIND CRACKS	NONE
9	Dec-88	FORGE LAP	YES, 0.4*
10	Mar-89	NICKED	YES, 2.5*
11	May-89	NICKED	YES, 1.0*
12	Mar-90	UNK	YES, 1.5*
13	Jul-90	UNK	YES, 2.0*
14	Jul-90	GRIND CRACKS	NONE
15	Jun-91	UNK	YES, 1.5*
16	Mar-92	UNK	YES, 2.5*
17	Mar-92	GRIND CRACKS	YES, 1.5*
18	Apr-92	UNK	YES, 2.5*
19	Apr-92	GRIND CRACKS	YES, 1.0*

\* FATIGUE PROPAGATION IN INCHES

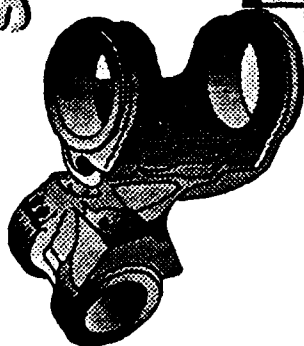
# H-46 CONNECTING LINK, P/N A02R2551

## CRACK LOCATIONS



BOTTOM VIEW

# Summary of Cracked Connecting Links



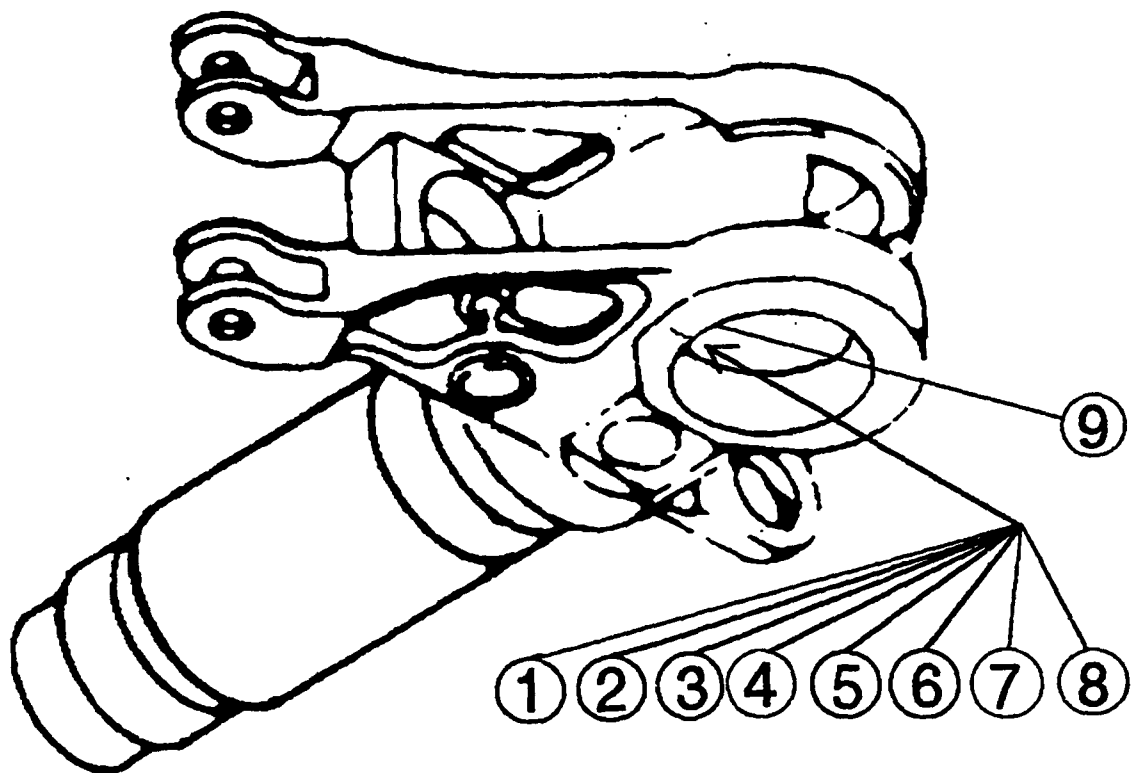
	DATE FOUND	SERIAL NUMBER	TSO	CRACK LENGTH
1	2 MAY 90	UY2374	480	1.75 inches
2	1 JUN 90	BN2003	290	1.05
3	6 JUN 90	BN4910	869	1.00
4	16 JUL 90	BN2007	60	0.25
5	19 JUL 90	BN6075	422	0.25
6	JUL 90	UY2039	1200	0.02
7	OCT 91	BN4365*	530	0.69
8	SEP 91	BN2450	836	1.25
9	18 JAN 92	BN821	578	1.13
10	JUN 92	BN2094	1200	0.50
11	JUL 92	BN6863*	1198	0.10
12	JUL 92	UY499*	1198	0.20
13	DEC 92	BN3883	954	1.88
14	JUL 93	BN954	1158	1.00
15	JUL 93	BN6271	1027	0.75

\* Not Nickel Plated



**H-46 PITCH SHAFT , P/N A02R2554**

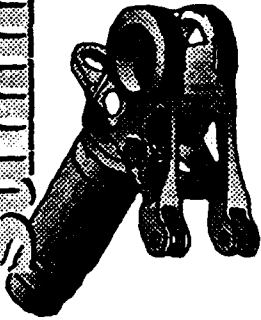
## CRACK LOCATIONS



### BOTTOM VIEW

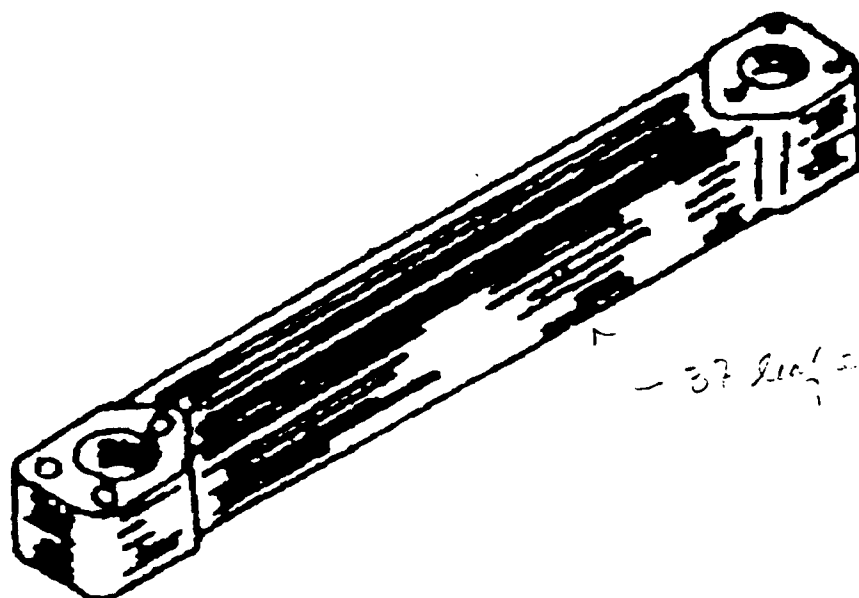


# Summary of Cracked Pitch Shafts



DATE	Reg No.	Am	Test Point	ISO	Survey	Crack Length	Remarks
June 90	BN9447	2	A5-776	1024	153412	3.4"	067-0M
June 90	BN6007	3	A5-776	1024	153412	3"	067-0M
June 90	BN10654	1	A5-776	1024	153412	Small	067-0M
November 90	BN6622	2	A5-644	681	153330	Very Small	N/A
February 91	BN8206	2	A5-1013	1135	154037	~3"	010-1R
February 91	BN9522	1	A5-1013	1135	154037	~.25"	010-1R
March 91	BN9133	3	A5-95	950	151948	~.03"	N/A
October 92	BN11066	?	?	1300	?	~.03"	N/A
July 93	BN9292	2	A5-772	267	153406	3.6"	117-3R

# H-46 TIE BAR, P/N A02R2505-2



- 37 1/2 inch

H-46 FAILED TIE BARS  
A02R2505-2



NR	SERIAL NUMBER	DATE FOUND	BROKEN ELEMENTS	TSN	HEAD	ARM	SQUADRON
1	A-12649	13-Jun-91	15	245	AFT	RED	HC 8
2	A-13119	18-Jun-91	2	103	AFT	YEL	HMM 166
3	A-12341	23-Jun-91	3	294	AFT	UNK	HMM 264
4	A-12350	23-Jun-91	3	234	AFT	YEL	HMM 268
5	A-12475	24-Jun-91	2	214	AFT	GRN	HMM 164
6	A-12789	24-Jun-91	2	274	AFT	YEL	HC 5
7	A-12754	27-Jun-91	4	274	AFT	RED	HC 5
8	A-12726	27-Jun-91	2	300	AFT	YEL	DEPLOYED
9	A-12474	27-Jun-91	2	869	FWD	RED	DEPLOYED
10	A-12652	29-Jun-91	5	324	FWD	UNK	HMM 264
11	A-12661	18-Aug-91	16	209	AFT	YEL	HC 6 DET 6
12	A-12662	18-Aug-91	22	209	AFT	RED	HC 6 DET 6
13	A-12827	30-Aug-91	2	356	AFT	RED	HC 8
14	A-12643	30-Aug-91	2	302	AFT	RED	HC 8
15	A-12306	21-Sep-91	3	751	AFT	RED	HMM 162
16	A-12655	27-Nov-91	4	UNK	AFT	RED	HC 6
17	A-12950	18-Feb-92	4	253	AFT	UNK	HMM 265
18	A-12755	17-Mar-92	6	808	AFT	GRN	HC 5
19	A-12763	17-Mar-92	7	808	AFT	YEL	HC 5
20	A-12726	6-May-92	13	870	AFT	YEL	HC 5 DET 1
21	A-12640	15-Jul-92	3	1018	UNK	UNK	HC 11
22	A-12691	3-Aug-92	3	632	UNK	UNK	HC 3
23	A-12927	5-Aug-92	4	536	UNK	UNK	UNK
24	A-12924	5-Aug-92	6	536	UNK	UNK	UNK
25	A-13714	11-Aug-92	4	349	AFT	YEL	HC 11
26	A-12647	2-Sep-92	15	1062	AFT	GRN	HC 5 DET 1
27	A-14510	17-Sep-92	13	573	AFT	UNK	HC 3
28	A-13900	22-Sep-92	8	398	AFT	YEL	HC 11 DET 10
29	A-14448	6-Oct-92	7	131	FWD	YEL	HMM 261
30	A-13692	6-Oct-92	5	398	AFT	YEL	HC 11 DET 10
31	A-13870	6-Oct-92	3	398	AFT	RED	HC 11 DET 10
32	A-15057	9-Oct-92	4	UNK	UNK	UNK	HC 8
33	A-14520	9-Oct-92	4	UNK	UNK	UNK	HC 8
34	A-14499	9-Oct-92	4	UNK	UNK	UNK	HC 8
35	A-13868	9-Oct-92	4	UNK	AFT	YEL	HC 6 DET 4
36	A-14455	13-Oct-92	3	46	AFT	GRN	HMM 164
37	A-14382	13-Oct-92	3	46	AFT	YEL	HMM 164
38	A-14468	14-Oct-92	3	409	FWD	RED	HC 8
39	A-14477	14-Oct-92	2	409	FWD	GRN	HC 8
40	A-14567	14-Oct-92	3	409	FWD	YEL	HC 8
41	A-14263	14-Oct-92	17	169	AFT	RED	HC 8
42	A-14225	14-Oct-92	15	169	AFT	GRN	HC 8
43	A-14238	14-Oct-92	11	169	AFT	YEL	HC 8
44	A-14550	16-Oct-92	5	323	AFT	RED	HC 11
45	A-14472	16-Oct-92	3	323	AFT	GRN	HC 11
46	A-14557	16-Oct-92	3	323	AFT	YEL	HC 11
47	A-13894	19-Oct-92	4	291	AFT	GRN	HC 11
48	A-12645	21-Oct-92	5	UNK	AFT	RED	HC 3
49	A-14142	28-Oct-92	2	UNK	AFT	UNK	HMM 364
50	A-14144	28-Oct-92	2	UNK	AFT	UNK	HMM 364



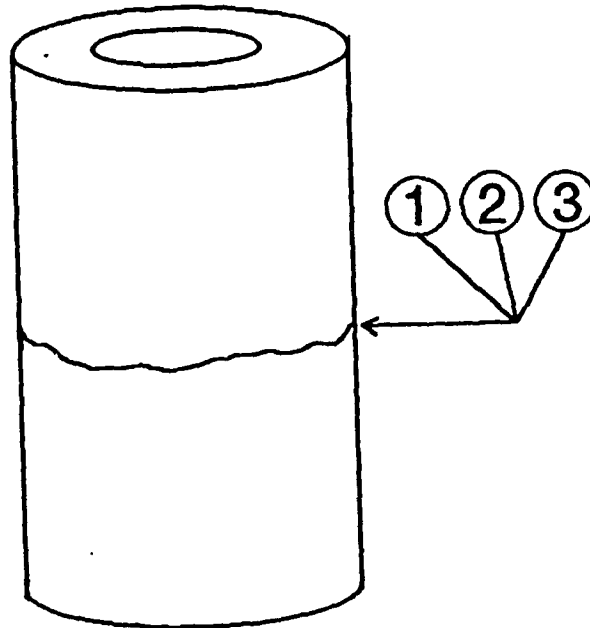


51	A-13540	18-Nov-92	4	UNK	AFT	UNK	HMM 364
52	A-14323	19-Nov-92	3	145	AFT	RED	HC 8 DET 1
53	A-14084	20-Nov-92	3	77	AFT	UNK	HMM 262
54	A-14305	3-Dec-92	3	UNK	FWD	UNK	HMM 364
55	A-14058	15-Dec-92	3	UNK	FWD	UNK	HMM 364
56	A-14254	15-Dec-92	3	UNK	FWD	UNK	HMM 364
57	A-14464	25-Dec-92	8	200	AFT	YEL	HC 6 DET 2
58	A-14087	2-Jan-93	6	219	UNK	UNK	HMM 261
59	A-14239	5-Jan-93	5	106	AFT	GRN	SOMS K-BAY
60	A-14531	5-Jan-93	5	106	AFT	YEL	SOMS K-BAY
61	A-14430	5-Jan-93	1	106	AFT	RED	SOMS K-BAY
62	A-13882	11-Jan-93	7	199	UNK	UNK	HMM 261
63	A-13856	11-Jan-93	11	199	UNK	UNK	HMM 261
64	A-13923	11-Jan-93	4	199	UNK	UNK	HMM 261
65	A-14347	11-Jan-93	4	188	AFT	UNK	HMM 262
66	A-13140	11-Jan-93	3	143	AFT	UNK	HMM 265
67	A-14139	20-Jan-93	3	352	FWD	UNK	HMX 1
68	A-14270	22-Jan-93	6	108	AFT	GRN	HMM 163
69	A-13957	28-Jan-93	2	291	UNK	UNK	HMM 261
70	A-13956	3-Feb-93	3	225	UNK	UNK	HMM 261
71	A-14035	17-Feb-93	5	UNK	AFT	RED	HMM 265
72	A-13809	5-Mar-93	2	163	UNK	UNK	HMM 261
73	A-13913	5-Mar-93	4	163	UNK	UNK	HMM 261
74	A-13910	6-Mar-93	4	321	UNK	UNK	HMM 261
75	A-14280	7-Mar-93	4	365	AFT	GRN	HC 8 DET 1
76	A-14721	1-Apr-93	3	UNK	AFT	UNK	HMM 364
77	A-13960	5-Apr-93	8	618	FWD	GRN	HC 11 D 11
78	A-12650	8-Apr-93	5	554	AFT	UNK	HMM 165
79	A-18980	12-Apr-93	5	104	AFT	UNK	HMM 262
80	A-13585	13-Apr-93	2	UNK	AFT	UNK	HMM 364
81	A-13885	11-May-93	6	409	AFT	GRN	HMM 264
82	A-13871	11-May-93	6	409	AFT	YEL	HMM 264
83	A-13888	11-May-93	2	409	AFT	RED	HMM 264
84	A-14290	11-May-93	3	313	FWD	GRN	HMM 264
85	A-14074	14-May-93	5	208	UNK	UNK	HMM 261
86	A-14466	24-May-93	8	106	FWD	GRN	HMM 264
87	A-12658	17-Jun-93	9	UNK	UNK	UNK	DEPOT CHPT
88	A-14722	21-Jun-93	7	275	AFT	UNK	HMM 364
89	A-14093	25-Jun-93	5	UNK	AFT	UNK	HMM 164
90	A-14109	25-Jun-93	13	UNK	AFT	UNK	HMM 164
91	A-14076	25-Jun-93	9	UNK	AFT	UNK	HMM 164
92	A-13489	14-Jul-93	11	500	AFT	YEL	HMM 166
93	A-14059	16-Jul-93	12	310	UNK	UNK	HMM 266
94	A-13522	17-Jul-93	9	817	AFT	RED	HC 11 D 3
95	A-14186	6-Aug-93	6	266	UNK	UNK	HMM 261
96	A-14157	18-Aug-93	8	624	UNK	UNK	HMM 266
97	A-1231	26-Aug-93	4	UNK	UNK	UNK	HMM 261
98	A-15012	26-Aug-93	4	312	UNK	UNK	HMM 261
99	A-13701	27-Aug-93	6	485	UNK	UNK	HMM 266
100	A-12794	7-Sep-93	3	454	UNK	UNK	HMM 261
101	A-13656	8-Sep-93	2	229	AFT	GRN	IWAKUNI
102	A-14193	15-Sep-93	13	300	UNK	UNK	HMM 262
103	A-14092	17-Sep-93	3	427	FWD	RED	HC 11
104	A-14827	17-Sep-93	4	301	AFT	RED	HC 11



# H-46 TIE BAR PIN, P/N A02R2644

## CRACK LOCATIONS





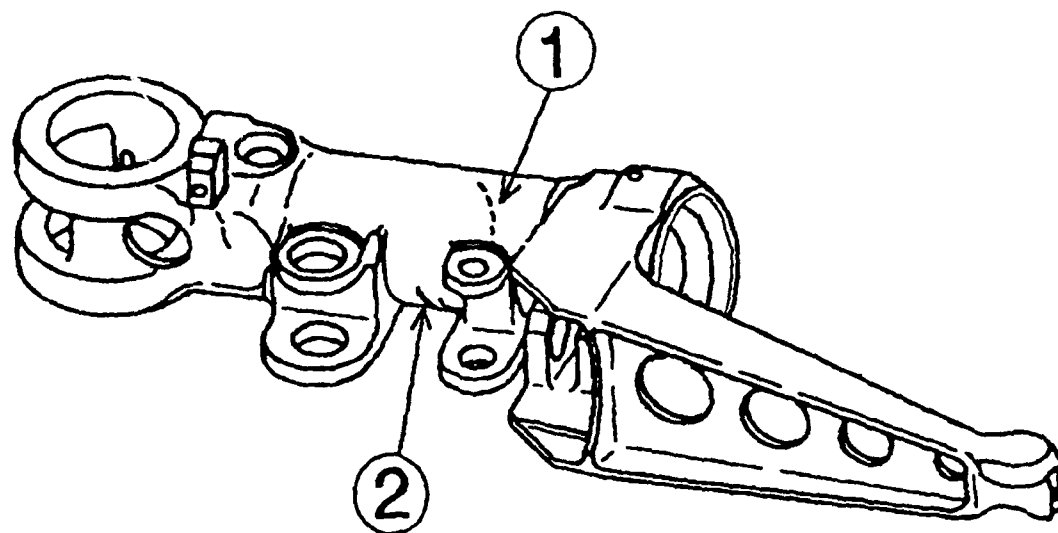
**H-46 TIE BAR PIN, P/N A02R2644**

**FAILURE LOCATIONS**

<b>NR</b>	<b>DATE</b>		<b>DEFECT</b>
	<b>FOUND</b>		
<b>1</b>	<b>27-Feb-84</b>		<b>STRESS CORR.</b>
<b>2</b>	<b>27-Mar-90</b>		<b>STRESS CORR.</b>
<b>3</b>	<b>1-Apr-90</b>		<b>STRESS CORR.</b>

# H-46 PITCH HOUSING, P/N A02R2553

## CRACK LOCATIONS



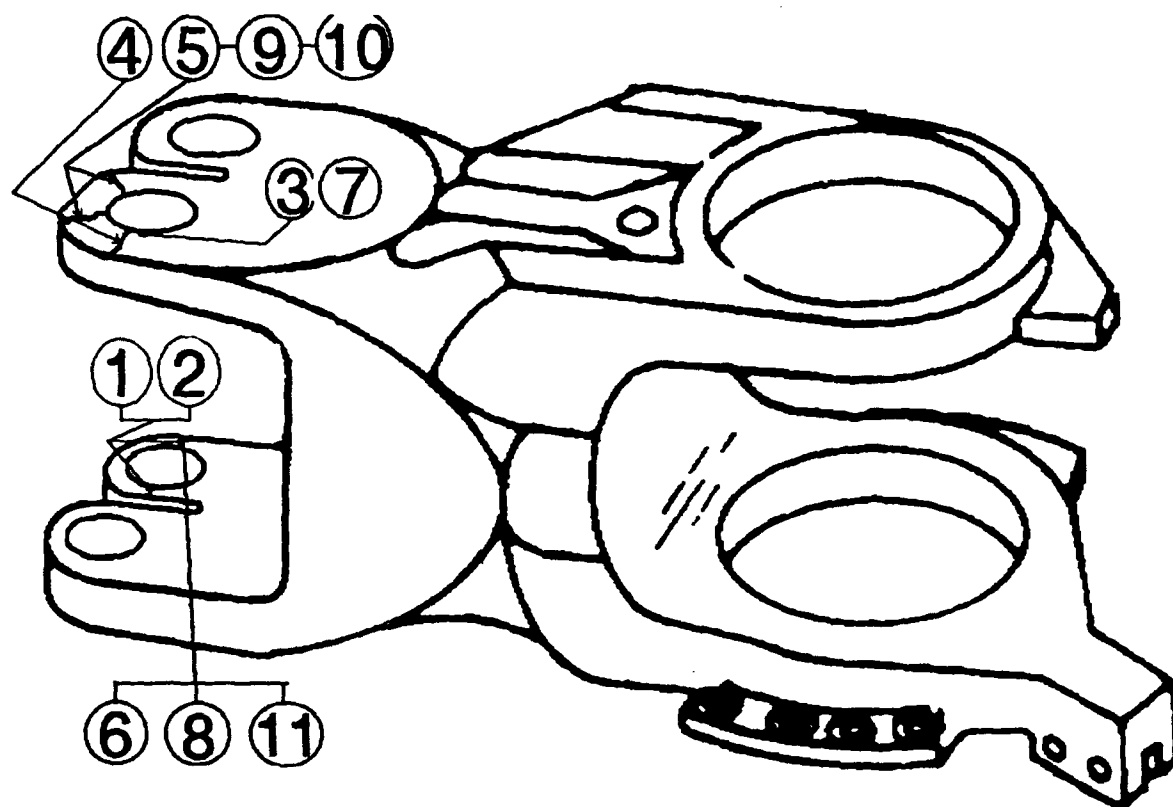


# H-46 PITCH HOUSING FAILURES

Nr.	Serial	Date	TSN	TSO	Crack length
	Number	Found			
1	BN11113	10-Jan-91	2217	1017	4.375"
2	BN10064	9-Jan-91	Unk	427	1.250"
3	*	9-Feb-91	Unk	469	1.000"

\* Rotor head, S/N A5-305, never received

H-46 BLADE FITTING, P/N A02R1710



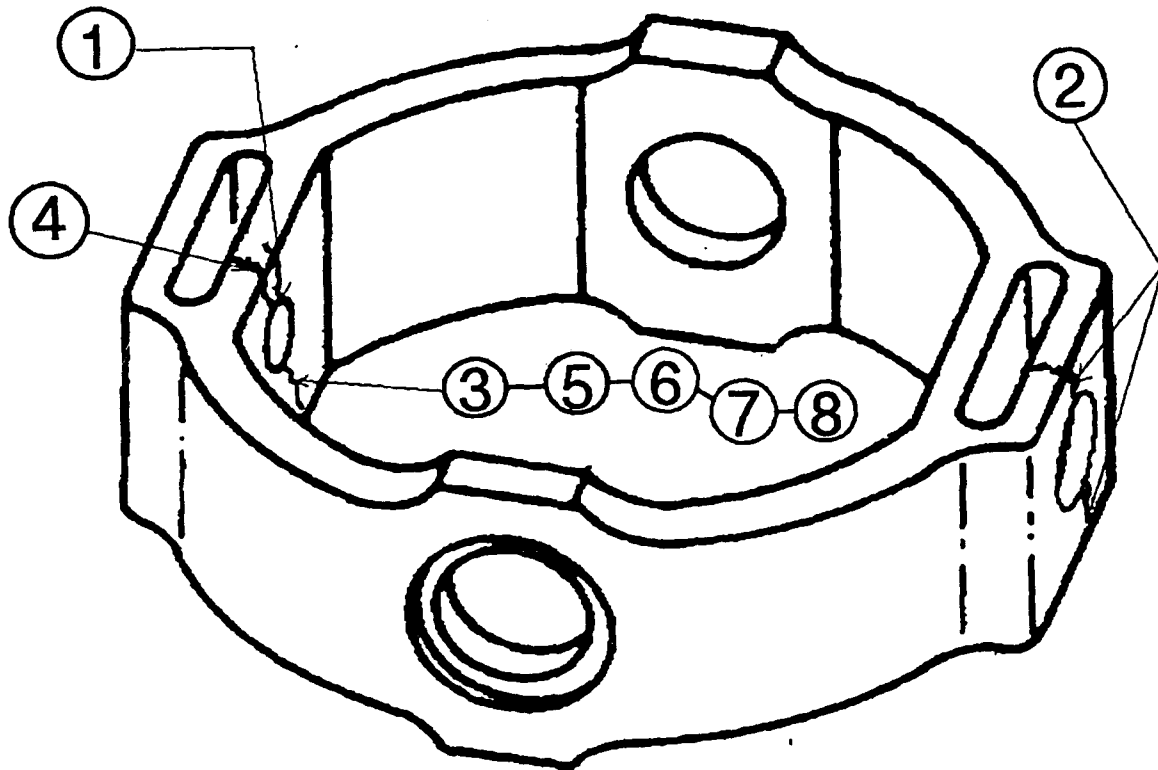
CRACK LOCATIONS

# H-46 FAILED FITTINGS

	DATE FOUND	TSN	TSO	DASH NO.	SERIAL NO.	LOCATION	EI NUMBER
1	Jul 91	5076	899	-9	RX 417	LOWER LAG	057-1R
2	Jul 91	3959	711	-9	UR 315	LOWER LAG	062-1R
3	Jan 92	UNK	292	-9	UW 151	UPPER LEAD	017-2R
4	Jan 92	UNK	231	-10	RX 132	UPPER LEAD	015-2R
5	Feb 92	2642	484	-10	RX 165	LOWER LAG	025-2R
6	Apr 92	3772	172	-11	AR 1248	UPPER LEAD	050-2R
7	Jun 92	UNK	229	-10	UW 1392	UPPER LEAD	078-2R
8	Jun 92	UNK	733	-12	UR 762	UNK	085-2R
9	Jul 92	UNK	518	-10	UR 1206	UPPER LEAD	091-2R
10	Oct 92	UNK	659	-11	RX 372	UPPER LEAD	134-2R
11	Nov 92	UNK	189	-11	UR1728	LOWER LAG	148-2R

# H-46 INNER RING, P/N 107R3582

## CRACK LOCATIONS



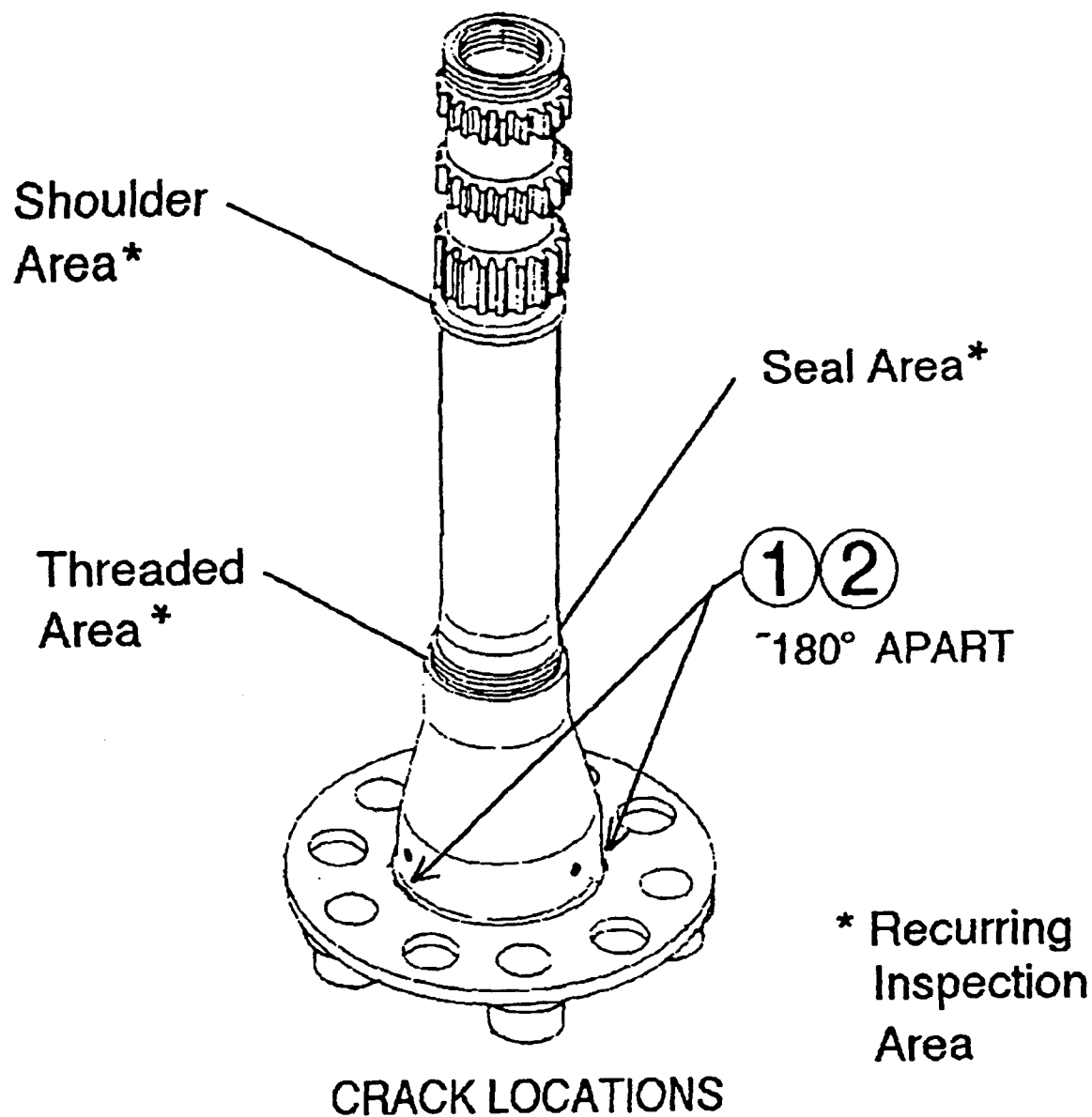
# H-46 SWASHPLATE INNER RING

## FAILURE LOCATIONS

NR	DATE		DEFECT	PROGRESSION
	FOUND			
1	25-Mar-87		CORR. PIT	YES, 1.0*
2	11-Jan-88		MATL INCLUSION	YES, 1.0*
3	23-Aug-88		CORR.	YES, 1.0*
4	31-Jan-89		FATIGUE	YES, 1.0*
5	27-Jun-89		STRESS CORR.	YES, 1.0*
6	4-Oct-91		UNK	
7	24-Dec-91		UNK	
8	27-Mar-92		UNK	

\* fatigue propagation in inches (thru crack)

# FORWARD SHAFT AND CARRIER P/N A02D1269





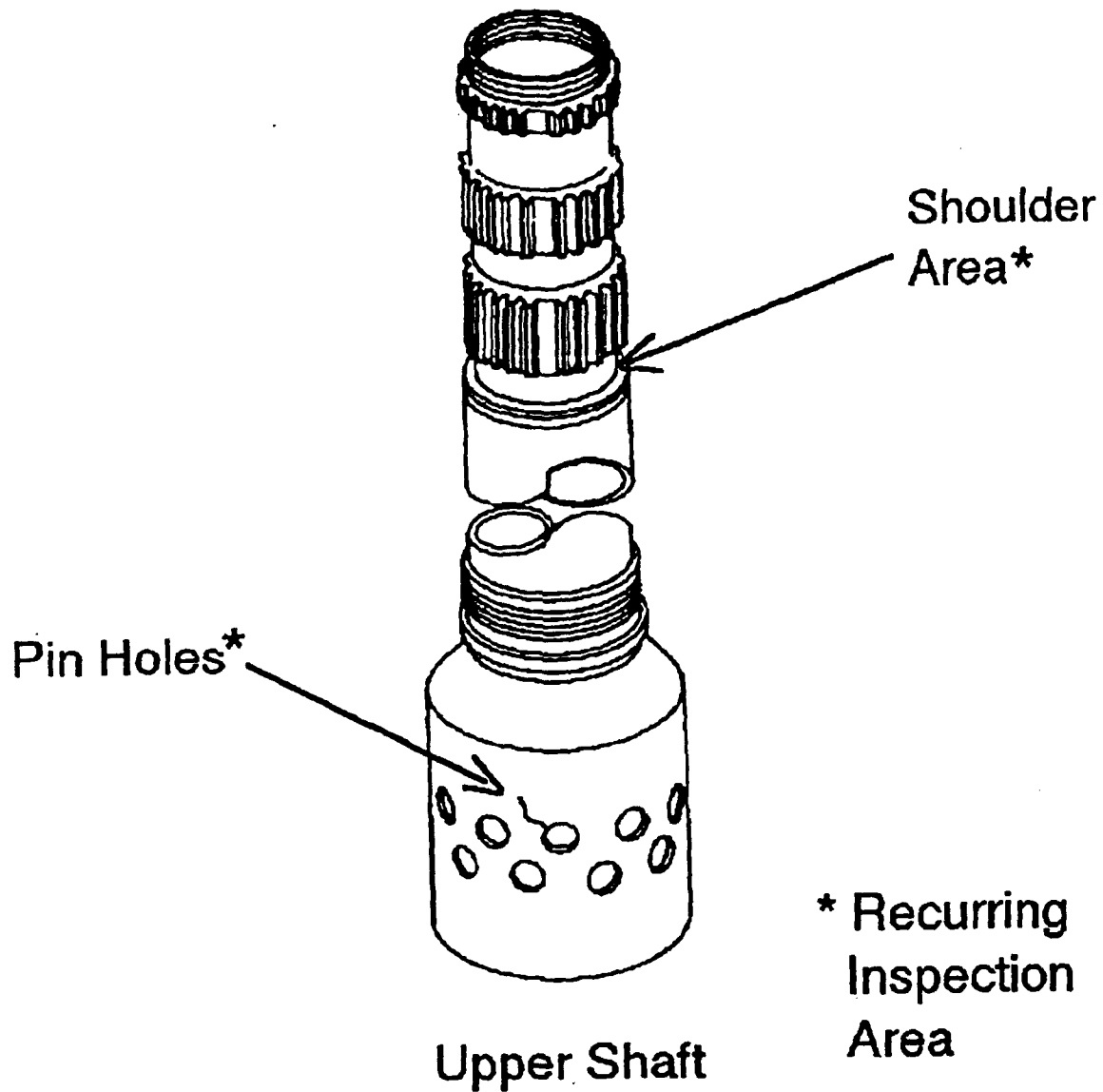
## H-46 FORWARD SHAFT AND CARRIER FAILURES

NR	SERIAL	DATE	TSN	TSO	CRACK
	NUMBER	FOUND			SIZE
1	P662	Nov-82	UNK	UNK	7" / 1.5"
2	TA826	23-Oct-90	>2000	1132	2.1" / .7"



# AFT ROTOR DRIVE SHAFT P/N A02D3011

CRACK LOCATIONS







# AFT VERTICAL SHAFT CRACKS

NUMBER	SERIAL NUMBER	DATE OF AND ->	BUREAU NUMBER	DATE FOUND	TSO	TSN	CRACK LOCATION	MISCHAP
1	A 471		156471	78SEP	114	2260	PIN HOLE	UNK NO
2	A 659		154827	77JUN	809	2279		YES/INCOMP
3	A 755		159913	78MAR	530	2489	PIN HOLE	UNK NO
4	A 917		UNK	78APR	979	UNK	THREADS	UNK NO
5	A 963		154020	78JAN	517	1521	PIN HOLE	UNK NO
6	A 423		154846	80AUG	263	2091	THREADS	UNK NO
7	A 594		154831	82AUG		4434	PIN HOLE	NO
8A	A 253	UNK	UNK	83031		2506	THREADS	NO
9	A 876	85262	151433	83081		1987	UNK	NO
10	A 305	85014	154857	83104		2000	UNK	NO
11	A 421	85182	157661	83119		2878	THREADS	NO
12	A 477	88217	151941	83147		3873	THREADS	NO
13	TA 138	84274	157704	83204	N/A	1327	THREADS	NO
14	A 949	84366	156465	83204	297	1714	PIN HOLE	NO
15	A 650	85295	156427	83300	789	1906	PIN HOLE	NO
16	A 555	84094	155317	83353		2732	THREADS	NO
17	A 517	87168	150957	84080		1517	PIN HOLE	NO
18	A 350	84361	151908	84206	1256	2305	THREADS	NO
19	A 750	84017	154789	84221		1966	THREADS	NO
20	A 930	85097	153372	84261		2637	THREADS	NO
21	A 269	84294	159651	85008	1659	2469	THREADS	NO
22	A 769	84285	156454	85046		3439	PIN HOLE	NO
23	A 946	UNK	UNK	85071		UNK	THREADS	NO
24	A 702	85161	150957	85083	1398	1882	UNK	NO
25	TA 170	85066	157702	85114	1	2564	UNK	NO
26	P 672	UNK	UNK	85201		UNK	PIN HOLE	NO
27	A 544	85300	154799	86037	1316	3027	THREADS	NO
28	A 684	87077	153405	87121		2331	THREADS	NO
29	A 864	88062	153998	88138		3693	UNK	NO
30	A 723	87305	157674	88239		2823	PIN HOLE	NO
31	A 536	88134	151937	88134		2470	UNK	NO
32	A 595	91282	151651	91308		4577	UNK	NO
33	A 791	90061	156472	92037		4374	PIN HOLE	NO

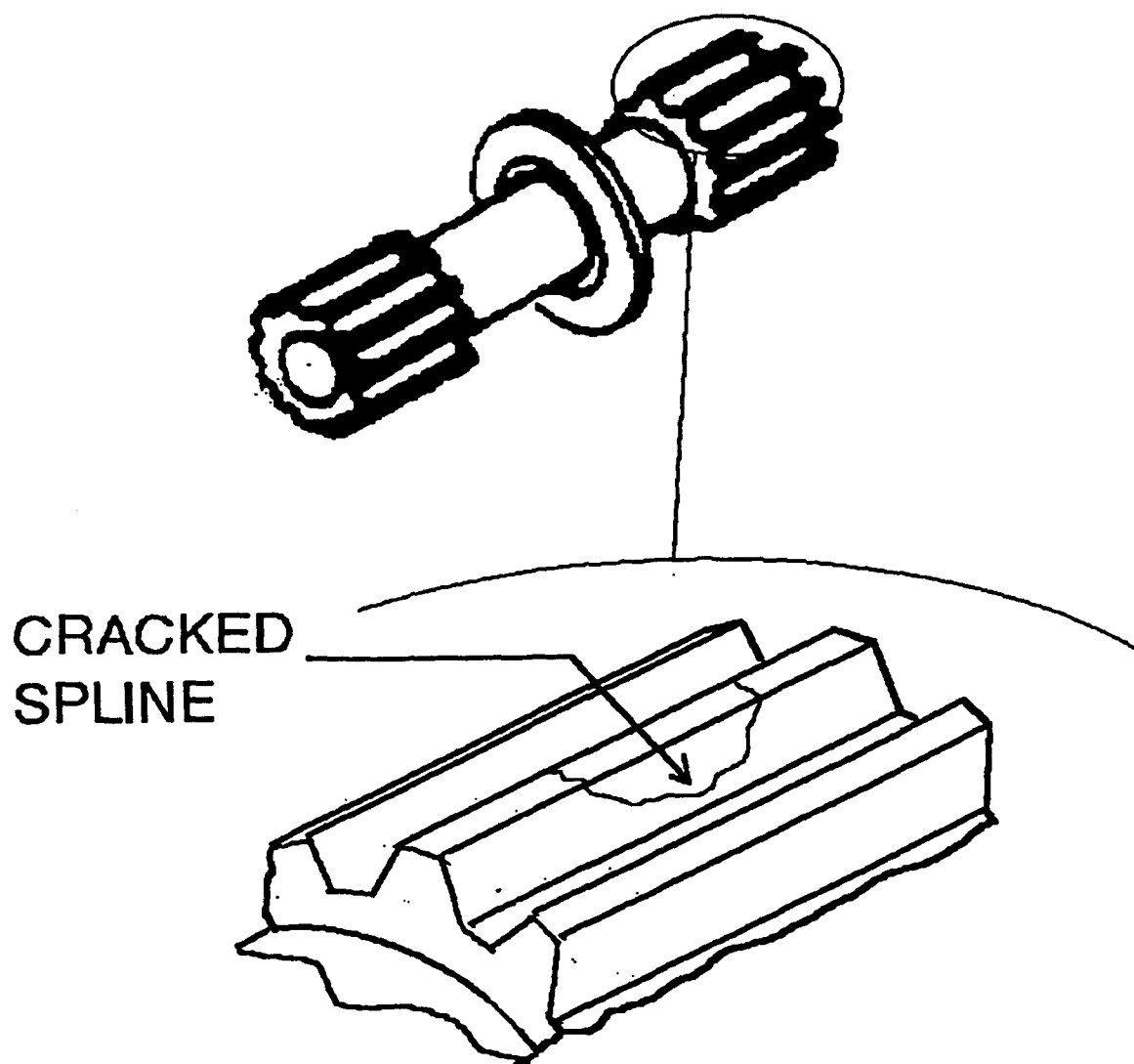
NOTES: Bureau numbers were not listed in the transmission records where a great ammount of this information was obtained. A search was made to locate the closest dated bureau number through COMPTRACK. Time since new and time since overhaul were obtained from the transmission records if they were listed otherwise these figures came from the COMPTRACK data.

CONCLUDING: Number's 8A through 33 were obtained by comparing inducted shafts with those receiving overhaul and repair because of failed NDI.

# H-46 QUILL SHAFT

## P/N A02D2067-2

### CRACK LOCATIONS

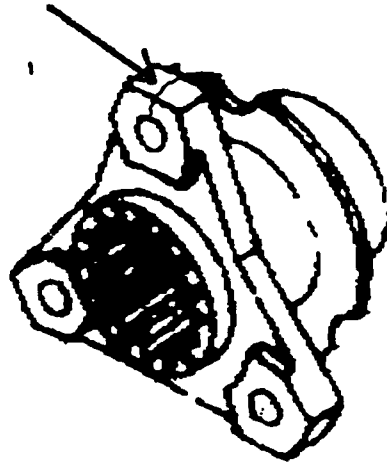


# H-46 QUILL SHAFT FAILURES

Nr	Serial		Date		Crack	
	Number	Found	TSN	Size		
1	XL787	4-May-90	315	720 Deg (Mishap)		
2	XL958	May-90	92	4 Splines Cracked .5"-.75"		
3	XL618	22-May-90	564	1 Spline Cracked		
4	XL200	23-May-90	851	1 Spline Cracked		
5	XL722	25-May-90	617	4 Splines Cracked		
6	XL796	27-May-90	206	4 Splines Broken		
7	XL914	28-May-90	367	1 Spline Broken		
8	XL792	29-May-90	212	1 Spline Broken		

# INPUT PINION ADAPTER P/N 107D3047

CRACK LOCATION





## H-46 INPUT PINION ADAPTER FAILURES

NR	SERIAL	DATE	TSN	TSO	CRACK
	NUMBER	FOUND			
1	A-302	1-Jun-90	UNK	UNK	Thru Lug



## H-46 DCU PROGRAM FEATURES

### REVISION H SOW

#### ROTOR HEADS

- MATERIAL CHANGES
- EPOXY FINISHES
- LOCAL BEEF-UPS
- NON-HYDROSCOPIC LINERS
- NEW SEALS
- NEW BEARINGS
- NEW DAMPER SEALS/SIGHT GLASS

#### TRANSMISSIONS

- NEW SHAFT SEALS
- AFT MIX SIGHT GLASS
- AIR DRIER SYSTEM
- #1 BOOST PUMP DRIVE SPLINE ADAPTER
- ACCESSORY GEARBOX
  - ALIGNMENT
  - NON-METALLIC SPLINE ADAPTERS
  - UTILITY PUMP SHEAR SHAFT

#### DRIVE SYSTEM

- SLIDER GUIDE BUSHINGS
- NEW FORWARD SHAFT
- NEW AFT SHAFT
- SYNCH SHAFTS EPOXY FINISHES
- NEW SYNCH SHAFTS MOUNTS

#### ROTOR CONTROLS SYSTEM

- SWASHPLATE GIMBAL MATERIAL CHANGE
- SWASHPLATE LOWER RING MATERIAL CHANGE
- NEW SWASHPLATE DRIVE LINK BEARING
- SCISSORS
  - MATERIAL CHANGES TO DVM
  - NEW BUSHINGS
  - NEW BEARINGS
- PITCH LINKS AND COLLECTIVE LINKS
  - MATERIAL CHANGES
  - NEW BEARINGS
- LCT ACTUATOR MODS
- NEW DASH ACTUATOR SHAFT SUPPORT



STATUS AS OF: 5/4/93

**PRELIMINARY**

## MAJOR MILESTONES

**ENGA DESIGN**

## VALVER PROCUREMENT

**VALIDATION KIT**  
**(COMPOSED OF 11 SUB KITS)**

**QUALIFICATION TEST**  
**(14 FATIGUE TESTS)**  
**(3 JOINT ENDURANCE TESTS)**  
**(DESTRUCT SPECIMENS)**

## FLIGHT TEST KIT

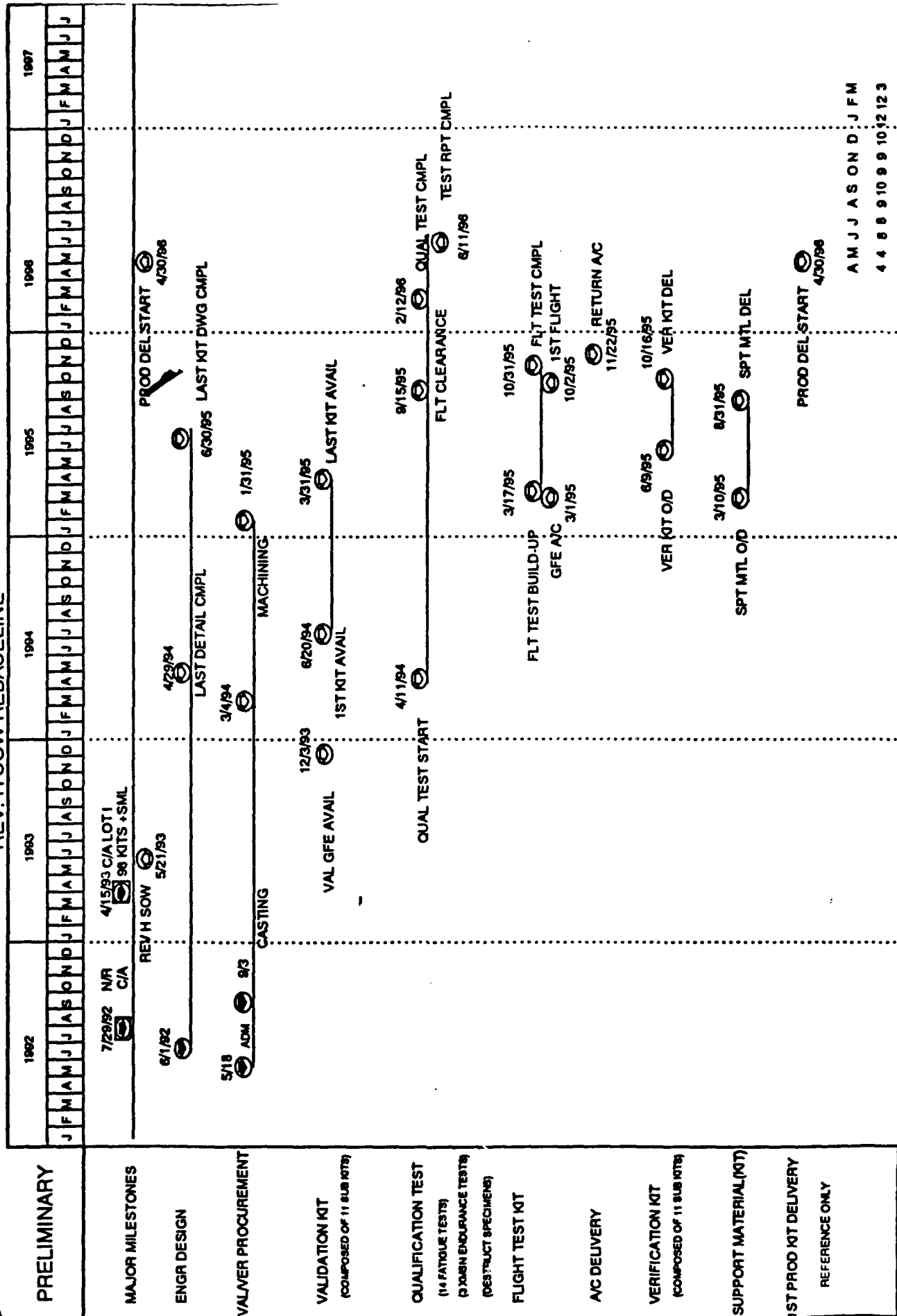
**A/C DELIVERY**

**VERIFICATION KIT  
(COMPOSED OF 11 SUB KITS)**

## SUPPORT MATERIAL (MTD)

REFERENCE ONLY

VALVEAH



**PREPARED BY PP&C**

**ONR-GA TECH WORKSHOP  
ON  
CONDITIONED BASED MAINTENANCE  
FINAL ATTENDANCE ROSTER  
NOVEMBER 15 - 17, 1993**

Achenbach, Jan D.  
Northwestern University  
Center for Quality Engineering &  
Failure Prevention  
Mechanical Engineering Department  
2137 North Sheridan Road  
Evanston, IL 60208  
708/491-5527

Bair, Scott  
Georgia Tech  
Woodruff School of Mechanical Engineering  
Atlanta, GA 30332-0405  
404/894-3273

Barron, Roger  
Barron Associates  
3046A Berkmar Dr.  
Charlottesville, VA 22901-1444  
804/973-1215  
804/973-4686 (fax)

Barsoum, Roshdy  
ONR-Mechanics  
Code 332 SM  
800 N. Quincy St.  
Arlington, VA 22217-5000  
703/696-4306  
703/696-0934 (fax)

Baugh, Kevin  
University of Texas-Austin  
Applied Research Laboratory  
PO Box 8029  
Austin, TX 78713-8029  
512/835-3405  
512/835-3259 (fax)

Ben-Amotz, Dor  
Purdue University  
Department of Chemistry  
West Lafayette, IN 47907  
317/494-5256  
317/494-0239 (fax)  
email:bendor@chem.purdue.edu

Benson, Tim  
System Planning Corp.  
1429 N. Quincy St.  
Arlington, VA 22207  
703/351-8632  
703/351-8662 (fax)

Board, David  
dme Corp.  
111 SW 33rd Street  
Ft. Lauderdale, FL 33315  
305/463-5066  
305/462-5503 (fax)

Bowen, John  
University of Texas-Austin  
Applied Research Lab  
PO Box 8029  
Austin, TX 78713-8029  
512/835-3707  
512/835-3259 (fax)

Brandt, Richard  
ONR-Physics Division  
Code 3121A1  
Ballston Center Tower One  
800 N. Quincy Street  
Alexandria, VA 22217-5660  
703/696-4206



Brown, Sherman D.  
University of Illinois  
Dept of Material Science & Engineering  
Ceramics Division  
105 S. Goodwin Ave.  
Urbana, IL 61001  
217/333-4766

Cammett, John  
Naval Aviation Depot  
Materials Engineering Division  
Cherry Point, NC 28533  
919/466-7168  
919/466-8108 (fax)

Cates, Mike  
Oak Ridge National Laboratory  
PO Box 2003  
Oak Ridge, TN 37831-8029  
615/574-8056  
615/576-0279 (fax)

Cowan, Rick  
Georgia Tech  
Woodruff School of Mechanical Engineering  
Atlanta, GA 30332-0405  
404/894-3277

Cox, Wesley J.  
BIRL Industrial Research Laboratories  
1801 Maple Avenue  
Evanston, IL 60202  
708/491-7648

Danyluk, Steven  
Georgia Tech  
Woodruff School of Mechanical Engineering  
Atlanta, GA 30332-0405  
404/894-9687

Fitzgerald, Paul  
Aerospace Engineer Code 361  
C-130 Aircraft NADEP  
Cherry Point, NC 28557  
919/466-8184  
919/466-8066 (fax)

Frison, Ted  
Randle, Inc.  
PO Box 1010  
Great Falls, VA 22066  
703/759-5257  
703/757-7639 (fax)  
email: ted@chaotic.com

Gaberson, Howard  
Naval Facilities Engineering Service Center  
560 Center Drive  
MC C21  
Port Hueneme, CA 93043-4328  
805/982-1345

Gibson, Ursula  
Dartmouth College  
Thayer School of Engineering  
Hanover, NH 03755  
603/646-3243

Glaeser, William  
Battelle Memorial Institute  
505 King Avenue  
Columbus, OH 43201  
614/424-4626

Hall, David L.  
Pennsylvania State University  
Applied Research Lab  
University Park, PA 16802  
814/863-4155  
814/863-7841 (fax)

Harris, Tedric A.  
Pennsylvania State University  
Department of Mechanical Engineering  
University Park, PA 16802  
814/863-6285

Hegner, Henry R.  
ECO Inc.  
1356 Cape St. Claire Rd.  
Annapolis, MD 21401  
410/757-3245  
410/757-8265 (fax)

Heshmat, Hooshang  
Mechanical Technology, Inc.  
986 Albany-Shaker Rd.  
Latham, NY 12109  
518/785-2322  
518/785-2420 (fax)

Howard, Paul  
Paul L. Howard Enterprises  
1212 Clearbrook Rd.  
West Chester, PA 19380  
610/692-0152  
610/692-5084 (fax)

Hsu, Steve  
NIST  
Building 223, Room A263  
Gaithersburg, MD 20899  
301/975-6120  
301/990-8729 (fax)

Hurd, Harry L.  
Harry L. Hurd Assoc.  
2301 Stonehenge Dr.  
Suite 104  
Raleigh, NC 17615  
919/676-9790

Jarzynski, Jacek  
Georgia Tech  
Woodruff School of Mechanical Engineering  
Atlanta, GA 30332-0405  
404/894-7479

Kadysewski, Ronald  
Vickers-Tedeco  
24 East Glenolden Avenue  
Glenolden, PA 19036  
215/583-9400 ext. 268  
215/583-3985 (fax)

Kennedy, Francis E.  
Dartmouth College  
Thayer School of Engineering  
Hanover, NH 03755  
603/646-2094

Kover, Don  
CDNSWC Code 825  
Annapolis, MD 21402  
410/267-2756

Krieder, K.G.  
NIST  
Process Measurements Division  
Building 221, Room A303  
Gaithersburg, MD 20899  
301/975-2619

Ling, Frederick F.  
The University of Texas  
Austin, TX 78712-1063  
512/471-3024

Marciano, Joseph  
Sikorsky Aircraft  
Engineering Department  
Reliability/Maintainability Section  
6900 Main Street  
Stratford, CT 06601  
203/386-4461

Mason, J.C.  
Aerospace Engineer, Code 361  
C-130 Scheduled Maintenance NADEP  
Cherry Point, NC 28533  
919/466-7136  
919/466-8066 (fax)

McKenna, Thomas  
ONR-Computational Neuro Science  
Code 342CN  
800 N. Quincy Street  
Arlington, VA 22217  
703/696-4503

McNeany, Steve  
Oak Ridge National Laboratory  
PO Box 2009  
Oak Ridge, TN 37831-8039  
615/574-0286  
615/574-9407

Ng, Kam  
ONR  
Code 452E4  
800 N. Quincy St.  
Arlington, VA 22217  
703/696-0816  
703/696-0308 (fax)

Nickerson, William (Bill)  
Pennsylvania State University  
Applied Research Laboratory  
PO Box 30  
State College, PA 16804  
410/479-4781  
814/863-1183 (fax)

O'Connor, Brian  
Lubrizol Corporation  
29400 Lakeland Blvd.  
Wickliffe, OH 44092  
216/943-1200  
216/943-9021 (fax)

Parker, Eugene  
Barron Assoc.  
3046A Berkmar Ave.  
Charlottesville, VA 22901-1444  
814/973-1215

Peterson, Marshall  
Wear Sciences  
925 Mallard Circle  
Arnold, MD 21012  
301/261-2342

Prine, David W.  
BIRL Industrial Research Laboratories  
1801 Maple Avenue  
Evanston, IL 60201  
708/491-2873

Ramalingam, S. "RAM"  
University of Minnesota  
Department of Mechanical Engineering  
111 Church Street, SE Room 215  
Minneapolis, MN 55455  
612/625-4017  
612/625-8884 (fax)

Reintjes, John  
NRL  
Laser Physics Branch  
Code 5642  
Washington, DC 20375  
202/767-2175  
202/404-7530 (fax)

Ruff, William  
NIST  
Surface Properties Group  
A215 Building 220  
Gaithersburg, MD 20899  
301/975-6010

Sauer, Carl  
Materials Engineering Code 341  
Naval Aviation Depot  
PSC Code 8021  
Cherry Point, NC 28533  
919/466-7151

Schmidt, Peter  
ONR-Materials Division  
800 N. Quincy Street  
Arlington, VA 22217-5660  
703/696-4362  
703/696-2611 (fax)

Sewersky, Rich  
Sikorsky Aircraft  
Engineering Department  
Diagnostics Section  
6900 Main St., Mail Stop S517B  
Stratford, CT 06601  
203/383-3402  
203/386-7016 (fax)

Shaffer, Steve  
Battelle Memorial Institute  
505 King Avenue  
Columbus, OH 43201  
614/424-4960

Singer, Irwin  
Naval Research Lab  
Code 6176  
4555 Overlook Ave., SW  
Washington, DC 20375-5320  
202/767-2327  
202/767-3321 (fax)  
email:singer@chem.nrl.navy.mil

Stancil, Charles M. (Chuck)  
Georgia Tech  
GTRI Aero Lab  
7220 Richardson Road  
Smyrna, GA 30080  
404/528-3229

Thornhill, Joe  
University of Texas-Austin  
Applied Research Lab  
PO Box 8029  
Austin, TX 78713-8029  
513/835-3732  
512/835-3259 (fax)

Turner, Nichelle  
Naval Air Warfare Center  
Aircraft Division  
Code RW82Q  
Building 3172  
Patuxent River, MD 20670-5304  
301/826-1239  
301/826-1232 (fax)

Wedeven, L. D.  
Wedeven Associates, Inc.  
5072 West Chester Pike  
Edgemont, PA 19028-0646  
215/356-7161  
215/235-0687 (fax)

Whitesel, Henry  
Naval Surface Warfare Center  
Carderock Division  
Code 853  
Annapolis, MD 21402  
410/267-2163

Wilsc  
Naval Aviation Depot  
H46 Drive Systems  
Cherry Point, NC 28533  
919/466-7381  
919/466-8108 (fax)

Winer, Ward  
Georgia Tech  
Woodruff School of Mechanical Engineering  
Atlanta, GA 30332-0405  
404/894-3200  
404/894-8336 (fax)